

Aus der Klinik und Poliklinik für Hals-Nasen-Ohrenheilkunde der
Ludwig-Maximilians-Universität München

Direktor: Prof. Dr. med. Alexander Berghaus

Leiter der HNO-Forschung: Prof. Dr. rer. nat. Olivier Gires

Innovative therapy modalities for solid EpCAM-positive tumors

Dissertation

zum Erwerb des Doktorgrades der Naturwissenschaften

an der Medizinischen Fakultät

der Ludwig-Maximilians-Universität München



vorgelegt von

Jana Ylva Tretter

aus Starnberg

2017

**Gedruckt mit der Genehmigung der Medizinischen Fakultät der Ludwig-
Maximilians-Universität München**

Betreuer: Prof. Dr. rer. nat. Olivier Gires

Zweitgutachter: Prof. Dr. Vigo Heissmeyer

Dekan: Prof. Dr. med. dent. Reinhard Hickel

Tag der mündlichen Prüfung: 08.11.2017

Eidesstattliche Versicherung

Tretter, Jana Ylva

Name, Vorname(n)

Ich erkläre hiermit an Eides statt,

dass ich die vorliegende Dissertation mit dem Thema

Innovative therapy modalities of solid EpCAM-positive tumors

selbstständig verfasst, mich außer der angegebenen keiner weiteren Hilfsmittel bedient und alle Erkenntnisse, die aus dem Schrifttum ganz oder annähernd übernommen sind, als solche kenntlich gemacht und nach ihrer Herkunft unter Bezeichnung der Fundstelle einzeln nachgewiesen habe.

Ich erkläre des Weiteren, dass die hier vorliegende Dissertation nicht in gleicher oder ähnlicher Form bei einer anderen Stelle zur Erlangung eines akademischen Grades eingereicht wurde.

Ort, Datum

Unterschrift DoktorandIn

“Nothing shocks me. I’m a scientist.”
Indiana Jones

Table of Contents

Abstract	1
Zusammenfassung	2
1 Introduction	4
1.1 The epithelial cell adhesion molecule (EpCAM)	5
1.1.1 The <i>EPCAM</i> gene	5
1.1.2 The EpCAM protein.....	6
1.1.3 EpCAM cleavage and signaling	7
1.1.4 EpCAM expression.....	10
1.1.5 EpCAM functions.....	11
1.1.6 EpCAM as target for immunotherapy of cancer	13
1.2 The Four and a Half LIM domains protein-2 (FHL2)	14
1.2.1 The <i>FHL2</i> gene	14
1.2.2 The FHL2 protein	15
1.2.3 FHL2 expression	16
1.2.4 FHL2 functions	16
1.3 Catenin beta-1	19
1.3.1 The CTNNB1 protein.....	20
1.3.2 The canonical Wnt signaling pathway	22
1.4 High-Content Screening	24
1.5 Aim of the project	24
2 Material and Methods	26
2.1 Chemicals and consumables	26
2.2 Oligonucleotides	26
2.2.1 DNA oligonucleotides for cloning	26
2.2.2 DNA oligonucleotides for qPCR	27
2.3 Plasmids	27
2.3.1 Commercial plasmids	27
2.3.2 Plasmids for recombinant protein expression in <i>E. coli</i>	28
2.3.3 Plasmid for recombinant protein expression in insect cells	28
2.4 Bacterial strains	28
2.5 Insect cell lines	29
2.6 Mammalian cell lines	29
2.7 Media and supplements for bacterial cell culture	30
2.8 Media and supplements for insect cell culture	30

2.9 Media and supplements for mammalian cell culture	30
2.10 Antibodies	31
2.11 General buffers and stock solutions.....	32
2.12 Molecular biology	32
2.12.1 Cloning	32
2.12.2 Transformation of <i>E. coli</i> and isolation of plasmid DNA	33
2.12.3 RNA isolation	33
2.12.4 Reverse transcription of RNA	33
2.12.5 Quantitative Real-Time PCR	33
2.13 Bioinformatics.....	34
2.13.1 Protein parameters	34
2.13.2 Sequence alignment.....	34
2.13.3 Mammalian cell line properties	34
2.14 Protein expression.....	34
2.14.1 Recombinant protein expression in <i>E. coli</i>	34
2.14.2 Recombinant protein expression in insect cells.....	34
2.15 Protein purification	35
2.15.1 Purification of GST-tagged proteins	35
2.15.2 Purification of MBP-tagged proteins	36
2.15.3 Purification of His-SUMO tagged proteins.....	36
2.16 SDS-PAGE	36
2.17 Methods for analyzing protein-protein interactions	37
2.17.1 <i>In vitro</i> pull-down assay	37
2.17.2 Isothermal titration calorimetric (ITC)	37
2.18 Cell culture	37
2.18.1 Cultivation of cells.....	37
2.18.2 Cryopreservation and thawing of cells.....	37
2.18.3 High-Content Screening (HCS)	38
2.18.3.1 Screening libraries	38
2.18.3.2 Performance and evaluation of High-Content Screening.....	38
2.18.4 Fluorescence-activated cell sorting (FACS) experiments.....	39
2.18.5 Viability/toxicity Assay	39
2.18.6 Proliferation Assay.....	40
2.19 Biochemical methods.....	40
2.19.1 Membrane-based cleavage assay.....	40
2.19.2 Preparation of whole cell lysates	40
2.19.3 Determination of protein concentration.....	40

2.19.4	Western blot	41
2.19.5	Determination of hEpCAM cleavage sites	41
2.19.5.1	Determination of γ -cleavage sites	41
2.19.5.2	Determination of ϵ -cleavage sites	42
3	Results	43
3.1	Structure determination of the nuclear complex	43
3.1.1	Expression and purification of FHL2 and EpICD	43
3.1.2	Expression and purification of β -catenin	45
3.1.3	<i>In vitro</i> pull-down experiments with FHL2, EpICD and β -catenin	46
3.1.4	ITC experiments with FHL2, EpICD and β -catenin	47
3.2	Identification of a small inhibitory molecule of the EpCAM-signaling cascade	49
3.2.1	Principle of the High-Content Screening	49
3.2.2	Image Analysis	50
3.2.3	Establishment of a High-Content Screening	51
3.2.3.1	Determination of optimal staining conditions	51
3.2.3.2	Determination of optimal magnification	52
3.2.3.3	Determination of optimal imaging method	54
3.2.3.4	Determination of optimal cell number	56
3.2.4	Performance of High-Content Screening and hit verification	57
3.2.5	Further characterization of hits	58
3.2.5.1	Cytotoxicity of compounds	59
3.2.5.2	Effects on target gene expression	60
3.2.5.3	Effects on regulated intramembrane cleavage	63
3.2.5.4	Effect on proliferation of cells	68
3.2.6	Screening of analogs	68
3.2.7	Further characterization of analogs	69
3.2.7.1	Cytotoxicity of analogs	69
3.2.7.2	Effects of analogs at transcriptional level	70
3.2.7.3	Effects of analogs on regulated intramembrane cleavage	71
3.2.7.4	Effects of analogs on proliferation	74
4	Discussion	75
4.1	Interaction of FHL2 with EpICD and β -catenin	75
4.2	Identification of a small inhibitory molecule	77
5	Appendix I	85
5.1	Abbreviations	85
5.2	Index of figures	86

5.3 Index of tables.....	88
6 Supplementary Data	89
7 References	94
Acknowledgments	113

Abstract

The epithelial cell adhesion molecule (EpCAM) is a type I transmembrane protein that is expressed on epithelial cells, cancer stem cells, carcinoma cells and embryonic stem cells. On epithelial cells, EpCAM is localized to the basolateral membranes, whereas on carcinoma cells, it is highly overexpressed and re-distributed all over the cell surface. EpCAM signaling is activated via regulated intramembrane proteolysis (RIP) by tumor-necrosis-factor alpha converting enzyme (TACE/ADAM17) and the γ -secretase complex. This leads to the release of the extracellular domain (EpEX) and of the intracellular domain (EpICD) into the cellular environment and the cytoplasm, respectively. EpICD becomes incorporated in a nuclear complex consisting of Four and a Half LIM domains protein-2 (FHL2), β -catenin and lymphoid enhancer-binding factor-1 (Lef-1). Translocation into the nucleus leads to activation of EpCAM-target genes, which are involved in cell growth and cell proliferation. Due to the expression pattern of EpCAM, it is perceived as a valuable target for cancer therapy. Therefore, several immunotherapeutic approaches have already been launched. However, targeting of the intracellular signaling cascade would be a completely new and promising way of interfering with the EpCAM signaling cascade.

The first part of this study served the structural determination of the nuclear complex and the design of a potential inhibitor for complex formation. Therefore, several interaction studies were performed with recombinantly produced FHL2, EpICD and β -catenin. Unfortunately, none of the performed experiments could confirm an interaction between these proteins, which is why a structural determination of the binding was not possible.

The second part of this project dealt with the establishment and the performance of a High-Content Screen (HCS) for the identification of a small inhibitory molecule, which inhibits the intracellular EpCAM-signaling cascade. First, the best conditions for this screen were identified. Subsequently, a screen with about 26,000 compounds was performed leading to eight high-confidence hits, which potentially inhibit the EpCAM-signaling cascade. These hits, and later on their analogs, were further characterized regarding their mode of action. It could be shown that compounds #4, #9, #10 and #13 as well as the analogs #13_1 and #10_12 interfere with γ -secretase cleavage of EpCAM. Compound #10 and its analog #10_16 seem to have an EpCAM-specific effect on cyclin D1 *CCND1* expression. Regarding cytotoxicity and cell proliferation, no EpCAM-dependent effect could be determined. Further analysis is needed to assess the compounds' substrate specificity and how they influence γ -secretase cleavage.

Zusammenfassung

Das epitheliale Zelladhäsionsmolekül (EpCAM) ist ein Typ I Transmembranprotein. EpCAM wird in Epithellzellen, Krebsstammzellen, Tumorzellen und embryonalen Stammzellen exprimiert. Auf Epithelzellen befindet sich EpCAM hauptsächlich in basolateralen Membranen, wohingegen es auf Krebszellen stark überexprimiert und auf der ganzen Zelloberfläche verteilt ist. Die EpCAM-Signalkaskade wird durch eine regulierte Intramembranproteolyse (RIP) aktiviert, die durch das Tumornekrosefaktor-alpha konvertierende Enzym (TACE/ADAM17) und den γ -Sekretase Komplex durchgeführt wird. Dies führt zu einer Freisetzung der extrazellulären Domäne von EpCAM (EpEX) in die Zellumgebung und der intrazellulären Domäne (EpICD) in das Zytoplasma. EpICD wird Teil eines Kernkomplexes mit dem *Four and a Half LIM domains protein-2* (FHL2), β -catenin und dem *Lymphoid enhancer-binding factor 1* (Lef-1). Nach der Translokation dieses Komplexes in den Zellkern aktiviert dieser die Expression von Zielgenen von EpCAM, die eine wichtige Rolle beim Zellwachstum und der Proliferation spielen. Aufgrund des Expressionsmusters ist EpCAM eine interessante Zielstruktur für die Krebstherapie. Daher wurden bereits EpCAM-basierte Ansätze für die Krebsimmuntherapie entwickelt. Ein komplett neuer Ansatz wäre allerdings die therapeutische Unterbrechung der intrazellulären EpCAM-Signalkaskade.

Der erste Teil dieses Projekts befasste sich mit der Strukturaufklärung des Kernkomplexes und dem anschließenden Design eines möglichen Inhibitors dieser Komplexbildung. Dafür wurden verschiedene Interaktionsstudien mit rekombinant hergestelltem FHL2, EpICD und β -Catenin durchgeführt. Leider konnte eine Interaktion dieser rekombinanten Proteine nicht bestätigt werden, weswegen auch die strukturelle Aufklärung der genauen Bindestelle nicht möglich war.

Der zweite Teil dieses Projekts befasste sich mit der Etablierung und Durchführung eines *High-Content Screens* (HCS). Dafür wurden zunächst die besten Bedingungen identifiziert. Anschließend wurden ca. 26.000 Moleküle getestet. Es wurden acht Verbindungen mit hohem Konfidenzniveau gefunden, welche potentiell die intrazelluläre EpCAM-Signalkaskade inhibieren. Anschließend wurde die Wirkungsweise dieser Hits und später ihrer Analoga untersucht. Es konnte gezeigt werden, dass die Verbindungen #4, #9, #10 und #13 und auch die Analoga #13_1 und 10_12 die γ -Sekretase Spaltung von EpCAM beeinflussen. Außerdem scheinen die Hits #10 and #10_12 einen EpCAM-spezifischen Effekt auf die Zyklin D1 (*CCND1*) Expression zu haben. Bezüglich der Zytotoxizität und der Zellproliferation konnte für keine Verbindung ein EpCAM-abhängiger Effekt festgestellt werden. Es sind weitere Untersuchungen not-

wendig, um die Substratspezifität und den Wirkmechanismus der gefundenen Verbindungen festzustellen.

1 Introduction

Cancer is one of the major causes of mortality worldwide (World Health Organization, 2014). In 2012, approximately 14 million new cases were reported, causing 8.2 million deaths per year. Cancer is characterized by a malignant transformation of cells leading to deregulated cell growth, evasion from cell death and invasion of nearby tissue. During cancer progression, some cancer cells disseminate from the primary tumor and spread to other parts of the body, giving rise to metastatic tumors. Metastases are the most common cause of cancer-related death (Hanahan and Weinberg, 2011). The most frequent cancer types are carcinomas of the lung (1.8 million cases, 13.0 % of the total), breast (1.7 million, 11.9 %) and large intestine (1.4 million, 9.7 %; World Cancer Report 2014). There are numerous reasons for the development of cancer. Approximately one third of cancer deaths are related to an unhealthy lifestyle: tobacco use, excessive alcohol consumption, lack of physical activity, poor diet and obesity. Other reasons might be viral infections such as hepatitis B (HBV), hepatitis C (HCV) or human papillomavirus (HPV), which lead to genetic changes within the infected cells (Cogliano *et al.*, 2011; Wicki and Hagmann, 2011; World Health Organization, 2014; World Cancer Report 2014). More than 50 % of hepatocellular carcinomas are caused by chronic infections by HBV and HPV is known to be associated with cervical cancer and carcinomas of the head and neck (Leemans *et al.*, 2011; Ljubojevic and Skerlev, 2014, Lafaro *et al.*, 2015, Njei *et al.*, 2015). An example for a carcinogenic bacterium is the gram-negative *Helicobacter pylori*, which is usually found in the stomach and might lead to chronic gastritis and ultimately stomach cancer (Correa and Piazuelo, 2011). Furthermore, there are some genetic mutations that are associated with an increased risk of cancer formation. In 1990, the gene breast cancer 1 (*BRCA1*) was described to play a role in tumor formation (Hall *et al.*, 1990). Mutations in this tumor-suppressor gene are associated with an increased risk for breast cancer and ovarian cancer (Weitzel *et al.*, 2007). Other known tumor-suppressor proteins are Retinoblastoma protein (pRb), p53 or phosphatase and tensin homolog (PTEN), which are known to be dysfunctional in several cancer types (Hollstein *et al.*, 1991; Levine *et al.*, 1991; Sansal and Sellers, 2004; Steelman *et al.*, 2004; Dick and Rubin, 2013; Uchida, 2016). Nowadays, cancer can be treated through chemotherapy, radiation therapy, hormonal therapy, immunotherapy and/or surgery in various combinations depending on the disease status. However, all treatment methods have certain limitations: radiation or chemotherapy have side effects on healthy cells and surgery will be less efficient or even not feasible for metastatic cancer. Therefore, despite current treatment options, cancer remains a disease that is in need of more efficacious and compatible therapies.

1.1 The epithelial cell adhesion molecule (EpCAM)

1.1.1 The *EPCAM* gene

The human *EPCAM* gene is located on chromosome 2 (location 2p21), consists of nine coding exons and has a size of approximately 17.9 kb (Figure 1-1A). Its transcript has a size of 1.5 kb (Balzar *et al.*, 1999a; NCBI 2017). Exons 1-6 encode for the proteins' extracellular domain (hEpEX), including the signal peptide. The transmembrane domain (TMD) is encoded by exon 7, whereas exon 8 and 9 encode for the intracellular part of hEpCAM (hEpICD; Linnenbach *et al.*, 1989; Balzar *et al.*, 1999a).

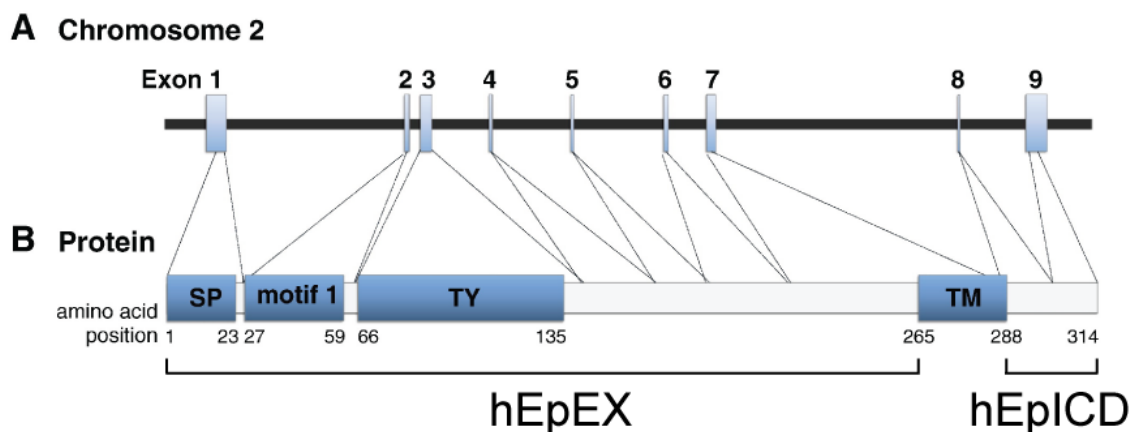


Figure 1-1 Scheme of the *EPCAM* gene (A) and protein (B). *EPCAM* is located on chromosome 2 and consists of nine exons, which encode as indicated. hEpCAM consists of 314 aa and can be subdivided in a 265 aa extracellular domain (EpEX), a 23 aa transmembrane domain (TMD) and a 26 aa intracellular domain (hEpICD). SP = signal peptide; TY = thyroglobulin-like domain (modified from Schnell *et al.*, 2013a).

The 5'-regulatory region of *EPCAM* does not contain a TATA- or CAAT-box. However, consensus transcription factor recognition sequences for the epithelial specific factors Initiator (Inr), specificity protein 1* (Sp-1), activator protein-1 (AP-1) and AP-2, Ets, epithelial specific ets-1 (ESE-1) and E-pal-like are present (Behrens *et al.*, 1991; Lee *et al.*, 1996; McLaughlin *et al.*, 2004). 177 bp of the 5'-flanking sequence are sufficient in order to obtain the maximal promoter activity, whereas 687 bp of the 5'-flanking region are necessary for epithelial specificity (McLaughlin *et al.*, 2004). *EPCAM* expression is enhanced by TCF/ β -catenin (Yamashita *et al.*, 2007) and diminished by $\text{INF}\gamma$, $\text{NF}\kappa\text{B}$ and $\text{TNF}\alpha$ (Gires *et al.*, 2001; Gires *et al.*, 2003).

Homozygous mutations of *EPCAM* have been identified in patients suffering from congenital tufting enteropathy (CTE). This is a rare autosomal recessive form of severe chronic diarrhea, which occurs in the first few days of life. Several mutations were identified leading to single amino acid (aa) exchange, truncation, partial deletion or frameshifts (Sivagnanam *et al.*, 2008; Al-Mayouf *et al.*, 2009; Ko *et al.*, 2010; Sivagnanam *et al.*, 2010; Salomon *et al.*, 2011). All these mutations cause an absence of

EpCAM from the plasma membrane, which results in dysplasia and therefore malfunction of the intestine (Sivagnanam *et al.*, 2008; Schnell *et al.*, 2013b). This dysplasia was also shown in EpCAM knock-out mice, which died shortly after birth due to hemorrhagic diarrhea. The reason for this intestinal defect might be a dysregulation of β -catenin and E-cadherin caused by the loss of EpCAM (Guerra *et al.*, 2012). Another explanation for the intestinal dysplasia is a morphologically abnormal tight junction due to the lack of EpCAM. In healthy tissue, EpCAM together with claudin-7 forms cell-cell junctions. In EpCAM knock-out mice however, claudin-7 was down-regulated to undetectable levels causing the abnormal morphology of the tight junctions what eventually results in an impaired barrier function of the intestinal epithelium (Lei *et al.*, 2012).

The *EPCAM* gene belongs to the tumor-associated antigen gene family GA-733 (Linnenbach *et al.*, 1989; Szala *et al.*, 1990; Alberti *et al.*, 1994). Since EpCAM is overexpressed on a variety of carcinomas, it has been discovered numerous times by different groups and has been given various names. These names are based on the antibody or cDNA that were used for the identification of this antigen (Schnell *et al.*, 2013a; Dollé *et al.*, 2015). However, EpCAM is used as its primary name since 2007 (Baeuerle and Gires, 2007)

1.1.2 The EpCAM protein

EpCAM is a calcium-independent homophilic cell adhesion molecule that belongs to the family of cellular adhesion molecules (CAM; Litvinov *et al.*, 1994a). It is a 34 to 42 kDa type I membrane protein consisting of 314 aa, and can be divided in three domains: a large extracellular domain of 242 aa, a TMD of 23 aa and a short intracellular domain (ICD) of 26 aa (Figure 1-1B; Strnad *et al.*, 1989; Gires, 2008; Munz *et al.*, 2009). The extracellular domain contains a signal peptide that is removed by signal peptidases in the endoplasmic reticulum (ER). The primary cleavage site is located between Ala23 and Gln24. However, approximately 1 % of EpCAM gets cleaved between Ala21 and Ala22 (Strnad *et al.*, 1989; Szala *et al.*, 1990; Chong and Speicher, 2001). The matured protein consists of an epidermal growth factor (EGF)-like domain (aa 27-59), a thyroglobulin (TY) type 1A domain (aa 66-135) and a third cysteine-free motif that is unrelated to any other known molecule (Molina *et al.*, 1996; Chong and Speicher, 2001; Schnell *et al.*, 2013a). EpCAM shows three N-glycosylation sites: Asn74, Asn111 and Asn198. Depending of the glycosylation status of these sites, the molecular weight of EpCAM ranges between 34 – 42 kDa (Thampoe *et al.*, 1988; Schon *et al.*, 1993; Gires, 2008). Glycosylation of Asn198 seems to be important for protein stability, since mutation of this site leads to a reduced overall EpCAM protein-level (Munz *et al.*, 2008). Furthermore, EpCAM has been shown to be hyperglycosylat-

ed in head and neck carcinoma in comparison to healthy tissue (Pauli *et al.*, 2003). This differential glycosylation pattern might cause different EpCAM functions in healthy versus malignant tissue (Schnell *et al.*, 2013a). EpEX is followed by TMD, which mediates the interaction with claudin-7 (Nubel *et al.*, 2009). The TMD is followed by the 26 aa intracellular domain of EpCAM, which contains two potential α -actinin binding sites (Arg289 – Lys296 and Glu304 – Ala314; Balzar *et al.*, 1998). Furthermore, the three C-terminal amino acids Leu312, Asn313 and Ala314 might be a putative PDZ binding site, which plays an important role in binding of signaling proteins (Schnell *et al.*, 2013a).

The EpCAM protein is conserved among different species, including rat, dog, mouse and zebrafish. Among higher vertebrates the gene is even more conserved showing an amino acid sequence homology of 81 % between human and mouse and even 99 % between man and gorilla (Schnell *et al.*, 2013a; Dollé *et al.*, 2015).

1.1.3 EpCAM cleavage and signaling

Since the signal peptide is already removed in the ER, it is never part of EpCAM full length (FL) protein, which can be found at the plasma membrane. The N-terminus of matured EpCAM can be cleaved between Arg80 and Arg81, which are located in the TY-domain. Predictably, the cleavage products will stay bound together by the disulfide bridge in this domain (Schnell *et al.*, 2013c). This cleavage step occurs in different epithelial cancer types and several proteases have been shown to perform this N-terminal cleavage (Thampoe *et al.*, 1988; Schon *et al.*, 1993). Recently it has been shown that EpCAM gets cleaved at Arg80 by the cell surface protease matriptase. This cleavage step is regulated by hepatocyte growth factor activator inhibitor-2 (HAI-2). Cleaved EpCAM has a reduced ability to associate with claudin-7. Additionally, it gets targeted for internalization and lysosomal degradation together with claudin-7 (Wu *et al.*, 2017).

Furthermore, EpCAM appears to be processed by RIP (Figure 1-2; Maetzel *et al.*, 2009). RIP is a conserved mechanism for the regulation of transmembrane proteins and includes sequential cleavage steps performed by sheddases and the γ -secretase complex. Eventually, this leads to the release of a soluble extracellular domain, A β -like peptides and an ICD. The latter translocates into the nucleus where it activates target gene transcription (Brown *et al.*, 2000; Medina and Dotti, 2003; Kopan and Ilagan, 2004; Lal and Caplan, 2011). RIP of EpCAM is induced by juxtacrine signaling (Denzel *et al.*, 2009). Thereby, EpCAM molecules on two different cells interact with each other or with an yet unknown ligand, which leads to the activation of RIP. The first step is a cleavage by the tumor necrosis factor alpha converting enzyme (TACE, ADAM17), a member of the ADAM protein family, in which the extracellular domain (EpEX) is shed-

ded from the remaining C-terminal fragment (CTF) of EpCAM (Edwards *et al.*, 2008; Maetzel *et al.*, 2009). Extracellular shedding of EpCAM occurs at one of the two distinct α -cleavage sites Asp243/Pro244 or Pro244/Gly245 (Tsaktanis *et al.*, 2015). Soluble EpEX can act as ligand for EpCAM, thereby enhancing the EpCAM signaling cascade in a paracrine way. The TACE/ADAM17 cleavage is the prerequisite for the second step of RIP, which is conducted by a γ -secretase complex containing presenilin-2 (PS-2; Maetzel *et al.*, 2009). This subsequent step leads to the release of three distinct A β -like fragments (arising from γ -cleavage) in the surroundings of the cell and two cytoplasmatic hEpICD fragments (arising from ϵ -cleavage). γ -cleavage occurs at Val273/Val274, Val274/Val275 or Val275/Val276, ϵ -cleavage at Val284/Val285 or Val285/Leu286. The function of the A β -like fragments is still unknown (Tsaktanis *et al.*, 2015). hEpICD is part of a large nuclear complex together with FHL2 (see section 1.2), β -catenin (see section 1.3) and the transcription factor Lef-1. This complex translocates into the nucleus and activates the transcription of EpCAM-target genes, which are genes involved in cell proliferation and growth, cell death and reprogramming (Munz *et al.*, 2004; Barolo *et al.*, 2006; Maaser and Borlak, 2008; Maetzel *et al.*, 2009; Imrich *et al.*, 2012; Chavez-Perez, 2013). Via the interaction with FHL2 and its binding to β -catenin and Lef-1, EpCAM is linked to the Wnt pathway (see section 1.3.2; Imrich *et al.*, 2012). Additionally, hEpICD as well as its murine counterpart mEpICD are prone to rapid degradation by the proteasome, which could represent a regulatory feature and/or a means of disposal for EpCAM (Hachmeister *et al.*, 2013; Tsaktanis *et al.*, 2015).

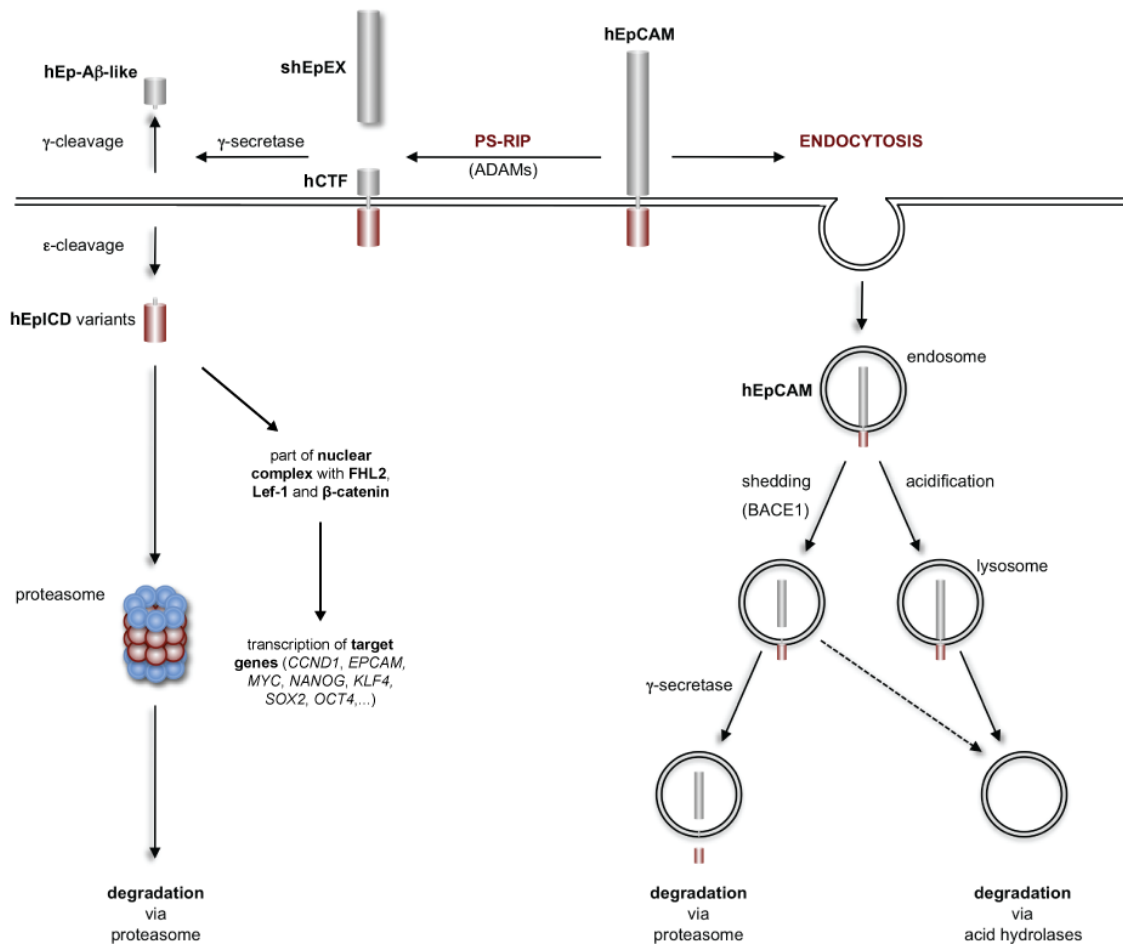


Figure 1-2 Scheme of EpCAM cleavage and signaling. Human EpCAM (hEpCAM) is cleaved at the plasma membrane by ADAM17, which generates soluble EpEX (shEpEX) and hCTF. The resulting CTF gets cleaved by γ -secretase to create A β -like fragments (γ -cleavage) and intracellular (hEpiCD) fragments (ϵ -cleavage). hEpiCD is either degraded by the proteasome or it becomes incorporated into a nuclear complex together with FHL2, β -catenin and Lef-1, which activates the transcription of EpCAM-target genes. Moreover, hEpCAM can be endocytosed and cleaved either by BACE1 in endosomes or by acidic hydrolases in lysosomes (modified from Hachmeister *et al.*, 2013).

Furthermore, it was shown that in carcinoma cell lines hEpCAM is subject to clathrin-dependent endocytosis and subsequent cleavage at the residues Tyr250/Tyr251 (β -cleavage) by β -secretase BACE1 (Figure 1-2; Tsaktanis *et al.*, 2015).

The crystal structure of hEpCAM represented a heart-shaped cis-dimer at the cell surfaces (Pavsic *et al.*, 2014). By mapping of the extracellular α - and β -cleavage sites onto the protein surface, it could be shown that α -sites are in a groove and β -sites are in an even more shielded part of the dimeric protein. Therefore, the dimer most probably needs to undergo a partial or temporal dissociation or conformational change to allow for cleavage of hEpCAM (Tsaktanis *et al.*, 2015). At pH 4.5, the great majority of hEpCAM-FL molecules is cleaved, whereas at pH 7 only a minor fraction of the total protein is affected (Hachmeister *et al.*, 2013; Tsaktanis *et al.*, 2015). It is likely that the acidic milieu of endosomes and lysosomes leads to a destruction of the cis-dimer, which provides a readily accessible cleavage site for BACE1 (Pavsic and Lenarcic,

2011; Pavsic *et al.*, 2014). Cleavage at α -sites might require a conformational change by a yet unknown ligand or by ADAM17 itself or by a certain amount of EpCAM molecules that remained in a monomeric form (Tsaktanis *et al.*, 2015).

1.1.4 EpCAM expression

EpCAM is expressed at the basolateral cell membrane of healthy epithelial cells (Moldenhauer *et al.*, 1987; Momburg *et al.*, 1987). In most organs and glands, EpCAM expression can be found, however, to varying extents. The colon shows a high level of EpCAM expression, whereas EpCAM is weakly expressed in the stomach (Moldenhauer *et al.*, 1987). Other organs displaying a high EpCAM expression are the respiratory tract, the gall bladder, certain cells of the kidney and pancreas, the endocrine system and the bile duct (Moldenhauer *et al.*, 1987; Cirulli *et al.*, 1998; Pauli *et al.*, 2003; Breuhahn *et al.*, 2006; Trzpis *et al.*, 2007). Skin cells vary regarding their expression levels of EpCAM ranging from high levels at the proliferative zone and the respiratory glands to a lack of expression in melanocytes and keratinocytes (Momburg *et al.*, 1987; Tsubura *et al.*, 1992). EpCAM expression is usually high in proliferating cells and low in differentiated cells. For example, an expression gradient of EpCAM can be found in the intestinal epithelium: the differentiated cells at the top of the villi show low levels of EpCAM, whereas EpCAM is highly expressed in intestinal stem cells of the crypts (Balzar *et al.*, 1999; Schnell *et al.*, 2013a).

Furthermore, EpCAM has been identified as surface marker for pluripotent human and murine embryonic stem cells (ESC; Gonzalez *et al.*, 2009; Sundberg *et al.*, 2009; Lu *et al.*, 2010; Ng *et al.*, 2010). Additionally, it shows a co-expression with the transcription factors required for cellular reprogramming sex-determining Y-Box-2 (SOX2) and Octamer 4 (OCT4; Lu *et al.*, 2010; Ng *et al.*, 2010). By inducing cell differentiation, a down-regulation of EpCAM alongside with other pluripotency markers like SOX2 or OCT4 could be observed (Gonzalez *et al.*, 2009). The maintenance of the undifferentiated state of ESCs is strongly connected with EpCAM expression levels (Schnell *et al.*, 2013a).

In carcinomas, EpCAM is highly overexpressed and distributed over the whole cell surface, which is frequently associated with cytoplasmatic and nuclear staining (Gosens MJ *et al.*, 2007; Yanamoto *et al.*, 2007; Ralhan *et al.*, 2010a; Ralhan *et al.*, 2010b; Schnell *et al.*, 2013a). In many cancer types, EpCAM overexpression is associated with a poor prognosis for the patient, e.g. lung, ovarian and breast cancer as well as pancreatic, gallbladder and prostate carcinoma (Spizzo *et al.*, 2004; Varga *et al.*, 2004; Brunner *et al.*, 2008; Fong *et al.*, 2008; Kim *et al.*, 2009; van der Gun *et al.*, 2010; Massoner *et al.*, 2014). Exceptions to this are renal and thyroid carcinomas, in which high

EpCAM expression is associated with an increased survival (Went *et al.*, 2005; Ralhan *et al.*, 2010). Furthermore, there are cancer types in which EpCAM expression was associated with both better and worse outcome for the patient (van der Gun *et al.*, 2010). Recently, EpCAM was found to also be expressed on tumor cells of acute myeloid leukemia (AML), with EpCAM-positive leukemic cells showing a greater resistance to chemotherapy (Zheng *et al.*, 2017).

Regarding EpCAM expression on circulating tumor cells (CTCs) and metastases no clear conclusion can be drawn yet. Liver metastases from colorectal cancer and lung metastases derived from colon cancer showed a high EpCAM expression comparable to that in the primary tumor, whereas metastases derived from head and neck carcinoma showed a lower EpCAM expression level than the respective primary tumor (Jojovic *et al.*, 1998; Takes *et al.*, 2001; Kuhn *et al.*, 2007). For retrieving CTCs in cancer patients, EpCAM is the most used antigen, which indicates an expression in these cells (Cohen *et al.*, 2006; Criscitiello *et al.*, 2010). However, there is also data suggesting a reduction of EpCAM expression in CTCs from colon and breast carcinomas (Jojovic *et al.*, 1998; Rao *et al.*, 2005; Gorges *et al.*, 2012).

1.1.5 EpCAM functions

Already in 1979, EpCAM was identified as tumor-associated antigen (Herlyn *et al.*, 1979). Up to now, a variety of functions of EpCAM have been described, ranging from cell adhesion to cell signaling. Additionally, it is used as prognostic and therapeutic marker in carcinomas.

The name EpCAM was introduced because this molecule was shown to mediate Ca^{2+} -independent homophilic cell-cell adhesion. However, this interaction can be inhibited by treatment with an EpCAM-specific antibody (Litvinov *et al.*, 1994a; Litvinov *et al.*, 1994b). All motifs in EpCAM's extracellular domain and also the short ICD are required for the homophilic interaction (Balzar *et al.*, 1998; Balzar *et al.*, 2001). Compared to E-cadherin, EpCAM is a rather weak cell-cell adhesion molecule. In fact, co-expression of EpCAM and E-cadherin weakens E-cadherin-mediated cell adhesion, most probably due to disruption of E-cadherin association with the cytoskeleton. The mediator of this process is phosphatidylinositol-3 kinase (PI3K). Furthermore, in contrast to E-cadherin expressing cells, EpCAM expressing cells are only loosely interconnected (Litvinov *et al.*, 1994a; Litvinov *et al.*, 1997; Winter *et al.*, 2007). Conditional knock-out of murine EpCAM in E-cadherin expressing Langerhans cells led to an attenuated motility and migration, which is due to an increased adhesion. This result together with the metastasis-promoting role of EpCAM indicates that EpCAM is rather a negative regulator of adhesion (Gaiser *et al.*, 2012). Furthermore, it was shown that neither cleavage inhibi-

tion nor cellular knockdown or knockout of hEpCAM in cancer cell lines had an effect on cell-cell adhesion. It is thus doubtful if hEpCAM acts as homophilic cell-cell adhesion molecule in carcinoma cells (Tsaktanis *et al.*, 2015). In general, the role of EpCAM in adhesion has yet to be resolved.

EpCAM seems to have a promoting role in cell proliferation. Several *in vitro* and *in vivo* studies demonstrated an induction of cell proliferation due to EpCAM overexpression and a decreased cell proliferation after EpCAM down-regulation (Munz *et al.*, 2004; Osta *et al.*, 2004; Maetzel *et al.*, 2009; Wenqi *et al.*, 2009; Chaves-Perez *et al.*, 2013). Induction of EpCAM expression leads to an upregulation of the oncogenic transcription factor c-Myc, which eventually results in upregulation of Cyclin A, D and E (Munz *et al.*, 2004; Chaves-Pérez *et al.*, 2013). Moreover, matrix metalloproteinase-7 (MMP-7) and epidermal fatty acid binding protein (E-FABP) are regulated by EpCAM (Munz *et al.*, 2005; Denzel *et al.*, 2012). EpICD seems to be necessary and also sufficient for c-Myc upregulation (Munz *et al.*, 2004; Munz *et al.*, 2005). The signaling cascade leading to these effects is initiated by RIP (see section 1.1.3).

Tetraspanin-enriched microdomains (TEMs) act as signaling platforms and are organized macromolecular complexes consisting of integral transmembrane proteins, certain lipids, tetraspanins and a variety of transmembrane and cytosolic proteins (Hemler, 2005; Le Naour *et al.*, 2006a; Zoller, 2009). In human colon cancer cells, EpCAM has been identified as a TEM-member by interacting with tetraspanin CD9 (Le Naour *et al.*, 2006b). In rat carcinoma cells, EpCAM has been found in a complex with tetraspanin CD9, CO-029 (tetraspanin8) and CD44 isoforms (Figure 1-3; Schmidt *et al.*, 2004). Claudin-7 is an essential part of this complex as well, since it is responsible for the recruitment of EpCAM. The different EpCAM mediated processes (apoptosis resistance, promotion of cell proliferation and tumorigenicity) are only functional in a complex of claudin-7 and EpCAM (Ladewein *et al.*, 2005; Kuhn *et al.*, 2007; Nubel *et al.*, 2009).

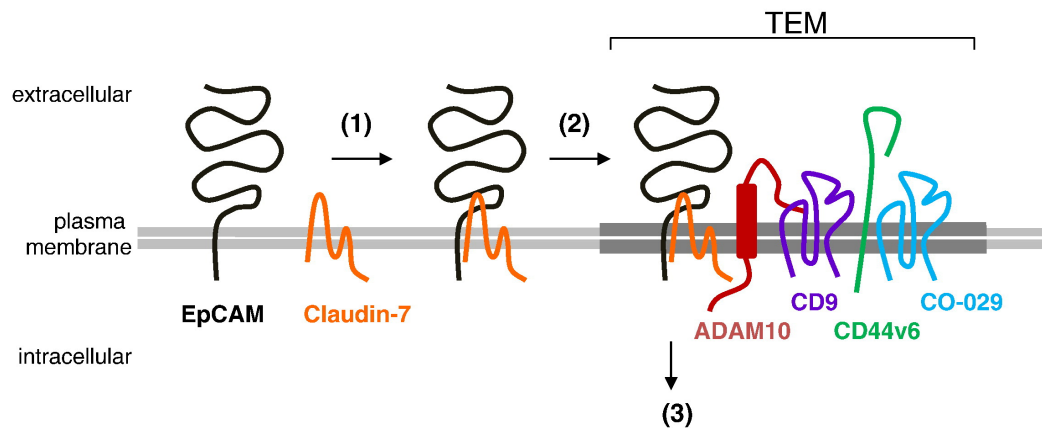


Figure 1-3 EpCAM in tetraspanin-enriched microdomains (TEMs). EpCAM forms a complex with claudin-7 (1) and is afterwards recruited into TEMs (2). There, it forms a complex with tetraspanin 9, CO-029, a CD44 isoform and ADAM10. The formation of this complex might play a crucial role in regulation of EpCAM signaling (3; from Schnell *et al.*, 2013a).

1.1.6 EpCAM as target for immunotherapy of cancer

Due to its tumor-specific overexpression, EpCAM is a suitable target for cancer therapy (Munz *et al.*, 2010; Schnell *et al.*, 2013a). Therefore, this antigen has been used for the development of different immunotherapeutic approaches, e.g. monoclonal antibodies, vaccination and toxin- or tumor necrosis factor-related apoptosis-inducing ligand (TRAIL)-conjugated antibodies, (Riesenberg *et al.*, 2001; Neighbors *et al.*, 2008; Groth *et al.*, 2012; Lund *et al.*, 2014; Waldron *et al.*, 2014; Schmohl *et al.*, 2016). The first immunotherapeutic anti-EpCAM antibody was Edrecolomab, which was produced in ascites of mice (Sears *et al.*, 1982; Sears *et al.*, 2009). However, a clinical activity in adjuvant setting could not be confirmed (Fields *et al.*, 2009; Schmoll and Arnold, 2009). Another downside of this antibody was the high immunogenicity and short serum half-life. Therefore, chimeric, humanized, human-engineered and fully human therapeutic antibodies were developed (Munz *et al.*, 2010). Examples of these are humanized and human-engineered antibodies 3622W94 and ING-1, respectively. Both showed high binding affinities, however already low concentrations caused acute pancreatitis (Goel *et al.*, 2007; Lewis, 2003; LoBuglio *et al.*, 1997). The fully human antibody Adecatumab only led to minor side effects like chill, fatigue, nausea and diarrhea when applied in higher doses in a clinical phase II study and no pancreatitis could be observed. Furthermore, this antibody showed a good prognosis in terms of metastasis development and overall survival in patients with high EpCAM metastasizing breast cancer (Schmidt *et al.*, 2010). In April 2009, the rat-mouse hybrid monoclonal antibody Catumaxomab (Removab®) was approved in the European Union for treatment of malignant ascites (Linke *et al.*, 2010). However, other EpCAM-directed antibodies are currently under development (Schnell *et al.*, 2013a; Liao *et al.*, 2015).

1.2 The Four and a Half LIM domains protein-2 (FHL2)

The Four and a Half LIM (FHL)-only protein subfamily is a member of the LIM-only protein family and consists of FHL1, FHL2, FHL3, FHL4 and activator of CREM in testis (ACT; Johannessen *et al.*, 2006). The two last-named proteins are expressed only in testis (Morgan and Madgwick, 1999). FHL1, FHL2 and FHL3 are mainly expressed in muscle, however, FHL1 and FHL2 can also be found in other tissues (see section 1.2.3; Samson *et al.*, 2004). This family is characterized by having four and a half cysteine-rich LIM domains. The half LIM-domain is always located at the N-terminus (Cao *et al.*, 2015; Kurakula *et al.*, 2015). The consensus sequence of the LIM domain is $CX_2CX_{16-23}C/HX_{2/4}C/H/EX_2CX_2CX_{14-21}C/HX_{1/2/3}C/H/D/EX$ with X depicting any amino acid. It contains two zinc fingers, each of which binding one Zn^{2+} ion (Figure 1-5; Schmeichel and Beckerle, 1994; Johannessen *et al.*, 2006). The acronym LIM is deduced from the first letters of LIN-11, ISL-1 and MEC-3, the transcription factors in which the domain was originally found (Way and Chalfie, 1988). A potential direct interaction of LIM-domains and DNA is not yet fully resolved (Cao *et al.*, 2015).

1.2.1 The *FHL2* gene

The *FHL2* gene is located on chromosome 2 (location 2q12-q14), consists of seven exons (the first three are non-coding exons) and has a size of approximately 78 kb. Its transcript has a size of around 1.5 kb (Chan *et al.*, 1998; Johannessen *et al.*, 2006; NCBI 2017). So far five transcript variants were reported, which are regulated by two alternative promoters. Promoter 1a regulates the transcription of variant 4 and promoter 1b regulates transcription of variants 1, 2, 3 and 5. All variants are translated into the identical FHL2 protein (see section 1.2.2). Promoter 1b was shown to have a higher activity than promoter 1a (Ng *et al.*, 2011; Xu *et al.*, 2014). The transcription of *FHL2* is regulated by a variety of transcription factors (Figure 1-4). FHL2 expression is associated with the cellular level of p53. However, there is no direct interaction between these proteins (Tanahashi and Tabira, 2000). A p53-dependent FHL2 expression was observed in different cell lines (Scholl *et al.*, 2000; Amaar *et al.*, 2002). It seems very likely that the 1a promoter serves as binding site for p53 (Xu *et al.*, 2014). Another transcription factor that was shown to bind to the *FHL2* promoter is the serum response factor (SRF). Nkx2.5, an interaction partner of SRF and one of the earliest markers of the cardiac lineage is also a regulator of FHL2 expression (Johannessen *et al.*, 2006; Philippar *et al.*, 2004). Other transcription factor binding sites found in the *FHL2* promoter are the myocyte enhancer factor-2 (MEF-2) and AP-1 (Johannessen *et al.*, 2006; Morlon and Sassone-Corsi, 2003).

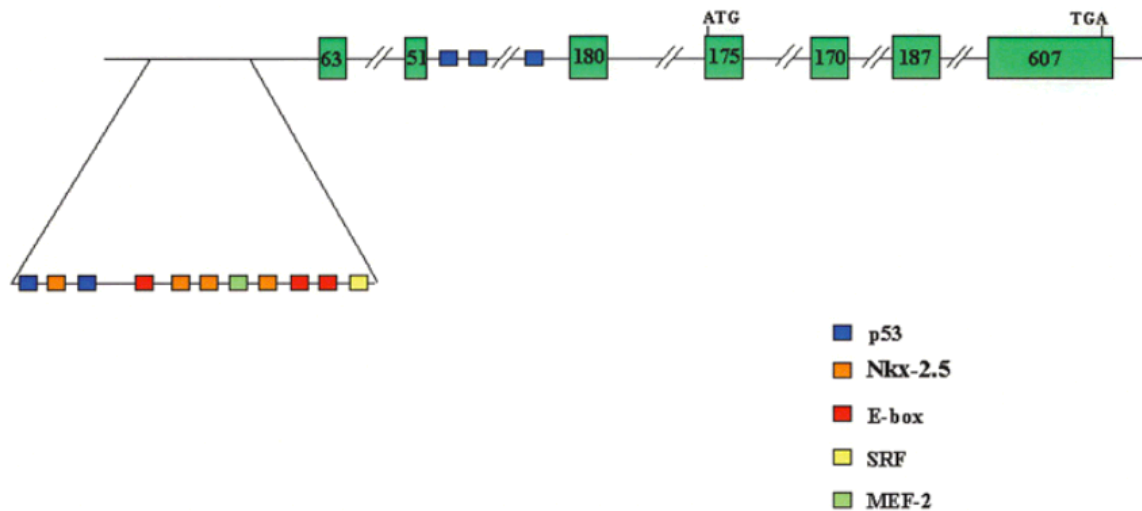


Figure 1-4 Scheme of the FHL2 gene. The seven exons are depicted with green boxes. Lines connecting the boxes with each other represent the introns. Exon sizes in bp are given by the number inside the boxes. Transcription factor binding sites in the respective color (see legend on the bottom right) are depicted by smaller boxes in front of exon 1 and in intron 2. Start- and stop-codon are indicated as well (from Johannessen *et al.*, 2006).

1.2.2 The FHL2 protein

FHL2 is a member of the FHL-only protein subfamily, which belongs to the LIM-only protein family (Cao *et al.*, 2015). It is a 32 – 41 kDa protein that consists of 279 aa (Johannessen *et al.*, 2006). The mass difference is due to post-translational modifications since FHL2 contains one O-glycosylation site and several potential phosphorylation sites (El Mourabit *et al.*, 2003). Furthermore, a 25 kDa peptide could be detected by anti-FHL2 antibodies. This might be a proteolytic fragment, since a potential cleavage site was found between LIM2 and LIM3. The resulting destruction of FHL2 might be a way of inhibiting interactions with other proteins. The subcellular localization of FHL2 is cell-type specific. In HeLa cells, FHL2 was predominantly found in the nucleus whereas in HEK293 or HepG2 cells, a distribution all over the cell was detected (Johannessen *et al.*, 2006). More than 50 FHL2 interactions partners are known, all of which belong to different functional classes: receptors (e.g. integrin), enzymes (e.g. ERK2, TACE), transcription factors and cofactors (e.g. β -catenin, androgen receptor), structural proteins (e.g. α -actin ACTA1), splicing factors (e.g. hNP220) or DNA replication and repair enzymes (e.g. BRCA1; Muller *et al.*, 2000; Wixler *et al.*, 2000; Martin *et al.*, 2002; Ng *et al.*, 2002; Yan *et al.*, 2003; Purcell *et al.*, 2004; Samson *et al.*, 2004; Johannessen *et al.*, 2006). These proteins do not show sequence or structure homology. However, for most interactions, the functional relevance remains unsolved. The binding of FHL2 to its interaction partner occurs via single or multiple LIM domains or sometimes requires the FL protein. FHL2 plays a role in several biological processes such as invasion, cell adhesion, apoptosis, differentiation and proliferation (Johannessen *et al.*, 2006; Cao *et al.*, 2015).

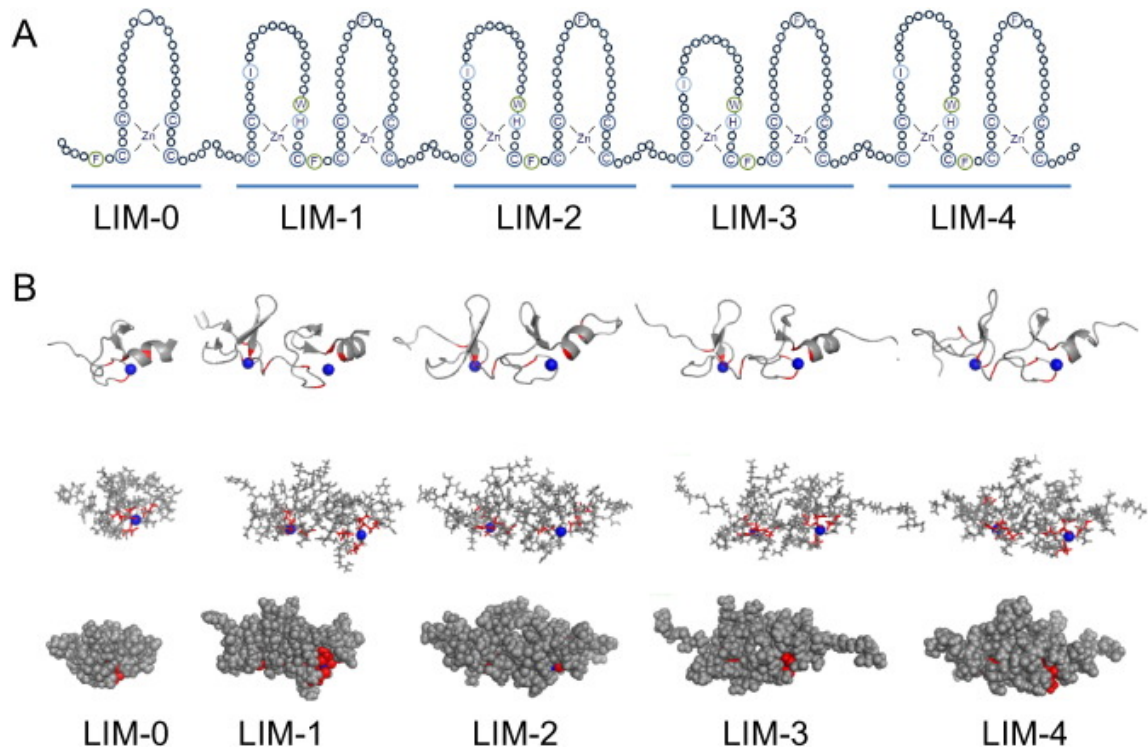


Figure 1-5 Structure of Four-and-a-half-LIM-only protein-2 (FHL2). (A) FHL2 consists of four (LIM1-4) and a half N-terminal (LIM0) LIM-domain. Every LIM-domain shows two zinc fingers and coordinates two Zn²⁺ ions in total except for the half LIM-domain, which possesses only one zinc finger. The conserved aa in the zinc fingers are indicated by single-letter aa code. (B) Structures of LIM-domains as ribbon diagram (upper panel), sticks (middle panel) and spheres (lower panel). The coordinated Zn²⁺ ions are depicted in blue, the conserved aa in red. LIM0 & LIM1: 2MIU; LIM2: 1X4K; LIM3: 2D8Z; LIM4: 1X4L (from Tran *et al.*, 2016).

1.2.3 FHL2 expression

The highest FHL2 expression level can be found in the heart. However, this protein was also observed in several other tissues, e.g. kidney, lung, ovary, pancreas, liver, colon, prostate and cortex. FHL2 could not be detected in tissues related to the immune system such as thymus, spleen and leukocytes (Chan *et al.*, 1998; Zheng and Zhao, 2007). In cancer cells, the expression levels display a high variation according to the respective cancer type. Lung cancer, breast cancer and colon cancer show high FHL2 expression levels, whereas hepatocellular carcinoma or prostate cancer have lower FHL2 expression (Tanahashi and Tabira, 2000; Chen *et al.*, 2003; Kinoshita *et al.*, 2005; Gabriel *et al.*, 2006; Chen *et al.*, 2012; Xu *et al.*, 2014; Cao *et al.*, 2015).

1.2.4 FHL2 functions

As already mentioned, FHL2 is abundantly expressed in the adult heart. Additionally, high FHL2 expression levels were also found in the embryonic heart, which suggests a role both in the development of the cardiac circulatory system and in cardiac physiology (Chu *et al.*, 2000; Kong *et al.*, 2001; Johannessen *et al.*, 2006). There are various presumptions about FHL2's role in heart physiology. FHL2 might antagonize the cardiac hypertrophic response by binding and negatively interfering with the mitogen-

activated protein (MAP) kinase ERK2, whose signaling pathway is crucial in hypertrophic growth response in cardiomyocytes (Purcell *et al.*, 2004). Another FHL2 specific response to hypertrophic stimuli might be a modulation of the ventricular functions by structural remodeling (Wan *et al.*, 2002). Furthermore, FHL2 might play a role in repolarization in cardiac cells via interaction with minK, a subunit of K⁺ channel. FHL2 probably connects minK to the cytoskeleton (Krishnamurthy *et al.*, 2004). In patient samples obtained after cardiopulmonary bypass, an increase in FHL2 expression was detected, implicating a role in myocardial injury (Wan *et al.*, 2002).

Moreover, high FHL2 expression levels can be found in human osteoblasts. In mouse bone marrow cells, a threefold increase of FHL2 could be determined during differentiation into osteoblasts (Chu *et al.*, 200; Amaar *et al.*, 2002). It was shown that in *fhl2* knock-out mice, osteoblasts showed a decreased activity which led to osteopenia. The number of osteoblasts however was not affected by the FHL2 deficiency (Kong *et al.*, 2001). A strong overexpression of FHL2 in osteoblasts led to an increase in bone mass in the respective animals, whereas the number of osteoblasts again remained unchanged (Günther *et al.*, 2005).

FHL2 might also play a role in muscular processes. Expression of FHL2 in mouse myoblasts induced differentiation into myotubes (Martin *et al.*, 2002). Titin is an important protein in human muscles since it contributes to muscle contraction (Itoh-Satoh *et al.*, 2002). FHL2 was shown to interact with titin, thereby acting as an adapter molecule that recruits metabolic enzymes, which provide energy needed during muscle contraction (Lange *et al.*, 2002). An additional interaction was found between FHL2 and integrins in heart muscle cells. However, the biological function of this interaction is not yet elucidated (Samson *et al.*, 2004).

The importance of FHL2 in splicing remains under debate. Although it was shown that FHL2 interacts with splicing factors NP220 and pyrimidine tract-binding protein-associated splicing factor (PSF), the facts that FHL2 deficient mice are viable and that the expression of FHL2 is tissue specific are arguments against an essential role in splicing (Inagaki *et al.*, 1996; Dye and Patton, 2001; Ng *et al.*, 2002; Johannessen *et al.*, 2006).

It was shown that overexpressed FHL2 is able to induce apoptosis in a plethora of cells by an unknown mechanism (Scholl *et al.*, 2000; Johannessen *et al.*, 2006). However, FHL2 was also found to suppress apoptosis by eventually negatively regulating the activity of the transcription factor Forkhead box protein O1 (FOXO1; Yang *et al.*, 2005). FHL2 could possibly be a transducer of apoptotic signals from extracellular matrix to

mitochondria, since FHL2 was detected inside these organelles (Li *et al.*, 2001). The role of FHL2 in apoptosis is still not understood since this protein can act both as enhancer and repressor of apoptosis (Tran *et al.*, 2016).

FHL2 also affects cell proliferation. It supports β -catenin-induced cyclin D1 promoter activity, which leads to an abolishment of the inhibitory effect of FOXO1 on this promoter (Wei *et al.*, 2003; Yang *et al.*, 2005). However, FHL2 also impedes cell proliferation in differentiating myoblasts by transcriptional inhibition of cyclin A and down-regulation of cyclin D1 expression (Martin *et al.*, 2002; McLoughlin *et al.*, 2002).

Moreover, FHL2 might have a function as scaffolding protein in signaling pathways (Scholl *et al.*, 2007). This assumption is supported by the localization of FHL2 in various intracellular compartments and the binding to different kinds of proteins such as receptors, chaperones, molecules involved in ubiquitination, signal transmitter proteins, receptor-linked proteins and transcription factors (Wixler *et al.*, 2000; El Mourabit *et al.*, 2004; Gabriel *et al.*, 2004).

There were indications that FHL2 might be a transcription factor itself, based on structural similarities between the half LIM-domain and the DNA-binding domain of the transcription factor GATA-1 (Morgan and Madgwick, 1996). However, a direct FHL2-DNA binding was not yet observed, which suggests that FHL2 rather acts as a transcriptional co-factor. The LIM-domains appear to play different roles depending on the respective cell line. These specific effects might depend on the cell-specific expression of co-activators or –repressors (Johannessen *et al.*, 2006). The first transcription factor for which a modulating activity of FHL2 was described is the androgen receptor (AR; Muller *et al.*, 2000). The transcriptional activity of AR was increased by synergistic action of FHL2, CBP/P300 and β -catenin (Labalette *et al.*, 2004). In contrast, FHL2 suppresses transcriptional activity of FOXO1 and SRF (Philippar *et al.*, 2004; Yang *et al.*, 2005). Furthermore, FHL2 interacts with β -catenin (see section 1.3), a modulator of the T-cell factor/lymphoid enhancer factor family (TCF/Lef). The effect of this interaction is cell- and promoter-specific. An activation of transcription could be observed in HEK293 or SE480 cells, whereas this interaction led to a repression in I28 or chinese hamster ovary (CHO) cells (Martin *et al.*, 2002; Wei *et al.*, 2003; Labalette *et al.*, 2004). The specificity might be explained by the cell- or promoter-specific recruitment of co-activators or co-repressors via FHL2. Another hypothesis is that FHL2 blocks or competes for cell-specific β -catenin binding sites (Johannessen *et al.*, 2006).

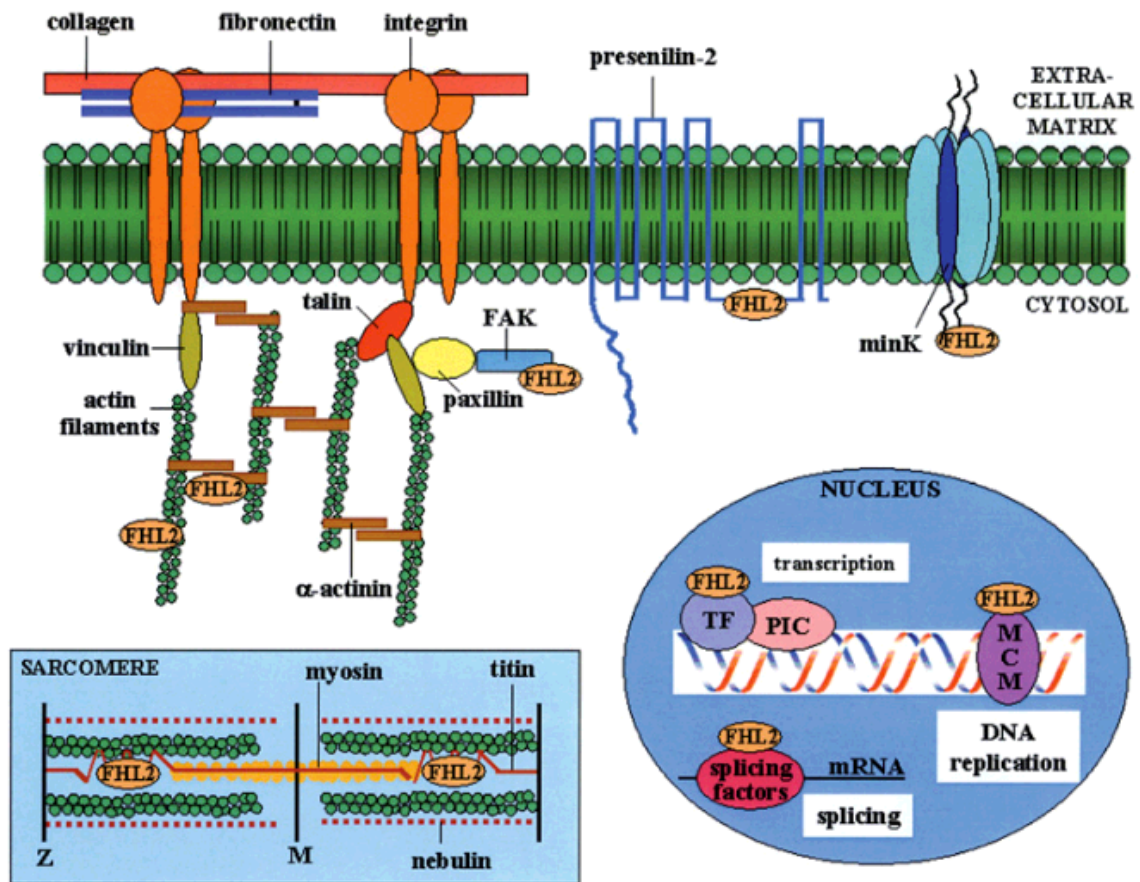


Figure 1-6 Functional diversity of FHL2. FHL2 (orange) can be found in different subcellular compartments, where it conducts diverse functions. In muscle, FHL2 interacts with titin (see light blue box bottom left). In the nucleus, FHL2 might be a modulator of splicing and DNA replication. Additionally, it has the ability to affect signal transmission of transcription factors, thereby influencing gene expression (see dark blue circle bottom right). At the plasma membrane (green), FHL2 can interact with integrin, presenilin-2 and voltage-gated K⁺ channel receptors. Moreover, FHL2 binds to structural proteins, actin filaments or α -actinin (from Johannessen *et al.*, 2006).

1.3 Catenin beta-1

In the 1980s, Catenin beta-1 (CTNNB1), which is usually referred to as β -catenin, was independently discovered twice based on its structure and signaling (Valenta *et al.*, 2012). β -catenin was isolated together with α -catenin and γ -catenin/plakoglobin as E-cadherin associated proteins. Therefore, these proteins were termed catenins (Ozawa *et al.*, 1989). Its ortholog in *Drosophila melanogaster* is called Armadillo (Arm) through which the role of β -catenin in intracellular signaling was discovered. Further studies of this protein showed a structural conservation in adherens junctions (McCrea *et al.*, 1990; Peifer and Wieschaus, 1990; Orsulic and Peifer, 1996). It was shown that *armadillo* segmentation, which is required for normal patterning within the embryo, is regulated by Wingless (Wg). This was the key observation triggering further characterization of the Wg/Arm (Wnt/ β -catenin in human) signaling cascade (Riggelman *et al.*, 1990). Another discovery contributing to an understanding was the pathway leading from Wg to an eventual stabilization of Arm by Shaggy/Zeste-white-3 (glycogen syn-

thase 3 (GSK3)) in vertebrates; Siegfried *et al.*, 1994). Finally, it was shown that the signaling function of Arm/ β -catenin in the nucleus is mediated via TCF/Lef (Behrens *et al.*, 1996; Huber *et al.*, 1996; Molenaar *et al.*, 1996; Brunner *et al.*, 1997; van de Wetering *et al.*, 1997). β -catenin belongs to the armadillo family of proteins and is a multitasking protein, which plays a role in several developmental and homeostatic processes. β -catenin can be found in different subcellular locations such as junctions, cytoplasm and in the nucleus (Valenta *et al.*, 2012; Daugherty *et al.*, 2007; Voronkov and Krauss, 2013).

The *CTNNB1* gene is located on chromosome 3 (location 3p22.1), consists of 17 exons and has a size of approximately 41 kb. The transcript has a size of roughly 3.5 kb (NCBI 2017).

1.3.1 The CTNNB1 protein

β -catenin is a highly conserved protein in the Wnt signaling cascade (Valenta *et al.*, 2012). β -catenin from sponges, ctenophores, and cnidarians show a high sequence similarity to mammalian β -catenin, e.g. cnidarian β -catenin has > 60 % aa identity. The biggest differences can be found in the C-terminal domain (CTD), which is less conserved in general (Xing *et al.*, 2008; Zhao *et al.*, 2011). The central region exhibits an approximately 80 % structural identity. Furthermore, even the exon/intron structure of *ctnnb1* is conserved among cnidarians, sponges and later developed metazoans (Holland *et al.*, 2005, Adamska *et al.*, 2010). Also in early metazoans, Wnt/ β -catenin signaling has strong impacts on their development. In sponges, the inhibition of β -catenin degradation leads to canal openings. In *Hydra* (cnidarian) a reduction of β -catenin leads to a loss of head structures whereas ectopic accumulation of β -catenin results in multiple heads and tentacle formation (Broun *et al.*, 2005; Muller *et al.*, 2007; Lapébie *et al.*, 2009; Gee *et al.*, 2010). These findings indicate that the Wnt/ β -catenin signaling cascade is a primeval pathway playing a crucial role in body plan and axis formation (Valenta *et al.*, 2012).

β -catenin belongs to the catenin family, which consists of three subfamilies: p120 (e.g. p120 and plakophilin), β - (β -catenin and plakoglobin) and α subfamily (alpha 1-3 catenin; Anastasiadis and Reynolds, 2000; Schneider *et al.*, 2003; Kobiela and Fuchs, 2004; Zhao *et al.*, 2011). The subfamilies differ in the number of their Arm repeats. Each of these repeats is comprised of three helices (approximately 42 aa per helix), which are arranged in a triangular shape. The p120 subfamily contains nine arm repeats and the β subfamily contains even twelve Arm repeats. The α subfamily, however, contains three vinculin homology domains instead of Arm repeats and therefore belongs to the Vinculin superfamily (Zhao *et al.*, 2011).

The human β -catenin protein consists of 781 aa and can be subdivided into a 130 aa N-terminal domain (NTD), a central region of 523 aa and a CTD consisting of 100 aa (Figure 1-7A). The central region, which is the most conserved one, is made up of twelve imperfect ARM repeats (R1-12). Altogether, the twelve repeats form a superhelix that features along a positively charged groove (Figure 1-7B). The central region forms a rigid scaffold for interactions partners, whereas the NTD and CTD are structurally flexible. A specific conserved helix, which is referred to as Helix-C (residues 667-683), is located between the center region and the CTD (Huber *et al.*, 1997; Xu and Kimelman, 2007; Xing *et al.*, 2008). Via structural and biochemical analysis, it has been shown that the binding sites in the charged groove of several β -catenin binding partners are overlapping. This means that the respective proteins cannot bind simultaneously. This is the case for instance for E-cadherin, the Adenomatous-polyposis-coli protein (APC) and TCF/Lef, which all bind β -catenin at Arm repeats R3-R9 (Figure 1-7A). All these interacting proteins form salt bridges between Lys435 and Lys312 of β -catenin and Asp and Glu residues in the binding partners. Other Arm repeats might strengthen the interaction (Graham *et al.*, 2000; Eklof *et al.*, 2001; Huber and Weis, 2001; Poy *et al.*, 2001). Both NTD and CTD are negatively charged and sensitive to trypsin digestion (Xu and Kimelman, 2007). They act as an intramolecular chaperone of Arm repeat domains and furthermore prevent self-aggregation of the central region (Xing *et al.*, 2008). GSK3, α -catenin and β -transducin repeat containing E3 ubiquitin protein ligase (β -TrCP) all bind β -catenin at the NTD (Xu and Kimelman, 2007). Additionally, this part of the protein contains phosphorylation sites. The phosphorylation is performed by a large multiprotein complex consisting of GSK3, Axin and APC (Schneider *et al.*, 2003). Moreover, it was suggested that Helix-C is crucial for interactions with β -catenin binding proteins, especially those involved in signaling. For β -catenin's role in cell-cell adhesion, this helix does not seem to be required (Xing *et al.*, 2008).

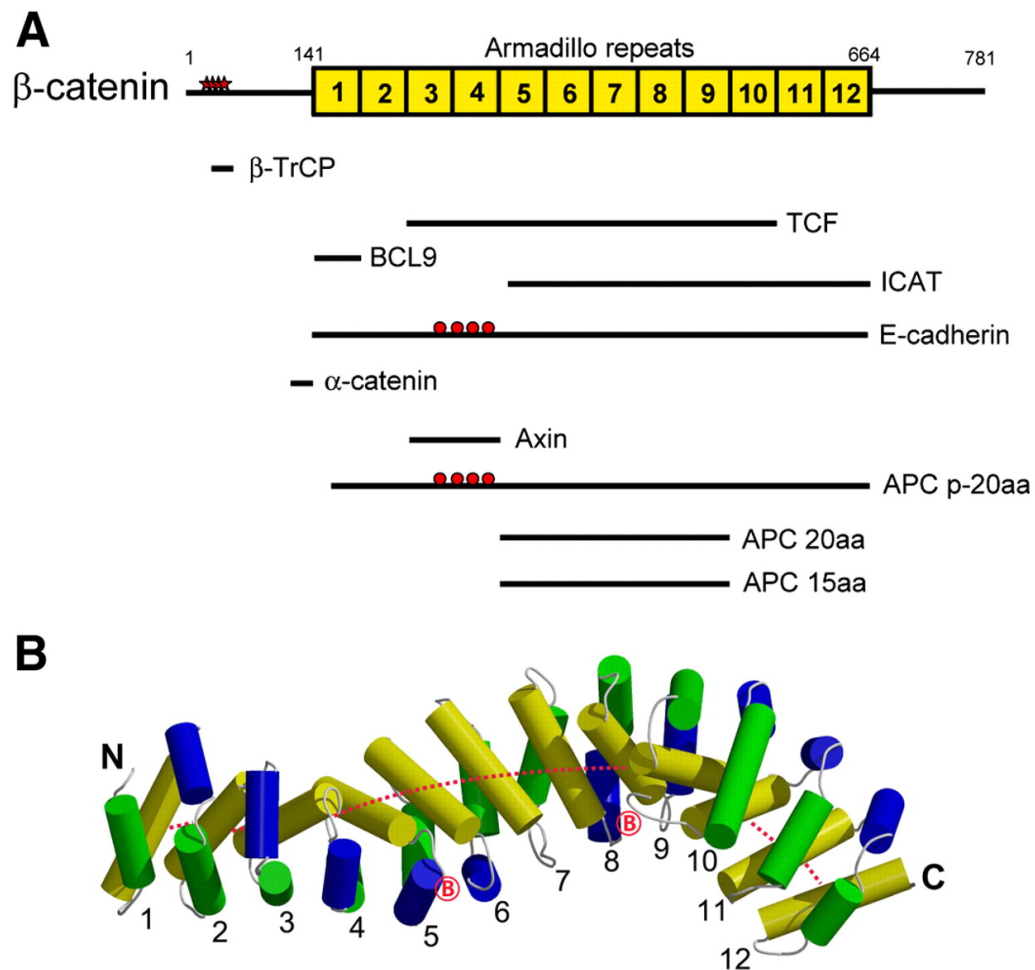


Figure 1-7 Structure of h β -catenin and interaction sites. (A) β -catenin consists of a NTD (aa 1-140), a central region consisting of twelve Arm repeats (yellow boxes) and a CTD (aa 665-781). The red stars indicate the CK1 phosphorylation sites. The black bars represent the binding sites of the respective interacting protein. Proteins sharing the same regions for binding cannot bind simultaneously. The red dots show phosphorylated Ser or Thr residues, which are bound by β -catenin. Helix-C is not depicted in this scheme. (B) Structure of the Arm repeats (R1-R12). Each repeat is formed by three helices (yellow, green and blue), which are arranged in a triangular shape. The positively charged groove is shown as a red dotted line. Lys312 and Lys435 are depicted as circled Bs (from Xu and Kimelman, 2007).

1.3.2 The canonical Wnt signaling pathway

The Wnt signaling pathway is a crucial cascade, which is involved in cell polarity, cell renewal and tissue homeostasis (Logan and Nusse, 2004). The intracellular signaling can be divided into three subtypes: the β -catenin dependent canonical pathway, the β -catenin independent non-canonical pathway and the non-canonical Wnt/ Ca^{2+} pathway (Nusse, 2005; Sugimura and Li, 2010; Thrasivoulou *et al.*, 2013). Without Wnt signaling, cytoplasmic β -catenin gets constantly degraded by a multiprotein destruction complex. This complex consists of APC, casein kinase-1 (CK1), the scaffolding protein Axin and GSK3. β -catenin is phosphorylated at the NTD by CK1 and GSK3 (see section 1.3.1), which eventually results in ubiquitination by β -TrCP and finally proteosomal degradation (Figure 1-8; He *et al.*, 2004; Voronkov and Krauss, 2013). The canonical Wnt pathway also referred to as Wnt/ β -catenin pathway leads to accumulation of β -catenin

in the cytoplasm and subsequent translocation into the nucleus where it stimulates transcription factors belonging to the TCF/Lef family (Kimelmann and Xu, 2006; MacDonald *et al.*, 2009). This pathway is activated by binding of a Wnt ligand to the Frizzled (Fz) receptor and co-receptor lipoprotein receptor related protein 6 (LRP6) or LRP5. Thereby, LRP6 gets phosphorylated by CK1 and GSK3 resulting in binding of Axin to LRP6. This causes the disruption of the destruction complex (Mao *et al.*, 2001; Tamai *et al.*, 2004; Davidson *et al.*, 2005; Zeng *et al.*, 2005). The translocation of the complex to the plasma membrane allows for the accumulation of β -catenin in the cytoplasm and subsequent translocation in the nucleus, where it activates the transcription of Wnt target genes (MacDonald *et al.*, 2009).

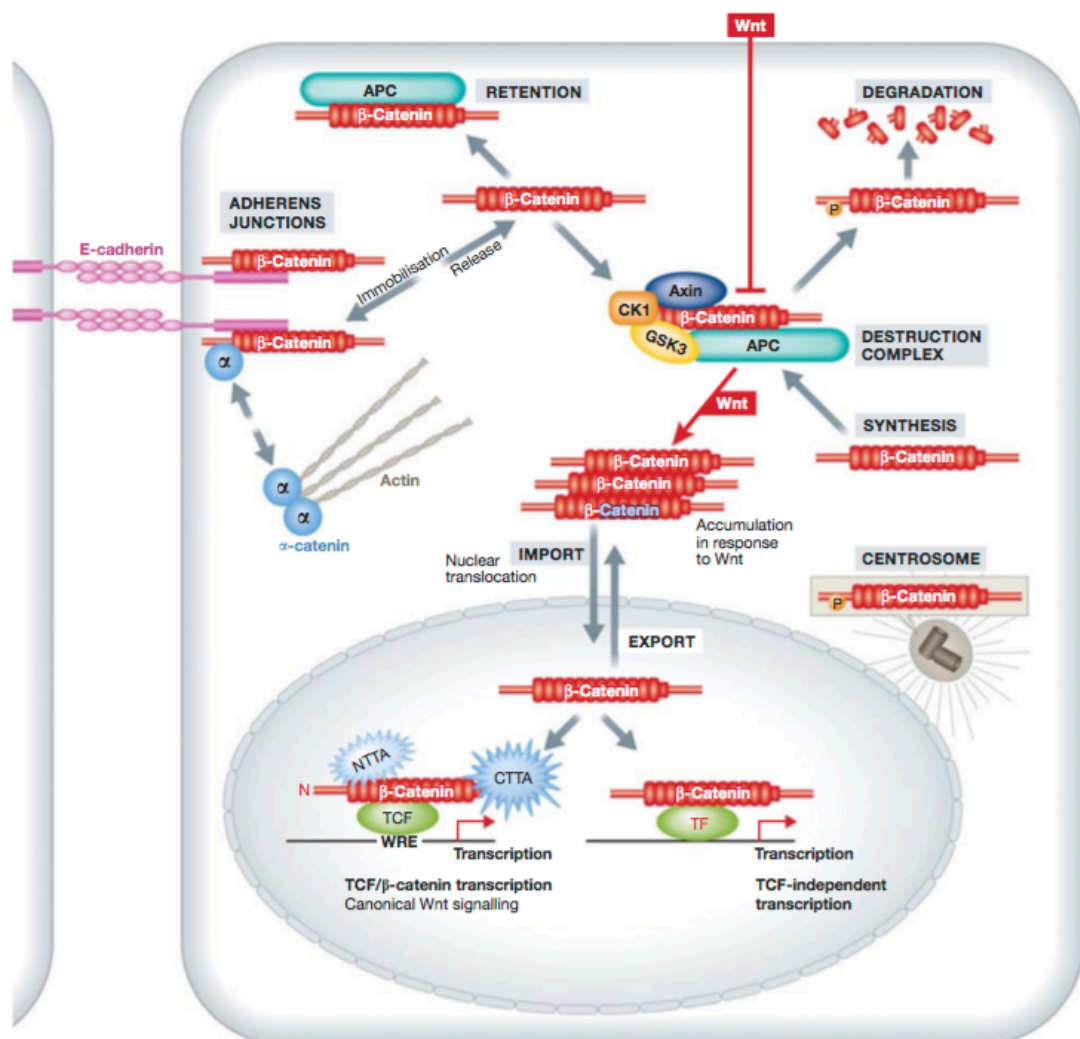


Figure 1-8 β -catenin's life cycle within the cell. Newly synthesized β -catenin (red) can interact both with E-cadherin (pink) and α -catenin (light blue), thereby having an influence on the actin cytoskeleton. Either by E-cadherin down-regulation or protein kinase activity β -catenin can be released. The released protein is immediately bound and phosphorylated by the destruction complex consisting of Axin (dark blue), APC (turquoise), CK1 (orange) and GSK3 (yellow). Phosphorylated β -catenin gets degraded by the proteasome. A small amount of β -catenin is retained in the cytoplasm by APC. After activation of Wnt signaling, the destruction complex gets disrupted, which leads to an accumulation of β -catenin in the cytoplasm and subsequent translocation into the nucleus. β -catenin interacts with TCF/Lef transcription factors (green) and thereby increases Wnt target gene transcription. β -catenin might also bind to other transcrip-

tion factors and drives transcription of TCF-independent genes. By modulating the nuclear import and export, β -catenin's signaling activity can be regulated. Additionally, β -catenin might interact with the centrosome (CTTA: C-terminal transcriptional activators; NTTA: N-terminal transcriptional activators; from Valenta *et al.*, 2012).

1.4 High-Content Screening

High-Content Screening (HCS) is a method which uses living cells to investigate cellular pathways in healthy and/or diseased cells and the effects of small inhibitory molecules on these pathways. Cells accomplish all functions of life. The tightly regulated spatial and temporal interplay of ions, DNA, RNA, proteins, metabolites, and organelles is responsible for the performance of life functions. Minor changes in this regulated network often make the difference between healthy and diseased. HCS facilitates obtaining more information about the spatial or temporal distribution of certain proteins within the cell, even at the single-cell level (Giuliano *et al.*, 1997; Gasparri, 2009). Fluorescently labeled antibodies can detect the localization of target proteins. However this only allows measurement of one time point. Another possibility is the creation of a cell line that expresses a fusion of the target protein with e.g. green fluorescent protein (GFP) or yellow fluorescence protein (YFP). This allows for detection at several time points. Another possibility is fluorescence resonance energy transfer (FRET), which can be used for the investigation of protein-protein interactions (Giuliano *et al.*, 1997; Liptrot, 2001). There is a large number of known biochemical pathways that involve translocations from the plasma membrane to the nucleus or other organelles. Diseases are often the result of a dysfunction or -regulation of these pathways. In order to discover a new drug candidate, HCS can be used to screen for perturbation of a cellular process of interest. Cells are first treated with compounds and afterwards the temporal or spatial changes in e.g. target protein distribution are detected and characterized using image analysis. Compared to High-Throughput Screening (HTS), HCS consumes more time. However, the yielded data contain much more biological information, which can provide a deeper insight into drug effects or the function of proteins, genes or signaling pathways in healthy and diseased cells (Giuliano *et al.*, 1997; Abraham *et al.*, 2004; Zanella *et al.*, 2010).

1.5 Aim of the project

EpCAM is a transmembrane molecule that is expressed on epithelial cells, stem cells, tumor-initiating cells and cancer cells. On epithelial cells, EpCAM can mainly be found in the intercellular space whereas on cancer cells, EpCAM is highly overexpressed and distributed all over the cell surface. The EpCAM target genes are involved in cell growth and cell proliferation. Due to its cancer-specific overexpression, EpCAM is an attractive target for cancer therapy. Compared to existing immunotherapeutic ap-

proaches, targeting the intracellular EpCAM signaling represents a completely new approach.

The first aim of this study was to obtain the structure of the FHL2/EpICD complex to understand the binding mode. This could be used in order to find or design a small inhibitory molecule, which disrupts the binding and therefore interrupts the EpCAM signaling cascade. This should be accomplished by biochemical assays and additional structural methods.

The aim of the second part was the establishment and performance of an HCS for finding a small inhibitory molecule that inhibits the EpCAM signaling cascade. The obtained hits should then be further characterized regarding their toxicity and specificity towards EpCAM in order to obtain a lead compound for a potential pharmaceutical drug. The HCS was performed with a cell line expressing an EpCAM-YFP construct, which allows for detection of the localization of EpCAM cleavage products within the cell. Further investigation of hits was done by different cellular, biochemical and protein-biochemical assays.

2 Material and Methods

2.1 Chemicals and consumables

All commonly used chemicals were purchased from Roth (Karlsruhe, Germany), Sigma-Aldrich (Taufkirchen, Germany) or Merck (Darmstadt, Germany), unless stated otherwise. Enzymes and nucleotides for molecular biology as well as molecular weight markers and loading dyes for gel electrophoresis were ordered from New England Biolabs (Frankfurt, Germany) and Invitrogen (Karlsruhe, Germany). DNA oligonucleotides were synthesized by Eurofins MWG (Ebersberg, Germany). Bacterial cell culture material was obtained from Becton, Dickinson & Co (Heidelberg, Germany) and Sigma-Aldrich. Media and supplements for mammalian cell culture were purchased from Life Technologies (Carlsbad, USA). Cell culture plates were ordered from Eppendorf (Hamburg, Germany) and Perkin Elmer (Waltham, USA). Chromatography was performed using columns and material from GE Healthcare (Munich, Germany). Transfer membranes for Western blots were ordered from Merck Millipore (Darmstadt, Germany). Chemically synthesized peptides were ordered from JPT peptide technologies (Berlin, Germany). Sequencing was done by Eurofins MWG. All reactions were performed using ddH₂O.

2.2 Oligonucleotides

2.2.1 DNA oligonucleotides for cloning

Table 2-1 DNA oligonucleotides for cloning

No.	Name	Sequence 5' -> 3'
1	EpiCD_BamHI_for	aaaggatccatgtccagaaagaagagaatg
59	EpiCD_stop_xho_rev	gaactcgagttatgcattgagttccctatgatctc
10	FHL2_NcoI_fwd	aaaccatgggcatgactgagcgccttgactgccac
11	FHL2_XhoI_rev	aaactcgaggatgtctttccacagtcggggcacag
17	FHL2_XhoI_stop	aaactcgagttagatgtctttccacagtcggggcacag
18	pOPINM_FHL2_for	aagttctgtttcagggcccgatgactgagcgccttgac
19	pOPINM_FHL2_rev	atggtctagaaagctttagatgtctttccacagtc
29	pFastBacI_FHL2f	aaaggatccatgaaaatcgaagaaggt
30	pFastBacI_FHL2r	aaaaagctttcagtggtggtggtggtggtg
15	mut_pETM43_fwd	gttcaggggcccatgtccagaaagaagagaatg
16	mut_pETM43_rev	cattctcttcttctggacatgggcccctggaac
53	LIM1_fwd_BamHI	aaaggatcctgccaccattgcaac
55	LIM2_fwd_BamHI	aaaggatcctgccaggaatgcaag
54	LIM2_rev_XhoI	aaactcgagttagcagggcacacagaa
51	LIM3_BamHI_fwd	aaaggatcctcgttcagtgcaaa

52	LIM3_XhoI_rev	aaactcgagttagcagttcaggcagta
49	LIM4_BamHI_fwd	aaaggatcctgtgctgggtgcacc
50	LIM4_XhoI_rev	aaactcgagttaacagtcggggcacag
56	pETM43_LIM1_fwd	aaaccatgggctgccaccattgcaac
57	pETM43_LIM2_fwd	aaaccatgggctgccaggaatgcaag
58	pETM43_LIM3_fwd	aaaccatgggctgcttcagtgcaaa
33	β -cat_fwd_pOPIN	aagttctgtttcaggggcccgaactgattaactatcaagatgat
34	β -cat_rev_pOPIN	atggctagaaagctttacaggtcagatcaaacaccaggc

2.2.2 DNA oligonucleotides for qPCR

Table 2-2 DNA oligonucleotides for qPCR

No.	Name	Sequence 5' -> 3'
35	GAPDH_for	tgaccaccaactgcttagc
36	GAPDH_rev	ggcatggactgtggcatgag
37	CycD1_for	tattgcgctgctaccgttga
38	CycD1_rev	ccaatagcagcaacaatgtgaaa
39	cmyc_qPCR_fwd	gtcaagaggcgaacacacaac
40	cmyc_qPCR_rev	ttggacggacaggatgtatgc
41	qPCR_EpCAM_fwd	gctggccgtaaactgctttg
42	qPCR_EpCAM_rev	acatttggcagccagctttg
43	HSPCB_fwd	tctgggtatcggaaagcaagcc
44	HSPCB_rev	gtgcacttcctcaggcatctg
45	RPS13_fwd	cgaaagcatcttgagaggaaca
46	RPS13_rev	tcgagccaaacggtgaatc
47	18s_fwd	agaaacggctaccacatcca
48	18s_rev	caccagacttgcctcca

2.3 Plasmids

2.3.1 Commercial plasmids

Table 2-3 Commercial plasmids

Name	Application	Tag	Antibiotic	Source
pGEX-6P-1	Protein expression in <i>E. coli</i>	GST	Amp	GE Healthcare EMBL
pETM43	Protein expression in <i>E. coli</i>	MBP	Kan	(Heidelberg, Germany)
pOPINM	Protein expression in <i>E. coli</i>	His ₆ -MBP	Amp	Addgene (Cambridge, USA)
pOPINS3C	Protein expression in <i>E. coli</i>	His ₆ -Sumo	Amp	Addgene
pFastBac	Bac-to-Bac Baculovirus expression system	-	Amp/Gen	Invitrogen

2.3.2 Plasmids for recombinant protein expression in *E. coli*

Table 2-4 Plasmids for recombinant protein expression in *E. coli*

No.	Name/Insert	Vector	Primer	Restriction sites	Template	Note
8	GST-FHL2 FL	pGEX-6P-1	-	BamHI/XhoI	-	a)
27	FHL2 (288-314)	pGEX-6P-1	-	BamHI/XhoI	-	a)
28	β -catenin (138-781)	-	-	-	-	b)
2	MBP-FHL2 FL-His	pETM43	10/11	NcoI/XhoI	8	
3	MBP-FHL2 FL	pETM43	10/17	NcoI/XhoI	8	
9	pOPINM-FHL2	pOPINM	18/19	KpnI/HindIII	8	
19	GST-LIM1-2	pGEX-6P-1	53/54	BamHI/XhoI	8	
20	GST-LIM2-3	pGEX-6P-1	55/52	BamHI/XhoI	8	
21	GST-LIM3-4	pGEX-6P-1	51/50	BamHI/XhoI	8	
23	MBP-LIM1-2	pETM43	56/54	NcoI/XhoI	8	
24	MBP-LIM2-3	pETM43	57/52	NcoI/XhoI	8	
25	MBP-LIM3-4	pETM43	58/50	NcoI/XhoI	8	
1	GST-EpicD	pGEX-6P-1	1/59	BamHI/XhoI	27	
22	β -catenin (138-781)	pOPINS3C	33/34	KpnI/HindIII	28	

a) Created by Patrick Schrepfer

b) Obtained from Prof. Dr. Tobias Madl, Medizinische Universität Graz, Austria

2.3.3 Plasmid for recombinant protein expression in insect cells

Table 2-5 Plasmid for recombinant protein expression in insect cells

No.	Name/Insert	Vector	Primer	Restriction sites	Template
16	FHL2 FL	pFastBac	29/30	BamHI/HindIII	2

2.4 Bacterial strains

Table 2-6 Bacterial strains

Name	Genotype	Source
XL1-Blue	recA1 endA1 gyrA96 thi-1 hsdR17 supE44 relA1 lac [F'proAB lac1 ^q Z Δ M15Tn10(Tet ^r)]	Stratagene (La Jolla, USA)
BL21 Star (DE3)	B F ⁻ ompT hsdS(_{r_B} m _B) dcm+ Tet ^r gal λ (DE3) EndA Hte [argU ile Y leu W Cam ^r]	Stratagene
DH10Bac	F- <i>mcrA</i> Δ (<i>mrr-hsdRMS-mcrBC</i>) ϕ 80/ <i>lacZ</i> Δ M15 Δ <i>lacX74</i> <i>recA1</i> <i>endA1</i> <i>araD139</i> Δ (<i>ara</i> , <i>leu</i>)7697 <i>galU</i> <i>galK</i> λ <i>rpsL</i> <i>nupG/bMON14272/pMON7124</i>	Invitrogen

2.5 Insect cell lines

Table 2-7 Insect cell lines

Name	Description	Source
Sf21	Derived from <i>Spodoptera frugiperda</i> ovarian cells. Used for isolation and propagation of recombinant baculovirus stocks.	Invitrogen
High Five	Derived from <i>Trichoplusia ni</i> ovarian cells. Used for recombinant protein expression upon baculovirus infection.	Invitrogen

2.6 Mammalian cell lines

Table 2-8 Mammalian cell lines

Name	Description	Source	Note
HEK293	Cell line derived from human embryonic kidney cells	Obtained from Prof. Dr. Olivier Gires, Klinikum der LMU München, Germany	
HEK293 EpCAM FL-YFP	HEK293 cells transfected with 141 pCAG::EpCAM-YFP	Created by Karolina Bobowski (Labor für molekulare Onkologie, Klinikum der LMU München, Germany)	
HEK293 EpCAM-CTF-YFP	HEK293 cells transfected with 141 pCAG::EpCAM-CTF-YFP	Created by Karolina Bobowski	Construct consists of Myc-Tag, EpCAM-CTF sequence (251-315), FLAG-Tag, TEV-cleavage site and YFP
HEK293 EpCAM FL	HEK293 cells transfected with 141 pCAG::EpCAM-FL	Created by Karolina Bobowski	
HEK293 Δ EpCAM YFP	HEK 293 cells transfected with 141 pCAG::YFP	Obtained from Prof. Dr. Olivier Gires, Klinikum der LMU München, Germany	
FaDu	Human hypopharynx carcinoma cell line	Obtained from Prof. Dr. Olivier Gires, Klinikum der LMU München, Germany	
HCT-8	Human colon carcinoma cell line	Obtained from Prof. Dr. Olivier Gires, Klinikum der LMU München, Germany	
HCT-8 KO	CRISPR-Cas9-mediated EpCAM KO clones of HCT-8 cells	Created by Thanos Tsaktanis (Labor für molekulare Onkologie, Klinikum der LMU München, Germany)	

2.7 Media and supplements for bacterial cell culture

Table 2-9 Media for bacterial cell culture

Medium	Composition
Luria-Bertani (LB) medium	1 % (w/v) bacto tryptone, 0.5 % (w/v) bacto yeast extract, 0.5 % NaCl, add 1.5 % (w/v) agar for plates
SOC	2 % (w/v) bacto tryptone, 0.5 % (w/v) bacto yeast extract, 10 mM NaCl, 2.5 mM KCl, 10 mM MgCl ₂ , 10 mM MgSO ₄ , pH 7.0
DH10Bac medium	1 % (w/v) bacto tryptone, 0.5 % (w/v) bacto yeast extract, 0.5 % (w/v) NaCl, 1 M IPTG, 100 µg/mL bromo-chloro-galactopyranoside (X-Gal), 7 mg/mL gentamycin, 10 mg/mL tetracycline, 50 mg/mL kanamycin, pH 7.0

Table 2-10 Supplements for bacterial cell culture

Supplements	Application	Final concentration
Ampicillin	<i>E. coli</i> selection	100 µg/mL
Kanamycin	<i>E. coli</i> selection	50 µg/mL
Carbenicillin	<i>E. coli</i> selection	100 µg/mL
Gentamycin	<i>E. coli</i> DH10Bac selection	7 µg/mL
Tetracyclin	<i>E. coli</i> DH10Bac selection	10 µg/mL
X-Gal	Substrate for blue/white screening on plates	100 µg/mL
Isopropyl-β-D-thiogalactosid (IPTG)	Induction of protein expression in <i>E. coli</i>	0.25 mM

2.8 Media and supplements for insect cell culture

Table 2-11 Media for insect cell culture

Medium	Composition
SF-900 III SFM	Protein-free insect cell culture medium
HyClone medium	4.13 % (w/v) HyClone, 4.16 mM NaHCO ₃ , 0.15 % (v/v) glycerol, pH 6.1-6.4

Table 2-12 Supplements for insect cell culture

Supplement	Application	Final concentration
Gentamycin	Insect cell selection	10 µg/mL

2.9 Media and supplements for mammalian cell culture

Table 2-13 Media for mammalian cell culture

Medium	Composition	Application
Complete Medium	90 % (v/v) DMEM, 10 % (v/v) FBS, 100 U/mL penicillin/streptomycin, 2.5 µg/mL fungizone	Normal cell culture
Cryo medium	(v/v) 70 % DMEM, (v/v) 20 % FBS, (v/v) 10 % DMSO	Freezing of cells

Table 2-14 Supplements for mammalian cell culture

Supplements	Application	Final concentration	Source
Gibco® DMEM (4.5 g/L D-Glucose, L-glutamine, phenol red)	Cell culture	70 or 90 % (v/v)	Life Technologies
FBS (fetal bovine serum)	Cell culture	10 or 20 % (v/v)	Life Technologies
Penicillin/streptomycin	Antibiotic in cell culture	100 U/mL	Life Technologies
Fungizone	Antimycotic in cell culture	2.5 µg/mL	Life Technologies
10x Trypsin/EDTA	Splitting of cells	1x	Life Technologies
DMSO (dimethylsulfoxid)	Cryo medium	10 % (v/v)	Carl Roth
1x PBS (phosphate buffered saline)	Washing of cells	1x	Life Technologies
Puromycin	Cell selection	1 µg/mL	Life Technologies

2.10 Antibodies

Table 2-15 Primary antibodies

Primary Antibody	Clonality/Source	Dilution/Application	Source
Anti-β-actin-HRP	Monoclonal/mouse	1:1000/ Western blot	Santa Cruz (Heidelberg, Germany)
Anti-cyclin D1	Polyclonal/rabbit	1:5000/Western blot	Epitomics (Burlingame, USA)
Anti-EpCAM-FITC	Monoclonal/mouse	1:200/FACS	Life Technologies
Anti-EpCAM	Monoclonal/mouse	1:1000/Western blot	Santa Cruz
Anti-EpICD	Polyclonal/guinea pig	1:1000/Western blot	Peptide Specialty Laboratories (Heidelberg, Germany)
Anti-FLAG	Monoclonal/mouse	1:1000/Western blot	Sigma-Aldrich
Anti-GFP	Polyclonal/rabbit	1:5000/Western blot	Abcam (Cambridge, UK)
Anti-GAPDH	Polyclonal/rabbit	1:5000/Western blot	Bethyl Laboratories (Montgomery, USA)
Anti-MBP-HRP	Monoclonal/mouse	1:1000/Western blot	Abcam

Table 2-16 Secondary antibodies

Secondary Antibody	Clonality/Source	Dilution/Application	Source
Anti-guinea-pig-HRP	polyclonal/rabbit	1:1000/Western blot	Thermo Fisher Scientific (Walham, USA)
Anti-mouse-HRP	Polyclonal/goat	1:5000/Western blot	Dako (Hamburg, Germany)
Anti-mouse-HRP	polyclonal/goat	1:3000/Western blot	BioRad (Munich, Germany)
Anti-rabbit-HRP	Polyclonal/goat	1:5000/Western blot	Dianova (Hamburg, Germany)

2.11 General buffers and stock solutions

Table 2-17 General buffers and stock solutions

Name	Composition	Application
4x stacking gel buffer	0.5 M Tris, 0.4 % (w/v) SDS, pH 6.8	SDS PAGE
4x separating gel buffer	3 M Tris, 0.4 % (w/v) SDS, pH 8.5	SDS PAGE
10x TGS	0.25 M Tris, 1 % (w/v) SDS, 1.9 M glycine	SDS PAGE
4x loading dye	110 mM Tris/HCl pH 6.8, 40 % (v/v) glycerol, 0.5 % (w/v) bromophenol blue, 4 % (w/v) SDS, 40 mM DTT	SDS PAGE
Coomassie staining solution	50 % (v/v) ethanol, 7 % (v/v) acetic acid, 0.2 % (w/v) Coomassie Brilliant blue R-250	SDS PAGE
50x TAE	2 M Tris-base, 5.71 % (v/v) acetic acid, 50 mM EDTA (pH 8.0)	Agarose-gel electrophoresis
10x PBS	80 g NaCl, 2 g KCl, 14.2 g Na ₂ HPO ₄ , 2.4 g KH ₂ PO ₄ in 1 L H ₂ O, pH 7.4	Western blot
PBS-T	1x PBS, 1:1000 Tween@20	Western blot
Lysis buffer	1x PBS, 1 % (v/v) Triton X-100, two tablets protease inhibitor cocktail	Western blot
Laemmli buffer	140 mM Tris-HCl, 30 % (w/v) glycerine, 4 % (w/v) SDS, 16 % (v/v) β-mercaptoethanol, 0.1 % (w/v) bromophenol blue	Western blot
Running buffer	250 mM Tris, 2 M glycine, 1 % (w/v) SDS	Western blot
10x Blotting buffer	30 g Tris, 95 g glycine in 1 L H ₂ O	Western blot
Washing buffer	1x PBS, 0.2 % (v/v) Tween@20	Western blot
Blocking buffer	5 % (w/v) milk powder in washing buffer	Western blot
Primary antibody solution	3% (w/v) BSA in washing buffer	Western blot
Secondary antibody solution	5 % (w/v) milk powder in washing buffer	Western blot
Homogenisation buffer	10 mM MOPS, 10 mM KCl, 1x protease inhibitor cocktail	Membrane Assay
Assay buffer	120 mM Na ₃ C ₆ H ₅ O ₇ , 10 μM ZnCl ₂ , 1x protease inhibitor cocktail	Membrane Assay
Lysis buffer_IP	10 mM Tris/HCl pH 7.5, 150 mM NaCl, 0.5 mM EDTA, 0.5 % (v/v) NP-40, 1 tablet protease inhibitor cocktail	IP
Dilution buffer	10 mM Tris/HCl pH 7.5, 150 mM NaCl, 0.5 mM EDTA	IP
Elution buffer_IP	100 mM glycine, pH 2.7	IP
TEV buffer	25 mM Tris/HCl pH 8.0, 150 mM NaCl, 10 mM DTT	TEV cleavage

2.12 Molecular biology

2.12.1 Cloning

Cloning of genes of interest was performed according to Sambrook and Russel, 2001. DNA was amplified by polymerase chain reaction (PCR). The resulting PCR products were analyzed by agarose-gel electrophoresis (1x TAE buffer, stained with GelRed (Biotium, Hayward, USA)) and purified with the NucleoSpin® PCR clean-up kit (Macherey-Nagel, Düren, Germany) according to manufacturer's instructions. The insert and the vector were digested with restriction enzymes and ligated. Restriction en-

zymes, buffers and T4 DNA ligase (Thermo Scientific, Waltham, USA) were used according to manufacturer's instructions. Point mutations were introduced using the QuickChange II Site-Directed Mutagenesis Kit (Agilent Technologies, Waldbronn, Germany). For cloning into pOPIN expression vectors, the purified PCR products were ligated with the linearized plasmid by using the In-Fusion Cloning Kit (Clontech, Mountain View, USA) according to manufacturer's protocol. Concentrations of nucleic acids were measured with NanoDrop Spectrophotometer (Thermo Fisher, Ulm, Germany). Cloning strategies for all constructs and sequences of the corresponding oligonucleotides are summarized in Table 2-1 and Table 2-4.

2.12.2 Transformation of *E. coli* and isolation of plasmid DNA

Preparation of chemically competent *E. coli* cells was done according to Hanahan, 1983. Plasmid DNA was transformed as described in Sambrook and Russel, 2001. Transformed cells were selected on LB agar plates supplemented with antibiotics. For small-scale plasmid preparation, 5 mL LB medium supplemented with respective antibiotics were inoculated with a single colony and grown o/n at 37 °C. Plasmid DNA was isolated using the NucleoSpin® Plasmid kit (Macherey-Nagel) according to manufacturer's instructions. Cloning was verified by sequencing.

2.12.3 RNA isolation

RNA isolation from mammalian cells was performed with the High Pure RNA Isolation Kit (Roche, Mannheim, Germany) according to manufacturer's protocol. For removal of contaminating DNA, isolated RNA was treated twice with Turbo DNasefree kit (Ambion, Austin, USA). Concentration was measured with NanoDrop Spectrophotometer.

2.12.4 Reverse transcription of RNA

Reverse transcription (RT) of RNA was performed with PrimeScript™ RT Master Mix (Takara, Paris, France) according to manufacturer's instructions. RT was generally performed from 1 µg total RNA. cDNA samples were stored at 4 °C until further use.

2.12.5 Quantitative Real-Time PCR

Quantitative Real-Time- (qRT-) PCR experiments were performed in a LightCycler® 480 instrument (Roche) using the KAPA SYBR FAST Universal Kit according to the manufacturer's protocol. Reactions were performed in triplicates on FrameStar® 480/96 (4titude, Wotton, UK) plates. To ensure specific amplification, melting curves were analyzed. For normalization, the house-keeping gene GAPDH was included. Evaluation was done by using the $\Delta\Delta C_p$ method (Pfaffl, 2001). For statistical analysis, the paired-sample t-test was applied and statistical significance was determined by a p-

value where $p < 0.05$ was considered significant. The DNA oligonucleotides used for qRT-PCR are summarized in Table 2-2.

2.13 Bioinformatics

2.13.1 Protein parameters

Protein parameters such as molecular weight (MW), isoelectric point (pI) and the extinction coefficient (ϵ) were calculated using the ExPASy Proteomics Server (<http://web.expasy.org/protparam/>). Protein concentration was determined by measuring A_{280} with NanoDrop Spectrophotometer.

2.13.2 Sequence alignment

DNA and protein sequences for primer design and determination of protein parameters were obtained from the NCBI database (<https://www.ncbi.nlm.nih.gov/>).

2.13.3 Mammalian cell line properties

The properties of the cultivated mammalian cell lines such as medium, sub-culturing, culture conditions and cryopreservation were obtained from ATCC (https://www.lgcstandards-atcc.org/?geo_country=de) and DSMZ (<https://www.dsmz.de/>).

2.14 Protein expression

2.14.1 Recombinant protein expression in *E. coli*

All cloned constructs (see section 2.12.1) were used to recombinantly express the proteins of interest in *E. coli* BL21 Star (DE3) cells. Freshly transformed cells were used to inoculate 50 mL LB medium supplemented with the respective antibiotic. After cultivation for 4 h at 37 °C, the preculture was transferred into 3 L prewarmed LB medium supplemented with the respective antibiotic. In case of maltose-binding protein (MBP)-fusion proteins, 2 g/L glucose were added. For zinc binding proteins, 100 μ M $ZnCl_2$ was added. After reaching an OD_{600} of 0.3-0.4, cell cultures were cooled to 18 °C. Expression was induced at an OD_{600} of 0.6 by adding 0.25 mM Isopropyl- β -D-thiogalactopyranosid (IPTG). The cells were harvested after 12-16 h by centrifugation (4,000 rpm, 20 min, 4 °C). Cell pellets were resuspended in the respective lysis buffer, flash frozen in liquid nitrogen and stored at -80 °C until further use.

2.14.2 Recombinant protein expression in insect cells

Recombinant baculovirus was prepared according to the protocol of the Bac-to-Bac baculovirus expression system (Invitrogen; Ciccarone *et al.*, 1998). MBP-FHL2 fusion protein was cloned into pFastBac1, amplified in XL-1 Blue cells (see section 2.12.1 and

2.12.2) and then transformed into DH10Bac *E. coli* cells. Transformed cells were plated on DH10Bac agar plates and grown at 37 °C for 48 h. Positive colonies were detected by blue/white screening. 5 mL LB medium supplemented with the corresponding antibiotic were inoculated with a white colony and grown o/n at 37 °C. Isolation of bacmid DNA was done with the NucleoSpin® Plasmid kit (Macherey-Nagel), however, instead of using the provided columns, the DNA was precipitated with isopropanol. For transfection of SF21 cells, 2 µg bacmid DNA and 3 µL FuGeneHD reagent (Roche, Mannheim, Germany) were mixed with 300 µL Hyclone SF medium and incubated for 45 min at RT. This was added to 2 mL of insect cell suspension (0.4×10^6 cells/mL) and incubated for 4 d at 27.5 °C. Afterwards, the cells were centrifuged (3,000 rpm, 10 min) and the supernatant (P0) was used for infection of 10 mL SF21 cells (1.4×10^6 cells/mL). After another cultivation for 4 d at 27.5 °C and 95 rpm, the cells were centrifuged (3,000 rpm, 10 min) and the supernatant (P1) was used for the infection of 500 mL SF21 cells (0.4×10^6 cells/mL). These cells were cultivated for 4 d at 27.5 °C and 95 rpm and afterwards pelleted (3,000 rpm, 10 min). The supernatant (P2) was sterile filtered and stored at 4 °C. 10-30 mL of P2 were used for the infection of 500 mL High Five cells (1×10^6 cells/mL). Afterwards, cells were incubated for 60-70 h at 27.5 °C and then harvested by centrifugation (2,000 x g, 15 min, 4 °C). Cell pellets were resuspended in the respective lysis buffer, flash frozen in liquid nitrogen and stored at -80 °C until further use.

2.15 Protein purification

All purification steps were performed at 4 °C or on ice. All buffers used were filtered and degassed prior to use. Furthermore, all buffers contained 1 mM DTT or 1 mM TCEP when the protein was used for ITC. pH of the buffers was adjusted according to the protein's pI.

2.15.1 Purification of GST-tagged proteins

After thawing of cell pellets, cells were resuspended in lysis buffer (50 mM HEPES, 500 mM NaCl, 1 mM EDTA, 20 % (v/v) glycerol, 1 % (v/v) triton X) and one tablet of EDTA-free protease inhibitor cocktail (Roche) was added. Cells were disrupted by sonication on ice with a Branson Sonifier 250 (Emerson, Danbury, USA). The cell debris was removed by centrifugation (16,000 rpm, 30 min, 4 °C). Afterwards, the lysate was loaded on a pre-equilibrated 5 mL GSTrap FF column (GE Healthcare). After extensive washing with washing buffer (50 mM HEPES, 500 mM NaCl) and high salt buffer (50 mM HEPES, 1 M NaCl), the protein was eluted by elution buffer (50 mM HEPES, 150 mM NaCl, 25 mM glutathione; GSH) using a linear gradient. Fractions containing proteins were identified by their A_{280} , analyzed by SDS-PAGE and pooled. If necessary,

GST was removed by adding 50 µg PreScission Protease (GE Healthcare), whilst dialysing against dialysis buffer (50 mM Hepes, 100 mM NaCl) o/n at 4 °C. The protein was further purified using a HiTrap Q column (GE Healthcare). The eluted fractions were analyzed by SDS-PAGE, pooled and concentrated in a centrifugal filter device (Amicon Ultra, Millipore Billerica, USA). Prior to purification by size exclusion (SEC) with a Superdex 75 10/30 GL column (GE Healthcare) in SEC buffer (20 mM HEPES, 100 mM NaCl), the protein was centrifuged (16,000 rpm, 20 min, 4 °C). Peak fractions were again analyzed on SDS-PAGE, pooled, concentrated, flash frozen in liquid nitrogen and stored at -80 °C until further use.

2.15.2 Purification of MBP-tagged proteins

MBP-tagged proteins were purified analogously to GST-tagged proteins (see section 2.15.1). The cleared lysate was loaded onto a pre-equilibrated amylose column. After washing steps, the protein was eluted with 75 mL elution buffer (20 mM HEPES, 150 mM NaCl, 10 mM maltose). The eluted fractions were analyzed by SDS-PAGE. After concentration of the protein, the final purification step was carried out on a HiLoad 16/600 Superdex S75 with SEC buffer.

2.15.3 Purification of His-SUMO tagged proteins

The cell pellet was thawed and resuspended in lysis buffer (20 mM HEPES, 500 mM NaCl, 20 % (v/v) glycerol, 1 % (v/v) triton X) and one tablet of EDTA-free protease inhibitor cocktail (Roche). Afterwards, the cells were sonified and centrifuged as previously described (see 2.15.1). The cleared lysate was loaded onto a pre-equilibrated 5 mL HisTrap column (GE Healthcare). The column was washed with washing buffer (20 mM HEPES, 300 mM NaCl, 20 mM imidazole) and afterwards eluted by elution buffer (20 mM HEPES, 100 mM NaCl, 500 mM imidazole) in a linear gradient over 20 column volumes (CV). The protein-containing fractions were identified by their A_{280} and analyzed on a SDS-PAGE, pooled and dialyzed o/n at 4 °C against dialysis buffer (20 mM HEPES, 100 mM NaCl). For removal of the His-SUMO-Tag, 50 µg PreScission protease were added. The protein was further purified analogously to GST-tagged proteins (see section 2.15.1).

2.16 SDS-PAGE

For assessing amount and purity of proteins, they were analyzed by sodium dodecyl-sulfate polyacrylamide gel electrophoresis (SDS-PAGE; Laemmli, 1970). Depending on the size of the proteins, 12-19 % polyacrylamide gels were used. Gels were stained either with Coomassie blue (Thermo Scientific) or Silver staining solution according to standard procedures (Thermo Fisher).

2.17 Methods for analyzing protein-protein interactions

2.17.1 *In vitro* pull-down assay

For pull-down experiments, the respective resin was washed with SEC buffer. The proteins were mixed in a total volume of 100 μL , incubated for 30 min at 4 °C and centrifuged (max. speed, 10 min, 4 °C). Afterwards, the resin was resuspended in SEC buffer, added to the proteins and incubated for 30 min at 4 °C on the overhead shaker. After the incubation, the resin was washed five times (3,000 rpm, 3 min, 4 °C) with SEC buffer before eluting the proteins with elution buffer. Samples of every step were analyzed by SDS-PAGE (see section 2.16).

2.17.2 Isothermal titration calorimetric (ITC)

ITC experiments were performed with SEC buffer in MicroCal iTC200 or MicroCal VP-ITC (Malvern Instruments, Malvern, UK). Before starting the experiment, all samples were centrifuged. The syringe was filled with a 40–110 μM protein solution and was titrated into the sample cell, which was filled with a ten times less concentrated putative interacting protein solution. ITC experiments were either performed with 20 injections of 2 μL protein solution every 2 min or with 36 injections of 4 μL protein at 4 min interval. The data was analyzed using the MicroCal Origin program.

2.18 Cell culture

2.18.1 Cultivation of cells

All cells were grown in Complete medium. For cultivation of transfected HEK293 cells, 1 $\mu\text{g}/\text{mL}$ puromycin was added to the medium. Upon 90 % cell density, cells were split. Therefore, medium was removed and cells were washed with PBS. For the detachment of the cells, Trypsin/EDTA was added and incubated for 5 min at 37 °C. Afterwards, medium was added to stop the activity of trypsin and the cell suspension was transferred to Falcon tubes (BD Biosciences, Heidelberg, Germany) and centrifuged (1,500 rpm, 5 min). The supernatant was discarded, the pellet was resuspended and cells were transferred to a new cell culture flask (Greiner Bio-One, Frickenhausen, Germany). For seeding the cells in 6-, 96- or 384-well plates, cells were counted with a Luna Cell Counter (Logos Biosystems, Annandale, USA) and the cell number was adjusted. All cell lines were cultivated at 37 °C in a humidified incubator with 5 % CO_2 .

2.18.2 Cryopreservation and thawing of cells

Cells were detached from the flask as previously described (see section 2.18.1), resuspended and frozen in cryo-conservation medium (see Table 2-13).

Cells were thawed, transferred to 10 mL pre-warmed Complete medium and centrifuged (1,500 rpm, 5 min). The supernatant was removed, the cell pellet was resuspended and transferred to a new cell culture flask.

2.18.3 High-Content Screening (HCS)

2.18.3.1 Screening libraries

For HCS, four in-house screening libraries of small inhibitory molecules were used. The compounds of these libraries were selected according to the following rules:

- Good solubility
- Molecular weight less than 600 g/mol
- Purity > 90 %
- Non-reactive, unstable and toxic chemical groups
- Meeting criteria of Lipinski's rule of five (Lipinski *et al.*, 2001)

Each library should contain diverse structures and differ from other libraries. The following diversity libraries were used: ChemDiv (10,000 compounds), ChemBridge (5,000 compounds), Enamine (10,000 compounds) and ChemDiv Protein-Protein Interaction (PPI; 5,000 compounds). Furthermore, an additional library was used that consists of FDA approved drugs (Prestwick library, 1,280 compounds; Prestwick Chemical, Illkirch, France). Compounds were reordered from the respective company as powder stocks and dissolved to a concentration of 10 mM in deuterated DMSO (DMSO D6). Aliquots were frozen and stored at -80 °C.

2.18.3.2 Performance and evaluation of High-Content Screening

Due to the imaging settings, it was not possible to image all of the 31,280 compounds. For recording pictures, the high numerical aperture (NA) objective has to come very close to the plate, which is not possible on the plate edge. Therefore, in order to identify small molecules that inhibit the EpCAM signaling cascade, only 26,000 compounds were screened. HEK293 EpCAM-CTF-YFP cells were automatically seeded (ELX406 plate washer and dispenser, BioTek, Winooski, USA; 3,000 cells in 50 µL/well) on 10 % (w/v) PDL-coated 384-well plates. In the initial HCS, compounds were tested at a concentration of 8 µM (0.8 % DMSO). Compound-treated cells were incubated o/n at 37 °C. Afterwards, cells were stained with Hoechst33342 (1:1000 in Complete medium) and 3.5 µg/mL CellMask™ Deep Red Plasma membrane Stain (Invitrogen) and fixed with 2 % (w/v) paraformaldehyde (PFA) solution. Cells were imaged with Operetta High-Content-Imaging System (Perkin Elmer) at 40x magnification and confocal imaging method, and results were evaluated with the Harmony High Content Imaging and

Analysis Software version 3.5.2. With the help of this software, different cell regions were defined: the median of the YFP intensity within these regions was calculated and compared to the one of the DMSO treated negative control. If the intensity exceeded a predefined threshold, the respective compound was regarded as hit. 128 hits were defined as primary hits and were subsequently tested in a five-point (80-5 μM) and ten-point (80-0.15 μM) titration. Results were evaluated in the Microsoft Excel program. In order to determine the quality of the HCS, the Z-factor was calculated. Thereby, the mean and the standard deviation of the positive control are compared to the mean and the standard deviation of the negative control. If $0.5 < \text{Z-factor} < 1$, the assay results are considered to be excellent.

Autofluorescence of the compounds was assessed as described earlier in this chapter. However, YFP-negative HEK293 EpCAM-FL cells were used instead. The absence of YFP in these cells was confirmed by FACS (see 2.18.4)

2.18.4 Fluorescence-activated cell sorting (FACS) experiments

Cells that were analyzed by FACS in this study were either expressing YFP or stained with a FITC-conjugated antibody. Cells were harvested as previously described (see section 2.18.1). The cell number was determined, 5×10^5 cells were transferred to a new tube, centrifuged (1,500 rpm, 5 min), resuspended in 1x PBS and measured with a BD LSR II Flow Cytometer (BD Biosciences). In case of staining with an antibody, cells were washed once with 1x PBS and then incubated with the antibody diluted in 1x PBS (1:200) for 30 min at RT in the dark. The cells were washed once again and then resuspended in 1x PBS and transferred to FACS measurement. The results were evaluated with the FlowJo program version 10.0.8.

2.18.5 Viability/toxicity Assay

Viability, toxicity and apoptosis of compound-treated cells were assessed using the ApoTox-Glo™ Triplex Assay (Promega, Madison, USA). Cells were automatically seeded on 384-well plates (5,000 cells in 50 μL /well), treated with compounds and incubated at 37 °C o/n. Viability/Cytotoxicity Reagent and Caspase-Glo® 3/7 Reagent were prepared according to manufacturer's instructions. 5 μL Viability/Cytotoxicity reagent were added per well and plates were again incubated for 30 min at 37 °C. Then, fluorescence was measured at 400_{Ex}/505_{Em} (viability) and 484_{Ex}/520_{Em} (cytotoxicity) in EnVision plate reader (Perkin Elmer). After adding 25 μL Caspase-Glo® 3/7 Reagent per well, plates were incubated for 30 min at RT in the dark and luminescence was measured. To evaluate the toxicity of the compounds, the measured intensities were related to the DMSO control using the program Microsoft Excel.

2.18.6 Proliferation Assay

Cells were harvested as previously described (see section 2.18.1) and seeded onto 96-well plates. After 6 h, one row was stained with 0.25 μ L Hoechst33342 and imaged with Operetta High-Content-Imaging System (Perkin Elmer). Afterwards, medium was removed and new medium containing the compounds or controls was added. Every 24 h, one row was stained with Hoechst33342 and imaged (D0-D7). Results were evaluated with the program Microsoft Excel.

2.19 Biochemical methods

2.19.1 Membrane-based cleavage assay

For the analysis of EpCAM cleavage products, membrane-based cleavage assays were performed. Cells were grown to confluence in cell culture dishes. Subsequently, cells were washed twice with ice cold 1x PBS, harvested by using a cell scraper and transferred to a new 15 mL reaction tube. After one more washing step, cells were homogenized in 1 mL homogenisation buffer by douncing them 10 times with a micro-lance 3/23G 1.25'' syringe (Becton Dickinson, Franklin Lakes, USA). The homogenized cells were centrifuged (1,000 x g, 15 min, 4 °C) and the post nuclear supernatant containing membranes, proteins and small organelles was transferred into a new reaction tube. Another centrifugation step was performed (16,000 x g, 20 min, 4 °C) to pellet the membranes. The supernatant was discarded and pellets were washed with 500 μ L homogenisation buffer. Finally, pellets were resuspended in 100 μ L assay buffer containing compounds in the desired concentration and incubated o/n at 37 °C. Subsequently, samples were further processed as described below in 2.19.2 and 2.19.4.

2.19.2 Preparation of whole cell lysates

Cells were harvested as described in section 2.18.1. Afterwards, lysis buffer was added and cells were incubated for 30 min on ice while vortexing every 10 min. After centrifugation (16,000 x g, 20 min, 4 °C), the protein containing supernatant was transferred into a new tube and stored at -20 °C until further use.

2.19.3 Determination of protein concentration

For the determination of the protein concentration in cell lysates and membrane fractions, respectively, the Pierce™ BCA Protein Assay Kit (Thermo Fisher Scientific) was used. The BCA Working Reagent and diluted bovine serum albumin (BSA) standards were prepared according to manufacturer's instructions. 100 μ L Working Reagent and 5 μ L sample or BSA standard were mixed and incubated for 15 min at 37 °C. A_{562} was measured for all samples and standards with GeneQuantPro spectrophotometer (GE

Healthcare). Background levels of Working Reagent-only samples were subtracted. All measurements were performed in triplicates.

2.19.4 Western blot

For whole cell lysates and membrane fractions, 20 µg and 2 µg of protein were loaded onto a 12 % SDS-PAGE (see section 2.16) and separated for 15 min at 30 mA and 2 h at 30 mA. For protein MW estimation, the Cozy™ Prestained Protein Ladder (highQu, Kraichtal, Germany) was used. Afterwards, proteins were transferred onto a methanol-equilibrated PVDF blotting membrane (Immobilon-P) at 100 V for 50 min. To prevent unspecific binding, the membrane was incubated in 5 % (w/v) milk powder/washing buffer for 30 min at RT in a rolling device. Subsequently, the blot was incubated with the respective primary antibody diluted in Primary antibody solution o/n at 4 °C. For removal of unbound antibody, the membrane was washed with washing buffer for 30 min. The secondary antibody was diluted in the secondary antibody solution and was incubated with the blot for 30 min at RT, followed by washing for 30 min. Protein bands were detected by incubation with HRP substrate and imaging with ImageLab software version 5.2.1 (Biorad). Analysis and quantification of protein bands was also done with the ImageLab software. For statistical analysis, the paired-sample t-test was applied and statistical significance was determined by a p-value.

2.19.5 Determination of hEpCAM cleavage sites

For the determination of the cleavage sites, HEK293 EpCAM-CTF-YFP cells were grown to confluence in T175 cell culture flask. Afterwards, the medium was replaced by medium containing compound or DMSO. To have a sufficient amount of protein, two T175 cell culture flasks were used and pooled per sample.

2.19.5.1 Determination of γ -cleavage sites

24 h after the replacement of the medium, the supernatant was collected for Myc-immunoprecipitation (IP). 50 mL of supernatant were mixed with 30 µL Myc-beads (Biomol GmbH, Hamburg, Germany) and incubated o/n at 4 °C on a rolling device. Subsequently, the supernatant was centrifuged (2,500 x g, 5 min, 4 °C), washed three times with 1x PBS buffer and twice with ddH₂O (300 x g, 2 min, 4 °C). After that, proteins were eluted in 10 µL acetonitrile (Sigma) and ddH₂O saturated with α -cyano-4-hydroxy-cinnamic acid (Sigma) and analyzed with MALDI-TOF mass spectrometry on an Ultraflex Extreme mass spectrometer (Bruker Daltonics, Bremen, Germany). Peptides were measured in a range of 3,000 – 5,000 m/z, protein fragments in a range of 10,000 – 100,000 m/z. Single spectra were accumulated for better visualization. Spectra were smoothed and baseline subtracted for further evaluation using flexAnalysis software version 3.4 (Bruker).

2.19.5.2 Determination of ϵ -cleavage sites

Cells were harvested in 4 mL lysis buffer_IP (see Table 2-17) by scratching and incubated on ice for 30 min with extensive pipetting every 10 min. Cell lysate was centrifuged (20,000 x g, 10 min 4 °C), the supernatant transferred into a new falcon and 0.6 x vol. of dilution buffer was added. 20 μ L pre-equilibrated GFP-Trap®_A beads (Chromotek, Planegg, Germany) were added and incubated for 4 h at 4 °C on a rolling device. After washing the beads three times with 1x PBS and two times with ddH₂O (2,500 x g, 2 min, 4 °C), proteins were eluted with 40 μ L elution buffer_IP on ice for 20 min. After centrifugation (280 x g, 5 min, 4 °C), eluted proteins were transferred into a new tube and neutralized by 200 μ L Tris/HCl (100 mM, pH 8.0). Subsequently, 10 μ L TEV buffer, 0.75 μ L DTT (1 M) and 3 μ L TEV protease (2 mg/mL) were added and incubated at 4 °C o/n. Afterwards Flag-beads (Sigma-Aldrich) were added und incubated for 4 h at 4 °C. All following steps were performed as described previously (see section 2.19.5.1).

3 Results

3.1 Structure determination of the nuclear complex

The EpCAM signaling cascade plays an important role since it has a stimulating effect on the cell cycle and cell proliferation (Munz *et al.*, 2004). Furthermore, EpCAM-positive cells have a tumorigenic effect in immunodeficient mouse models (Maetzel *et al.*, 2009). Thereby, EpCAM is sequentially cleaved by TACE and γ -secretase, which eventually results in the release of EpICD into the cytoplasm. EpICD forms an intracellular complex with FHL2, β -catenin and Lef-1. This complex is translocated into the nucleus, where it activates the transcription of EpCAM target genes (Maetzel *et al.*, 2009). The goal of this part of the project was to confirm the already published interaction between EpICD, FHL2 and β -catenin (Maetzel *et al.*, 2009) and afterwards to solve the structure of this complex and identify the key elements responsible for this interaction. After characterization of the binding site, small inhibitory molecules could be designed (structure-based drug design) that prevent the formation of the nuclear complex and thereby inhibiting the intracellular EpCAM signaling cascade.

3.1.1 Expression and purification of FHL2 and EpICD

For all interaction studies, FHL2 derivatives (FHL2 LIM1-2 (17 kDa), FHL2 LIM2-3 (13 kDa), FHL2 LIM3-4 (13 kDa) and FHL2 FL (32 kDa)) were cloned and expressed as described in sections 2.12.1 and 2.14.1. To achieve the best stability and yield of the purified proteins, several purification procedures and tags were tested (Figure 3-1). Initially, FHL2 FL was purified with a GST-tag (26 kDa). This protein was well expressed, soluble and could be enriched using a GSTrap column. However, after the removal of the GST-tag the protein was degraded leading to a very poor yield after SEC (Figure 3-1A). Replacing the GST-tag by an MBP-tag (42 kDa) did not overcome this problem. Although the protein was well expressed, soluble and could be enriched using an amylose resin, it still became degraded and also partially precipitated after the removal of the MBP-tag. The result was again a very poor yield after SEC (Figure 3-1B). Hence, it was decided to purify FHL2 FL without removal of the tag. Furthermore, the stability of the protein was improved by adding a His-tag to the carboxy-terminus. By adding ZnCl_2 to the growth medium, the expression level and also the yield could be substantially improved for both GST-FHL2 FL (58 kDa) and MBP-FHL2 FL (74 kDa). Both proteins were stable and the achieved purity was $\geq 90\%$ (Figure 3-1C). Here, removal of the tag was only possible by the addition of 0.1% (v/v) Triton to the dialysis buffer. Yet, the ZnCl_2 containing protein still was degraded after the removal of the tag (Figure 3-1D). FHL2 FL for expression in insect cells was cloned and ex-

pressed as described in 2.14.2. This protein also showed good expression, solubility and could be enriched using an amylose resin. During concentrating, the protein already precipitated at very low concentrations. Therefore, it was not possible to perform a SEC, which is why buffer exchange and concentration of the protein was done by adding 25 % or 50 % glycerol to the dialysis buffer. The purified protein was stable and pure ≥ 85 % (Figure 3-1E).

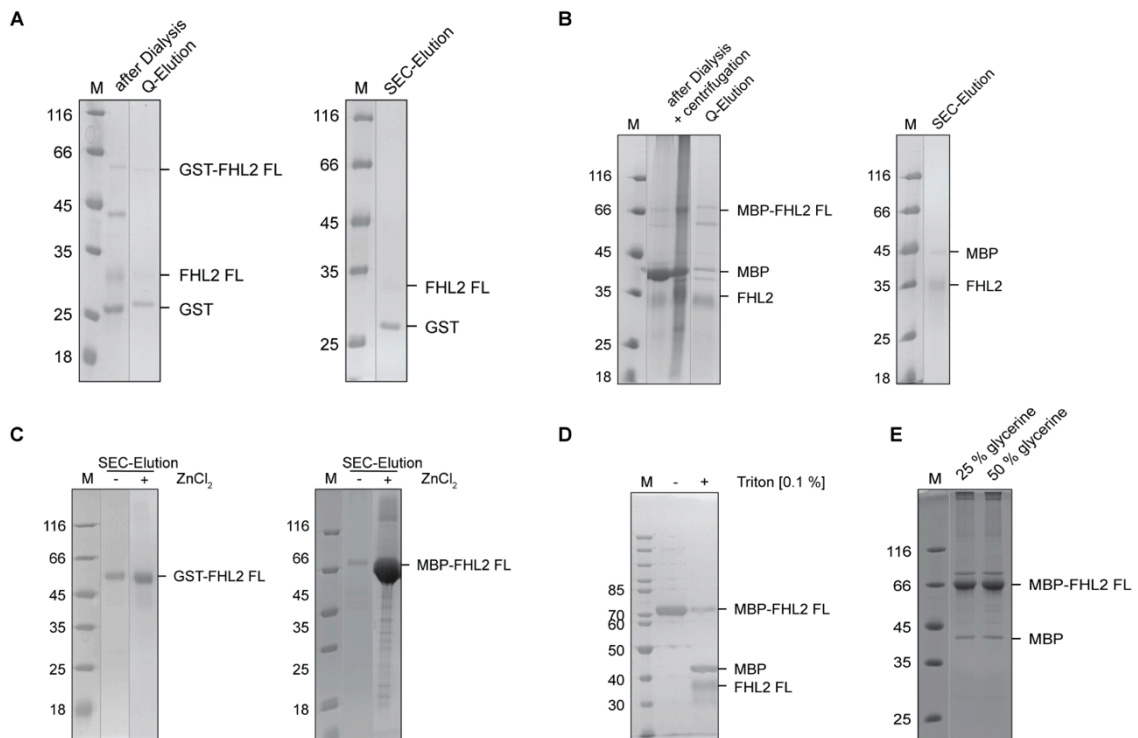


Figure 3-1 Purification procedures and tags of FHL2 derivatives. (A) Purification of GST-FHL2 FL (58 kDa). After the removal of the tag, the protein is degrading. (B) Purification of MBP-FHL2 FL (74 kDa). The protein also degrades after removal of the tag. (C) After adding ZnCl₂ to the expression, the yield of both proteins could be clearly improved. (D) Removal of the tag of ZnCl₂ containing proteins was only possible after the addition of Triton but still led to degradation of the protein. (E) MBP-FHL2 FL expressed in insect cells was concentrated by using glycerol.

The different LIM-constructs were purified according to the FL protein with the respective tag. All of the GST-LIM constructs were well expressed and showed good solubility. After the final purification step by SEC, quality and purity of all proteins were assessed via SDS-PAGE. Purified GST-LIM1-2 was stable and a purity of ≥ 90 % was achieved. Purified GST-LIM2-3 showed slight degradation and purity of ≥ 90 %. The yield of GST-LIM3-4 was comparatively poor. The protein showed a rather strong degradation and a purity of ≥ 90 % (Figure 3-2A-C). Both MBP-LIM1-2 and MBP-LIM2-3 showed good expression but were not completely soluble. After enrichment by amylose resin and SEC, both purified proteins were stable and pure (≥ 90 %). MBP-LIM3-4

showed a very strong expression and solubility. The purified protein was also stable and a purity of $\geq 95\%$ was achieved (Figure 3-2D-F).

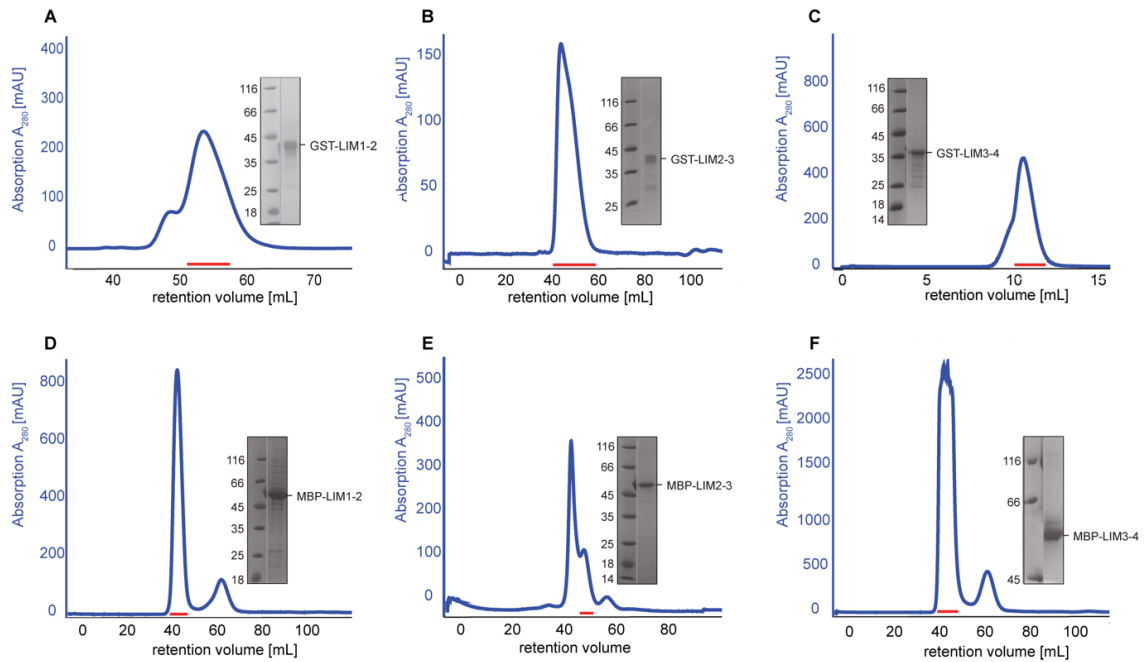


Figure 3-2 Purification of LIM-constructs. (A-F) SEC chromatograms (blue) of the final purification step with Superdex 75 10/300 GL column (C) or HiLoad 16/600 Superdex S75 (A+B, D-F). Peak fractions were analyzed by SDS-PAGE and the best fractions (red dash) were pooled, concentrated and frozen. (A) GST-LIM1-2 (43 kDa). (B) GST-LIM2-3 (39 kDa). (C) GST-LIM3-4 (39 kDa). (D) MBP-LIM1-2 (59 kDa). (E) MBP-LIM2-3 (55 kDa). (F) MBP-LIM3-4 (55 kDa).

Since EpICD already heavily precipitated in the cell pellet, which could not be improved by the addition of arginine to the lysis buffer, it was decided to order a chemically synthesized peptide. Hachmeister *et al.*, 2013 showed that EpCAM-CTF cleavage results in different EpICD variants of which the one consisting of 28 AA (starting with V288 I289) is the most stable one. Therefore, it was decided to order this EpICD fragment N-terminally fused to a 3x FLAG-tag (6 kDa).

3.1.2 Expression and purification of β -catenin

For interaction studies, β -catenin (138-781; 82 kDa) was cloned and expressed as described in sections 2.12 and 2.14.1. The protein was well expressed, soluble and was enriched using a nickel-affinity column. After removal of the His₆-SUMO tag, the protein (70 kDa) remained stable. After SEC, the purified protein was stable and pure ($\geq 90\%$; Figure 3-3). Since purified β -catenin precipitated after freeze and thaw cycles, it had to be freshly purified for every interaction study.

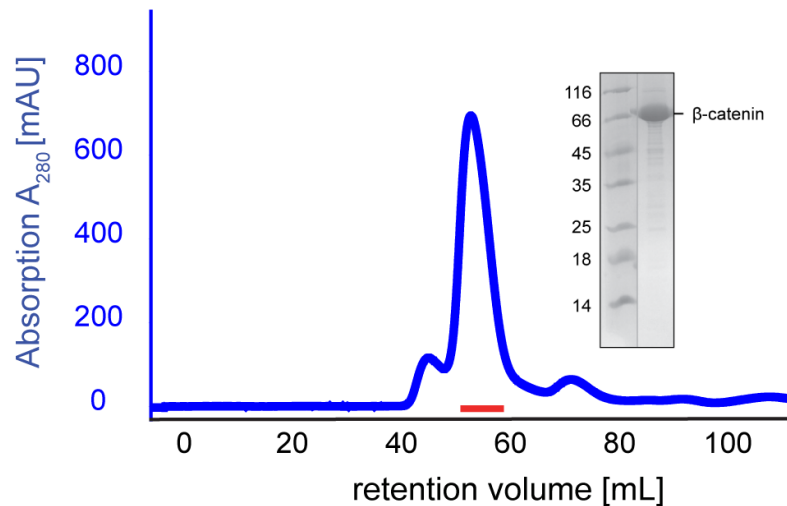


Figure 3-3 Purification of β -catenin. SEC chromatograms (blue) of the final purification step with HiLoad 16/600 Superdex S75. Peak fractions were analyzed by SDS-PAGE and the best fractions (red dash) were pooled, concentrated and directly used for interaction studies.

3.1.3 *In vitro* pull-down experiments with FHL2, EpICD and β -catenin

Yeast two-hybrid screens and immunoprecipitation experiments have already shown an interaction between FHL2 and EpICD. β -catenin was identified as member of the nuclear complex as well (Maetzel *et al.*, 2009). In order to reconfirm the already published interaction between FHL2, EpICD and β -catenin *in vitro* and to show a direct interaction, *in vitro* pull-down experiments were carried out. Since MBP-tagged FHL2 FL protein did not bind to the amylose resin (Figure 3-4A), the GST-tagged version was used. Pull-down experiments with either FHL2 FL and EpICD or β -catenin were performed. GST-FHL2 FL and either 3x FLAG EpICD or untagged β -catenin were mixed with GSH-beads, washed and the bound proteins were eluted with GSH and visualized and analyzed via SDS-PAGE. However, none of these experiments showed a direct interaction between these proteins (Figure 3-4A+B). To check whether posttranslational modifications are required for an interaction of FHL2 FL and EpICD, pull-down experiments with MBP-tagged FHL2 FL purified from insect cells and 3x FLAG-tagged EpICD were carried out. Both proteins were mixed with anti-FLAG beads, washed and the bound proteins were eluted by heating in SDS-containing buffer and visualized by SDS-PAGE. Small amounts of FHL2 FL could be found in the elution fraction; however, the same effect could be seen in the negative control. This indicates that FHL2 FL found in the elution fraction is due to unspecific binding of MBP-FHL2 FL to the anti-FLAG beads. The two additional bands in the elution fraction very likely correspond to the heavy chain (50 kDa) and the light chain (23 kDa) of anti-FLAG antibodies (Figure 3-4C).

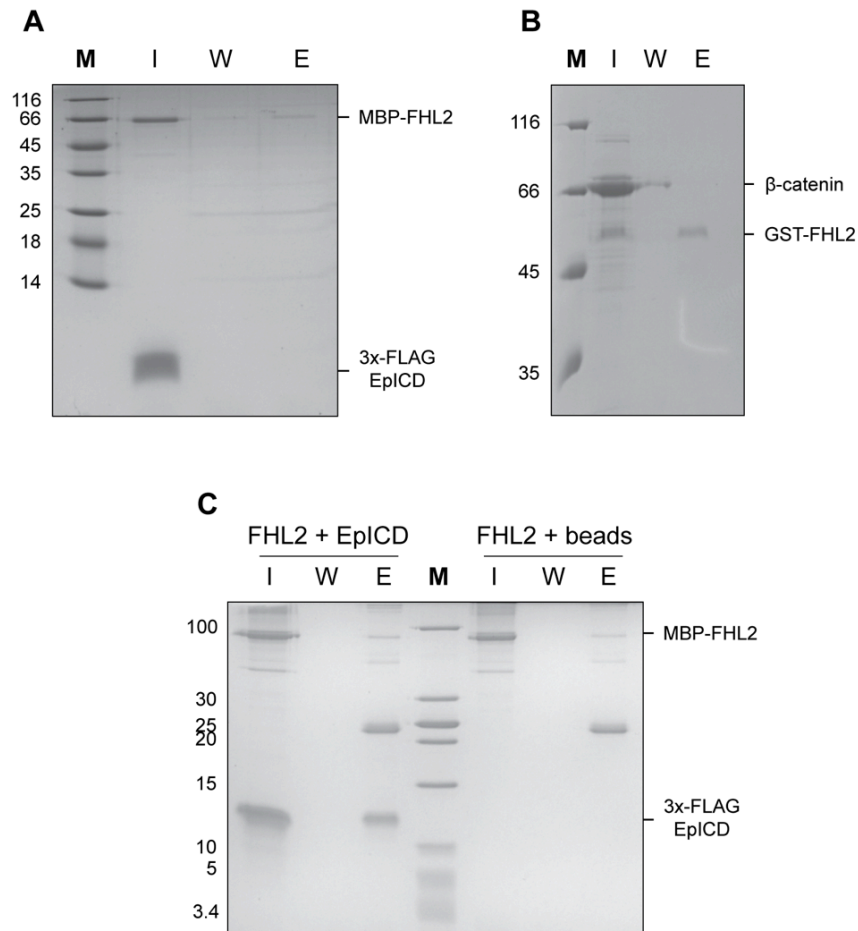


Figure 3-4 Pull-down experiments with FHL2, β -catenin and EpICD. *In vitro* pull-down assays were performed with MBP-FHL2 and EpICD (**A**), GST-FHL2 and β -catenin (**B**), and insect cell MBP-FHL2 and EpICD (**C**). None of these assays showed an interaction. I: input; W: wash; E: elution.

3.1.4 ITC experiments with FHL2, EpICD and β -catenin

Since the interaction between FHL2 and EpICD or β -catenin could be transient and thus not detectable by pull-down experiments, ITC was used to further investigate this possible interaction. By titrating 200 μ M EpICD into 20 μ M FHL2, no interaction could be detected (Figure 3-5A). One potential scenario is that the binding of EpICD and β -catenin is a prerequisite for the interaction with FHL2. Therefore, 200 μ M EpICD was titrated into 20 μ M β -catenin. However, no interaction could be detected either (Figure 3-5B). Next, a possible interaction between FHL2 and β -catenin was assessed. 90 μ M FHL2 was titrated into 7 μ M β -catenin. In doing so, an interaction of these two proteins could be detected, revealing a $K_d \approx 1.08$ μ M and a stoichiometry of FHL2 : β -catenin = 1.06 ± 0.09 (Figure 3-5C). Since β -catenin already starts precipitating at even low concentrations, it was not possible to conduct this experiment with higher concentrations. To verify that this result is not due to binding of β -catenin to the MBP-tag, 70 μ M MBP was titrated in 7 μ M β -catenin and no interaction could be detected. Since the

FHL2- β -catenin interaction could be a prerequisite for EpICD-binding to the complex, FHL2 and β -catenin (11 μ M) were pre-incubated before 110 μ M EpICD was added. However, no interaction could be detected (Figure 3-5D).

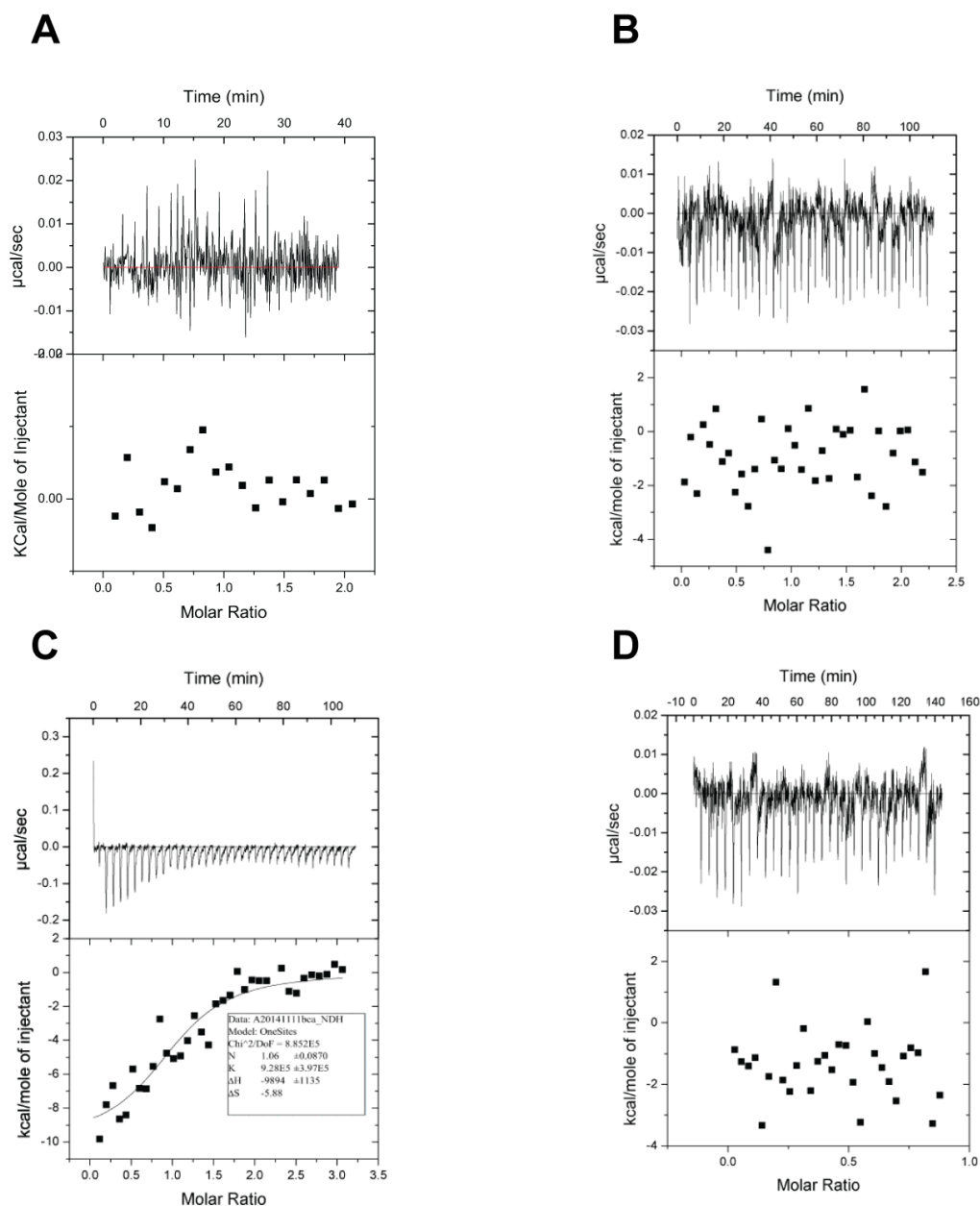


Figure 3-5 ITC experiments with β -catenin, FHL2 and EpICD. In order to identify a possible interaction, ITC experiments with EpICD and FHL2 (A), EpICD and β -catenin (B), FHL2 and β -catenin (C), and EpICD and FHL2- β -catenin (D) were performed. Only for FHL2 and β -catenin, an interaction could be shown, revealing a $K_d \approx 1.08 \mu$ M and a stoichiometry of 1:1.

To further analyze the observed FHL2- β -catenin interaction, different FHL2-constructs containing diverging sets of LIM-domains (see section 3.1.1) were planned to be tested. Since, on the one hand the GST-tagged constructs precipitated at a comparatively low concentration ($\approx 25 \mu$ M) and on the other β -catenin showed an interaction with GST, it was decided to perform these experiments as MBP-tagged fusion proteins.

However, it was not possible to obtain evaluable results. This was probably due to the already mentioned precipitation of β -catenin at very low concentrations. Another explanation might be the formation of bubbles induced upon the contact of the cold sample (β -catenin) and the warm cell walls.

3.2 Identification of a small inhibitory molecule of the EpCAM-signaling cascade

On healthy, polarized epithelial cells, EpCAM is predominantly found at basolateral membranes, whereas on tumor (-initiating) cells, EpCAM is highly overexpressed and re-distributed all over the cell surface. Therefore, EpCAM is much less accessible on normal epithelial cells, which makes it a very attractive target for immunotherapy. However, the non-tumor specific expression might also cause side effects in EpCAM-directed immunotherapy (Baeuerle and Gires, 2009; Balzar *et al.*, 1999; Munz *et al.*, 2010). Therefore, targeting the intracellular EpCAM-signaling might reveal a more specific way for treatment of EpCAM-positive cancers. Hence, the aim of this part of the project was the establishment and performance of a cell-based HCS and a subsequent analysis and characterization of the potential hits in order to obtain a possible lead compound for the development of a pharmaceutical drug.

3.2.1 Principle of the High-Content Screening

HCS is a phenotypic screen used in drug discovery for the identification of small inhibitory molecules, which change the spatial and temporal distribution of e.g. a target protein in a desired manner (Giuliano KA and Haskins JR, 2010; Haney, 2008). For the here-performed screening, human embryonic kidney 293 (HEK293) wild-type cells were stably transfected with hEpCAM-CTF C-terminally fused to YFP. This hEpCAM-CTF-YFP construct allows for the spatial detection of EpCAM-CTF-YFP and its cleavage product EpICD-YFP within the cell (Figure 3-6A). The CTF-fragment was chosen to exclude hits, which target the ADAM17 cleavage because inhibition of this step would not be specific for EpCAM (Figure 3-6A, centre scheme). Treatment of the cells with compounds could have three possible effects: i) the compound does not affect the EpCAM-signaling cascade and therefore no accumulation of YFP would be visible (Figure 3-6B, left), ii) the compound inhibits hEpCAM-CTF-YFP cleavage and thereby leads to accumulation of hEpCAM-CTF, which would be recognizable by cortical cell staining (Figure 3-6B, middle) or iii) the compound leads to accumulation of the intracellular fragment hEpICD-YFP, which would cause completely green shining cells (Figure 3-6C, right). If the cells are treated with a compound that has an effect on the intracellular EpCAM-signaling cascade, there will be accumulation of YFP-fluorescence intensity at the cell membrane, in the cytoplasm or in the nucleus. The fluorescence

intensity is calculated separately for each cell region by the Harmony High-Content Imaging and Analysis Software and is compared with the intensity measured in the respective region in the DMSO control (negative control). If the intensity in the compound-treated cells exceeds a certain predefined threshold, then this compound will be regarded as a hit.

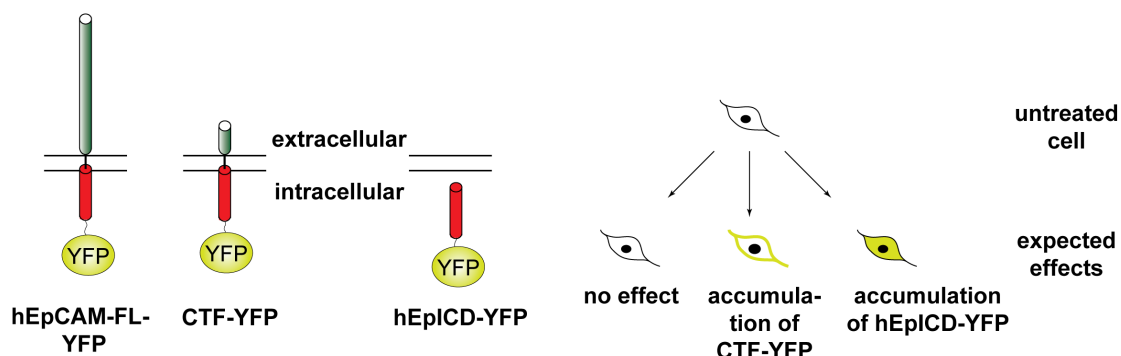


Figure 3-6 Principle of High-Content Screen (HCS) and possible effects. (A) HEK293 cells expressing hEpCAM-CTF-YFP (middle) were used for the performance of the HCS. Due to the fusion of YFP to the carboxy-terminus of EpCAM, it is possible to determine the localization of EpCAM within the cell. (B) Treatment of cells with compounds could have no effect at all (left), lead to accumulation of hEpCAM-CTF-YFP (middle) or to accumulation of hEplCD-YFP (right).

3.2.2 Image Analysis

In order to calculate the YFP intensities in the different cell regions and to compare them with the negative control, the images had to be quantitatively analyzed. Due to the staining of the cells (see section 3.2.3.1), the analysis software was able to distinguish between three different subcellular compartments: nucleus, cytoplasm and membrane. The image analysis comprised several steps. Based on the input image, the cells were detected through Hoechst33342 staining. All nuclei that did not meet certain criteria regarding roundness and shape were excluded from further analysis (marked red on the image). Afterwards, the cytoplasm was determined through CellMask staining. Based on this now defined cell structure and the selected population, three subcellular compartments were selected: nucleus, cytoplasm, and membrane. Subsequently, YFP-intensities were calculated for all three subcellular compartments (Figure 3-7). Since not all of the compartments had the same size and not all of the analyzed images showed the same number of cells, the YFP-intensities were normalized to region size and number of cells. Every pixel in a specific region has a given intensity. All these intensities in this region were summed and then divided by the number of pixels composing the region. This was done for every object in the image, i.e. for every cell included in the population. These values were summed and then divided by the number of objects in the image. This calculation procedure provided values that were normal-

ized to the region size (dividing the value for the region by the number of pixels) and the number of cells (dividing the summed values of all regions by the number of cells).

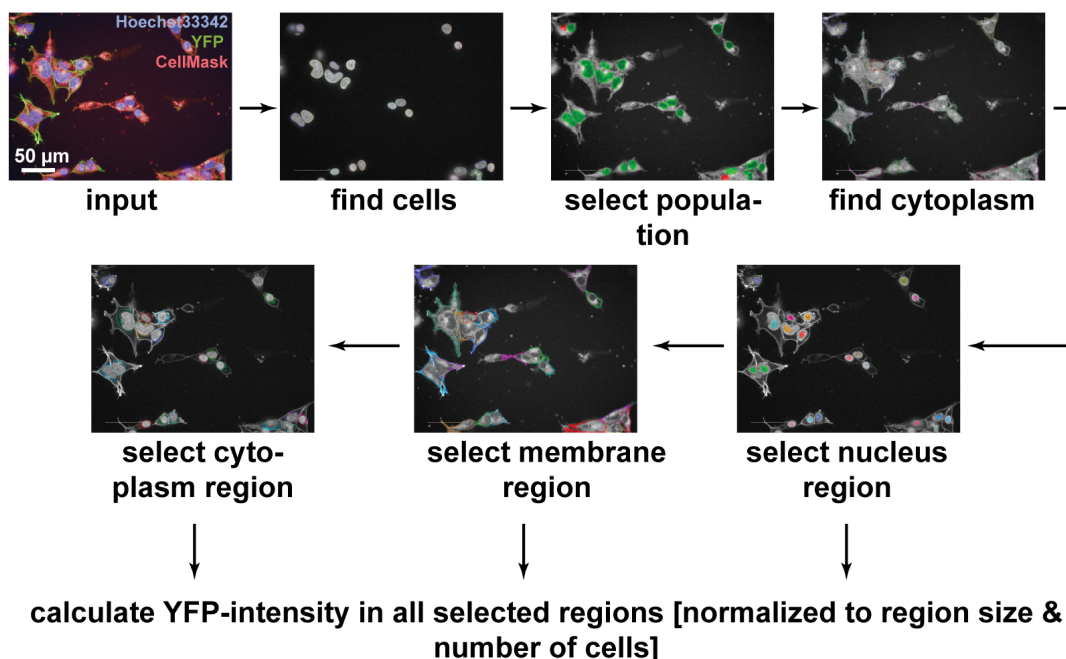


Figure 3-7 Image analysis. According to the nuclear staining by Hoechst33342 (blue) and cytoplasmic staining by CellMask (red), the cells were identified, the population was selected and the cytoplasm was defined by the analysis software. Subsequently, the nuclear region, membrane region and cytoplasmic regions were selected and the fluorescence intensities were calculated for each region (normalized to region size and number of cells). Scale bar represents 50 μm.

Sometimes nuclei are located close to the membrane of the cells. This may result in wrongly included parts of the membrane region to the nucleus region, which would lead to a higher intensity in the nucleus region. Therefore, it was decided that only the inner 40 % of the nucleus should be included into the nucleus region. This led to smaller ratios compared with the negative control, which rather corresponded to the observations on the images. The same process was done for the cytoplasm region.

3.2.3 Establishment of a High-Content Screening

For the identification of small inhibitory molecules targeting the intracellular EpCAM signaling cascade, a suitable HCS setting had to be established. Hence, the optimum conditions for imaging (magnification and imaging method), staining of the cells and the optimal cell number per well had to be determined. For both, the establishment and the performance of the HCS, the Operetta High-Content Imaging System and corresponding analysis software provided by Perkin Elmer were used.

3.2.3.1 Determination of optimal staining conditions

To facilitate an automated discrimination between the three different cellular compartments by the software, the cells had to be stained with fluorescent dyes. Cells were

plated on 384-well plates and treated with DMSO (negative control) or the γ -secretase inhibitor DAPT. DMSO does not have any influence on the EpCAM-signaling cascade, whereas DAPT inhibits γ -secretase cleavage and therefore leads to accumulation of EpCAM-CTF at the cell membrane (Maetzel *et al.*, 2009). After staining DMSO- or DAPT-treated HEK293 EpCAM-CTF-YFP cells with DRAQ5 (DNA stain), the software was able to find the nuclei of the cells. However, detection of the cytoplasm was too imprecise in order to obtain reliable results (Figure 3-8A, middle and right pictures). This problem was solved by staining with Hoechst33342 (DNA stain) and CellMask (plasma membrane stain). As a result, the analysis software was able to find both, the nuclei and the cytoplasm (Figure 3-8B, middle and right pictures).

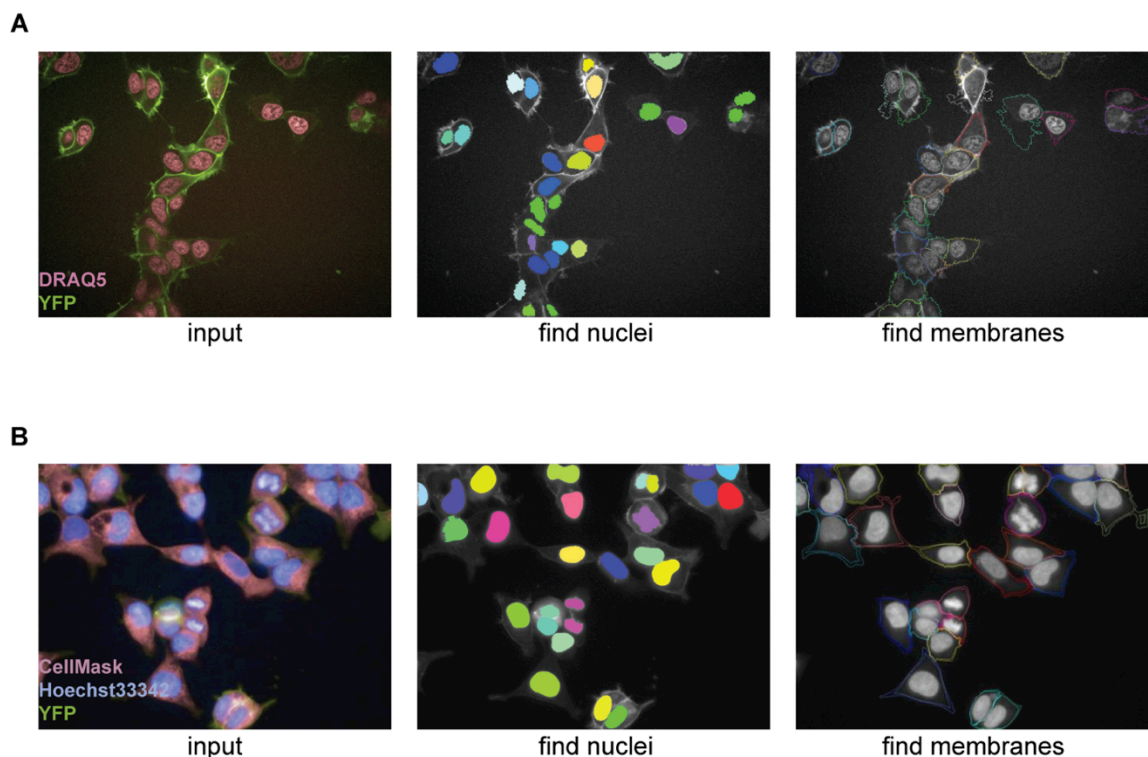


Figure 3-8 Determination of optimal staining method. DAPT-treated HEK293 hEpCAM-CTF-YFP cells were stained with DRAQ5 (red) (**A**) or Hoechst33342 (blue) and CellMask (red) (**B**). Detection of the nuclei was possible with both staining methods (middle pictures) whereas detection of the membranes could only be accomplished after Hoechst33342 and CellMask staining (pictures on the right).

Since the staining of the cells requires a number of additional washing steps and HEK293 cells are prone to surface detachment, the screening plates were coated with poly-D-lysine prior to seeding of the cells.

3.2.3.2 Determination of optimal magnification

For image analysis, it was important that the cells were sufficiently large on the images in order to enable the analysis software to distinguish between different cellular compartments. Additionally, for time limitations it was not possible to image the complete wells but only three sections of each well. Therefore, it was crucial to find a magnifica-

tion, which, on the one hand, would allow for cell analysis and, on the other hand, would cover a sufficiently large area to ensure sufficient cell counts. For the determination of the optimal magnification, HEK293 hEpCAM-CTF-YFP cells were plated on 384-well plates, incubated for 22 h with DMSO or the γ -secretase inhibitor DAPT, stained, imaged at 40x- and 60x magnification and analyzed. DAPT led to accumulation of hEpCAM-CTF-YFP at the cell membrane whereas DMSO did not have any effect on the EpCAM signaling cascade (Figure 3-9). Evaluation showed that imaging at 40x magnification led to bigger DMSO:DAPT ratios for the YFP-intensity in every cell region, which corresponds to the manual analysis of the pictures (Figure 3-9A + B). Furthermore, by using the lower magnification, a bigger area of the well was covered, which reduced the risk of having an image devoid of cells. Comparison of the evaluation of confocal versus non-confocal imaging revealed that non-confocal led to higher ratios (Figure 3-9B + D). However, the differences between the subcellular compartments were considerably smaller.

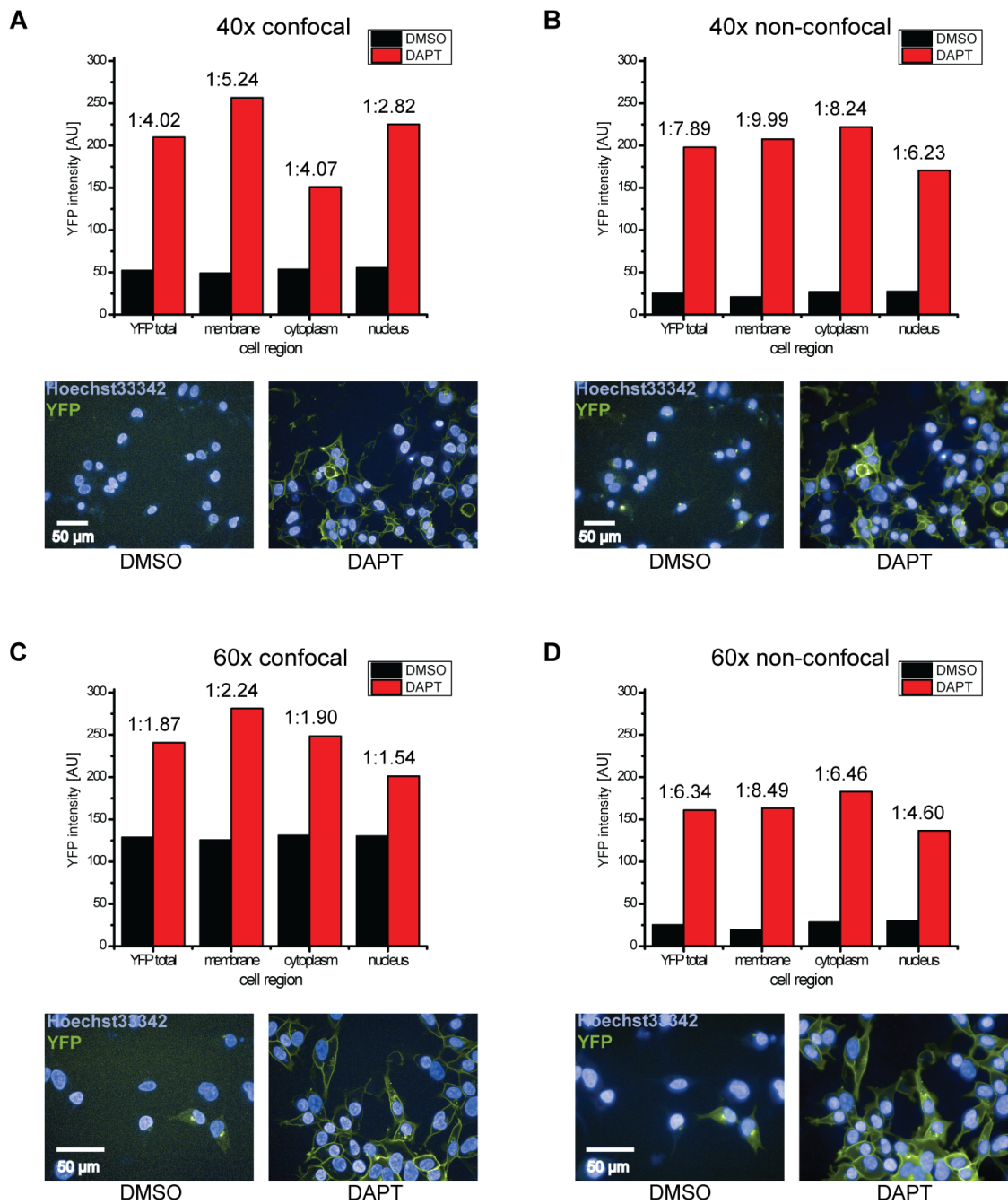


Figure 3-9 Determination of optimal magnification. Pictures and evaluation of DMSO (black) or DAPT (red) treated hEpCAM-CTF-YFP cells imaged at 40x magnification, confocal (**A**) and non-confocal imaging (**B**) and at 60x magnification, confocal (**C**) and non-confocal imaging (**D**). Shown is the YFP intensity for the whole cell (YFP total) and each region after DMSO- and DAPT treatment. Ratio of DMSO:DAPT is depicted above the bars. Scale bar represents 50 μ m. Pictures are taken with auto-contrast.

3.2.3.3 Determination of optimal imaging method

For the identification of the imaging method allowing for the best analysis, HEK293 hEpCAM-CTF-YFP cells were plated on 384-well plates, incubated with DMSO or four different DAPT concentrations, stained, imaged with confocal and non-confocal imaging and analyzed. It was decided to perform this experiment with several DAPT concentrations in order to reveal if our analysis method is sensitive enough for showing a

concentration dependent effect. Treatment with 10 nM DAPT did not have any effect on the cells. After treatment with 20 nM DAPT, YFP-accumulation could be seen in some of the cells. Incubation of cells with 200 nM DAPT showed an even stronger accumulation of YFP when compared to 10 μ M DAPT, which is very likely due to the much higher DMSO concentration (1:50 instead of 1:1,000), which was mistakenly used. The evaluation also showed a concentration-dependent increase in YFP-fluorescence intensity. In images taken with non-confocal imaging, there is no difference in YFP-intensity between membrane, cytoplasm, and nucleus visible. In images taken with confocal imaging, this difference is visible and is also reflected in the evaluation; here, a significant difference in YFP-intensity is detected between membrane and nucleus region ($p < 0.01$) and between cytoplasm and nucleus region ($p < 0.05$).

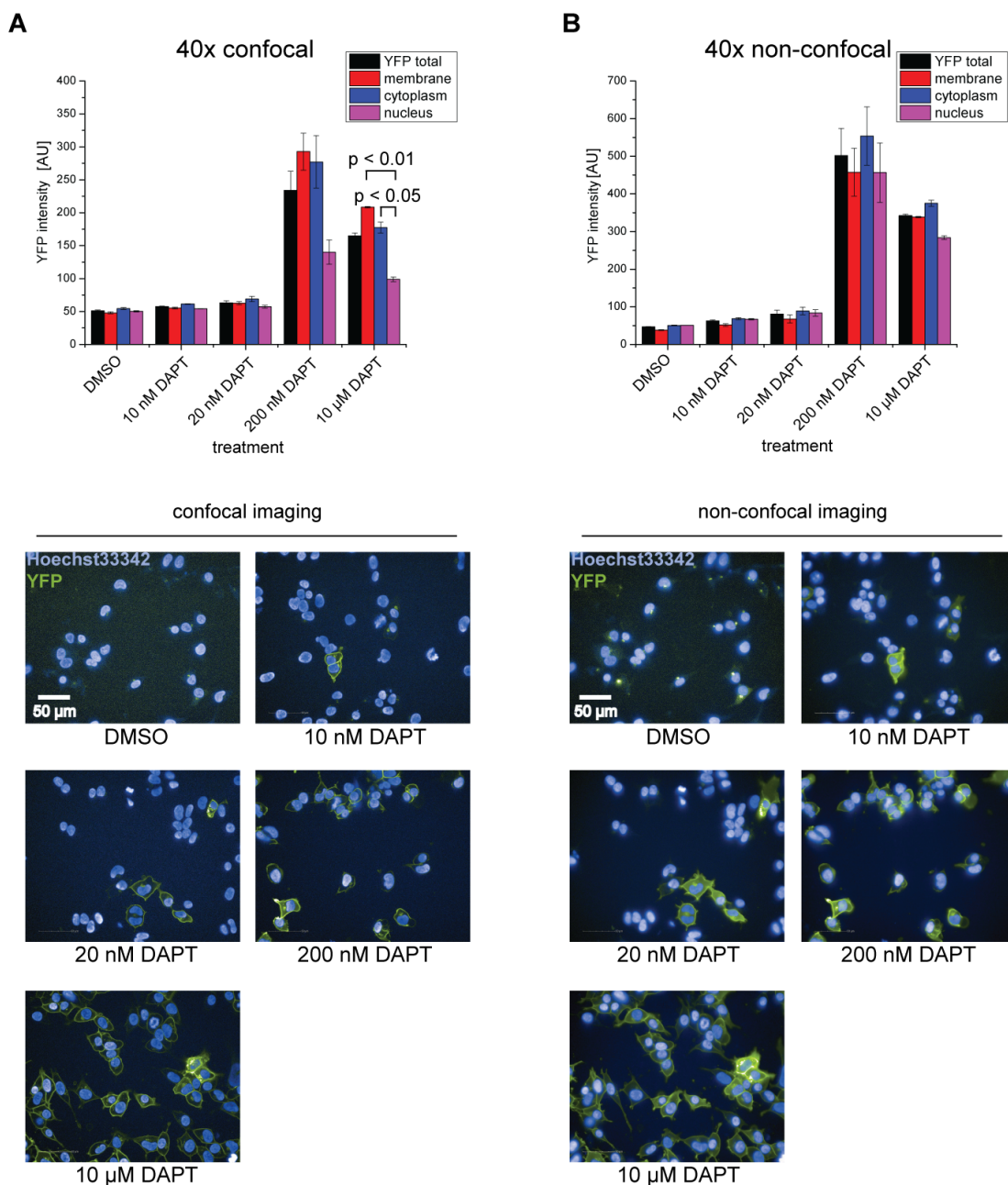


Figure 3-10 Determination of optimal imaging method. Evaluation and pictures of DMSO and DAPT treated HEK293 hEpCAM-CTF-YFP cells at 40x magnification taken with confocal (A) and non-confocal imaging (B). Shown is the YFP-intensity in the whole cell (black), in the membrane region (red), in the cytoplasm (blue) and in the nucleus (purple). Confocal imaging is the only way to show the significant difference in YFP-intensity between membrane and nucleus region and cytoplasm and nucleus region, respectively. Shown are mean values and standard deviations of two independent experiments. Scale bar represents 50 μm . Images are taken with auto-contrast. Statistical analysis was performed using paired-sample t-test. P-values are given above the brackets.

For obtaining bright images, it was necessary to use a high numerical aperture (NA) microscope objective. By using a long working distance objective, the images were pale and blurred, which makes image analysis impossible. The disadvantage of the high NA objective is that the plates' edges could not be visualized and thus compounds in these wells not be evaluated.

3.2.3.4 Determination of optimal cell number

For a proper screening, it was crucial to use cell densities of a sufficient amount of cells for analysis, which simultaneously do not form too large cell clusters. The latter would hamper single cell detection. In order to find the optimal cell number per well, 3,000 or 5,000 HEK293 hEpCAM-CTF-YFP cells per well were plated on 384-well plates, treated with DMSO or DAPT, stained, imaged with confocal imaging and analyzed. Evaluation showed that both cell numbers led to similar results (Figure 3-11A+B). As can be seen in the pictures below (Figure 3-11), plating 5,000 cells per well led to comparably large cell clusters, which complicate detection of subcellular compartments. Therefore it was decided to perform the HCS with 3,000 cells per well.

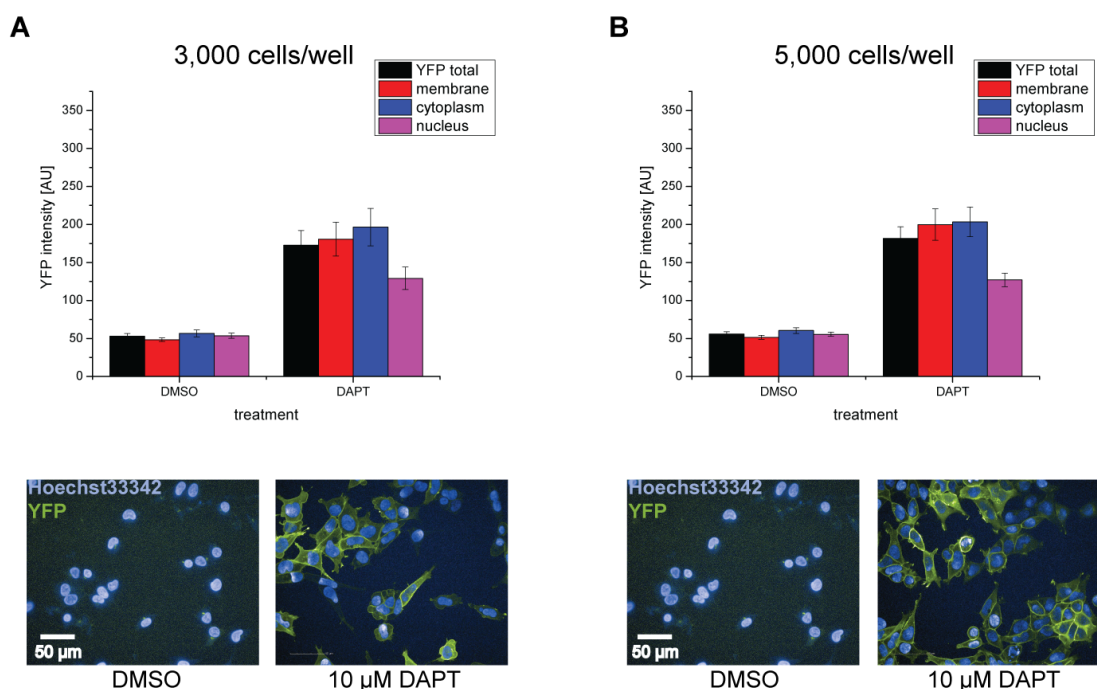


Figure 3-11 Determination of optimal cell number. Evaluation and pictures of DMSO and DAPT treated HEK293 hEpCAM-CTF-YFP cells at 40x magnification taken with confocal imaging. Either 3,000 cells/well (A) or 5,000 cells/well (B) were plated. Shown is the YFP-intensity in the whole cell (black), in the mem-

brane region (red), in the cytoplasm (blue) and in the nucleus (purple). Both cell numbers led to similar results. Shown are mean values and standard deviations.

3.2.4 Performance of High-Content Screening and hit verification

After establishing the HCS, the following conditions were chosen for the performance of the full screening experiment:

- 40x magnification, confocal imaging
- Black 384-well plates coated with poly-D-lysine
- 3,000 cells/well in 50 μ L
- DMSO (1:1000) and DAPT (10 μ M) as negative and positive control, respectively
- Staining with Hoechst33342 and CellMask
- Incubation for 16 h

For the identification of small molecules inhibiting the intracellular EpCAM-signaling cascade, four in-house libraries (ChemDiv, ChemBridge, Enamine and Protein-Protein Interaction) and one commercial library (FDA-approved drugs) were screened. In the screening process each compound was tested in a final concentration of 8 μ M, which corresponds to a final DMSO concentration of 0.8 %. A DMSO killing curve was conducted prior to the screening in order to confirm the nontoxicity of this DMSO concentration (see supplementary data, Figure 6-1). At least 16 plates were imaged at once. Since this process takes several hours, the cells were fixed with paraformaldehyde solution so that all images of all cells are taken at equal status. Out of the 100 screening plates, 66 met the criteria for Z' factor ($0.5 \leq Z' \leq 0.9$). In total, 128 out of 26,000 tested compounds showed an effect on the intracellular EpCAM-signaling cascade, which corresponds to a primary hit rate of 0.49 %. Afterwards, a hit picking campaign was performed for verification of the 128 small molecules. Therefore, these compounds were tested in a five-point serial dilution (80 – 5 μ M final concentration) under the same conditions as in the initial HCS. In doing so, 81 small inhibitory molecules could be confirmed. In order to validate the 81 verified hits, all compounds were re-ordered from the respective suppliers and tested in a ten-point serial dilution (80 – 0.15 μ M final concentration). With this approach, 59 small molecules could be confirmed (Figure 3-12A). Since the read-out of the screen was fluorescence, it was important to exclude false-positive results arising from the autofluorescent compounds. HEK293 cells stably transfected with hEpCAM-FL were subjected to flow cytometry assessment of YFP fluorescence (Figure 3-12B). HEK293 wild-type cells (red) served as reference for YFP-negative cells, HEK293 hEpCAM-CTF-YFP cells (orange) as reference for YFP-positive cells. HEK293 EpCAM-FL cells (blue) did not show any shift compared to the

HEK293 wild-type cells, which confirms that those cells are indeed YFP-negative. HEK293 hEpCAM-FL cells were treated with the respective compounds (80 – 0.15 μ M final concentration) and were analyzed with regard to fluorescence signal. As a result, 51 additional compounds were excluded due to autofluorescence (Figure 3-12A). An example of an autofluorescent hit is given in Figure 3-12C. Both cell lines, YFP-positive (upper panel) and YFP-negative (lower panel) show a fluorescent signal, which decreased when reducing the compound concentration. This indicates that the fluorescence is due to autofluorescence of the compound. Summarizing the HCS campaign, out of 26,000 small inhibitory molecules eight hit molecules were obtained which are likely to target the intracellular EpCAM-signaling cascade (Figure 3-12A).

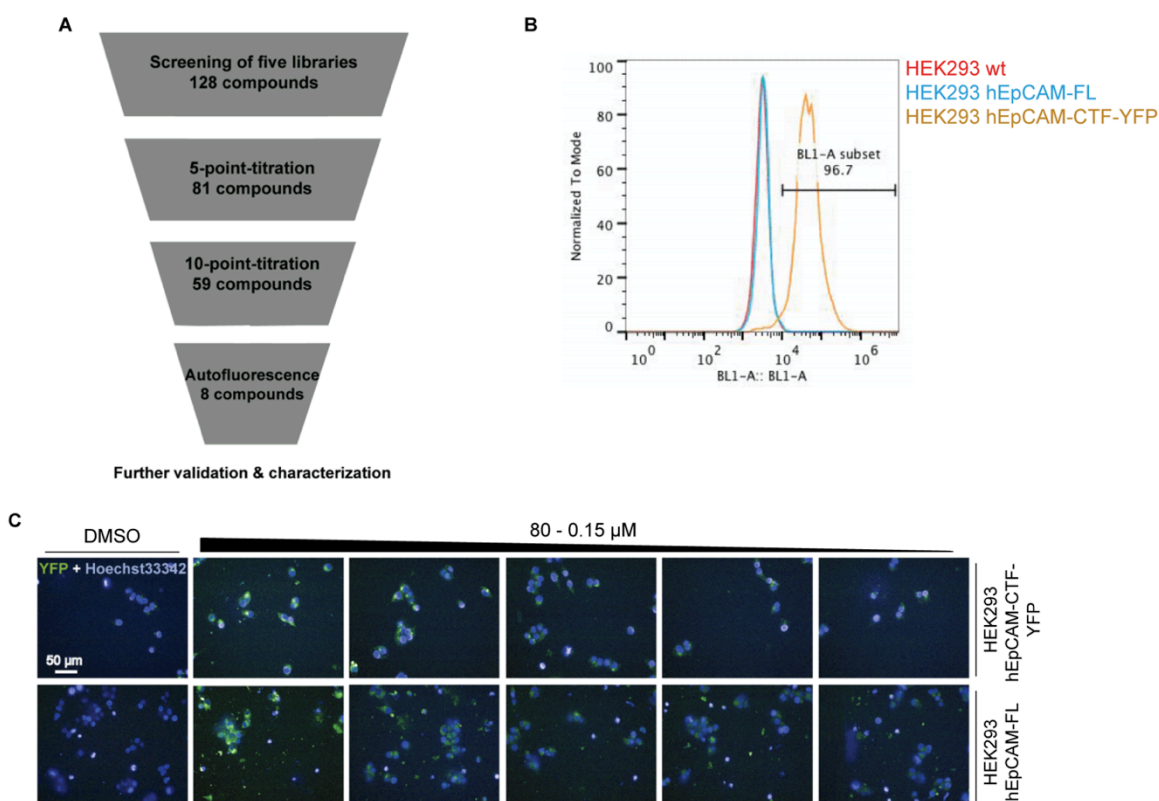


Figure 3-12 Hit verification procedure. (A) Scheme for selecting compound including the number of compounds left as well as the verification procedure leading to exclusion. (B) YFP-fluorescence was assessed by FACS analysis by comparing HEK293 hEpCAM-CTF-YFP cells (orange) with HEK293 hEpCAM-FL cells (blue). HEK293 wild-type cells (red) served as positive control for YFP-negative cells. (C) Example for an autofluorescent compound (compound #12). HEK293 hEpCAM-CTF YFP (upper panel) and HEK293 hEpCAM-FL cells (lower panel) were treated with a ten-point serial dilution of compounds and analyzed with regard to fluorescence. Scale bar represents 50 μ m.

3.2.5 Further characterization of hits

Of the remaining eight compounds, seven compounds showed EpCAM-accumulation at the membrane up to a concentration of 20 μ M (40 μ M for compound #51), only compound #66 showed accumulation in the cytoplasm at a concentration of 80 μ M (Figure 3-13).

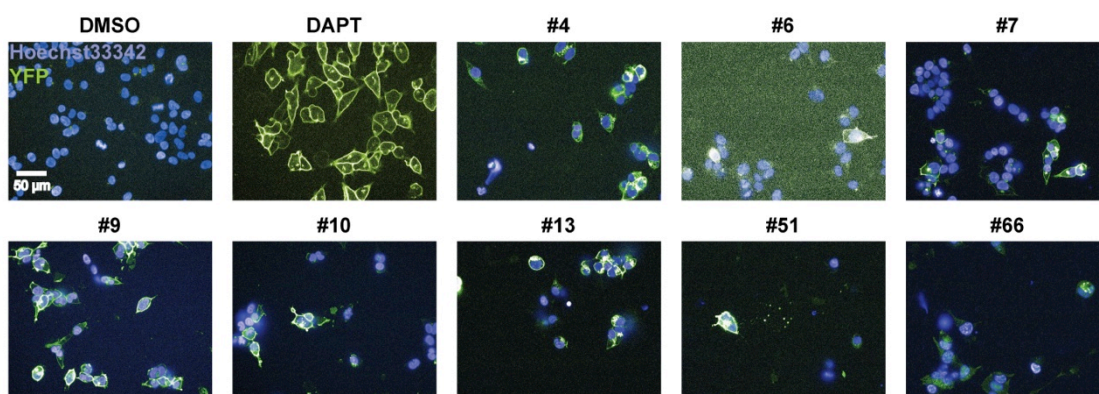


Figure 3-13 Effects of eight high confidence hits on HEK293 hEpCAM-CTF-YFP cells. HEK293 hEpCAM-CTF-YFP cells were treated with DMSO, DAPT or compounds. Pictures of compounds are taken without auto-contrast. Compound used for treatment of the cells is depicted above the respective picture. Scale bar represents 50 μm .

These eight compounds were considered as high-confidence hits and studied further with regards to toxicity, effect on the intramembrane cleavage of hEpCAM, effect on the transcriptional level of EpCAM target genes and effect on cell proliferation. Unless stated otherwise, compounds were tested at 20 μM concentration, since this was the lowest concentration at which most of the compounds showed an effect. All compounds were tested at the same concentration for better comparison.

3.2.5.1 Cytotoxicity of compounds

Since general cytotoxicity of a compound is detrimental to its use as a potential drug, the effects of the eight compounds on viability, cytotoxicity and apoptosis were assessed. For this purpose, the ApoToxGlo-Kit was used, which allows to simultaneously measure cell viability, cytotoxicity and apoptosis within one well and therefore enables the determination of the mechanism of cell death. For the determination of conditions that lead to most reproducible results, different cell numbers, cell plates and positive controls were tested. Since the drug staurosporine is known to be toxic and a potent inducer of apoptosis, it was decided to use it as positive control. After optimization the following conditions were chosen for the performance of the assay:

- Black 384-well plates
- 5,000 cells/well in 50 μL
- DMSO (0.8 %) and staurosporine (80 – 0.15 μM final concentration) as negative and positive control, respectively
- Compounds tested in a ten-fold serial dilution (80 – 0.15 μM final concentration)

For the detection of a potential EpCAM-specific effect, four different EpCAM-positive and –negative cell lines were used. These are EpCAM-negative HEK293 wild-type cells, HEK293-hEpCAM-FL cells, and two endogenously EpCAM-expressing cell lines,

human colon carcinoma cell line HCT-8 and human hypopharyngeal carcinoma cell line FaDu. These cell lines were automatically seeded onto 384-well plates, treated with compound, the drug staurosporine as positive control or DMSO as negative control, and analyzed after 16 h incubation. Results were related to the DMSO control (Table 3-1). The experiment was performed in technical triplicates and was conducted twice. There were no differences in viability, cytotoxicity or apoptosis between the different cell lines, which indicates that there is no EpCAM-specific effect of any compound on cell death. Staurosporine, expectedly, led to a strongly decreased viability (--) and strongly increased cytotoxicity and apoptosis (++) . Compound #7 did not show any effects on the cells, whereas compounds #13 and #66 very strongly impaired cell viability. Compounds #4, #6, #9, #10 and #51 had only minor effects on the cells (for a detailed presentation of the results, see appendix II).

Table 3-1 Effects of compounds on cell viability, cytotoxicity and apoptosis. Results are depicted in comparison to DMSO control. Since there were no differences between the different cell lines, they are not indicated individually. ++: strong increase; +: increase; 0: no difference; -: decrease; --: strong decrease.

Compound No.	Viability	Cytotoxicity	Apoptosis
DMSO	0	0	0
Staurosporine	--	++	++
#4	0	0	+
#6	-	+	+
#7	0	0	0
#9	-	0	0
#10	-	0	0
#13	--	++	+
#51	0	0	+
#66	--	+	--

3.2.5.2 Effects on target gene expression

For the investigation of a possible effect of compound-treatment on EpCAM-target gene transcription, the expression levels of *CCND1*, *MYC* and *EPCAM* were assessed. In order to find an EpCAM-specific effect, HCT-8 wild-type and a CRISPR-Cas9-mediated EpCAM knock-out clone of HCT-8 cells (Tsaktanis *et al.*, 2015; HCT-8 KO) were tested and results were compared. The EpCAM-expression level of these two cell lines was confirmed by FACS-analysis (see supplementary data, Figure 6-2). Both cell lines were manually plated on 6-well plates and incubated with compounds or DMSO

(1:500) or DAPT (10 μ M) as controls for 18 h. RNA was extracted from cell lysates and reversely transcribed into cDNA, which was then used as a template for RT-PCR. Several housekeeping-genes were considered as reference genes and therefore their variations in expression level after compound treatment were assessed. After comparing the c_p -values, it was decided to use GAPDH as reference gene. The experiment was performed in technical triplicates and was carried out five times. Analysis of relative expression levels revealed a significant decrease of *CCND1* expression after treatment with compound #4, #6, #9, #10, #13, #51 and #66 in HCT-8 wild-type cells (Figure 3-14A, left panel). In HCT-8 KO cells, compound #4 and #6 led to a significant decrease of *CCND1* expression level, suggesting an EpCAM-independent effect (Figure 3-14A, right panel). Comparison of expression levels in wild-type cells and in KO cells showed that compound #10 led to significant reduction of *CCND1* in HCT-8 wild-type cells, which indicates an EpCAM-specific effect. For *MYC*, none of the compounds showed a significant down-regulating effect in any cell line upon compound treatment (Figure 3-14B). *EPCAM* expression levels could only be assessed in HCT-8 wild-type cells. Treatment with compound #6, #10 or #51 led to a statistically significant reduction (Figure 3-14C).

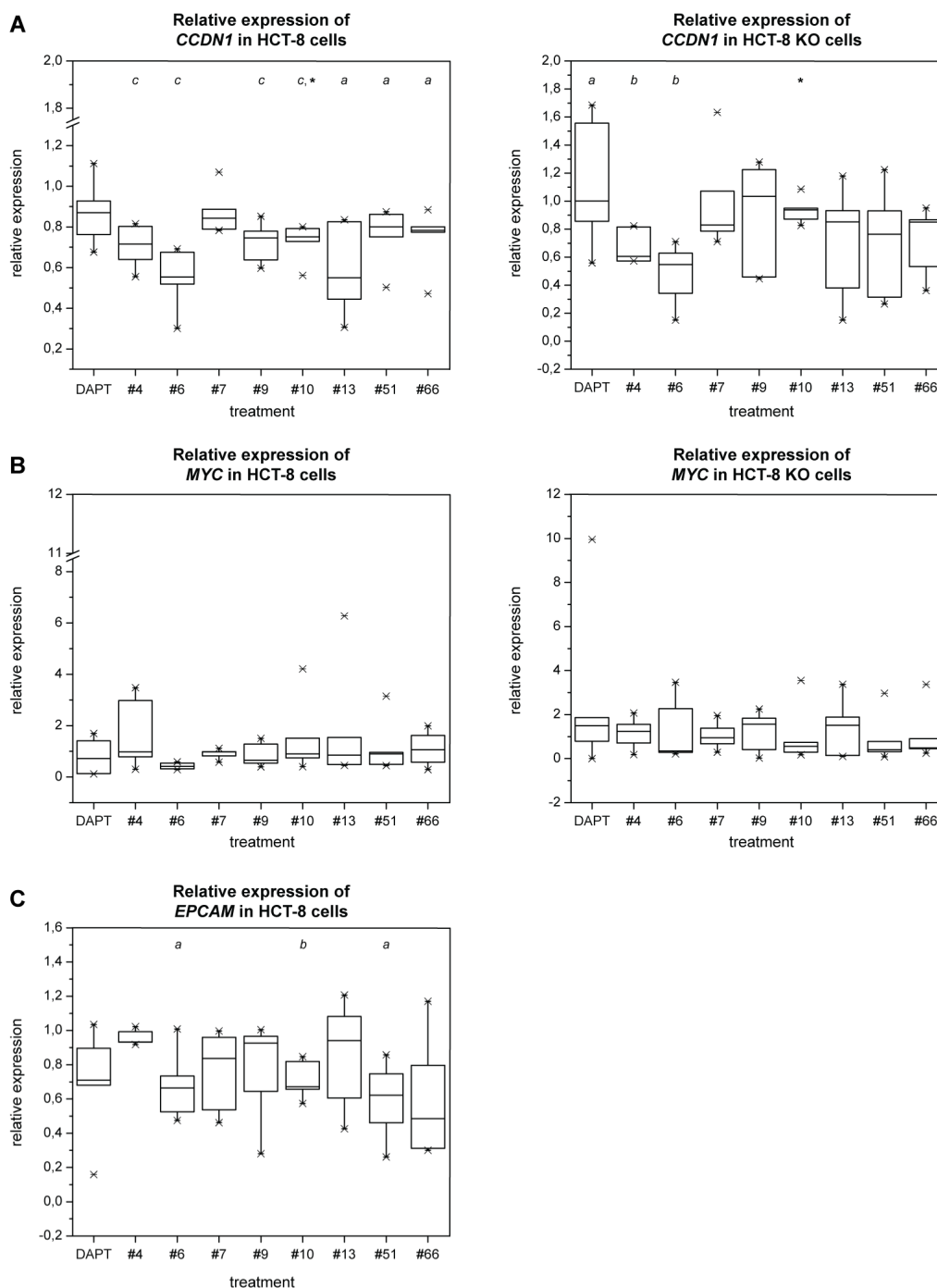


Figure 3-14 Effects on target gene expression. Effects on *CCND1* (A), *MYC* (B) and *EPCAM* (C) expression were assessed by RT-PCR with EpCAM-positive HCT-8 wild-type cells (left panels) and EpCAM-negative HCT-8 KO cells (right panels). For *CCND1*, compounds #4, #6, #9, #10, #13, #51 and #66 showed an EpCAM-independent effect in wild-type cells (A, left panel), compounds #4 and #6 in KO cells (A, right panel). #10 showed an EpCAM-specific effect. No compound had a down-regulating effect on *MYC* (B). Compounds #6, #10 and #51 reduced *EPCAM* expression levels in wild-type cells (C). Shown is the evaluation of five independent experiments. Whiskers span the 10-90 percentiles. Statistical analysis was performed using paired-sample t-test. Small letters depict p-values of t-tests within cell lines (a: $p < 0.05$; b: $p < 0.01$; c: $p < 0.005$; d: $p < 0.001$), p-values of t-tests between the cell lines are depicted by an asterisk (*: $p < 0.01$).

These results should be confirmed via Western blot by testing the amount of cyclin D1 (34 kDa) and EpCAM (35 kDa) after compound treatment in the cells. Therefore, HCT-8 wild-type cells were manually plated on 6-well plates and treated with DMSO, DAPT

or compounds for 18 h. Afterwards, cells were harvested, lysed and cell lysates were separated in a 10 % SDS-PAGE and analyzed in immunoblot experiments using anti-cyclin D1 or anti-EpCAM antibodies. β -actin (46 kDa) was used as loading control. The experiment was performed in three biological replicates. Unfortunately, the RT-PCR results could not be confirmed by Western blots. Neither of the two proteins showed a significant down-regulation upon compound treatment (for blots and evaluation, see supplementary data, Figure 6-3).

3.2.5.3 Effects on regulated intramembrane cleavage

The effect of compounds on regulated intramembrane cleavage of hEpCAM was analyzed in membranes isolated from HEK293-hEpCAM-FL-YFP cells. The fused YFP increases the size of the cleavage products and therefore facilitates their detection. Cells were cultivated for several days and then harvested and lysed. Via several centrifugation steps, isolated membrane fractions were obtained. Either both, cells and isolated membrane fractions (Figure 3-15A), or the isolated membrane fractions alone (Figure 3-15B) were incubated with DMSO (control), compounds or a combination of known cleavage inhibitors. Cleavage products were separated in a 10 % SDS-PAGE and analyzed in immunoblot experiments using anti-GFP antibodies. GAPDH (35 kDa) was used as loading control (see supplementary data, Figure 6-4). After 22 h incubation without inhibitor or with DMSO, hEpCAM-FL-YFP (66 kDa) was cleaved into the membrane-associated CTF-YFP (35 kDa) and the soluble ICD of EpCAM (hEpICD-YFP; 31 kDa). Since the given molecular weights refer to the YFP-fusion constructs, 25 kDa have to be subtracted in order to determine the actual size of the EpCAM cleavage products. Incubation with the ADAM protease inhibitor GI254023X (GI) and β -secretase inhibitor (C3) led to inhibition of cleavage of hEpCAM-FL-YFP. This inhibits the formation of hEpCAM-CTF-YFP, but still allows cleavage of already formed fractions of this fragment to hEpICD-YFP (Figure 3-6A). Inhibition with the aforementioned inhibitors and additional inhibition with the γ -secretase inhibitor DAPT, which prevents the cleavage of hEpCAM-CTF-YFP, abrogates hEpICD-YFP formation and strongly reduces hEpCAM-CTF-YFP formation (Figure 3-15). Treatment of cells and isolated membrane fractions with compound #4, #9, #10 and #13 led to slightly weaker hEpICD-YFP band on the blots (Figure 3-15B). In order to confirm that these effects indeed are EpCAM-dependent effects and not due to the fusion to YFP, HEK293 wild-type cells stably transfected with YFP were treated and analyzed in the same way. After all treatments (DMSO, combinations of known inhibitors or compounds), only the YFP band could be detected for all samples at the same intensity, which indicates that the detected effects on the EpCAM-cleavage products are not influenced by the YFP-

fusion. Here again, GAPDH was used as loading control (see supplementary data, Figure 6-5). This test was performed in three independent experiments.

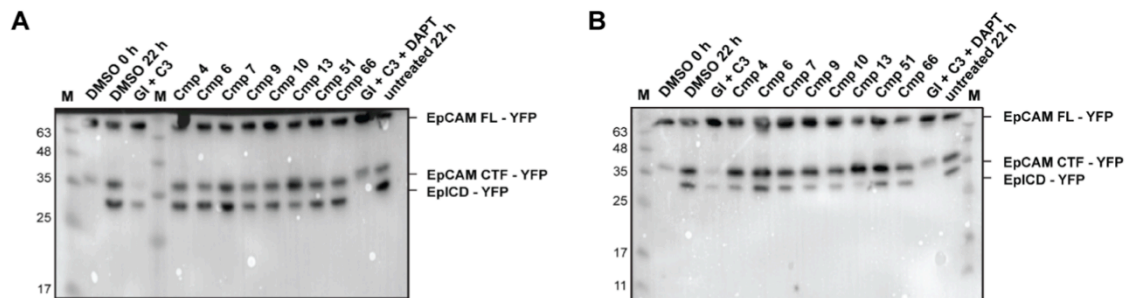


Figure 3-15 Membrane-based EpCAM-cleavage assay. Isolated membrane fractions from HEK293 hEpCAM-FL-YFP cells (**A**) or both isolated membrane fractions and cells (**B**) were treated as indicated and cleavage products were separated in a 10 % SDS-PAGE and probed with anti-GFP antibodies. Incubation with Gl and C3 led to inhibition of hEpCAM-CTF-YFP formation. Additional DAPT treatment inhibited hEpICD formation. Incubation of both cells and isolated membrane fractions with compounds #4, #9, #10 and #13 led to a reduction of hEpICD-YFP (**B**).

The effects of the compounds on EpCAM cleavage were quantified from Western blots by calculating intensities of different hEpCAM-YFP bands relative to the respective band of the DMSO control (Figure 3-16). Since the HCS was conducted with HEK293 hEpCAM-CTF-YFP cells, the compounds expectedly did not have any influence on hEpCAM-FL-YFP cleavage (Figure 3-16A + D). For hEpCAM-CTF-YFP no significant accumulation or decrease could be detected as well (Figure 3-16B + E). In contrast, a change in the amount of hEpICD-YFP could be detected: Compound #4 (0.88 ± 0.04 AU), #9 (0.50 ± 0.16 AU), #10 (0.51 ± 0.16 AU) and #13 (0.28 ± 0.12 AU) showed a significant decrease of hEpICD-YFP intensity, which indicates that these compounds have an influence on γ -secretase cleavage (Figure 3-16F). According to this evaluation, compound #13 has the strongest effect on regulated intramembrane cleavage, followed by compounds #9, #10 and #4. The results of the analysis match the observations on the Western blots. However, this effect was only visible when cells and the isolated membrane fractions were incubated with the compounds. In general it seems that this set-up is more efficient than inhibition of the membrane fractions alone, since Gl/C3/DAPT treatment leads to an even more significant hEpICD-YFP decrease after *in vitro* and *in vivo* inhibition (Figure 3-16C + F).

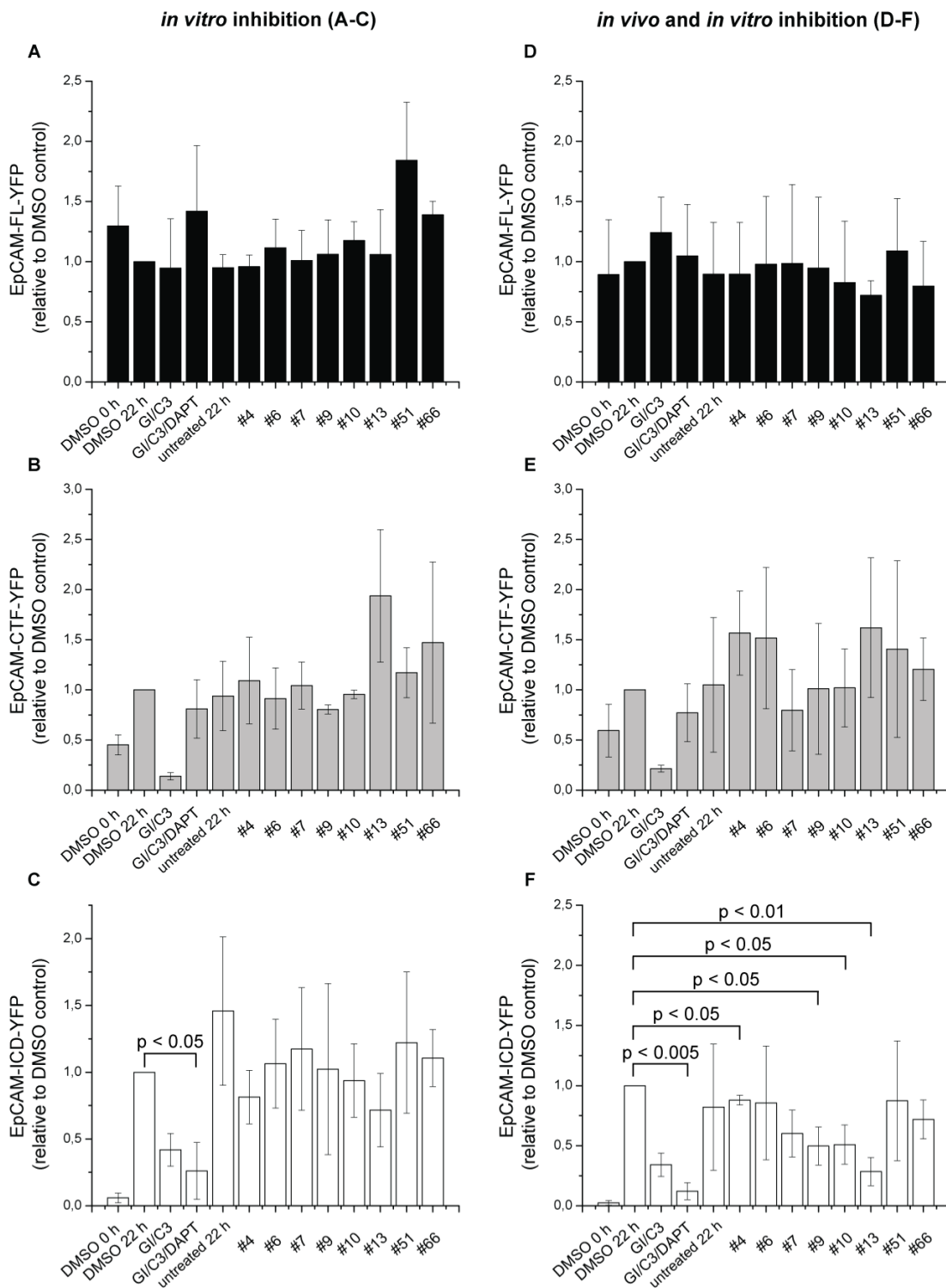


Figure 3-16 Quantitative Western blot analysis from membrane based EpCAM-cleavage assays. Intensities of different hEpCAM-YFP bands relative to the respective DMSO 22 h control band were calculated. Compound treatment was either performed in isolated membrane fractions only (**A-C**) or in cells and in isolated membrane fractions (**D-F**). Only after double-treatment, significant changes in hEpICD-YFP intensities could be detected. Compounds #4, #9, #10 and #13 show significant down-regulation. Shown are mean values and standard deviations from three independent experiments. Statistical significance was assessed using paired-sample t-test. P-values are given above the brackets.

Tsaktanis *et al.*, 2015 showed that γ -secretase cleavage occurs at two distinct sites in the hEpCAM TMD, referred to as γ - and ϵ -cleavage site. Cleavage at the γ -site is leading to three A β -like cleavage products (γ 1, γ 2, and γ 3), which are released into the surroundings of the cell, whereas γ -secretase cleavage at ϵ -sites is leading to two hEpICD-fragments (ϵ 1 and ϵ 2), which are released into the cytoplasm. These cleavage products do not occur to the same extent. Treatment of cells with DAPT abrogates all of these cleavage fragments. The effect of compounds #4, #10, and #13 on the formation of these cleavage products was assessed in a MS-based approach followed by MALDI-TOF read-out. For this experiment, HEK293 hEpCAM-CTF-YFP cells were used. The hEpCAM-CTF-YFP construct consists of an N-terminal c-Myc-epitope, 15 aa of the extracellular domain, TMD and ICD fused to YFP. Furthermore, FLAG-tag and TEV-cleavage site were added between hEpICD and YFP (Figure 3-17A). Those were added in order to process the cleavage products into smaller fragments and for detection. Otherwise a distinction between the cleavage products would not have been possible, since MALDI has too low resolution at greater masses for such small size differences.

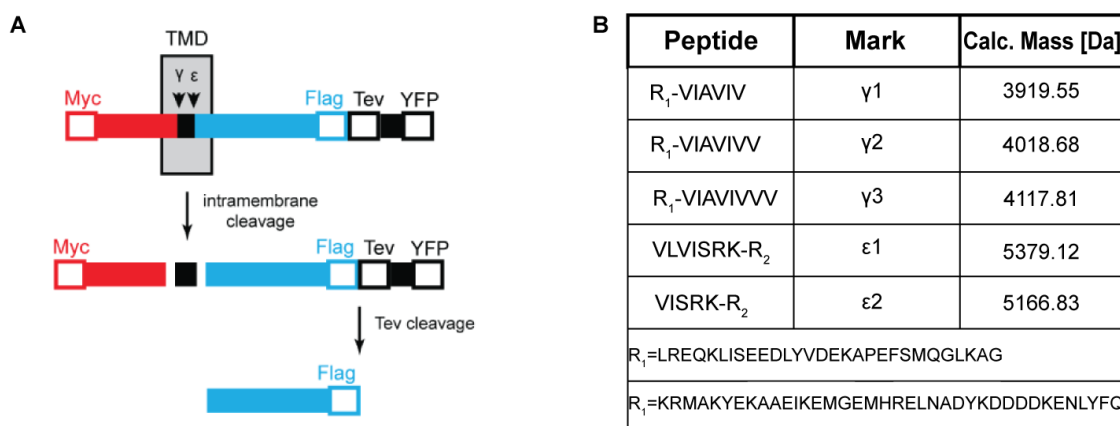


Figure 3-17 Analysis of intramembrane hEpCAM-cleavage by MS. (A) Scheme of construct used for this analysis. A c-Myc-tag was fused N-terminally to CTF-YFP. In order to further process the cleavage products, FLAG-tag and TEV-cleavage site were added between hEpICD and YFP. Cleavage products in the supernatant (red) or intracellular cleavage products (blue) were enriched by immunoprecipitation before analyzing them using mass spectrometry. **(B)** Tabular presentation of expected cleavage fragments showing peptide sequence, mark and calculated mass in Dalton (modified from Tsaktanis *et al.*, 2015).

HEK293-hEpCAM-CTF-YFP cells were treated with DMSO, DAPT or compounds for 24 h. In order to analyze the cleavage products by mass spectrometry, the supernatants were collected and subjected to anti-c-Myc immunoprecipitation (Figure 3-17A, red fragment). For analysis of ϵ -cleavage products, HEK293 hEpCAM-CTF-YFP cells were lysed, subjected to anti-YFP immunoprecipitation, followed by TEV-cleavage and anti-FLAG immunoprecipitation before the samples were analyzed by mass spectrometry (Figure 3-17A, blue fragment). Expected sizes of the cleavage fragments are shown

in Figure 3-17B. It was not possible to detect cleavage products after c-Myc immunoprecipitation in the supernatant. This might be due to a weak binding of the antibody to the protein. Another more likely explanation is that the protein in the sample is only available in low levels. In a test experiment, γ -cleavage products were detectable in very small amounts compared to ϵ -cleavage products (30-50 AU and 4,000-10,000 AU, respectively; see supplementary data, Figure 6-6). While analyzing the cleavage products enriched from cell lysates, only fragments with a molecular weight of approximately 30 kDa could be detected, which refers to the CTF-FLAG-TEV-YFP fragment. This might indicate that TEV-cleavage was not working properly. Since TEV-cleavage and the following FLAG-specific immunoprecipitation are sources of error, it was decided to not conduct these steps. However, this limited the ability to distinguish between ϵ_1 and ϵ_2 , since MALDI has too low resolution at 30 kDa for such small size differences (212.29 Da). It could be shown that the amount of hEpICD-FLAG-TEV-YFP, which arises by cleavage at ϵ -cleavage sites, was reduced after treatment with compound #4, #10 or #13. However, DAPT treatment led to an even more pronounced effect (Figure 3-18). This experiment was conducted in three biological independent experiments.

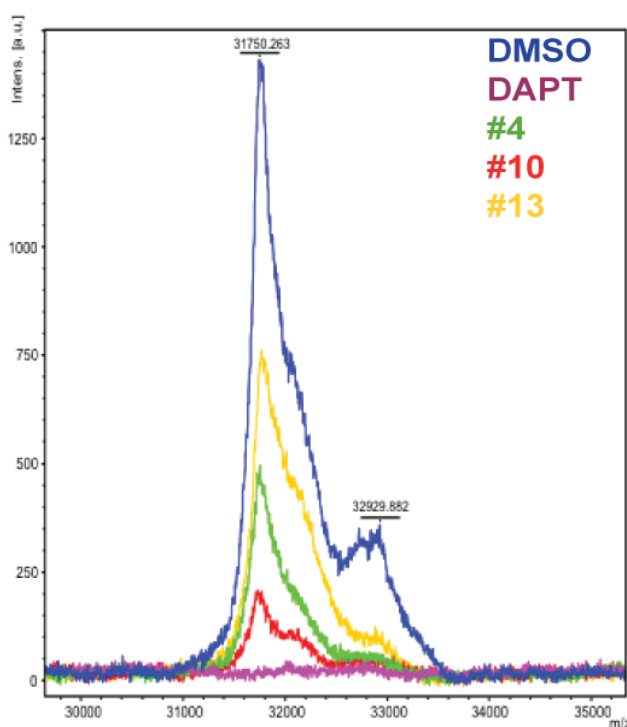


Figure 3-18 Representative mass spectrum of ϵ -cleavage. Shown are peaks of hEpICD-FLAG-TEV-YFP (\approx 30 kDa) after treatment of cells with DMSO (blue), DAPT (purple), compound #4 (green), #10 (red) and #13 (yellow). Treatment with compounds distinctly reduced the amount of cleavage products compared to DMSO treatment, however, to a lesser extent than DAPT treatment. Shown is one representative spectrum out of three independent experiments.

3.2.5.4 Effect on proliferation of cells

For addressing a potential EpCAM-specific effect of the compounds on cell proliferation, HCT-8 wild-type (Figure 3-19A) and EpCAM-KO cells (Figure 3-19B) were automatically seeded on a 96-well plate and treated with compounds, DAPT or DMSO. Over a period of seven days, the cell numbers were determined on a daily basis using Hoechst3342 staining and the automated Operetta Imaging System. The experiment was performed in duplicates and conducted two times. None of the compounds showed a significant difference between EpCAM-positive and -negative cells. Compound #66 did not have any effect on cell proliferation. Compounds #9, #10 and #7 had minor effects on the proliferation of HCT-8 wild-type and KO cells, whereas compounds #4, #6, #13 and #51 almost completely inhibited proliferation of both cell lines (Figure 3-19).

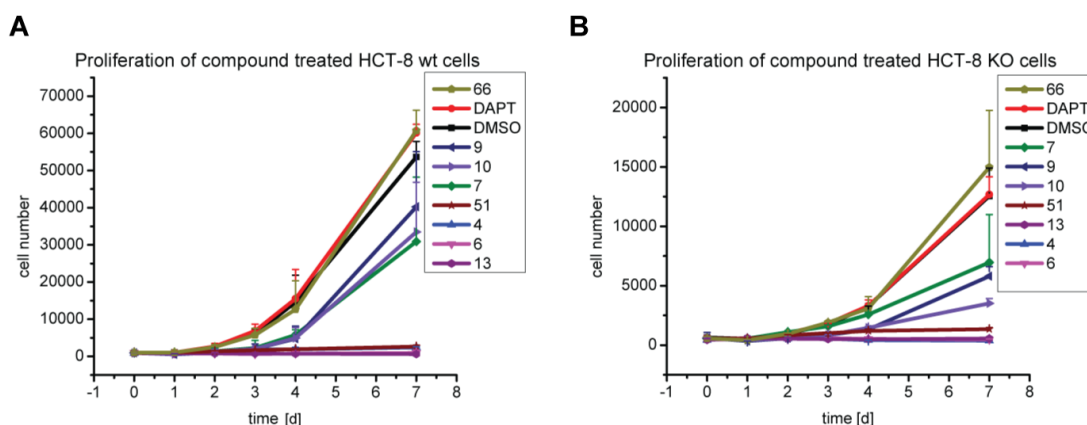


Figure 3-19 Effect on cell proliferation. HCT-8 wild-type (A) and KO-cells (B) were treated with DMSO, DAPT or compounds and cell number was assessed on a daily basis. None of the compounds showed an EpCAM-specific effect. Compound #66 did not have any influence on cell proliferation, compounds #7, #9 and #10 had a slight influence and compounds #51, #13, #4 and #6 almost completely inhibited cell proliferation. Shown are mean values and standard deviations from two independent experiments.

3.2.6 Screening of analogs

Based on the above-described results, analogs of compounds #4, #9, #10 and #13 were selected. In total, 39 new compounds were assessed: 13 analogs of compound #4, four analogs of compound #9, 13 analogs of compound #10 and nine analogs of compound #13 were ordered from the respective supplier. All of these compounds, including the four original compounds, were tested in a ten-point serial-dilution (80 – 0.15 μ M final concentration) with HEK293 hEpCAM-CTF-YFP cells under the same conditions as in the original screening campaign as described in section 3.2.4. The effects of the analogs were manually assessed and compared with the results of the original hits regarding their efficiency and toxicity. If an analog showed comparable or a better effect with simultaneously less toxicity, this compound was used for further studies. Furthermore, a possible autofluorescence of the analogs was assessed. Therefore,

YFP-negative HEK293 hEpCAM-FL cells were also treated with a ten-point serial-dilution (80 – 0.15 μM final concentration) of the compounds and analyzed with regard to fluorescence signal. This confirmed that none of the analogs showed autofluorescence. In summary, nine out of 39 analogs were chosen for further studies (Figure 3-20): one analog of compound #4 (#4_7), none of the analogs of compound #9, five analogs of compound #10 (#10_4, #10_6, #10_9, #10_10 and #10_12) and two analogs of compound #13 (#13_1 and #13_7).

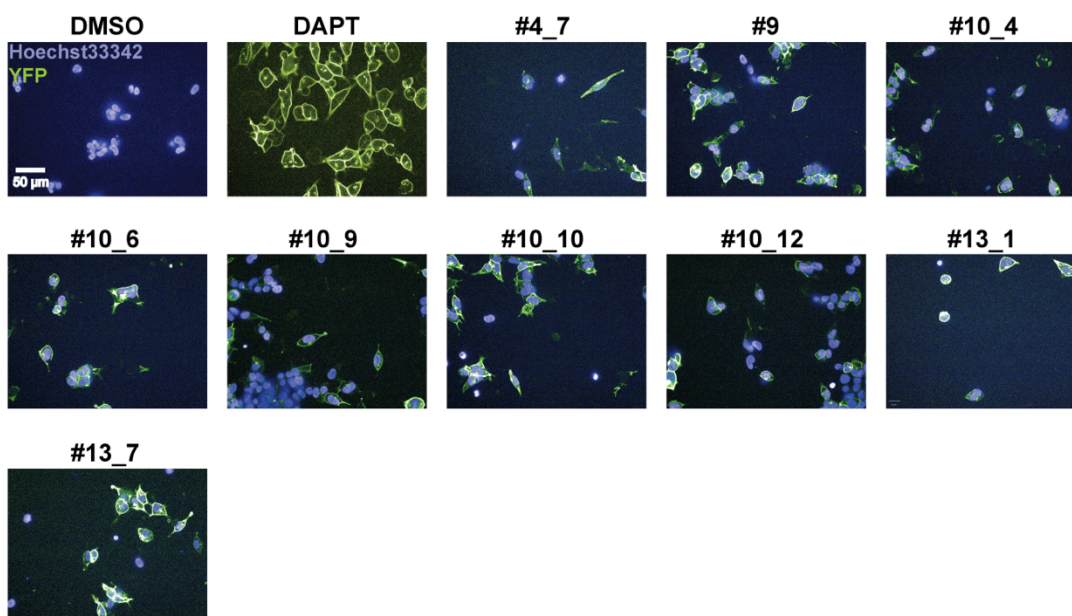


Figure 3-20 Effects of analogs on cells. HEK293 hEpCAM-CTF-YFP cells were treated with DMSO, DAPT or analogs. Pictures of analogs are taken without auto-contrast and show effects after treatment at 20 μM . Treatment of the cells is depicted above the respective picture. Scale bar represents 50 μm .

3.2.7 Further characterization of analogs

As before, the chosen analogs were analyzed regarding their toxicity effects, effects on regulated intramembrane cleavage of hEpCAM, effects on the transcriptional level of EpCAM target genes and effects on cell proliferation. In order to figure out if there is an improvement in any of these characteristics, the results of these analyses were compared with the results of the original compounds. Here again, for ensuring a better comparability with the original compounds, all analogs were used at a concentration of 20 μM if not stated otherwise.

3.2.7.1 Cytotoxicity of analogs

For identification of analogs with improved cellular toxicity characteristics, their effects on the viability of the cells were tested. As before, EpCAM-positive (HEK293 hEpCAM-FL, HCT-8 wild-type and FaDu wild-type cells) and –negative cells (HEK293 wild-type

cells) were automatically plated on 384-well plates, treated with DMSO, staurosporine (positive control) or compounds and analyzed with the ApoTox Glo Kit after 16 h incubation. The assay was conducted under the same conditions as already described in section 3.2.5.1. The experiment was performed in technical triplicates and was carried out two times. Results were related to the DMSO control (Table 3-2). There were no observable differences in viability, cytotoxicity or apoptosis between the different cell lines, which indicate that there is no EpCAM-specific effect. As expected, staurosporine led to a strongly decreased viability (--) and strongly increased cytotoxicity and apoptosis (++) . Compounds #4_7, #10_4, #10_6, #10_10 and #10_12 had some minor effects on the viability of the cells. Compound #9 did not show any influence on cell viability. Remarkably, none of the analogs of compound #13 showed any toxic effects on the cells, whereas the original compound #13 showed a strong reduction in viability (compare Table 3-1). Thus, analogs of compound #13 have an improved toxicity profile.

Table 3-2 Effects of analogs on cell viability, cytotoxicity and apoptosis. Results are depicted in comparison to DMSO control. Since there were no differences between the different cell lines, they are not indicated individually. ++: strong increase; +: increase; 0: no difference; -: decrease; --: strong decrease.

Compound No.	Viability	Cytotoxicity	Apoptosis
DMSO	0	0	0
Staurosporine	--	++	++
#4_7	-	+	0
#9	0	0	0
#10_4	-	0	0
#10_6	-	0	0
#10_9	0	0	0
#10_10	-	0	0
#10_12	-	0	0
#13_1	0	0	0
#13_7	0	0	0

3.2.7.2 Effects of analogs at transcriptional level

Since *CCND1* was the only gene for which an EpCAM-specific effect could be shown (see section 3.2.5.2), the effect of the analogs on its expression level was analyzed. For the investigation of a possible EpCAM-dependent effect on *CCND1* expression, HCT-8 wild-type (Figure 3-21, left panel) and EpCAM-KO cells (Figure 3-21, right panel) were treated with DMSO (control) or analogs of compound #10. Since this com-

pound was the only one with an EpCAM-specific effect (section 3.2.5.2), it was decided only to test analogs of compound #10. Both cell lines were manually plated on 6-well plates and treated with DMSO (1:500), DAPT or analogs. As template for RT-PCR, RNA extracted from cell lysates and reversely transcribed into cDNA was used. Just as before, GAPDH was used as reference gene. All experiments were performed in triplicates and were conducted five times. Evaluation was done in boxplots. Analysis of relative expression levels revealed a significant decrease of *CCND1* expression after treatment with compound #10_4 and #10_12 in wild-type cells and for #10_12 in KO cells. Comparison of the expression levels between wild-type cells and KO-cells revealed a significant down-regulating effect for compound #10_12, which indicates an EpCAM-dependent effect (Figure 3-21).

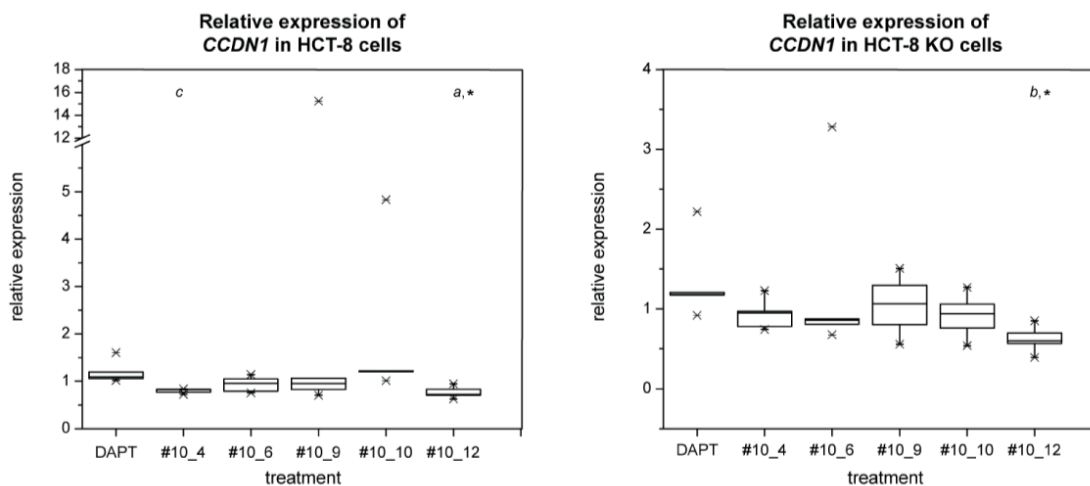


Figure 3-21 Effects on target gene expression. Effects on *CCND1* expression were assessed by RT-PCR with EpCAM-positive HCT-8 wild-type cells (left panel) and EpCAM-negative HCT-8 KO cells (right panel). Compounds #10_4 and #10_12 showed an EpCAM-independent effect in wild-type cells, compounds #10_12 as well in KO cells. #10_12 showed an EpCAM-specific effect. Shown is the evaluation of five independent experiments. Whiskers span the 10-90 percentiles. Statistical analysis was performed using paired-sample t-test. Small letters depict p-values of t-tests within cell lines (a: $p < 0.05$; b: $p < 0.01$; c: $p < 0.005$), p-values of t-tests between the cell lines are depicted by an asterisk (*: $p < 0.01$).

3.2.7.3 Effects of analogs on regulated intramembrane cleavage

The effect of the selected nine analogs on regulated intramembrane cleavage of hEpCAM was analyzed in isolated membranes of HEK293 hEpCAM-YFP cells. As before, cells were cultivated for several days and then harvested, lysed and membrane fractions were obtained via different centrifugation steps. Either the cells and the membrane fractions (Figure 3-22B) or the isolated membrane fractions alone (Figure 3-22A) were incubated with DMSO, analogs or a combination of known cleavage inhibitors. After 22 h incubation, the cleavage products were separated in a 10 % SDS-PAGE and visualized in immunoblot experiments using anti-GFP antibodies. GAPDH (35 kDa) was used as loading control (see supplementary data, Figure 6-7). The experiment was performed in three biological replicates. For detailed explanation of expected cleavage

products after treatment with already known inhibitors, see section 3.2.5.3. After incubation of both cells and isolated membrane fractions with compound #13_1, #13_7, #10_6 and #10_12, the hEpICD-YFP band seemed to have a lesser intensity than the respective band of the DMSO 22 h control.

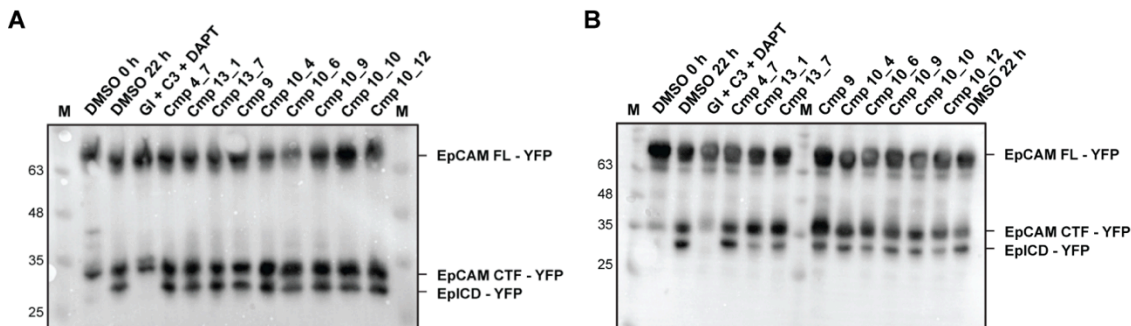


Figure 3-22 Membrane based EpCAM-cleavage assay. HEK293 hEpCAM-FL-YFP cells and isolated membrane fractions (**B**) or membrane fractions only (**A**) were treated as indicated and cleavage products were separated in a 10 % SDS-PAGE and probed with anti-GFP antibodies. Incubation of both cells and isolated membrane fractions with compounds #13_1, #13_7, and #10_12 led to a reduction of hEpICD-YFP (**B**).

The effects of the analogs on regulated intramembrane cleavage of EpCAM were quantified from Western blot analysis. Thereby, intensities of different hEpCAM-YFP bands were calculated and normalized to the respective band of the control with 22 h of DMSO treatment. As before, none of the analogs showed a significant effect on hEpCAM-FL-YFP, which was as expected (Figure 3-23A + D). The results of hEpCAM-CTF-YFP are difficult to interpret due to the high standard deviations (Figure 3-23B + E). However, a significant change in the intensities of hEpICD-YFP could be detected: Compound #10_12 (0.42 ± 0.22 AU) and #13_1 (0.34 ± 0.21 AU) led to a significant decrease of hEpICD-YFP intensity, which indicates that these compounds have an influence on γ -secretase cleavage (Figure 3-23F). For compounds #10_6 and #13_7, the EpICD-YFP band seemed to be weaker than the band of the DMSO control (Figure 3-22B). However, this apparent observation made after Western blot was not reflected in the quantitative analysis. The changes in intensity (0.5 ± 0.31 AU and 0.74 ± 0.36 AU, respectively) were not significant (Figure 3-23F). According to this evaluation, compound #13_1 has a stronger effect on regulated intramembrane EpCAM-cleavage than compound #10_12. However, compared with the effects of the original compounds #10 and #13, the two analogs showed much weaker effects (compare Figure 3-16F and Figure 3-23F). Here again, effects were only visible when cells and the isolated membrane fractions were incubated with the compounds.

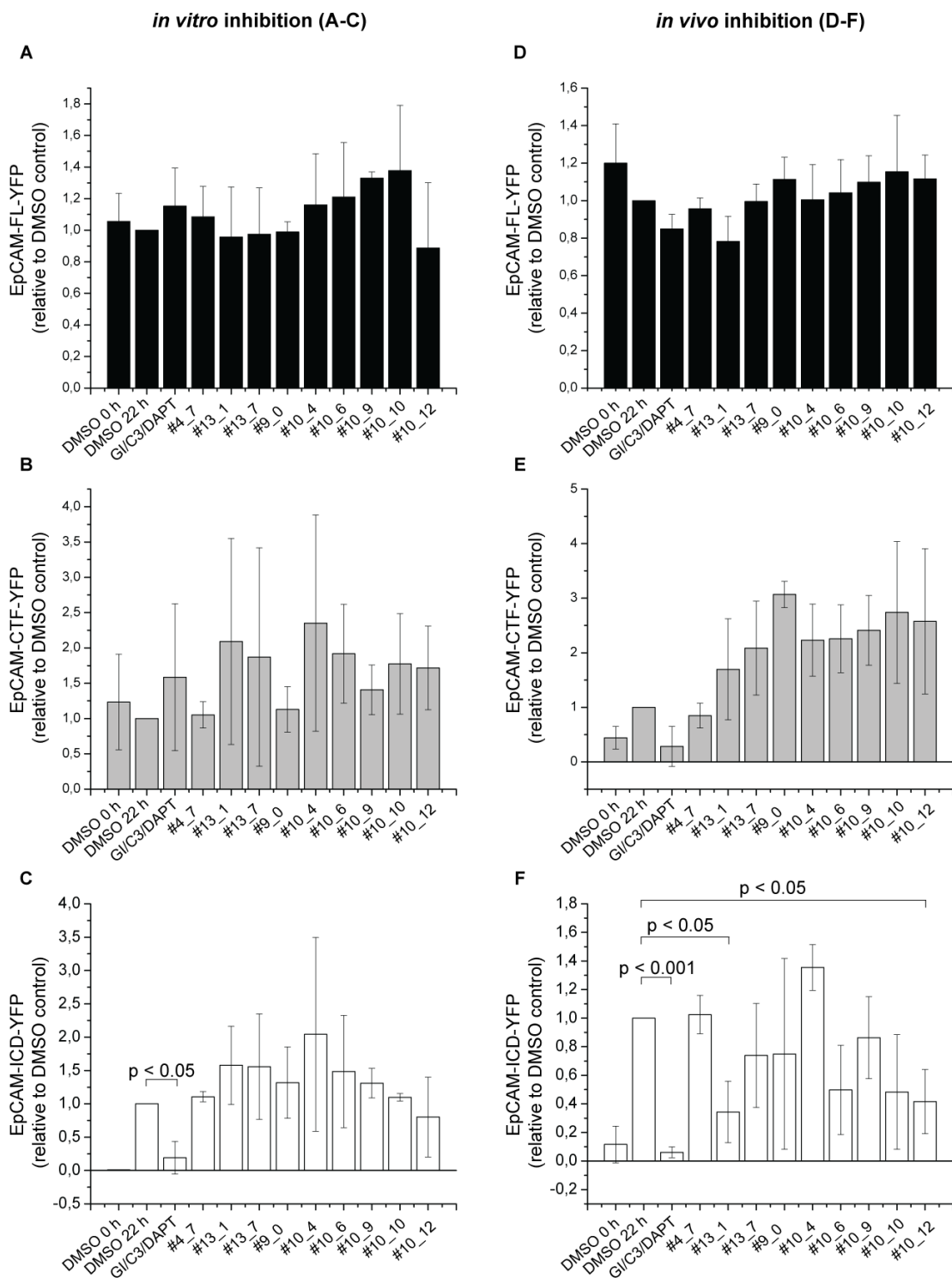


Figure 3-23 Quantitative Western blot analysis from membrane based EpCAM-cleavage assays. Intensities of different hEpCAM-YFP bands relative to the respective DMSO control band were calculated. Treatment with analogs was either performed in isolated membrane fractions only (**A-C**) or in cells and in isolated membrane fractions (**D-F**). Only after double-treatment, significant changes in hEpiCD-YFP intensities could be detected. Compounds #10_12 and #13_1 show significant down-regulation. Shown are mean values and standard deviations from three independent experiments. Statistical significance was assessed using paired-sample t-test. P-values are given above the brackets.

3.2.7.4 Effects of analogs on proliferation

In order to address a potential EpCAM-specific effect of analogs on cell proliferation, HCT-8 wild-type and EpCAM-KO cells were treated with analogs of compound #10, DAPT or DMSO as control. Both cell lines were automatically plated on 96-well plates and treated as indicated. Cell numbers were automatically counted every day for a total duration of seven days based on Hoechst3342 staining using the automated Operetta Imaging System. The experiments were performed in duplicates and were carried out twice. No difference could be detected between EpCAM-positive and -negative cells for any compound. Additionally, none of the analogs of compound #10 showed any effect on cell proliferation (Figure 3-24A + B). Analogues of compound #4 and #13 were only tested regarding their effects on proliferation of HCT-8 wild-type cells. Compound #4_7 and compound #13_7 had minor effects on the proliferation of HCT-8 wild-type cells (Figure 3-24A). In contrast, compound #13_1 strongly inhibited proliferation of these cells. The original compounds #4 and #13 showed a much stronger inhibition of proliferation of both cell lines (compare Figure 3-19 and Figure 3-24A). The effects of analogs of compounds #4 and #13 on cell proliferation of HCT-8 KO cells were not tested, since compound #10 seems to be the only molecule which displayed EpCAM-specific effects (see section 3.2.5.4).

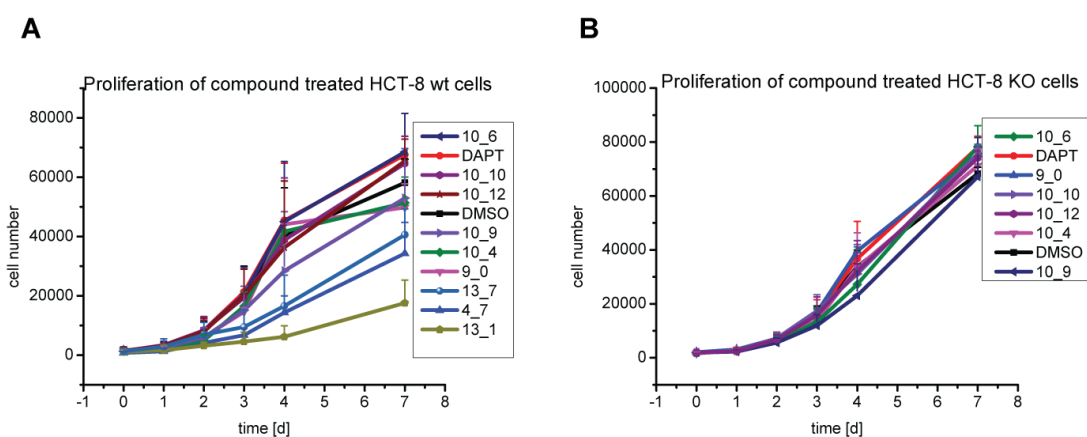


Figure 3-24 Effect on proliferation. HCT-8 wild-type (A) and KO-cells (B) were treated with DMSO, DAPT or compounds and cell number was assessed on a daily basis. None of the compounds showed an EpCAM-specific effect. Compound #13_1 strongly inhibited cell proliferation of wild-type cells whereas compounds #4_7 and #13_7 only had a minor influence. All the other analogs did not have an influence on cell proliferation. Shown are the mean values and standard deviations from two independent experiments.

4 Discussion

4.1 Interaction of FHL2 with EpICD and β -catenin

EpCAM is a transmembrane protein which is highly overexpressed in carcinoma cells. After sequential cleavage by TACE/ADAM17 and γ -secretase, EpICD is released into the cytoplasm. This fragment is part of a complex furthermore consisting of FHL2 and β -catenin. The complex translocates into the nucleus and activates the transcription of EpCAM target genes (Maetzel *et al.*, 2009). Due to the cancer-specific overexpression, EpCAM is an attractive target for cancer therapy. There have been immunotherapeutic approaches. However, targeting of the intracellular EpCAM signaling cascade is a completely new and promising approach (Oishi *et al.*, 2014). For instance, inhibition of formation of the nuclear complex is one possibility of specifically disrupting the intracellular EpCAM signaling cascade. If the binding sites of the participating proteins were known, it could be easier to design/find a small inhibitory molecule. However, in this study it was not possible to confirm the interaction between the key players FHL2 and EpICD.

A yeast two-hybrid screen revealed an interaction of EpICD and FHL2, which was later reconfirmed in combined immunoprecipitation and blotting experiments (Maetzel *et al.*, 2009). A serial deletion analysis showed that the fourth LIM domain is required for the binding (Maetzel *et al.*, 2009). However, the present study did not demonstrate any binding of EpICD and FHL2 FL at all: neither *in vitro* pull down assays nor ITC experiments could reveal an interaction between these two proteins. This seemingly contradicting result might be caused by the different experimental methods, which led to this finding. The rate of false positive and false negative results in yeast two-hybrid screens was estimated as high as 70 % (Deane *et al.*, 2002). One reason for this is that proteins, which naturally never occur in the same cell compartment or at the same time point, might interact when artificially co-expressed. Furthermore, mammalian proteins might not be correctly modified in yeast. The yeast two-hybrid system takes place in the nucleus, however, there are some proteins, which are not able to interact in the yeast nucleus, e.g. proteins of the secretory compartments (Clark, 2006; Koegl and Uetz, 2007). Since the FHL2-EpICD interaction could be confirmed by immunoprecipitation, it is unlikely that this result is a false positive result. The immunoprecipitation experiments were performed in HEK293 and HCT-8 cells, whereas the *in vitro* pull down assays and ITC experiments in this study were done with recombinant proteins from bacteria and insect cells (Maetzel *et al.*, 2009). Proteins that are expressed in bacteria do not contain most of the post-translational modifications (PTMs) found in

eukaryotes, which however have a strong impact on protein localization, turnover, activity state and its interactions (Schein, 1989; Mann and Jensen, 2003). Expression in insect cells provides protein with PTMs, however, not all of the mammalian PTMs occur in insect cells and furthermore some of them such as glycosylation differ between the cell types (Hoss *et al.*, 1990; O'Reilly *et al.*, 1994). Therefore, mammalian cells are most suitable for the expression of mammalian proteins since protein folding and PTMs are the way they naturally occur in the endogenous protein (Khan *et al.*, 2013). The differences in these expression systems could be the reason for the here presented divergent results. The FHL2-EpICD interaction might require a PTM that is neither provided by insect cells nor bacterial cells. Another reason might be a change in protein folding due to the expression system or due to the protein-tag, which could not be removed because of protein stability issues (see section 3.1.1). It would also be conceivable that intact, membranous EpCAM is necessary for FHL2 binding, which would mean that this interaction would occur before EpCAM cleavage.

In immunoprecipitation experiments in HEK293 and FaDu cells, β -catenin was co-precipitated with FHL2, EpICD (and Lef-1 in nuclear extracts; Maetzel *et al.*, 2009). In this study, the already published interaction between β -catenin and FHL2 could be re-confirmed by ITC (Wei *et al.*, 2003). It is difficult to speculate about the physiological relevance of the measured K_d , since the concentrations used for ITC experiments are much higher than naturally occurring protein concentrations in cells. It was not possible to show this interaction by *in vitro* pull down-assays, which indicates a transient interaction of FHL2 and β -catenin (see section 3.1.3). However, no interaction between β -catenin and EpICD or β -catenin, EpICD and FHL2 was observed (see section 3.1.3 and 3.1.4). The reason might be again a missing or changed PTM due to the expression system. Another possible explanation would be that this interaction requires an additional so far unknown binding partner, which mediates the binding between these proteins. Since all constructs are cloned in pOPIN vectors, which contain a mammalian expression promoter, the next step would be transfection of these constructs into mammalian cells in order to harvest molecules more closely representing endogenous proteins.

Since the ternary FHL2-EpICD- β -catenin interaction was not confirmed in this study, it was not possible to solve the structure of the nuclear complex. In general, structural determination of the nuclear complex might be problematic. Due to the size of purified β -catenin (82 kDa) and tagged FHL2 (58 kDa and 74 kDa with GST- and MBP-tag, respectively) it is not possible to perform NMR-studies with these proteins. Structural determination by X-ray crystallography is restricted insofar that FHL2 is a flexible pro-

tein, which makes it inaccessible to this method (Buck, 2003; Kadrmas and Beckerle, 2004). In a yeast two-hybrid system it was shown that FHL2 FL is required for the interaction with β -catenin. Deletion of one or more LIM-domains drastically reduced the binding of these proteins (Wei *et al.*, 2003). Due to the above-mentioned downsides of yeast two-hybrid systems, it might be possible that experiments performed with proteins expressed in mammalian cells lead to different results. If the LIM-domains interacting with β -catenin (or EpICD) are known, it would be easier to define the structure of the nuclear complex, since the complex size and the flexibility is reduced.

4.2 Identification of a small inhibitory molecule

Another possibility of finding a small inhibitory molecule is the establishment and performance of a HCS. For the identification of a compound that specifically inhibits the intracellular EpCAM signaling cascade, about 26,000 molecules were tested and analyzed in an HCS campaign. The primary hits were reconfirmed in a five-point and ten-point dilution series. The eight obtained hits were regarded as high-confidence hits and were further characterized in cell based and *in vitro* assays regarding their toxicity, specificity and effects on cell proliferation and regulated intramembrane proteolysis. Compound #4 had minor effects on the intramembrane EpCAM cleavage, but showed strong inhibition of cell proliferation. Compound #9 and #10 also showed minor effects on regulated intramembrane proteolysis. Furthermore, compound #10 seemed to have an EpCAM-specific effect on the down-regulation of *CCND1*. Compound #13 has a strong influence on γ -secretase cleavage, however strongly impaired cell viability as well as cell proliferation. No compound showed an EpCAM-dependent effect on cell proliferation. In order to improve the effects of these inhibitory molecules, a screening of compound analogs was performed. These analogs were tested under the very same conditions as the initial compounds. Compounds #13_1 and #13_7 have an improved toxicity profile. Compound #10_12 showed an EpCAM-specific down-regulating effect on *CCND1* expression. However, all analogs had a less effective influence on γ -secretase cleavage. Moreover, none of the analogs seemed to have an EpCAM-specific effect on cell proliferation.

The five-point and ten-point serial dilutions were performed with compounds from stock aliquots and newly provided by the supplier, respectively. In some cases, the effect shown in the initial HCS campaign was not reproducible. Several reasons might account for this. Since the whole screening campaign took several months, it might be possible that the cells themselves changed in cell culture, which influenced their sensitivity towards the compounds. However, this is rather unlikely since cells were freshly thawed for every screening set-up from same cell batches. Furthermore, some other

compounds continued to show reproducible effects, including DAPT, which was used as positive control. The compounds for HCS are stored in compound plates in DMSO at -20 °C and underwent several freeze-thaw cycles, which might have led to degradation of the compounds. Thus, a degradation product might have been the cause of these effects. Moreover, newly provided compound samples might differ in their purity and identity of possible contaminants.

A similar screen has already been performed (Henrich *et al.*, 2013). This identified compounds, which inhibited EpCAM-dependent growth of hepatocellular carcinoma cells (HCCs) in consequence of reduction of EpCAM expression. EpCAM-positive and -negative HCCs were treated with compounds and confirmed differentially active compounds were further characterized regarding their effect on EpCAM expression. In doing so, three compounds that affect EpCAM-dependent growth have been found. These were identified as STAT5 inhibitor, α -adrenoreceptor antagonist and ROR γ inhibitor. Since this screen was based on changes in cell numbers and expression levels, it was not possible to elucidate the molecular mechanism of action for these compounds. A clear advantage of the here-performed HCS is that by measuring an increase in YFP-fluorescence in a specific subcellular compartment, one is able to narrow down the possible mode of actions of the hits. Additionally, further characterization of a given compound and its effect can be done in a more focused way.

A downside of the here-performed HCS campaign is that with the employed evaluation method, it is not possible to discriminate whether an autofluorescent compound might not also have an actual effect on the intracellular EpCAM-signaling cascade. So there is a certain possibility that a compound was excluded from further investigation due to autofluorescence despite of being effective (false negative result). No compound which led to YFP-accumulation at the cell membrane was excluded because of autofluorescence. All autofluorescent compounds caused an increase of YFP-fluorescence in the cytoplasm and/or nucleus. This effect could be caused by proteasome inhibition, inhibition of nuclear complex formation or inhibition of nuclear translocation of the complex. In order to be able to exclude the possibility of a false negative result, all autofluorescent compounds need to be tested if they inhibit one of the above mentioned steps. This could be done by IP experiments or with the aid of special kits e.g. proteasome activity kit or nuclear translocation assay. However, due to the large number of autofluorescent compounds (51 molecules), this would be a very time and money consuming process.

After investigating the effects of the eight high-confidence hits on cell viability, proliferation, target gene expression and regulated intramembrane proteolysis, four compounds

showed promising results: Compounds #4, #9, #10 and #13. Therefore, analogs of these compounds were chosen and investigated under the same considerations as before. By comparing the effects of the analogs with the original compound, it was possible to analyze the structure-activity relationship (SAR; conducted by Dr. Manfred Rösner, Rösner Consulting Group). For the efficacy of compound #4, a 2-methoxysubstitution on the right-hand aromatic ring seemed to be crucial. If this substitution is in any other position, the compound will lose efficacy (e.g. compounds #4_2 and #4_5). The fluorine compounds have a very weak effect (#4_3 and #4_4). The only alternative is a Cl-substitution instead of a methoxysubstitution; however, this compound #4_6 was more toxic than #4_0 and less effective. Compounds #4_7 and #4_9 have a Cl and F substitution at the left aromatic ring, respectively. Additionally, they show a benzyl-cycloalkylamin at the right aromatic ring. The cycloalkyl seemed to be important, since derivatives without this residue do not have any effect (e.g. #4_10 and #4_13). The structures of compound #9 and #10 have a very similar scaffold. It seems that a secondary amine (R_1 -NH- R_2) has a somewhat better efficacy than N-substitution. For analogs of #13_0, it was shown that a benzyl group drastically reduces cytotoxicity but shows comparable effectiveness (#13_1). Moreover, compounds substituted at the exo-N (#13_5-#13_9) also show similar effects and toxicity as the analogs, which are substituted at the N within the aromatic ring. The benzyl group reduces the cytotoxicity of these compounds as well. In general, compound #4 and #13 are structurally similar. All benzyl-substituted derivatives show the best effects and additionally decrease cellular toxicity for analogs of compound #13_0. For molecular structures of compounds, see appendix II.

The effects of the compounds and their analogs on regulated intramembrane proteolysis were analyzed in membrane based EpCAM cleavage assays (see sections 3.2.5.3 and 3.2.7.3). Two different approaches have been applied: incubation of cells and isolated membrane fractions with compounds and incubation of only isolated membrane fractions. It was demonstrated, however, that incubation of isolated membrane fractions failed to have any significant effect on intramembrane EpCAM-cleavage. An effect was only detectable when the cells were treated with compounds as well. This indicates that the compounds do not directly interfere with EpCAM-cleavage by γ -secretase e.g. via blocking the cleavage sites of EpCAM but rather have an indirect effect e.g. via inhibition of binding of necessary co-factors for cleavage. It would be possible that FHL2-EpCAM binding is required for γ -secretase cleavage. If the cells are incubated with the compounds and binding is affected, there will not be any cleavage of EpCAM neither in the cells nor in the isolated membrane fractions. If, however, only the isolated membrane fractions are treated with the compounds, then FHL2-EpCAM bind-

ing will occur within the cell. The FHL2-EpCAM complex might be still bound together after isolation of the membrane fractions, which would then allow for intramembrane cleavage of EpCAM despite compound treatment. DAPT, which is a highly specific γ -secretase inhibitor, leads to a significant effect in both set-ups (Geling *et al.*, 2002). Since the compounds identified in the HCS only have an effect after additional incubation with the cells, it is an indication as well that they are not direct inhibitors of γ -secretase cleavage. Furthermore, it seems that the effect caused by the compounds does not lead to a complete inhibition of intramembrane EpCAM-cleavage, since there is still a reasonable amount of detectable EpICD compared to treatment with DAPT (Figure 3-16 and Figure 3-23).

Another important issue is the selectivity of the compounds: do the compounds interact with EpCAM or γ -secretase? An interaction with EpCAM is preferable since this would be a specific inhibition of the EpCAM signaling cascade. An interference with γ -secretase would also have an influence on numerous other signaling pathways, which would cause unintended side effects when this molecule is used as a drug in cancer therapy. If the identified compounds affect γ -secretase, then they should also influence the cleavage of other γ -secretase substrates such as β -amyloid precursor protein (APP) or Notch (De Strooper *et al.*, 1999; Zhang *et al.*, 2012). This issue should be clarified in collaboration with Johannes Trambauer (group of Prof. Dr. Harald Steiner, DZNE, München). Therefore, APP-expressing cells were treated with the compounds of interest (#4, #10, and #13) and their influence on the amount of cleavage products was investigated. Since all compounds influenced APP-cleavage, most likely none of the small inhibitory molecules specifically interfere with cleavage of EpCAM, but rather generally influence γ -secretase cleavage. However, the degree of influence differs between the cleavage products. Compound #13 has the strongest impact on EpCAM-cleavage followed by compound #10 and #4, whereas with respect to APP-cleavage compounds #4 and #10 had the strongest. Compound #13 did not have any significant effect on APP-cleavage. A next experimental step in the analyses would be to reveal if these compounds interfere with Notch-cleavage as well and if so, to what extent.

A possible explanation for this result might be that the compounds interfere with substrate recognition. It was shown that Nicastrin (Nct) is essential for the binding and recognition of the substrate as well as for the maturation of γ -secretase (Chung and Struhl, 2001; Shah *et al.*, 2005). After shedding of the substrate, Nct binds the free N-terminus (Figure 4-1A). Afterwards, the substrate is either translocated into the catalytic site or it kinks in order to position the scissile bond within the catalytic site (Figure 4-1B). Inhibition of this interaction dramatically reduces substrate binding and eventual-

ly γ -secretase activity (Beel and Sanders, 2008). The compounds could possibly influence substrate recognition by interacting with the N-terminus of the substrate. This would explain the differential activity towards different substrates. If the compounds affected substrate recognition via Nct-binding, then one compound should always have the same effect regardless of the substrate. An interference of the compounds with γ -secretase's catalytic site, which is separated from the substrate-binding site, seems also unlikely, since then a compound should have the same effect for every substrate as well (Kornilova *et al.*, 2005).

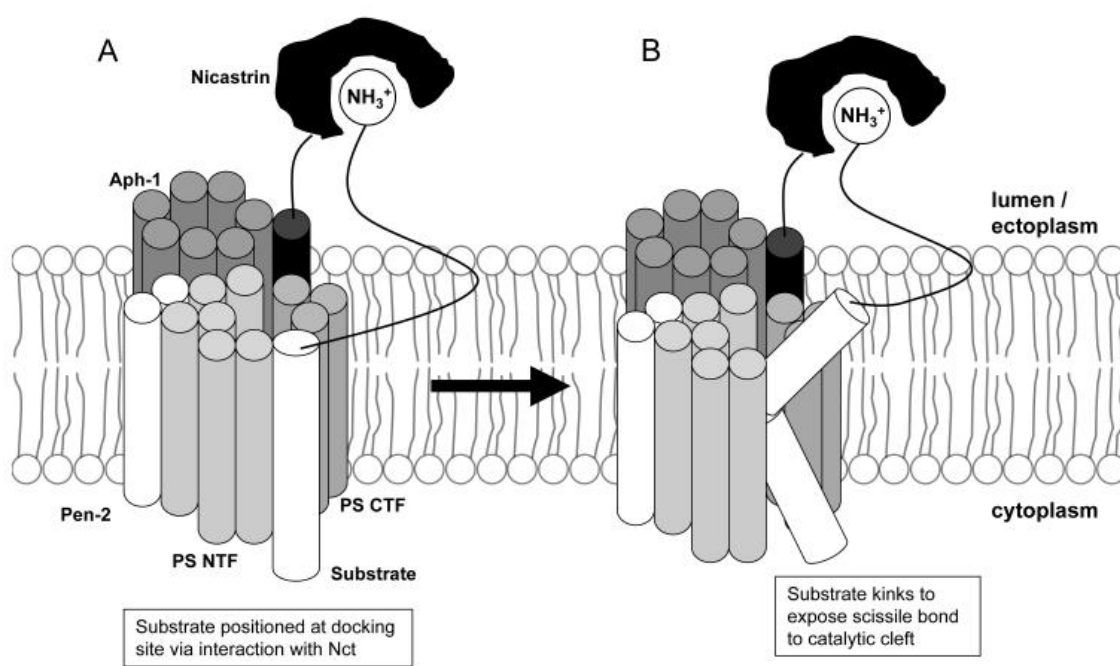


Figure 4-1 Model for substrate recognition and –cleavage of γ -secretase. (A) After ectodomain shedding, the free N-terminus of the substrate (white) is bound by Nicastrin (Nct, black). This leads to positioning of the substrate to the substrate-binding site. (B) Subsequently, the substrate either translocates or kinks in order to position the scissile bond within the catalytic site (from Beel and Sanders, 2008).

γ -secretase is a multiprotein complex consisting of Presenilin (PS), Nct, anterior pharynx defective-1 (Aph-1), and presenilin enhancer-2 (Pen2). All of these components are necessary for both *in vivo* and *in vitro* activity (Edbauer *et al.*, 2003; Kimberly *et al.*, 2003; Fraering *et al.*, 2004). PS represents the catalytic core of the complex, Nct is essential for substrate recognition, Aph-1 plays a crucial role in the assembly and stabilization of the γ -secretase complex and PS-2 causes PS endoproteolysis (Wolfe *et al.*, 1999; Brunkan *et al.*, 2005; Niimura *et al.*, 2005; Shah *et al.*, 2005). The molecular stoichiometry of the complex was determined to be 1:1:1:1 (for Ps:Nct:Aph-1:Pen-2). It has not yet been finally clarified whether there are non-essential co-factors (Sato *et al.*, 2007; Beel and Sanders, 2008). It seems unlikely that the here-identified compounds interfere with the assembly of the γ -secretase complex. This is a fundamental process and disruption should have a larger impact on the cleavage than by the compounds

seen in this study. Furthermore, all γ -secretase substrates should be affected to the same extent if the complex assembly is disturbed.

Another possibility for identification of compounds' binding partner is to analyze the changes in biophysical properties upon drug binding. The basis of this assay is that the thermal stability of a protein changes upon binding to a ligand (Lo *et al.*, 2004). Therefore, purified proteins are heated at increasing temperatures in the presence or absence of the small inhibitory molecule of interest. Due to the heat denaturation, the protein's hydrophobic parts are exposed, which can be measured with a fluorescence dye. Binding of the protein to the ligand causes differences in denaturation temperature (Niesen *et al.*, 2007). This principle can also be used in living cells or whole cell lysates and is called cellular thermal shift assay (CETSA). Thereby, cells are treated with compounds or the vehicle control and are heated with increasing temperatures. Afterwards, the protein of interest is detected via Western blot (Martinez Molina *et al.*, 2013; Jafari *et al.*, 2014). This experiment could be performed either with whole cell lysates or with isolated membrane fractions. Protein detection would occur either with anti-EpCAM or anti- γ -secretase antibodies. A variant of this assay is the isothermal dose response (ITDR): cells or cell lysates are incubated at the same temperature, but treated with increasing ligand concentrations. The protein stability increases with increasing concentrations and facilitates the determination of affinity values for half maximal stabilization (Martinez Molina *et al.*, 2013). Provided that the compounds interfere with FHL2-EpCAM binding and that this interaction is the prerequisite for γ -secretase cleavage (see above), it would be possible to identify the interaction partner by CETSA. The cells or cell lysates would be heated and protein detection would be done by either anti-EpCAM or anti-FHL2 antibodies.

EpCAM regulates both *CMYC* and *CCND1* expression at the transcriptional level (Munz *et al.*, 2004; Chaves-Perez *et al.*, 2013). Therefore, it was investigated if the compounds have an effect on the transcription of these EpCAM-target genes. None of the compounds had an effect on *CMYC* (see section 3.2.5.2). Except for compound #7, all eight high-confidence hits had a down-regulating effect on *CCND1* expression in HCT-8 wild-type cells. When comparing these results with the effects in HCT-8 EpCAM-KO cells, it was shown that only compound #10 had an EpCAM-dependent effect. This indicates that the other compounds have an influence on *CCND1* expression as well, however, in an EpCAM-independent manner. In comparison to the already published results, the down-regulating effect of compound #10 is very weak. The published results, however, were obtained after transfection with small interfering RNA (siRNA), which is possibly more effective than compound #10 (Chaves-Perez *et al.*, 2013). Ep-

CAM siRNA leads to degradation of EpCAM messenger RNA (mRNA), which leads to a strong down-regulation of EpCAM (Agrawal *et al.*, 2013). Compound #10, however, does not have an influence on *EPCAM* expression, it solely impairs intramembrane cleavage to a certain degree. This might explain the significantly poorer effect of this small inhibitory molecule in comparison to the published results.

The effect shown for *CCND1* and *EPCAM* on the transcriptional level (see section 3.2.5.2) should be investigated on the protein level as well, since down-regulation also led to a reduction of cyclin D1 at the protein level (Chaves-Perez *et al.*, 2013). Therefore, HCT-8 wild-type cells were treated with compounds and the lysates were analyzed by Western blot. Neither cyclinD1 nor EpCAM were significantly down-regulated after compound treatment (see section 3.2.5.2). A possible explanation is again a stronger effectiveness of siRNA-mediated down-regulation (Chaves-Perez *et al.*, 2013). Another reason might be the duration of the treatment. Cyclin D1 started to decrease after 24 h incubation time and almost completely disappeared after 48 h. In the present study, cells were treated with compounds for 18 h. Possibly, an extended incubation time could lead to a positive result. Strangely, treatment with the γ -secretase inhibitor DAPT did not affect target gene expression at all. After being subjected to RIP, the cleaved intracellular EpCAM fragment is thought to be responsible for the activation of target genes (Maetzel *et al.*, 2009; Chaves-Perez *et al.*, 2013). Therefore, inhibition of formation of this fragment should inhibit target gene expression. It was already shown that DAPT treatment, which inhibits cleavage of EpCAM-CTF, eventually results in reduced expression of c-Myc and E-FABP (Maetzel *et al.*, 2009). However, this experiment was performed in HEK293 hEpCAM-YFP cells whereas the experiments in the present study were conducted with endogenously EpCAM-expressing HCT-8 cells. There might be small differences in the EpCAM signaling pathways between these two cell lines, which might account for the differing outcomes.

It was shown that EpCAM directly influences cell cycle regulation and eventually cell proliferation via the cyclin-regulated pathway. In general, EpCAM overexpression is associated with an increased cell proliferation, whereas EpCAM down-regulation causes a decrease of cell proliferation (Munz *et al.*, 2004; Wenqi *et al.*, 2009; Chaves-Perez *et al.*, 2013). Thus, it was decided to examine if an inhibition of the intracellular signaling cascade will lead to a decreased cell proliferation. Therefore, the compounds were tested regarding their effect on cell proliferation in HCT-8 wild-type and HCT-8 EpCAM-KO cells. Thereby, it was shown that compounds #4, #6, #13 and #51 strongly impaired cell proliferation for both cell lines. This indicates that these compounds influence cell proliferation in an EpCAM-independent way. If these compounds adversely

affect γ -secretase cleavage in general, it might be possible that several fundamental processes are disturbed in these cells, which eventually results in severely restricted cell proliferation. Again, DAPT treatment did not influence cell proliferation, which was unexpected.

In summary, the present study describes the discovery of small inhibitory molecules, which interfere with the regulated intramembrane proteolysis of EpCAM. However, the molecular targets and mechanisms of inhibition still remain elusive. Furthermore, it needs to be investigated in more depth if these identified compounds may not actually influence EpCAM target gene expression. Nevertheless, targeting the intracellular EpCAM signaling cascade is a very promising and innovative strategy for the identification of a specific small inhibitory molecule as a potential pharmaceutical drug for EpCAM-positive tumors.

5 Appendix I

5.1 Abbreviations

Table 5-1 Abbreviations

%	Percent	IP	Immunoprecipitation
°C	Degree Celsius	IPTG	Isopropyl-β-D-thiogalactopyranosid
x g	Times standard gravity	IDTR	Isothermal dose response
μ	Micro	k	Kilo
A ₂₆₀ , A ₂₈₀ , A ₅₆₂	Absorption at wavelength 260 nm/ 280 nm/ 562 nm	Kan	Kanamycin
A	Alanine (aa), adenine (DNA), Ampere	KCl	Potassium chloride
aa	Amino acid	L	Liter
ACT	Activator of CREM in testis	Lef-1	Lymphoid enhancer binding factor-1
Amp	Ampicillin	LRP5/6	Lipoprotein receptor related protein 5/6
AML	Acute myeloid leukemia	m	Milli, meter
AP-1/2	Activator protein-1/-2	M	Methionine (protein), mol/L
APC	Adenomatous-polyposis-coli pro- tein	MALDI	Matrix assisted laser desorption ioni- sation
Aph-1	Anterior pharynx defective-1	MBP	Maltose binding protein
AR	Androgen receptor	MEF-2	Myocyte enhancer factor-2
Arm	Armadillo	MES	Mesenchymal to epithelial transition
AU	Arbitrary unit	min	Minute
APP	Amyloid precursor protein	MAP	Mitogen activated protein
BAC	Bacterial artificial chromosome	MMP-7	Matrix metalloproteinase-7
BCA	Bicinchonic acid	MOPS	3-(N-Morpholino) propanesulfonic acid
BSA	Bovine serum albumin	(m/si)RNA	(messenger/small interfering) ribonu- cleic acid
β-TrCP	β-transducin repeats containing protein	MW	Molecular weight
bp	Base pair	n	Nano
C	Cysteine (protein), cytosine (DNA)	NaCl	Sodiumchloride
(c)DNA	(Complementary) desoxyribonu- cleic acid	Nct	Nicastrin
CETSA	Cellular Thermal Shift Assay	NFκB	Nuclear factor kappa-light-chain- enhancer of activated B-cells
CHO	Chinese hamster ovary	NMR	Nuclear Magnetic Resonance
CK1	Casein kinase-1	nt	Nucleotide
CTC	Circulating tumor cell	NTD	N-terminal domain
CTD	C-terminal domain	N-term	Amino terminus
CTE	Congenital tufting enteropathy	OD ₆₀₀	Optical density at 600 nm
CTF	C-terminal fragment	o/n	Overnight
CV	Column volume	PAGE	Polyacrylamide gel electrophoresis
Da	Dalton	PBS	Phosphate buffered saline
ddH ₂ O	Double distilled water	PCR	Polymerase chain reaction
DAPT	N-[(3,5-Difluorophenyl)acetyl]-L- alanyl-2-phenylglycine-1,1- dimethylethyl ester	PDL	Poly-D-lysine
DMEM	Dulbecco's Modified Eagle Medi- um	Pen-2	Presenilin enhancer-2
DMSO	Dimethylsulfoxide	PFA	Paraformaldehyde
dNTP	Deoxyribonucleotide triphosphate	pH	<i>Potentia hydrogenii</i>
DTT	Dithiothreitol	pI	Isoelectric point
<i>E. coli</i>	<i>Escherichia coli</i>	PI3K	Phosphatidylinositol-3 kinase
EDTA	Ethylenediaminetetraacetic acid	pRb	Retinoblastoma protein

E-FABP	Epidermal fatty acid binding protein	PS	Presenilin
EGF	Epidermal growth factor	PSF	Pyrimidine tract-binding protein-associated splicing factor
EpCAM	Epithelial cell adhesion molecule	PTEN	Phosphatase and tensin homolog
EpEX	Extracellular domain of EpCAM	PTM	Post-translational modification
(Ep)ICD	Intracellular domain (of EpCAM)	PVDF	Polyvinylidene fluoride
ESE-1	Ets epithelial specific ets-1	qRT-PCR	Quantitative Real Time PCR
ER	Endoplasmatic Reticulum	rev	Reverse
FACS	Fluorescence activated cell sorter	RIP	Regulated intramembrane proteolysis
FBS	Fetal bovine serum	rpm	Rounds per minute
FDA	Food and drug administration	RT	Room temperature, reverse transcriptase
FITC	Fluorescein isothiocyanate	s	Second
FHL2	Four-and-a-half LIM-domains protein 2	SAR	Structure-activity relationship
FL	Full length	SDS	Sodium dodecyl sulfate
for	Forward	SEC	Size exclusion chromatography
Fz	Frizzled	Sp-1	Specificity protein-1
g	Gram, standard gravity	SRF	Serum response factor
G	Guanine	TACE	Tumor necrosis factor alpha converting enzyme
Gent	Gentamycin	TCEP	Tris-(2-carboxyethyl)-phosphine hydrochloride
GFP	Green fluorescent protein	TCF	Transcription factor
GSH	Glutathione	TEM	Tetraspanin-enriched microdomains
GSK3	Glycogen synthase 3	Tet	Tetracycline
GST	Glutathione S-transferase	TMD	Transmembrane domain
h	Hour, human	TNF α	Tumor-necrosis factor α
HAI-2	Hepatocyte growth factor activator inhibitor-2	TRIS	Tris(hydroxymethyl)aminomethane
HBV	Hepatitis B virus	TY	Thyroglobulin
HCC	Hepatocellular carcinoma	UV	Ultraviolet
HCS	High Content Screen	V	Volt
HCV	Hepatitis C virus	v/v	Volume per volume
HEPES	(4-(2-hydroxyethyl)-1-piperazineethanesulfonic acid	Wg	Wingless
HRP	Horseradish peroxidase	WT	Wildtype
HPV	Human Papilloma Virus	w/v	Weight per volume
HTS	High-Throughput Screening	YFP	Yellow fluorescent protein
INF γ	Interferon γ	ZnCl ₂	Zinc chloride
Inr	Initiator		

5.2 Index of figures

Figure 1-1 Scheme of the <i>EPCAM</i> gene (A) and protein (B).....	5
Figure 1-2 Scheme of EpCAM cleavage and signaling.	9
Figure 1-3 EpCAM in tetraspanin-enriched microdomains (TEMs).	13
Figure 1-4 Scheme of the FHL2 gene.	15
Figure 1-5 Structure of four-and-a-half-LIM-only protein-2 (FHL2).	16
Figure 1-6 Functional diversity of FHL2.	19
Figure 1-7 Structure of h β -catenin and interaction sites.	22

Figure 1-8 β -catenin's life cycle within the cell.	23
Figure 3-1 Purification procedures and tags of FHL2 derivatives.	44
Figure 3-2 Purification of LIM-constructs.	45
Figure 3-3 Purification of β -catenin.	46
Figure 3-4 Pull-down experiments with FHL2, β -catenin and EpICD	47
Figure 3-5 ITC experiments with β -catenin, FHL2 and EpICD.	48
Figure 3-6 Principle of High-Content Screen (HCS) and possible effects.	50
Figure 3-7 Image analysis.	51
Figure 3-8 Determination of optimal staining method.	52
Figure 3-9 Determination of optimal magnification.	54
Figure 3-10 Determination of optimal imaging method.	56
Figure 3-11 Determination of optimal cell number.	56
Figure 3-12 Hit verification procedure.	58
Figure 3-13 Effects of eight high confidence hits on HEK293 hEpCAM-CTF-YFP cells.	59
Figure 3-14 Effects on target gene expression.	62
Figure 3-15 Membrane-based EpCAM-cleavage assay.	64
Figure 3-16 Quantitative Western blot analysis from membrane based EpCAM- cleavage assays.	65
Figure 3-17 Analysis of intramembrane hEpCAM-cleavage by MS.	66
Figure 3-18 Representative mass spectrum of ϵ -cleavage.	67
Figure 3-19 Effect on cell proliferation.	68
Figure 3-20 Effects of analogs on cells.	69
Figure 3-21 Effects on target gene expression.	71
Figure 3-22 Membrane based EpCAM-cleavage assay.	72
Figure 3-23 Quantitative Western blot analysis from membrane based EpCAM- cleavage assays.	73
Figure 3-24 Effect on proliferation.	74
Figure 4-1 Model for substrate recognition and γ -cleavage of γ -secretase.	81
Figure 6-1 DMSO killing curve for HEK293 EpCAM-CTF-YFP cells.	89
Figure 6-2 FACS-analysis of EpCAM-expression on HCT-8 wildtype and EpCAM-KO cells.	89
Figure 6-3 Western blot analysis of protein expression levels after compound treatment.	90

Figure 6-4 GAPDH loading control of membrane-based EpCAM-cleavage assays.....	90
Figure 6-5 YFP control of membrane-based EpCAM-cleavage assay.....	91
Figure 6-6 Mass spectra of γ -cleavage (A) and ϵ -cleavage sites (B) of Myc-CTF-Fag-TEV-YFP in HEK293..	92
Figure 6-7 GAPDH loading control of membrane-based EpCAM-cleavage assays.....	93
5.3 Index of tables	
Table 2-1 DNA oligonucleotides for cloning.....	26
Table 2-2 DNA oligonucleotides for qPCR.....	27
Table 2-3 Commercial plasmids.....	27
Table 2-4 Plasmids for recombinant protein expression in <i>E. coli</i>	28
Table 2-5 Plasmid for recombinant protein expression in insect cells.....	28
Table 2-6 Bacterial strains.....	28
Table 2-7 Insect cell lines.....	29
Table 2-8 Mammalian cell lines.....	29
Table 2-9 Media for bacterial cell culture.....	30
Table 2-10 Supplements for bacterial cell culture.....	30
Table 2-11 Media for insect cell culture.....	30
Table 2-12 Supplements for insect cell culture.....	30
Table 2-13 Media for mammalian cell culture.....	30
Table 2-14 Supplements for mammalian cell culture.....	31
Table 2-15 Primary antibodies.....	31
Table 2-16 Secondary antibodies.....	31
Table 2-17 General buffers and stock solutions.....	32
Table 3-1 Effects of compounds on cell viability, cytotoxicity and apoptosis.....	60
Table 3-2 Effects of analogs on cell viability, cytotoxicity and apoptosis.....	70
Table 5-1 Abbreviations.....	85

6 Supplementary Data

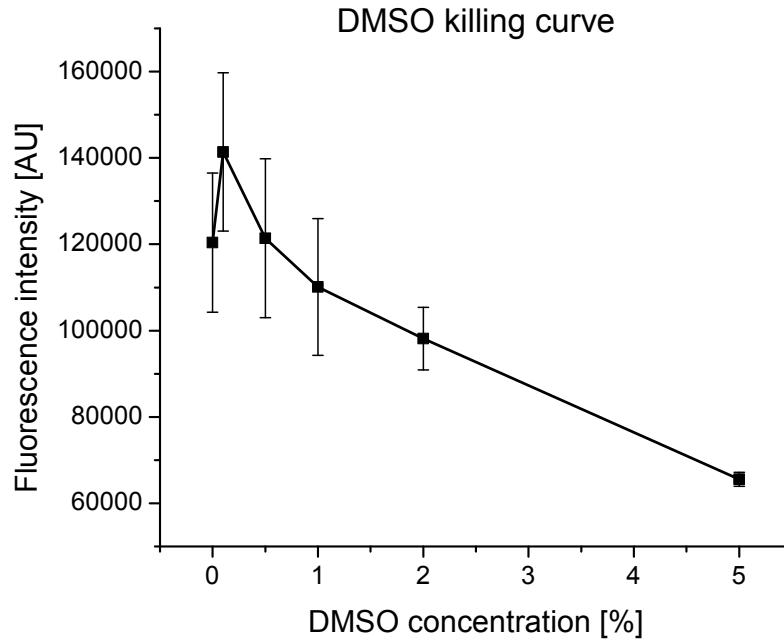


Figure 6-1 DMSO killing curve for HEK293 EpCAM-CTF-YFP cells. Cells were plated on a 96-well plate and treated with different DMSO concentrations for 18 h. A decrease of viability after DMSO treatment could be detected at a concentration of 2.0 % DMSO, which is far beyond the DMSO concentration used in the HCS (0.8 %). Cell viability was measured with CellTiter-Blue® Cell Viability Assay. Shown are mean values and standard deviations from two independent experiments.

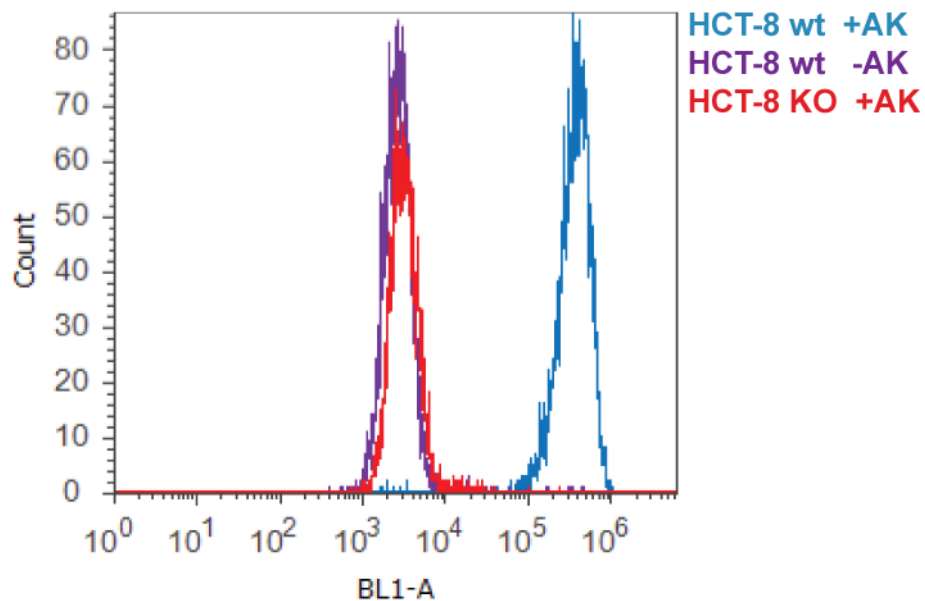


Figure 6-2 FACS-analysis of EpCAM-expression on HCT-8 wildtype and EpCAM-KO cells. HCT-8 wild-type (turquoise) and HCT-8 EPCAM-KO cells (purple) were stained with a GFP-coupled anti-EpCAM

antibody. Wild-type cells without antibody (red) were used as negative control. No EpCAM could be detected on the HCT-8 EPCAM-KO cells.

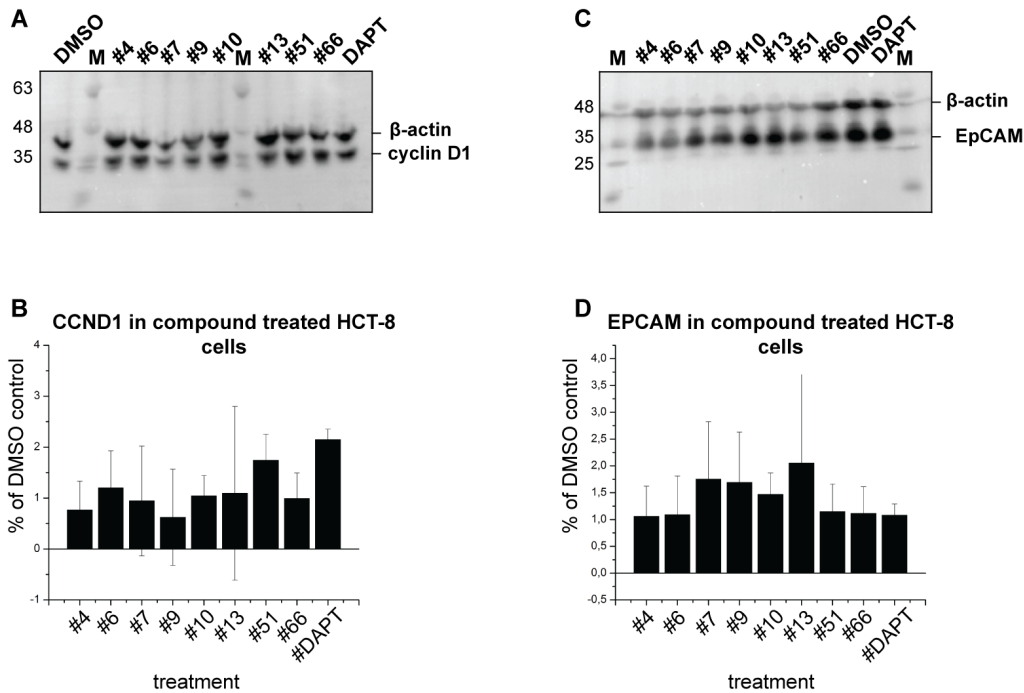


Figure 6-3 Western blot analysis of protein expression levels after compound treatment. HCT-8 wild-type cells were treated as indicated and cyclin D1 (**A**) and EPCAM (**C**) protein expression levels were analyzed by immunostaining and quantified (**B + D**). Neither the blots nor the quantification show any reduction of protein expression levels after compound treatment. Shown is one representative blot out of three independent experiments (**A + C**). Shown are mean values and standard deviations (**B + D**).

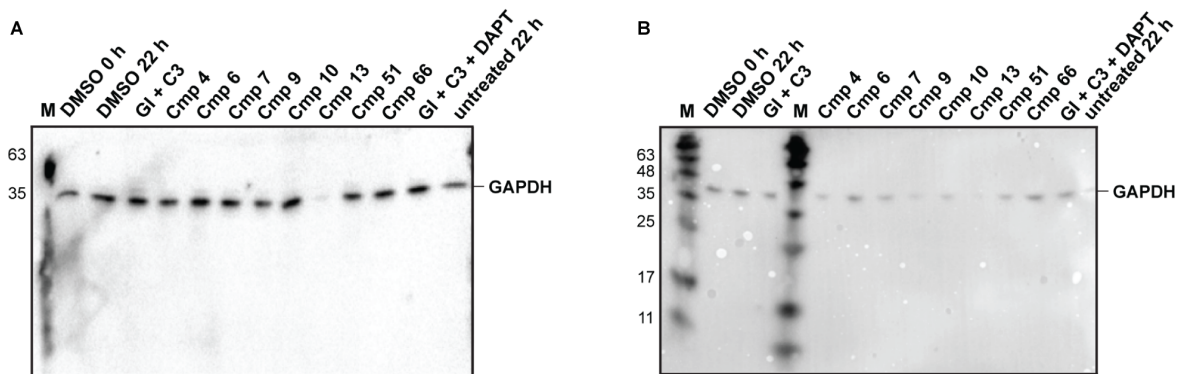


Figure 6-4 GAPDH loading control of membrane-based EpCAM-cleavage assays. HEK293 hEpCAM-FL-YFP cells and isolated membrane fractions (**B**) or membrane fractions only (**A**) were treated as indicated. Shown is the loading control from blots in **Figure 3-15**.

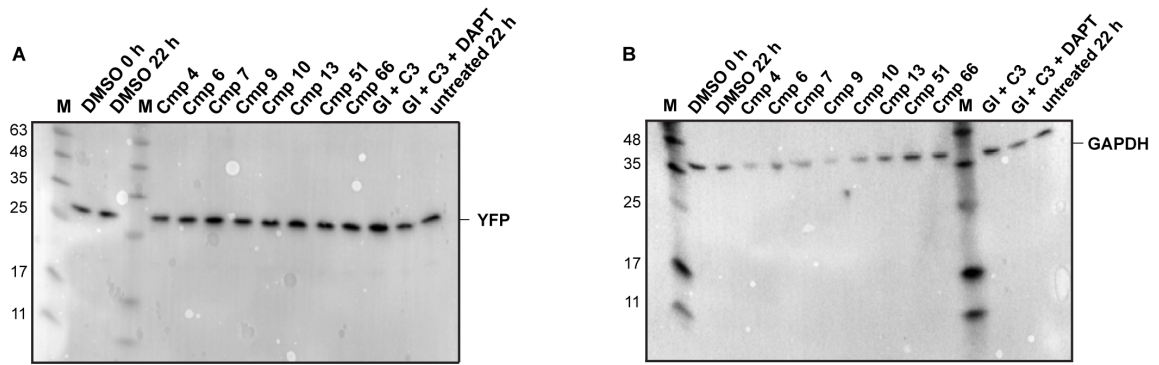


Figure 6-5 YFP control of membrane-based EpCAM-cleavage assay. Isolated membrane fractions from HEK293-YFP cells (**A**) were treated as indicated and cleavage products were separated in a 10 % SDS-PAGE and probed with anti-GFP antibodies. The YFP band was detected at the same intensity for every treatment. GAPDH was used as loading control (**B**).

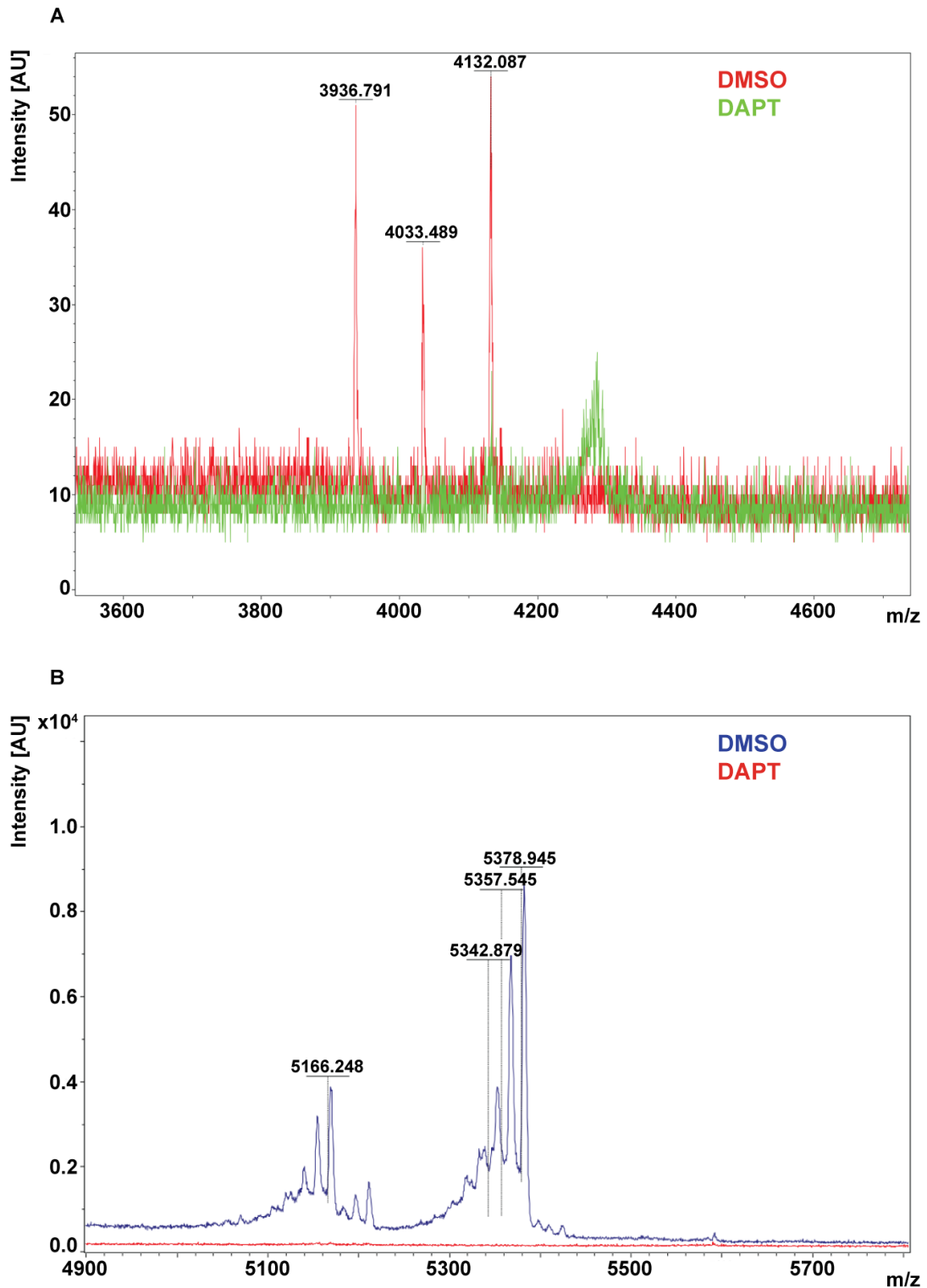


Figure 6-6 Mass spectra of γ -cleavage (A) and ϵ -cleavage sites (B) of Myc-CTF-Fag-TEV-YFP in HEK293. (A) HEK293 cells were treated with DMSO (red) or DAPT (green) to inhibit γ -secretase cleavage. Supernatant was collected and subjected to c-Myc IP. Peaks seen after DMSO treatment representing the three fragments resulting from γ -cleavage (3919.55 Da, 4018.68 Da, 4117.81 Da) were lacking after DAPT treatment. The size difference of approximately 15 Da is very likely due to oxidation of Methionine. (B) HEK293 cells were treated with DMSO (blue) or DAPT (red). Cells were lysed and subjected to GFP-IP followed by TEV-cleavage and Flag-IP. Peaks seen after DMSO treatment represent the two fragments resulting from ϵ -cleavage (5166.83 Da, 5379.12 Da) were lacking after DAPT treatment.

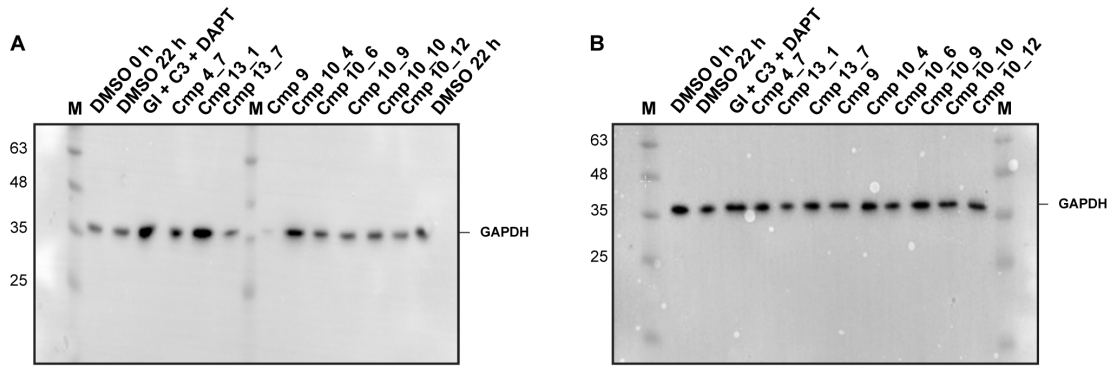


Figure 6-7 GAPDH loading control of membrane-based EpCAM-cleavage assays. HEK293 hEpCAM-FL-YFP cells and isolated membrane fractions (**B**) or membrane fractions only (**A**) were treated as indicated. Shown is the loading control from blots in [Figure 3-22](#).

7 References

Abraham VC, Taylor DL, Haskins JR (2004). **High Content Screening applied to large-scale cell biology.** Cell Press 22(1), 15-22.

Adamska M., Larroux C., Adamski M., Green K., Lovas E., Koop D., Richards GS, Zwafink C., Degnan BM (2010). **Structure and expression of conserved Wnt pathway components in the demosponge Amphimedon queenslandica.** Evolution & Development 12, 494-518.

Agrawal N., Dasaradhi PV, Mohammed A., Malhotra P., Bhatnagar RK, Mukherjee SK (2003). **RNA Interference: biology, mechanism and applications.** Microbiology and Molecular Biology Reviews 67(4), 657-685.

Al-Mayouf AM, Alswaied N., Alkuraya FS, Almehaidib A., Faqih M. (2009). **Case report tufting enteropathy and chronic arthritis: a newly recognized association with a novel EpCAM gene mutation.** Journal of Pediatric Gastroenterology & Nutrition 49(5), 642-644.

Alberti S., Nutini M., Herzenberg LA (1994). **DNA methylation prevents the amplification of TROP1, a tumor-associated cell surface antigen gene.** PNAS 91(13), 5833-5837.

Amaar YG, Thompson GR, Linkhart TA, Chen ST, Baylink DJ, Mohan S. (2002). **Insulin-like growth factor-binding protein 5 (IGFBP-5) interacts with a four and a half LIM protein 2 (FHL2).** The Journal of Biological Chemistry 277, 12053-12060.

Anastasiadis PZ and Reynolds AB (2000). **The p120 catenin family: complex roles in adhesion, signaling and cancer.** Journal of Cell Science 113(Pt 8), 13139-1334.

Baeuerle PA and Gires O. (2007). **EpCAM (CD326) finding its role in cancer.** British Journal of Cancer 96, 417-423.

Balzar M., Bakker HA Briaire-de-bruijn IH, Fleuren GJ, Warnaar SO, Litvinov SV (1998). **Cytoplasmic tail regulates the intercellular adhesion function of the epithelial cell adhesion molecule.** Molecular and Cell Biology 18(8), 4833-4843.

Balzar M., Braire-de Bruijn IH, Rees-bakker HAM, Prins FA, Helfrich W., De Leij L., Riethmüller G., Alberti S., Warnaar SO, Fleuren GJ, Litvinov SV (2001). **Epidermal growth factor-like repeats mediate lateral and reciprocal interactions of Ep-CAM molecules in homophilic adhesions.** Molecular and Cellular Biology 21(7), 2570-2580.

Balzar M., Winter MJ, de Boer CJ, Litvinov SV. (1999). **The biology of the 17-1A antigen (Ep-CAM).** Journal of Molecular Medicine 77(10), 699-712.

Barker N., van Es JH, Kuipers J., Kujala P., van den Born M., Cozijnsen M., Hagebarth A., Korving J., Begthel H., Peters PJ, Clevers H. (2007). **Identification of stem cells in small intestine and colon by marker gene *Lgr5*.** Nature 449, 1003-1007.

Barolo S. (2006). **Transgenic Wnt/TCF pathway reporters: all you need is Lef?** Oncogene 25(57), 7505-7511.

Beel AJ and Sanders CR (2008). **Substrate specificity of γ -secretase and other intramembrane proteases.** Cellular and Molecular Life Sciences 65(9), 1311-1334.

- Behrens J., von Kries Jp, Kuhl M., Bruhn L., Wedlich D., Grosschedl R., Birchmeier W. (1996). **Functional interaction of beta-catenin with the transcription factor LEF-1.** Nature 382, 638-642.
- Behrens, J., lowrick O., Klein-Hitpass L., Birchmeier W. (1991). **The E-cadherin promoter: functional analysis of a G.C-rich region and an epithelial cell-specific palindromic regulatory element.** PNAS 88(24), 11495-11499.
- Breuhahn K., Baeuerle PA, Peters M., Prang N., Töx U., Köhne-Volland R., Dries V., Schirmacher P., Leo E. (2006). **Expression of epithelial cellular adhesion molecule (Ep-CAM) in chronic (necro-)inflammatory liver diseases and hepatocellular carcinoma.** Hepatology Research: The Official Journal of the Japan Society of Hepatology 34(1), 50-56.
- Broun M., Gee L., Reinhardt B., Bode HR (2005). **Formation of the head organizer in hydra involves the canonical Wnt pathway.** Development 132, 2907-2916.
- Brown MS, Ye J., Rawson RB, Goldstein JL (2000). **Regulated intramembrane proteolysis: a control mechanism conserved from bacteria to humans.** Cell 100(4), 391-398.
- Brunkan AL, Martinez M., Walker ES, Goate AM (2005). **Presenilin endoproteolysis is an intramolecular cleavage.** 29(1), Molecular and Cellular Neuroscience 65-73.
- Brunner A., Schaefer G., Veits L., Brunner B., Prelog M., Ensinger C. (2008). **EpCAM overexpression is associated with high-grade urothelial carcinoma in the renal pelvis.** Anticancer Research 28(1A), 125-128.
- Brunner E., Peter O., Schweizer L., Basler K. (1997). **Pangolin encodes a Lef-1 homologue that acts downstream of Armadillo to transduce the Wingless signal in Drosophila.** Nature 385, 829-833.
- Buck M. (2003). **Crystallography: embracing conformational flexibility in proteins.** Structure 11(7), 735-736.
- Cao CY, Mok SWF, Cheng VWS, Tsui SKW (2015). **The FHL2 regulation in the transcriptional circuitry of human cancers.** Gene 572, 1-7
- Cehn YH, Wu ZQ, Zhao YL, Si YL, Guo MZ, Han WD (2012). **FHL2 inhibits the Id3-promoted proliferation and invasive growth of human MCF-7 breast cancer cells.** Chinese Medical Journal (Engl) 125, 2329-2333.
- Chan KK, Tsui SK, Lee SM, Luk SC, Liew CC, Fung KP, Waye MM, Lee CY (1998). **Molecular cloning and characterization of FHL2, a novel LIM domain protein preferentially expressed in human heart.** Gene 572, 1-7.
- Chaves-Perez A., Mack B., Maetzel D., Kremling H., Eggert C., Harreus U., Gires O. (2013). **EpCAM regulates cell cycle progression via control of cyclin D1 expression.** Oncogene 32(5), 641-650.
- Chen D., Xu W., Bales E., Colmenares C., Conacci-Sorrell M., Ishii S., Stavnezer E., Campisi J., Fisher DE, Ben-Zeév A., Medrano EE (2003). **SKI activates Wnt/beta-catenin signaling in human melanoma.** Cancer research 63, 6626-6634.
- Chong JM and Speicher DW (2001). **Determination of disulfide bond assignments and N-Glycosylation sites of the human gastrointestinal carcinoma antigen GA733-2 (CO17-1A, EGP, KS1-4, KSA, and EpCAM).** The Journal of Biological Chemistry 276, 5804-5813.

- Chu PH, Ruiz-Lozano P., Zhou Q., Cai C., Chen J. (2000). **Expression patterns of FHL/SLIM family members suggest important roles in skeletal muscle and cardiovascular system.** FEBS Letters 521, 259-265.
- Chung HM and Struhl G. (2001). **Nicastrin is required for Presenilin-mediated transmembrane cleavage in Drosophila.** Nature Cell Biology 3(12), 1129-1132.
- Cirulli V., Crisa L., Beattie GM, Mally MI, Lopez AD, Fannon A., Ptasznik A., Inverardi L., Ricordi C., Deerinck T., Ellisman M., Reisfeld RA, Hayek A. (1998). **KSA antigen Ep-CAM mediates cell-cell adhesion of pancreatic epithelial cells: morphoregulatory roles in pancreatic islet development.** Journal of Cell Biology 140(6), 1519-1534.
- Clark DP (2006). **Molecular Biology. Understanding the genetic revolution.** Spektrum Akademischer Verlag
- Cogliano VJ, Baan R., Straif K., Grosse Y., Lauby-Secretan B., El Ghissassi F., Bouvard V., Benbrahim-Tallaa L., Guha N., Freeman C., Galichet L., Wild CP (2011). **Preventable exposures associated with human cancers.** Journal of the National Cancer Institute 103(24), 1827-1839.
- Cohen SJ, Alpaugh RK, Gross S., O'Hara SM, Smirnov DA, Terstappen LW, Allard WJ, Bilbee M., Cheng JD, Hoffman JP, Lewis NL, Pellegrino A., Rogatko A., Sigurdson E., Wang H., Watson JC, Weiner LM, Meropol NJ (2006). **Isolation and characterization of circulating tumor cells in patients with metastatic colorectal cancer.** Clinical Colorectal Cancer 6(2), 125-132.
- Correa P. and Piazuelo, MB (2011). **Helicobacter pylori infection and gastric adenocarcinoma.** US Gastroenterology Hepatology Review 7(1), 59-64.
- Criscitiello C., Sotiriou C. Ignatiadis M. (2010). **Circulating tumor cells and emerging blood biomarkers in breast cancer.** Current Opinion in Oncology 22(6), 552-558.
- Daugherty RL and Gottardi CJ (2007). **Phospho-regulation of Beta-catenin adhesion and signaling functions.** Physiology 22, 303-309.
- Davidson G., Wu W., Shen J., Bilic J., Fenger U., Stannek P., Glinka A., Niehrs C. (2005). **Casein kinase 1 gamma couples Wnt receptor activation to cytoplasmic signal transduction.** Nature 438, 867-872.
- De Strooper B., Annaert W., Cupers P., Saftig P., Craessaerts K., Mumm JS, Schroeter EH, Schrijvers V., Wolfe MS, Ray WJ, Goate A., Kopan R. (1999). **A presenilin-1-dependent gamma-secretase-like protease mediates release of Notch intracellular domain.** Nature 398, 518-522.
- Deane CM, Salwinski L., Xenarios I., Eisenberg D (2002). **Protein interactions: two methods for assessment of the reliability of high throughput observations.** Molecular & Cellular Proteomics 1(5), 349-356.
- Denzel S., Mack B., Eggert C., Massoner P., Stocklein N., Kemming D., Harreus U., Gires O. (2012). **MMP7 is a target of the tumour-associated antigen EpCAM.** International Journal of Experimental Pathology 93(5), 341-353.
- Denzel S., Maetzel D., Mack B, Eggert C., Bähr G., Gires O. (2009). **Initial activation of EpCAM-cleavage via cell-to-cell contact.** BMC Cancer 9, 402
- Dick FA and Rubin SM (2013). **Molecular mechanisms underlying RB protein function.** Nature Reviews Molecular Cell Biology 14(5), 297-306.

- Dollé L., Theise ND, Schmelzer E., Boulter L., Gires O., van Grunsven LA (2015). **Ep-CAM and the biology of hepatic stem/progenitor cells**. *American Journal of Physiology* 308(4), G233-G250
- Dye BT and Patton JG (2001). **An RNA recognition motif (RRM) is required for the localization of PTB-associated splicing factor (PSF) to subnuclear speckles**. *Experimental Cell Research* 263, 131-144.
- Edbauer D., Winkler E., Regula JT, Pesold B., Steiner H., Haass C. (2003). **Reconstitution of gamma-secretase activity**. *Nature Cell Biology* 5(5), 486-488.
- Edwards DR, Handsley MM, Pennington CJ (2008). **The ADAM metalloproteinases**. *Molecular Aspects of Medicine* 29(5), 258-289.
- Eklof Spink K., Fridman SG, Weis WI (2001). **Molecular mechanisms of beta-catenin recognition by adenomatous polyposis coli revealed by the structure of an APC-beta catenin complex**. *The EMBO Journal* 20, 6203-6212.
- El Mourabit H., Muller S., Tunggal L., Paulsson M., Aumailley M. (2003). **Characterization of recombinant and natural forms of the human LIM domain-containing protein FHL2**. *Protein Expression and Purification* 32, 95-103.
- El Mourabit H., Muller S., Tunggal L., Paulsson M., Aumailley M. (2004). **Analysis of the adapter function of the LIM domain-containing protein FHL2 using an affinity chromatography approach**. *Journal of Cellular Biochemistry* 92(3), 612-625.
- Fields AL, Keller A., Schwartzberg L., Bernard S., Kardinal C., Cohen A., Schulz J., Eisenberg P., Forster J., Wissel P. (2009). **Adjuvant therapy with the monoclonal antibody Edrecolomab plus fluouracil-based therapy does not improve overall survival of patients with stage III colon cancer**. *Journal of Clinical Oncology* 27(12), 1941-1947.
- Fong D., Steurer M., Obrist P., Barbieri V., Margreiter R., Amberger A., Laimer K., Gastl G., Tzankov A., Spizzo G. (2008). **Ep-CAM expression in pancreatic and ampullary carcinomas: frequency and prognostic relevance**. *Journal of Clinical Pathology* 61(1), 31-35.
- Fraering PC, Ye W., Strub JM, Dolios G., LaVoie MJ, Ostaszewski BL, van Dorsselaer A., Wang R., Selkoe DJ, Wolfe MS (2004). **Purification and characterization of the human gamma-secretase complex**. *Biochemistry* 43(30), 9774-9789.
- Gabriel B., Fischer DC, orlowska-Volk M., zur Hausen A., Schule R., Muller JM, Hasenburger A. (2006). **Expression of the transcriptional coregulator FHL2 in human breast cancer: a clinicopathologic study**. *Journal of the Society for Gynecologic Investigation* 13, 69-75.
- Gabriel B., Mildenerger S., Weisser CW, Metzger E., Gitsch G., Schule R., Muller JM (2004). **Focal adhesion kinase interacts with the transcriptional coactivator FHL2 and both are overexpressed in epithelial ovarian cancer**. *Anticancer Research* 24(2B), 921-927.
- Gaiser MR, Lämmermann T., Feng X., Igyarto BZ, Kaplan DH, Tessarollo L., Germain RN, Udey MC (2012). **Cancer-associated epithelial cell adhesion molecule (Ep-CAM; CD326) enables epidermal Langerhans cell motility and migration in vivo**. *Proceeding of the National Academy of Sciences of the United States of America* 109(15), E889-897.

- Gasparri F. (2009). **An overview of cell phenotypes in HCS: limitations and advantages.** Expert Opinion on Drug Discovery 4(6), 643-657.
- Gee L., Hartig J., Law L., Wittlieb J., Khalturin K., Bosch TC, Bode HR (2010). **Beta-catenin plays a central role in setting up the head organizer in hydra.** Developmental Biology 340, 116-124.
- Geling A., Steiner H., Willem M., Bally-Cuif L., Haass C. (2002). **A γ -secretase inhibitor blocks Notch signaling *in vivo* and causes a severe neurogenic phenotype in zebrafish.** EMBO Reports 3(7), 688-694.
- Gires O. (2008). **EPCAM (tumor-associated calcium signal transducer 1).** Atlas of Genetics and Cytogenetics in Oncology and Haematology (February 2008).
- Gires O., Eskofier S., Lang S., Zeidler R., Munz M. (2003). **Cloning and characterization of a 1.1 kb fragment of the carcinoma-associated epithelial cell adhesion molecule promoter.** Anticancer Research 23(4), 3255-3261
- Gires O., Kieu C., Fix P., Schmitt B., Munz M., Wollenber B., Zeidler R. (2001). **Tumor necrosis factor alpha negatively regulates the expression of the carcinoma-associated antigen epithelial cell adhesion molecule.** Cancer 92(3), 620-628
- Giuliano KA, DeBiasio RL, Terry Dunlay R., Gough A., Volosky JM, Zock J., Pavlakis GN, Lansing Taylor D. (1997). **High-Content Screening: a new approach to easing key bottlenecks in the drug discovery process.** Journal of Biomolecular Screening 2(4), 249-259.
- Giuliano KA, Haskins JR, ed. (2010). **High Content Screening: A Powerful Approach to Systems Cell Biology and Drug Discovery.** Humana Press.
- Goel S., Bauer RJ, Desai K., Bulgaru A., Igbal T., Strachan BK, Kim G., Kaubisch A., Vanhove GF, Goldberg G., Mani S. (2007). **Pharmacokinetic and safety study of subcutaneously administered weekly ING-1, a human engineered monoclonal antibody targeting human EpCAM, in patients with advanced solid tumors.** Annals of Oncology 18(10), 1704-1707.
- Gonzalez B., Denzel S., Mack B., Conrad M., Gires O. (2009). **EpCAM is involved in maintenance of the murine embryonic stem cell phenotype.** Stem Cells 27(8), 1782-1792.
- Gorges TM, Tinhofer I., Drosch M., Rose L., Zollner TM, Krahn T., Ahsen O. (2012). **Circulating tumor cells escape from EpCAM-based detection due to epithelial-to-mesenchymal transition.** BMC Cancer 12, 178.
- Gosens MJ, van Kempen LC, van de Velde CJ, van Krieken JH, Nagtegaal ID. (2007). **Loss of membraneous Ep-CAM in budding colorectal carcinoma cells.** Modern Pathology: an Official Journal of the United States and Canadian Academy of Pathology 20(2), 221-232.
- Graham TA, Weaver C., Mao F., Kimelman D., Xu W. (2000). **Crystal structure of a beta-catenin/TCF complex.** Cell 103, 885-896.
- Groth A., Salnikov AV, Ottinger S., Gladkich J., Liu L., Kallifatidis G., Salnikoa O., Ryschich E., Giese N., Giese T., Momburg F., Büchler MW, Moldenhauer G., Herr I. (2012). **New gene-immunotherapy combining TRAIL-lymphocytes and Ep-CAMxCD3 bispecific antibody for tumor targeting.** Clinical Cancer Research 18(4), 1028-1038.

- Guerra E., Lattanzio R., La Sorda R., Dini F., Tiboni GM, Piantelli M., Alberti S. (2012). **mTrop1/Epcam knockout mice develop congenital tufting enteropathy through dysregulation of intestinal E-cadherin/ β -catenin.** PLoS One 7(11), e49302
- Günther T., Poli C., Muller JM, Catala-Lehnen P., Schinke T., Yin N., Vomstein S., Ameling M., Schule R. (2005). **Fhl2 deficiency results in osteopenia due to decreased activity of osteoblasts.** The EMBO Journal 24(17), 3049-3056.
- Hachmeister M., Bobowski KD, Hogl S., Dislich B., Fukumori A., Eggert C., Mack B., Kremling H., Sarrach S., Coscia F., Zimmermann W., Steiner H., Lichtenthaler SF, Gires O. (2013). **Regulated intramembrane proteolysis and degradation of murine epithelial cell adhesion molecule mEpCAM.** PLOS ONE 8(8), e71863.
- Hall JM, Lee MK, Newman B., Morrow JE, Anderson LA, Huey B., King MC (1990). **Linkage of early-onset familial breast cancer to chromosome 17q21.** Science 250 (4988), 1684-1689.
- Hanahan D. and Weinberg RA (2011). **Hallmarks of Cancer: The Next Generation.** Cell 144(5), 646-674.
- Haney SA ed. (2008). **High content screening: science, techniques and applications.** Wiley-Interscience.
- He B., Reguart N., You L., Mazieres J., Xu Z., Lee AY, Mikami I., McCormick F., Jablons DM (2005). **Blockade of Wnt-1 signaling induces apoptosis in human colorectal cancer cells containing downstream mutations.** Oncogene 24, 3054-3058.
- Hemler ME (2005). **Tetraspanin functions and associated microdomains.** Nature Reviews Molecular Cell Biology 6, 801-811.
- Henrich CJ, Budhu A., Yu Z., Evans JR, Goncharova EI, Ransom TT, Wang XW, McMahon JB (2013). **High-throughput Screening of identification of inhibitors of EpCAM-dependent growth of hepatocellular carcinoma cells.** Chemical Biology & Drug Design 82, 131-139.
- Herlyn M., Steplewski Z., Herlyn D., Koprowski H. (1979). **Colorectal carcinoma-specific antigen: detection by means of monoclonal antibodies.** Proceedings of the National Academy of Sciences 76(3), 1438-1442.
- Holland LZ, Panfilio KA, Chastain R., Schubert M., Holland ND (2005). **Nuclear beta-catenin promotes non-neural ectoderm and posterior cell fates in amphioxus embryos.** Developmental Dynamics 233, 1430-1443.
- Hollstein M., Sidransky D., Vogelstein B., Harris CC (1991). **P53 mutations in human cancers.** Science 253(5015), 49-53.
- Hoss A., Moarefi I., Scheidtmann KH, Cisek LJ, Corden JL, Dornreiter I., Arthur AK, Fanning E. (1990). **Altered phosphorylation pattern of simian virus 40 T antigen expressed in insect cells by using a baculovirus vector.** Journal of Virology 64, 4799-4807.
- Huber AH, Nelson WJ, Weis WI (1997). **Three-dimensional structure of the armadillo repeat region of beta-catenin.** Cell 90, 871-882.
- Huber AH, Weis WI (2001). **The structure of the beta-catenin/E-cadherin complex and the molecular basis of diverse ligand recognition by beta catenin.** Cell 105, 391-402.

- Huber O., Korn R., McLaughlin J., Ohsugi M., Herrmann BG, Kemler R. (1996). **Nuclear localization of beta-catenin by interaction with transcription factor LEF-1.** *Mechanisms of Development* 59, 3-10.
- Imrich S., Hachmeister M., Gires O. (2012). **EpCAM and its potential role in tumor-initiating cells.** *Cell Adhesion & Migration* 6(1), 30-38.
- Inagaki J., Matushima Y., Nakamura K., Oshima M., Kadowaki T., Kitagawa Y. (1996). **A large DNA-binding nuclear protein with RNA recognition motif and serine/arginine rich domain.** *The Journal of Biological Chemistry* 271, 12525-12531.
- Itoh-Satoh M., Hayashi T., Nishi H., Koga Y., Arimura T., Koyanagi T., Takahashi M., Hohda S., Ueda K., Nouchi T., Hiroe M., Marumo F., Imaizumi T., Yasunami M., Kimura A. (2002). **Itin mutations as the molecular basis for dilated cardiomyopathy.** *Biochemical and Biophysical Research Communications* 291(2), 385-393.
- Jafari R., Almqvist H., Axelsson H., Ignatuschenko M., Lundback T., Nordlund P., Martinez Molina D. (2014). **The cellular thermal shift assay for evaluating drug target interactions in cells.** *Nature Protocols* 9, 2100-2122.
- Johannessen M., Moller S., Hansen T., Moens U., Van Ghelue M. (2006). **The multifunctional roles of the four-and-a-half-LIM only protein FHL2.** *Cellular and Molecular Life Sciences* 63, 268-284.
- Jojovic M., Adam E., Zangemeister-Wittke U., Schumacher U. (1998). **Epithelial glycoprotein-2 expression is subject to regulatory processes in epithelial-mesenchymal transitions during metastases: an investigation of human cancers transplanted into severe combined immunodeficient mice.** *The Histochemical Journal* (30)10, 723-729.
- Kadmas JL and Beckerle MC (2004). **The LIM domain: from the cytoskeleton to the nucleus.** *Nature Reviews. Molecular Cell Biology* 5(11), 920-931.
- Khan KH (2013). **Gene expression in mammalian cells and its applications.** *Advanced Pharmaceutical Bulletin* 3(2), 257-263.
- Kim Y., Kim HS, Cui ZY, Lee HS, Ahn JS, Park CK, Park K., Ahn MJ (2009). **Clinicopathological implications of EpCAM expression in adenocarcinoma of the lung.** *Anticancer research* 29(5), 1817-1822.
- Kimberly WT, LaVoie MJ, Ostaszewski BL, Ye W., Wolfe MS, Selkoe DJ (2003). **Gamma-secretase is a membrane protein complex comprised of presenilin, nicastrin, Aph-1, and Pen-2.** *Proceedings of the National Academy of Science of the United States of America* 100(11), 6382-6387.
- Kimelman D. and Xu W. (2006). **beta-catenin destruction complex: insights and questions from a structural perspective.** *Oncogene* 25(57), 7482-7491.
- Kinoshita M., Nakagawa T., Schimizu A., Katsuoka Y. (2005). **Differently regulated androgen receptor transcriptional complex in prostate cancer compared with normal prostate.** *International Journal of Urology* 12, 390-397.
- Ko JS, Seo JK, Shim JO, Hwang SH, Park HS, Kang GH (2010). **Tufting enteropathy with EpCAM mutations in two siblings.** *Gut and Liver* 4(3), 407-410.
- Kobielak A. and Fuchs E. (2004). **Alpha-catenin: at the junction of intercellular adhesion and actin dynamics.** *Nature Reviews Molecular Cell Biology* 5(8), 614-625.

- Kong Y., Shelton JM, Rothermel B., Li X., Richardson JA, Bassel-Duby R., Williams RS (2001). **Cardiac-specific LIM protein FHL2 modifies the hypertrophic response to beta-adrenergic stimulation.** *Circulation* 103(22), 2731-2738.
- Kopan R. and Ilagan MX (2004). **Gamma-secretase: proteasome of the membrane?** *Nature Reviews. Molecular Cell Biology* 5(6), 499-504.
- Kornilova AY, Bihel F., Das C., Wolfe MS (2005). **The initial substrate-binding site of gamma-secretase is located on presenilin near the active site.** *Proceedings of the National Academy of Science of the United States of America* 102(9), 3230-3235.
- Krishnamurthy G., Patberg KW, Obreztkhikova MN, Rybin AV, Rosen MR (2004). **Developmental evolution of the delayed rectifier current IKs in canine heart appears dependent on the beta subunit mink.** *Heart Rhythm* 1(6), 704-711.
- Kuhn S., Koch M., Nubel T., Ladwein M., Antolovic D., Klingbeil P., Hildebrand D., Moldenhauer G., Langbein L., Franke WW, Weitz J., Zoller M. (2007). **A complex of EpCAM, claudin-7, CD44 variant isoforms, and tetraspanins promote colorectal cancer progression.** *Molecular Cancer Research* 5(6), 553-567.
- Kuhn S., Koch M., Nübel T., Ladwein M., Antolovic D., Klingbeil P., Hildebrand D., Moldenhauer G., Langbein L., Franke WW, Weitz J., Zoeller M. (2007). **A complex of EpCAM, claudin-7, CD44 variant isoforms, and tetraspanins promotes colorectal cancer progression.** *Molecular Cancer Research* 5(6), 553-567.
- Kurakula K., Sommer D., Sokolovic M., Moerland PD, Scheij S., van Loenen PB, Koenis DS, zelcer N., van Tiel CM, de Vries CJ (2015). **LIM-only protein FHL2 is a positive regulator of liver X receptors in smooth muscle cells involved in lipid homeostasis.** *Molecular and Cellular Biology* 35, 52-62.
- Labalette C., Renard CA, Neuveut C., Buendia MA, Wei Y. (2004). **Interaction and functional cooperation between the LIM protein FHL2, CBP/p300 and β -catenin.** *Molecular and Cellular Biology* 24, 10689-10702.
- Ladwein M., Pape UF, Schmidt DS, Schnolzer M., Fiedler S., Langbein L., Franke WW, Moldenhauer G., Zoller M. (2005). **The cell-cell adhesion molecule EpCAM interacts directly with the tight junction protein claudin-7.** *Experimental Cell Research* 309(2), 345-357.
- Lafaro KJ, Demirjian AN, Pawlik TM (2015). **Epidemiology of hepatocellular carcinoma.** *Surgical oncology clinics of North America* 24(1), 1-17.
- Lal M. and Caplan M. (2011). **Regulated intramembrane proteolysis: signaling pathways and biological functions.** *Physiology (Bethesda)* 26(1), 34-44.
- Lange S., Auerbach D., McLoughlin P., Perriard E., Schafer B., Perriard JC, Ehler E. (2002). **Subcellular targeting of metabolic enzymes to titin in heart muscle may be mediated by DRAL/FHL2.** *Journal of Cell Science* 115(Pt 24), 4925-4936.
- Lapébie P., Gazave E., Ereskovsky A., Derelle R., Bézac C., Renard E., Houliston E., Borchiellini C. (2009). **WNT/beta-catenin signaling and epithelial patterning in the homoscleromorpha sponge *Oscarella*.** *PLoS One* 4, e5823.
- Le Naour F., André M., Boucheix C., Rubinstein E. (2006). **Membrane microdomains and proteomics: lessons from tetraspanin microdomains and comparison with lipid rafts.** *Proteomics* 6 (2006a), 6447-6454.

- Le Naour F., André M., Greco C., Billard M., Sordat B., Emile JF, Lanza F., Boucheix C., Rubinstein E. (2006b). **Profiling of the tetraspanin web of human colon cancer cells.** *Molecular Cellular Proteomics* 5, 845-857.
- Lee JH, Jang SI, Yang JM, Markova NG, Steinert PM (1996). **The proximal promoter of the human transglutaminase 3 gene. Stratified squamous epithelial-specific expression in cultured cells is mediated by binding of Sp1 and ets transcription factors to a proximal promoter element.** *The Journal of Biological Chemistry* 271(8), 4561-4568
- Leemans CR, Braakhuis BJ, Brakenhoff RH (2011). **The molecular biology of head and neck cancer.** *Nature Reviews. Cancer* 11(1), 9-22.
- Lei Z., Maeda T., Tamura A., Nakamura T., Yamazaki Y., Shiratori H., Yashiro K., Tsukita S., Hamada H. (2012). **EpCAM contributes to formation of functional tight junctions in the intestinal epithelium by recruiting claudin proteins.** *Developmental Biology* 371(2), 136-145.
- Levine AJ, Momand J., Finlay CA (1991). **The p53 tumour suppressor gene.** *Nature* 351(6362), 453-456.
- Lewis LD (2003). **Technology evaluation: ING-1, XOMA.** *Current Opinion in Molecular Therapeutics* 5(4), 433-436.
- Li HY, Ng EK, Lee SM, Kotaka M., Tsui SK, Lee CY, Fung KP, Waye MM. (2001). **Protein-protein interaction of FHL3 with FHL2 and visualization of their interaction by green fluorescent proteins (GFP) two-fusion fluorescence resonance energy transfer (FRET).** *Journal of Cellular Biochemistry* 80(3), 293-303.
- Liao MY, Lai JK, Kuo MYP, Lu RM, Lin CW, Cheng PC, Liang KH, Wu HC (2015). **An anti-EpCAM antibody EpAB2-6 for the treatment of colon cancer.** *Oncotarget* 6(28), 24947-24968.
- Linke R., Klein A., Seimetz D. (2010). **Catumaxomab: clinical development and future directions.** *MAbs* 2(2), 129-136.
- Linnenbach AJ, Wojciorowski J., Wu S., Pyrc JJ, Ross AH, Dietzschold B., Speicher D., Koprowski H. (1989). **Sequence investigation of the major gastrointestinal tumor-associated antigen gene family, GA733.** *PNAS* 86(1), 27-31.
- Lipinski CA, Lombardo F., Dominy BW and Feeney PJ (2001). **Experimental and computational approaches to estimate solubility and permeability in drug discovery and development settings.** *Advanced Drug Delivery Reviews* 46(1-3), 2-26.
- Liptrot C. (2001). **High Content Screening – from cells to data to knowledge.** *Drug Discovery Today* 6(16), 832-834.
- Litvinov SV, Bakker HA, Gourevitch MM, Velders MP, Warnaar SO (1994b). **Evidence for a role of the epithelial flycoprotein 40 (Ep-CAM) in epithelial cell-cell adhesions.** *Cell Communication & Adhesion* 2(5), 417-428.
- Litvinov SV, Balzar M., Winter MJ, Bakker HA, Briaire-de Bruijn LH, Prins F., Fleuren GJ, Warnaar SO (1997). **Epithelial cell adhesion molecule (Ep-CAM) modulates cell-cell interactions mediated by classic cadherins.** *The Journal of Cell Biology* 139(5), 1337-1348.
- Litvinov SV, Velders MP, Bakker HA, Fleuren GJ, Warnaar SO (1994a). **Ep-CAM: a human epithelial antigen is a homophilic cell-cell adhesion molecule.** *The Journal of Cell Biology* 125(2), 437-446.

- Ljubojevic S. and Skerlev M. (2014). **HPV-associated diseases**. Clinics in Dermatology 32(2), 227-234.
- Lo MC, Aulabaugh A., Jin G., Cowling R., Bard J., Malamas M., Ellesatd G. (2004). **Evaluation of fluorescence-based thermal shift assays for hit identification in drug discovery**. Analytical Biochemistry 332(1), 153-159.
- LoBuglio A., Saleh M., Braddock J., Lampkin T., Khor S., Wissel P., *et al.* (1997). **A phase I trial of the humanized anti-EGP40 monoclonal antibody 3622W94**. Proceedings of the American Society of Clinical Oncology 16, 436.
- Logan CY and Nusse R. (2004). **The Wnt signaling pathway in development and disease**. Annual review of cell and developmental biology 20, 781-810.
- Lu TY, Lu RM, Liao MY, Yu J., Chung CH, Kao CF, Wu HC (2010). **Epithelial cell adhesion molecule regulation is associated with the maintenance of the undifferentiated phenotype of human embryonic stem cells**. The Journal of Biological Chemistry 285(12), 8719-8732.
- Lund K., Bostad M., Skarpen E., Braunagel M., Kiprijanov S., Krauss S., Duncan A., Hogset A., Selbo PK (2014). **The novel EpCAM-targeting monoclonal antibody 3-171 linked to saporin is highly cytotoxic after photochemical internalization in breast, pancreas and colon cancer cell lines**. MAbs 6(4), 1038-1050.
- Maaser K. and Borlak J. (2008). **A genome-wide expression analysis identifies a network of EpCAM-induced cell cycle regulators**. British Journal of Cancer 99, 1635-1643.
- MacDonald BT, Tamai K., He X. (2009). **Wnt/ β -catenin signaling: components, mechanisms and diseases**. Developmental Cell 17(1), 9-26.
- Maetzel D., Denzel S., Mack B., Canis M., Went P., Benk M., Kieu C., Papior P., Baeuerle PA, Munz M., Gires O. (2009). **Nuclear signalling by tumour-associated antigen EpCAM**. Nature Cell Biology 11(2), 162-171.
- Mann M. and Jensen ON (2003). **Proteomic analysis of post-translational modifications**. Nature Biotechnology 21, 255-261.
- Mao J., Wang J., Liu B., Pan W., Farr GH, Flynn C., Yuan H., Takada S., Kimelman D., Li L., Wu D. (2001). **Low-density lipoprotein receptor-related protein-5 binds to Axin and regulated the canonical Wnt signaling pathway**. Molecular Cell 7(4), 801-809.
- Martin B., Schneider R., Janetzky S., Waibler Z., Pandur P., Kuhl M., Behrens J., von der Mark K., Starzinski-Powitz A., Wixler V. (2002). **The LIM-only protein FHL2 interacts with beta-catenin and promotes differentiation of mouse myoblasts**. The Journal of Cell Biology 159(1), 113-122
- Martinez Molina D., Jafari R., Ignatuschenko M., Seki T., Larsson EA, Dan C., Sreekumar L., Cao Y., Nordlund P. (2013). **Monitoring drug target engagement in cells and tissues using the cellular thermal shift assay**. Science 341(6141), 84-87.
- Massoner P., Thomm T., Mack B., Untergasser G., Martowicz A., Bobowski K., Klocker H., Gires O., Puhr M. (2014). **EpCAM is overexpressed in local and metastatic prostate cancer, suppressed by chemotherapy and modulated by MET-associated miRNA-200c/205**. British Journal of Cancer 111(5), 955-964.
- McCrea PD, Turck CW, Gumbiner B. (1990). **A homolog of the armadillo protein in Drosophila (plakoglobin) associated with E-cadherin**. Science 254, 1359-1361.

- McLaughlin PMJ, Trzpis M., Kroesen BJ, Helfrich W., Terpstra P., Dokter WHA, Ruiters MHJ, de Leij LFMH, Harmsen MC (2004). **Use of the EGP-2//EpCAM promoter for targeted expression of heterologous genes in carcinoma derived cell lines.** *Cancer Gene Therapy* 11(9), 603-612.
- McLoughlin P., Ehler E., Carlile G., Licht JD, Schafer B. (2002). **The LIM-only protein DRAL/FHL2 interacts with and is a corepressor for the promyelocytic leukemia zinc finger protein.** *The Journal of Biological Chemistry* 277, 37045-37053.
- Medina M. and Dotti CG (2003). **RIPped out by presenilin-dependent gamma secretase.** *Cellular Signaling* 15(9), 829-841.
- Moegl M. and Uetz P. (2007). **Improving yeast two-hybrid screening systems.** *Briefings in Functional Genomics* 6(4), 302-312.
- Moldenhauer G., Momburg F., Moller P., Schwarz R., Hammerling GJ (1987). **Epithelium-specific surface glycoprotein of Mr 34,000 is a widely distributed human carcinoma marker.** *British Journal of Cancer* 56(6), 714-721.
- Molenaar M., van de Wetering M., Oosterwegel M., Peterson-Maduro J., Godsave S., Korinek V., Roose J., Destree O., Clevers H. (1996). **XTCF-3 transcription factor mediates beta-catenin induced axis in Xenopus embryos.** *Cell* 86, 391-399.
- Molina F., Bouanani M., Pau B., Granier C. (1996). **Characterization of the type-1 repeat from the thyroglobulin, a cysteine-rich module found in proteins from different families.** *European Journal of Biochemistry* 240(1), 125-133.
- Momburg F., Moldenhauer G., Hammerling GJ, Moller P. (1987). **Immunohistochemical study of the expression of a Mr 34,000 human epithelium-specific surface glycoprotein in normal and malignant tissues.** (*Cancer Research* 47(11), 2883-2891.
- Morgan MJ and Madgwick AJ (1996). **Slim defines a novel family of LIM-proteins expressed in skeletal muscle.** *Biochemical and Biophysical Research Communications* 225, 632-638.
- Morgan MJ and Madgwick AJ (1999). **The fourth member of the FHL family of LIM proteins is expressed exclusively in the testis.** *Biochemical and Biophysical Research Communications* 255, 251-255.
- Morlon A., Sassone-Corsi P. (2003). **The LIM-only protein FHL2 is a serum-inducible transcriptional coactivator of AP-1.** *Proceedings of the National Academies of Sciences of the United States of America* 100, 3977-3982.
- Muller JM, Isele U., Metzger E., Rempel A., Moser M., Pscherer A., Breyer T., Holubarsch C., Buettner R., Schule R. (2000). **FHL2, a novel tissue-specific coactivator of the androgen receptor.** *The EMBO Journal* 19(3), 359-369.
- Muller W., Frank U., Teo R., Mokady O., Guette C., Plickert G. (2007). **Wnt signaling in hydroid development: ectopic heads and giant buds induced by GSK-2beta inhibitors.** *The International Journal of Developmental Biology* 51, 211-220.
- Munz M., Baeuerle PA, and Gires O. (2009). **The Emerging Role of EpCAM in Cancer and Stem Cell Signaling.** *Cancer Research* 69(14), 5627-5629.
- Munz M., Fellingner K., Hofmann T., Schmitt B., Gires O. (2008). **Glycosylation is crucial for stability of tumour and cancer stem cell antigen EpCAM.** *Frontiers in Bioscience: A Journal and Virtual Library* 13, 5195-5201.

- Munz M., Kieu C., Mack B., Schmitt B., Zeidler R., Gires O. (2004). **The carcinoma-associated antigen EpCAM upregulates c-myc and induces cell proliferation.** *Oncogene* 23, 5748-5758.
- Munz M., Murr A., Kvesic M., Rau D., Mangold S., Pflanz S., Lumsden J., Volkland J., Fagerberg J., Riethmüller G., Rüttinger D., Kufer P., Baeuerle PA, Raum T. (2010). **Side-by-side analysis of five clinically tested antiEpCAM monoclonal antibodies.** *Cancer Cell International* 10(44).
- Munz M., Zeidler O., Gires O. (2005). **The tumour-associated antigen EpCAM up-regulates the fatty acid binding protein E-FABP.** *Cancer Letters* 225(1), 151-157.
- NCBI (2017). **CTNNB1 – catenin beta 1 [*Homo sapiens* (human)]** – Gene ID: 1499
- NCBI (2017). **EPCAM epithelial cell adhesion molecule [*Homo sapiens* (human)]** – Gene ID: 4072
- NCBI (2017). **FHL2 – four and a half LIM domains 2 [*Homo sapiens* (human)]** – Gene ID: 2274
- Neighbors M., Apt D., Chang JC, Brinkman A., Sipos-Solman I., Ong R., Leong S., Punnonen J. (2008). **EpCAM-specific vaccine response by modified antigen and chimeric costimulatory molecule in cynomolgus monkeys.** *Journal of Immunotherapy* 31(7), 644-655.
- Ng EK, Chan KK, Wong CH, Tsui SK, Ngai SM, Lee SM, Kotaka M., Lee CY, Waye MM, Fung KP (2002). **Interaction of the heart-specific LIM domain protein, FHL2, with DNA-binding nuclear protein, hNP220.** *Journal of Cellular Biochemistry* 84(3), 556-566.
- Ng VY, Ang SN, Chan JX, Choo AB. (2010). **Characterization of epithelial cell adhesion molecule as a surface marker on undifferentiated human embryonic stem cells.** *Stem Cells* 28(1), 29-35.
- Niesen FH, Berglund H., Vedadi M. (2007). **The use of differential scanning fluorimetry to detect ligand interactions that promote protein stability.** *Nature Protocols* 2(9), 2212-2221.
- Niimura M., Isoo N., Takasugi N., Tsuruoka M., Ui-Tei K., Saigo K., Morohashi Y., Tomita T., Iwatsubo T. (2005). **Aph-1 contributes to the stabilization and trafficking of the gamma-secretase complex through mechanisms involving intermolecular and intramolecular interactions.** *The Journal of Biological Chemistry* 280(13), 12967-12975.
- Njei B., Rotman Y., Ditah I., Lim JK (2015). **Emerging trends in hepatocellular carcinoma incidence and mortality.** *Hepatology* 61(1), 191-199.
- Nubel T., Preobraschenski J., Tuncay H., Weiss T., Kuhn S., Ladwein M., Langbein L., Zoller M. (2009). **Claudin-7 regulates EpCAM-mediated functions in tumor progression.** *Molecular Cancer Research* 7(3), 285-299.
- Nusse R. (2005). **Wnt signaling in disease and development.** *Cell Research* 15(1), 28-32.
- O'Reilly DR, Miller LK, Luckow VA (1994). **Baculovirus expression vectors: a laboratory manual.** Oxford University Press

- Ohlkippar U., Schrott G., Dieterich C., Muller JM, Galgoczy P., Engel FB, Keating MT, Gertler F., Schule R., Vingron M., Nordheim A. (2004). **The SRF target gene Fhl2 antagonizes RhoA/MAL-dependent activation of SRF.** *Molecular Cell* 16, 867-880.
- Oishi N., Yamashita T., Kaneko S. (2014). **Molecular biology of liver cancer stem cells.** *Liver Cancer* 3, 71-84.
- Orsulic S. and Peifer M. (1996). **An *In vivo* structure-function study of armadillo, the beta-catenin homologue, reveals both separate and overlapping regions of the protein required for cell adhesion and for wingless signaling.** *The Journal of Cell Biology* 134, 1282-1300.
- Osta WA; Chen Y., Mikhitarian K., Mitas M., Salem M., Hannun YA, Cole DJ, Gilanders WE (2004). **EpCAM is overexpressed in breast cancer and is a potential target for breast cancer therapy.** *Cancer Research* 64(16), 5818-5824.
- Ozawa M., Baribault H., Kemler R. (1989). **The cytoplasmic domain of the cell adhesion molecule uvomorulin associates with three independent proteins structurally related in different species.** *The EMBO Journal* 8, 1711-1717.
- Patriarca C., Macchi RM, Marschner AK, Mellstedt H. (2012). **Epithelial cell adhesion molecule expression (CD326) in cancer: A short review.** *Cancer Treatment Reviews* 38(1), 68-75.
- Pauli C., Munz M., Kieu C., Mack B., Breinl P., Wollenberg B., Lang S., Zeidler R., Gires O. (2003). **Tumor-specific glycosylation of the carcinoma-associated epithelial cell adhesion molecule EpCAM in head and neck carcinomas.** *Cancer Letters* 193(1), 25-32.
- Pavsic M., and Lenarcic B. (2011). **Expression, crystallization and preliminary X-ray characterization of the human epithelial cell-adhesion molecule ectodomain.** *Acta crystallographica. Section F, Structural biology and crystallization communications* 67, 1363-1366.
- Pavsic M., Guncar G., Djinovic-Carugo K., Lenarcic B. (2014). **Crysal structure and its bearing towards an understanding of key biological functions of EpCAM.** *Nature Communications* 5, 4764.
- Peifer M. and Wieschaus E. (1990). **The segment polarity gene armadillo encodes a functionally modular protein that is the Drosophila homolog of human plakoglobin.** *Cell* 63, 1056-1068.
- Pfaffl MW (2001). **A new mathematical model for relative quantification in real-time RT-PCR.** *Nucleic Acids Research* 29(9), e45.
- Poy F., Lepourcelet M., Shivdasani RA, Eck MJ (2001). **Structure of a human TCF4-beta catenin complex.** *Nature Structural & Molecular Biology* 8, 1053-1057.
- Prakash S. and Swaminathan U. (2015). **β catenin in health: A review.** *Journal of Oral and maxillofacial pathology* 19(2), 230-238.
- Purcell NH, Datwis D., Bueno OF, Muller JM, Schule R. Molkenstein JD (2004). **Extracellular signal-regulated kinase 2 interacts with and is negatively regulated by the LIM-only protein FHL2 in cardiomyocytes.** *Molecular and Cell Biology* 24, 1081-1095.
- Ralhan R., Cao J., Lim T., MacMillan C., Freeman JL, Walfish PG (2010b). **EpCAM nuclear localization identifies aggressive thyroid cancer and is a marker for poor prognosis.** *BMC cancer* 10, 33.

- Ralhan R., Cao T., Lim T., MacMillan C., Freeman JL, Walfish PG. **EpCAM nuclear localization identifies aggressive thyroid cancer and is a marker for poor prognosis.** BMC Cancer 10, 331.
- Ralhan R., He HC, So AK, Tripathi SC, Kumar M., Hasan MR, Kaur J., Kashat L., MacMillan C., Chauhan SS, Freeman JL, Walfish PG (2010a). **Nuclear and cytoplasmic accumulation of Ep-ICD is frequently detected in human epithelial cancers.** PLoS One 5(11), e14130.
- Rao CG, Chianese D., Doyle GV, Miller MC, Russell T., Sanders RA Terstappen LW (2005). **Expression of epithelial cell adhesion molecule in carcinoma cells present in blood and primary and metastatic tumors.** International Journal of Oncology 27(1), 49-57
- Reichert JM. (2012). **Marketed therapeutic antibodies compendium.** mAbs 4(3), 413-415.
- Riesenberg R., Buchner A., Pohla H., Lindhofer H. (2001). **Lysis of prostate carcinoma cells by trifunctional bispecific antibodies (alpha EpCAM x alpha CD3).** Journal of Histochemistry & Cytochemistry 49(7), 911-917.
- Riggleman B., Schedl P., Wieschaus E. (1990). **Spatial expression of the Drosophila segment polarity gene armadillo is posttranscriptionally regulated by wingless.** Cell 63, 549-560.
- Salomon J., Espinosa-Parrilla Y., Goulet O., Al-Qabandi W., Guigue P., Canioni D., Bruneau J., Alzahrani F., Almuhsen S., Cerf-Bensussan N., Jeanpierre M., Brousse N., Lyonnet S., Munnich A., Smahi A. (2011) **A founder effect at the EPCAM locus in congenital tufting enteropathy in the Arabic Gulf.** European Journal of Medical Genetics 54(3), 319-322.
- Sambrook J. and Russell, DW (2001). **Molecular cloning: a laboratory manual.** Cold Spring Harbor Laboratory Press 4.
- Samson T., Smyth N., Janetzky S., Wendler O., Muller JM, Schule R., von der Mark H., von der Mark K., Wixler V. (2004). **The LIM-only proteins FHL2 and FHL3 interact with alpha- and beta-subunits of the muscle alpha7beta1 integrin receptor.** The Journal of Biological Chemistry 279, 28641-28652.
- Sansal I. and Sellers WR (2004). **The biology and clinical relevance of the PTEN tumor suppressor pathway.** Journal of Clinical Oncology 22(14), 2954-2963
- Sato T., Diehl TS, Narayanan S., Funamoto S., Ihara Y., De Strooper B., Steiner H., Haass C., Wolfe MS (2007). **Active gamma-secretase complexes contain only one of each component.** The Journal of Biological Chemistry 282(47), 33985-33993.
- Schein CH (1989). **Production of soluble recombinant proteins in bacteria.** Nature Biotechnology 7, 1141-1149.
- Schmeichel KL and Beckerle MC (1994). **The LIM domain is a modulator protein-binding interface.** Cell 79, 211-219.
- Schmidt DS, Klingbeil P., Schnolzer M., Zollner M. (2004). **CD44 variant isoforms associate with tetraspanin and EpCAM.** Experimental Cell Research 297(2), 329-347.
- Schmidt M., Scheulen ME, Dittrich C., Obrist P., Marschner N., Dirix L., Schmidt M., Rüttinger D., Schuler M., Reinhardt C., Awada A. (2010). **An open-label, randomized phase II study of adecatumumab, a fully human anti-EpCAM antibody, as mono-**

- therapy in patients with metastatic breast cancer.** *Annals of Oncology* 21(2), 275-282.
- Schmohl JU, Felices M., Todhunter D., Taras E., Miller JS, Vallera DA (2016). **Tetra-specific scFv construct provides NK cell mediated ADCC and self-sustaining stimuli via insertion of IL-15 as a cross-linker.** *Oncogene* 7(45), 73830-73844.
- Schmoll HJ and Arnold D. (2009). **When wishful thinking leads to a misty-eyed appraisal: the sorry of the adjuvant colon cancer trials with edrecolomab.** *Journal of Clinical Oncology* 27(12), 1926-1929.
- Schneider SQ, Finnerty JR, Martindale MQ (2003). **Protein evolution: structure function relationships of the oncogene beta-catenin in the evolution of multicellular animals.** *Journal of Experimental Zoology Part B: Molecular and Developmental Evolution* 295(1), 25-44.
- Schnell U., Cirulli V., Giepmans BNG (2013a). **EpCAM: Structure and function in health and disease.** *Biochimica et Biophysica Acta* 1828, 1989-2001.
- Schnell U., Kuipers J., Giepmans BNG (2013c). **EpCAM proteolysis: new fragments with distinct functions?** *Bioscience Reports* 22(2), e00030.
- Schnell U., Kuipers J., Mueller JL, Veenstra-Algra A., Sivagnanam M., Giepmans BNG (2013b). **Absence of cell surface EpCAM in congenital tufting enteropathy.** *Human Molecular Genetics* 22 (13), 2566-2571.
- Scholl FA, McLoughlin P., Ehler E., de Giovanni C., Schafer BW (2000). **DRAL is a p53-responsive gene whose four and a half LIM protein domain protein product induces apoptosis.** *The Journal of Cell Biology* 151, 495-506.
- Schon MP, Schon M., Mattes MJ, Stein R., Weber L., Alberti S., Klein CE (1993). **Biochemical and immunological characterization of the human carcinoma-associated antigen MH 99/KS 1/4.** *International Journal of Cancer* 55(6), 988-995.
- Sears HF, Atkinson B., Mattis J., Ernst C., Herlyn D., Steplewski Z., Hayry P., Koprowski H. (1982). **Phase-I clinical trial of monoclonal antibody in treatment of gastrointestinal tumours.** *Lancet* 1(8275), 762-765.
- Sears HF, Herlyn D., Steplewski Z., Koprowski H. (1984). **Effects of monoclonal antibody immunotherapy on patients with gastrointestinal adenocarcinoma.** *Journal of Biological Response Modifiers* 3(2), 138-150.
- Shah S., Lee SF, Tabuchi K., Hao YH, Yu C., LaPlant Q., Ball H., Dann CE 3rd, Südhof T., Yu G. (2005). **Nicastrin functions as gamma-secretase-substrate receptor.** *Cell* 122(3), 435-447.
- Siegfried E., Wilder EL, Perrimon N. (1994). **Components of wingless signaling in Drosophila.** *Nature* 367, 76-80.
- Sivagnanam M., Mueller JL, Lee H., Chen Z., Nelson SF, Turner D., Zlotkin SH, Pencharz PB, Ngan BY, Libiger O., Schork NJ, Lavine JE, Taylor S., Newbury RO, Kolodner RD, Hoffman HM (2008). **Identification of EpCAM as the gene for congenital tufting enteropathy.** *Gastroenterology* 135, 429-437
- Sivagnanam M., Schaible T., Szigeti R., Byrd RH, Finegold MJ, Ranganathan S., Gopalakrishna GS, Tatevian N., Kellermayer R. (2010). **Further evidence for EpCAM as the gene for congenital tufting enteropathy.** *American journal of medical genetics* 152A(1), 222-224.

- Spizzo G., Went P., Dirnhofer S., Obrist P., Simon R., Spichtin H., Maurer R., Metzger U., von Castelberg B., Bart R., Stopatschinskaya S., Köchli OR, Haas P., Mross F., Zuber M., Dietrich H., Bischoff S., Mirlacher M., Sauter G., Gastl G. (2004). **High EpCAM expression is associated with poor prognosis in node-positive breast cancer.** Breast Cancer Research and Treatment 86(3), 207-213.
- Steelman LS, Bertrand FE, McCubrey JA (2004). **The complexity of PTEN: mutation, marker and potential target for therapeutic intervention.** Expert opinion on therapeutic targets 8(6), 537-550.
- Strnad J., Hamilton AE, Beavers LS, Gamboa GC, Apelgren LD, Taber LD, Sportsman JR, Bumol TF, Sharp JD, Gadski RA (1989). **Molecular cloning and characterization of a human adenocarcinoma/epithelial cell surface antigen complementary DNA.** Cancer Research 49, 314-317.
- Sugimura R. and Li L. (2010). **Noncanonical Wnt signaling in vertebrate development, stem cells, and diseases.** Birth Defects research 90(4), 243-256.
- Sundberg M., Jansson L., Ketolainen J., Pihlajamäki H., Suuronen R., Skottman H., Inzunza J., Hovatta O., Narkilahti S. (2009). **CD marker expression profiles of human embryonic stem cells in their neural derivatives, determined using flow-cytometry analysis, reveal a novel CD marker for exclusion of pluripotent stem cells.** Stem Cell Research 2(2), 113-124.
- Szala S., Froehlich M., Scollon M., Kasai Y., Steplewski Z., Koprowski H., Linnenbach AJ (1990). **Molecular cloning of cDNA for the carcinoma-associated antigen GA733-2.** PNAS 87(9), 3542-3546.
- Takes RP, Baatenburg de Jong RJ, Wijffels K., Schuurung E., Litvinov S., Hermans J., van Krieken JH (2001). **Expression of genetic markers in lymph node metastases compared with their primary tumours in head and neck cancer.** The Journal of Pathology 194 (3), 298-302.
- Tamai K., Zeng X., Liu C., Zhang X., Harada Y., Chang Z., He X. (2004). **A mechanism for Wnt coreceptor activation.** Molecular Cell 13, 149-156.
- Tanahashi H. and Tabira T. (2000). **Alzheimer's disease-associated presenilin 2 interacts with DRAL, an LIM-domain protein.** Human Molecular Genetics 9, 2281-2289.
- Thampoe I., Ng JSC, Lloyd KO (1988). **Biochemical analysis of a human epithelial surface antigen: Differential cell expression and processing.** Archives of Biochemistry and Biophysics 267(1), 342-352.
- Thrasivoulou C., Millar M., Ahmed A. (2013). **Activation of intracellular calcium by multiple ligand and translocation of β -catenin into the nucleus.** The Journal of Biological Chemistry 288, 35651-35659.
- Tran MK, Kurakula K., Koenis DS, de Vries CJM (2016). **Protein-protein interactions of the LIM-only protein FHL2 and functional implication of the interactions relevant in cardiovascular disease.** Biochimica et Biophysica Acta 1863(2), 219-228.
- Trzpis M., Popa E., McLaughlin PM, van Goor H., Timmer A., Bosman GW, de Leij LM, Harmsen MC (2007). **Spatial and temporal expression patterns of the epithelial cell adhesion molecule (EpCAM/EGP2) in developing and adult kidneys.** Nephron Experimental Nephrology 107(4), e119-131.

- Tsubura A., Senzaki H., Hilgers J., Morii S. (1992). **Immunohistochemical demonstration of breast-derived and/or carcinoma-associated glycoproteins in normal skin appendages and their tumors.** *Journal of Cutaneous Pathology* 19(1), 73-79.
- Uchida C. (2016). **Roles of pRB in the regulation of nucleosome and chromatin structures.** *BioMed Research International* 5959721
- Valenta T., Hausmann G., Basler K. (2012). **The many faces and functions of β -catenin.** *The EMBO Journal* 31, 2714-2736.
- Van de Wetering M., Cavallo R., Dooijes D., van Beest M., van Es J., Loureiro J., Ypma A., Hursh D., Jones T., Bejsovec A., Peifer M., Mortin M., Clevers H. (1997). **Armadillo coactivates transcription driven by the product of the *Drosophila* segment polarity gene dTCF.** *Cell* 88, 789-799.
- Van der Gun BTF, Melchers LJ, Ruiters MHJ, de Leij LFMH, McLaughlin PMJ, Rots MG (2010). **EpCAM in carcinogenesis: the good, the bad or the ugly.** *Carcinogenesis* 31(11), 1913-1921.
- Varga M., Obrist P., Schneeberger S. (2004). **Overexpression of epithelial cell adhesion molecule antigen in gallbladder carcinoma is an independent marker for poor survival.** *Clinical Cancer Research* 10(9), 3131-3136.
- Voronkov A. and Krauss S. (2013). **Wnt/beta-catenin signaling and small molecule inhibitors.** *Current Pharmaceutical Design* 19, 634-664.
- Waldron NN, Barsky SH, Dougherty PR, Vallera DA (2014). **A bispecific EpCAM/CD133-targeted toxin is effective against carcinoma.** *Targeted Oncology* 9(3), 239-249.
- Wan S., Yim AP, Wong CK, Arifi AA, Yip JH, Ng CS, Waye MY, Lam CW (2002). **Expression of FHL2 and cytokine messenger RNAs in human myocardium after cardiopulmonary bypass.** *International Journal of Cardiology* 86(2-3), 265-272.
- Way JC and Chalfie M. (1988). **Mec-3, a homeobox-containing gene that specifies differentiation of the touch receptor neurons in *C. elegans*.** *Cell* 54, 5-16.
- Wei Y., Renard CA, Labalette C., Wu Y., Levy L., Neuveut C., Prieur X., Flajolet M., Prigent S., Buendia MA (2003). **Identification of LIM protein FHL2 as a coactivator of beta-catenin.** *The Journal of Biological Chemistry* 278(7), 5188-5194.
- Weitzel JN, Lagos VI, Cullinane CA, Gambol PJ, Culver JO, Blazer KR, Palomares MR, Lowstuter KJ, MacDonald DJ (2007). **Limited family structure and BRCA gene mutation status in single cases of breast cancer.** *Journal of the American Medical Association* 297(23), 2587-2595.
- Wenqi D., Li W., Shanshan C., Bei C., Yafei Z., Feihu B., Jie L., Daiming F. (2009). **EpCAM is overexpressed in gastric cancer and its downregulation suppresses proliferation of gastric cancer.** *Journal of Cancer Research and Clinical Oncology* 135(9), 1277-1285.
- Went P., Dirnhofer S., Salvisberg T., Amin MB, Lim SD, Diener PA, Moch H. (2005). **Expression of Epithelial Cell Adhesion Molecule (EpCAM) in renal epithelial tumors.** *The American Journal of Surgical Pathology* 29(1), 83-88.
- Went PTH, Lugli A., Meier S., Bundi M., Mirlacher M., Sauter G., Dirnhofer S. (2004). **Frequent EpCam protein expression in human carcinomas.** *Human Pathology* 35(1), 122-128.

- Wicki A. and Hagmann J. (2011). **Diet and cancer**. *Swiss Medical Weekly* 141: w13250
- Winter MJ, Cirulli V., Briaire-de Bruijn IH, Litvinov SV (2007). **Cadherins are regulated by Ep-CAM via phosphatidylinositol-3 kinase**. *Molecular and Cellular Biochemistry* 302 (1-2), 19-26.
- Wixler V., Geerts D., Laplantine F., Westhoff D., Smyth N., Aumailley M., Sonnenberg A., Paulsson M. (2000). **The LIM-Only protein DRAL/FHL2 binds to the cytoplasmic domain of several alpha and beta integrin chains and is recruited to adhesion complexes**. *The Journal of Biological Chemistry* 275 (43), 33669-336678.
- Wolfe MS, Xia W., Ostaszewski BL, Diehl TS, Kimberly WT, Selkoe DJ (1999). **Two transmembrane aspartates in presenilin-1 required for presenilin endoproteolysis and gamma-secretase activity**. *Nature* 398(6727), 513-517.
- World Health Organization, 2014. *Cancer Fact Sheet N°297*. Retrieved 27 January 2017
- World Health Organization, 2014. *World Cancer Report 2014*.
- Wu CH, Feng X., Lu M., Morimura S., Udey MC (2017). **Matriptase-mediated cleavage of EpCAM destabilizes claudins and dysregulates intestinal epithelial homeostasis**. *The Journal of Clinical Investigation* 127(2), 623-634.
- Wu G., Xu G., Schulman BA, Jeffrey PD, Harper JW, Pavletich NP (2003). **Structure of a β -TrCP1-Skp1- β -catenin complex: destruction motif binding and lysine specificity of the SCF ^{β -TrCP1} ubiquitin ligase**. *Molecular Cell* 11(6), 1445-1456.
- Xing Y., Takemaru K., Liu J., Berndt JD, Zheng JJ, Moon RT, Xu W. (2008). **Crystal structure of a full-length beta-catenin**. *Structure* 16(3), 478-487.
- Xu J., Zhou J., Li MS, Ng CF, Ng YK, Lai PB, Tsui SK (2014). **Transcriptional regulation of the tumor suppressor FHL2 by p53 in human kidney and liver cells**. *PLoS One* 9, (e99359).
- Xu W. and Kimelman D. (2007). **Mechanistic insights from structural studies of beta-catenin and its binding partners**. *Journal of Cell Science* 120(Pt 19), 3337-3344.
- Yamashita, T., Budhu A., Forgues M., Wang XW (2007). **Activation of hepatic stem cell marker EpCAM by Wnt- β -catenin signaling in hepatocellular carcinoma**. *Cancer Research* 67(22), 10831-10839.
- Yan JH, Ye QN, Fang Y., Zhu JH, Huang CF (2003). **Mapping of FHL2 Transcription Activation Domain**. *Acta Biochimica et Biophysica Sinica* 35, 643-648.
- Yanamoto S., Kawasaki G., Yoshitomi I., Iwamoto T., Hirata K., Mizuno A. (2007). **Clinicopathologic significance of EPCAM expression in squamous cell carcinoma of the tongue and its possibility as a potential target for tongue cancer gene therapy**. *Oral Oncology* 43(9), 869-877.
- Yang Y., Hou H., Haller EM, Nicosia SV, Bai W. (2005). **Suppression of FOXO1 activity by FHL2 through SIRT1-mediated deacetylation**. *The EMBO Journal* 24, 1021-1032.
- Zanella F., Lorens JB, Link W. (2010). **High Content Screening: seeing is believing**. *Cell Press* 28(5), 237-245.

Zeng X., Tamai K., Doble B., Li S., Huang H., Habas R., Okamura H., Woodgett J., He X. (2005). **A dual-kinase mechanism for Wnt co-receptor phosphorylation and activation.** Nature 438, 873-877.

Zhan H., Ma Q., Zhang Y., Xu H. (2012). **Proteolytic processing of Alzheimer's β -amyloid precursor protein.** Journal of Neurochemistry 120, 9-21.

Zhao ZM, Reynolds AB, Gaucher EA (2011). **The evolutionary history of the catenin gene family during metazoan evolution.** BMC Evolutionary Biology 11, 198

Zheng Q., Zhao Y. (2007). **The diverse biofunctions of LIM domain proteins: determined by subcellular localization and protein-protein interaction.** Biology of the cell 99, 489-502.

Zheng X., Fan X., Fu B., Zheng M., Zhang A., Zhong K., Yan J., Sun R., Tian Z., Wei H. (2017). **EpCAM inhibition sensitizes chemoresistant leukemia to immune surveillance.** Cancer Research 77(2), 482-493.

Zoller M. (2009). **Tetraspanins: push and pull in suppressing and promoting metastasis.** Nature Reviews Cancer 9, 40-55.

Acknowledgments

This work would not have been possible without the support of many people.

First of all, I would like to thank Dierk Niessing for giving me the chance to discover a completely new field of work. Thank you for giving me the opportunity to carry out my PhD in your lab, your constant readiness to discuss scientific questions and your guidance.

I would like to thank Olivier Gires for being my official supervisor, being part of my thesis committee and constantly giving helpful advice.

I am also grateful to Kamyar Hadian for being part of my thesis committee and his valuable input.

A big thank you goes to Kenji Schorpp for the great collaboration. Thanks for your ideas and for introducing me to HCS. Thank you for your effort. I also would like to thank Elke Luxenburger for being a great help with all the Western blots and Membrane Assays. Thank you to Martin Viertler for his help with ITC.

Special thanks to all the former and present members of the Niessing lab, especially to Annika, Elena, Franzi, Janine, Rob and Simone. Thanks for the great atmosphere, scientific and mental support, lunch break runs, coffee & cake and so on. I could not have asked for better company during these years. Vera for her support and for keeping the lab running. Thank you to all of you for having a great time in and outside the lab.

Big thanks to all my friends for withstanding all my grumbling, their support and their encouragement, especially to Chrissy, Daniel, Frank, Josi, Katharina, Maggie, Maria and Susan (also for introducing me to MS). And most of all, a heartfelt thank you to Belli, who probably suffered the most;)

Last but not least, I would like to thank my family, in particular my grandparents, for providing constantly any kind of support, motivating and believing in me.

Aus der Klinik und Poliklinik für Hals-Nasen-Ohrenheilkunde der
Ludwig-Maximilians-Universität München

Direktor: Prof. Dr. med. Alexander Berghaus

Leiter der HNO-Forschung: Prof. Dr. rer. nat. Olivier Gires

Innovative therapy modalities for solid EpCAM-positive tumors

Dissertation

zum Erwerb des Doktorgrades der Naturwissenschaften

an der Medizinischen Fakultät

der Ludwig-Maximilians-Universität München



Jana Ylva Tretter

Appendix II

2017

Table of Contents

A. ApoTox raw data.....	1
B. ApoTox Evaluation.....	33
C. Compound structures	43

A. ApoTox raw data

The tables show the raw data from the ApoTox Assay. Results are shown for FaDu, HCT-8, HEK293 EpCAM-FL and HEK293 wild-type cells. The cell type is shown in the top left corner of each table. The compound number is given in the third column. Results for viability are shown with orange background, results for cytotoxicity with blue background, and results for apoptosis with green background. Depicted are mean values and standard deviations from two independent experiments, each consisting of three replicates.

Table A-1 Raw data for staurosporin treatment.

FaDu		Staurosporine [μM]	80	40	20	10	5	2,50	1,25	0,625	0,313	0,156
Viability	Average		0,228	0,209	0,205	0,251	0,317	0,347	0,352	0,376	0,73	0,491
	Standard Deviation		0,046	0,036	0,05	0,063	0,066	0,05	0,079	0,063	0,08	0,014
Cytotoxicity	Average		3,189	3,087	3,098	3,537	3,362	4,07	3,71	4,061	2,559	2,953
	Standard Deviation		1,138	0,997	1,204	1,338	0,194	1,072	0,441	1,312	0,502	0,936
Apoptosis	Average		2,784	2,652	2,582	3,491	4,924	4,978	5,016	5,605	3,311	4,929
	Standard Deviation		1,908	2,053	2,349	3,417	1,03	0,634	1,096	0,581	0,252	0,396

HCT-8		Staurosporine [μM]	80	40	20	10	5	2,50	1,25	0,625	0,313	0,156
Viability	Average		0,202	0,192	0,182	0,228	0,321	0,355	0,337	0,358	0,703	0,46
	Standard Deviation		0,065	0,055	0,057	0,08	0,071	0,107	0,115	0,109	0,192	0,016
Cytotoxicity	Average		3,653	3,805	3,447	4,009	5,163	5,409	4,954	5,536	4,474	3,523
	Standard Deviation		0,093	0,087	0,303	0,164	2,305	2,193	1,915	2,643	0,293	1,584
Apoptosis	Average		2,755	2,447	2,357	2,995	5,006	4,804	4,443	4,742	3,564	4,267
	Standard Deviation		1,74	1,778	1,94	2,095	0,093	0,485	0,283	0,174	0,65	0,384

HEK293 EpCAM FL											
	Staurosporine [μ M]	80	40	20	10	5	2,50	1,25	0,625	0,313	0,156
Viability	Average	0,207	0,19	0,198	0,283	0,353	0,456	0,504	0,553	0,886	0,736
	Standard Deviation	0,06	0,057	0,074	0,112	0,123	0,058	0,1	0,139	0,143	0,112
Cytotoxicity	Average	3,045	2,844	2,687	2,239	2,118	1,823	1,655	1,403	2,303	1,037
	Standard Deviation	1,083	0,682	0,666	0,755	0,234	0,757	0,406	0,299	1,991	0,17
Apoptosis	Average	6,486	5,835	3,896	2,367	4,723	4,292	2,671	2,384	1,105	1,317
	Standard Deviation	1,573	1,418	1,224	1,454	0,581	1,791	0,848	1,031	0,292	0,505

HEK293 wt											
	Staurosporine [μ M]	80	40	20	10	5	2,50	1,25	0,625	0,313	0,156
Viability	Average	0,249	0,253	0,247	0,256	0,284	0,376	0,396	0,424	0,798	0,665
	Standard Deviation	0,031	0,014	0,011	0,026	0,06	0,107	0,145	0,096	0,085	0,033
Cytotoxicity	Average	3,479	3,282	2,777	2,247	2,598	2,573	1,893	1,838	1,448	1,441
	Standard Deviation	0,037	0,059	0,29	0,002	0,679	1,757	1,169	1,194	0,642	0,537
Apoptosis	Average	3,725	3,209	2,765	2,222	3,803	3,02	2,593	1,976	1,216	1,17
	Standard Deviation	2,811	2,553	2,019	1,568	2,556	2,745	2,448	1,869	0,418	0,553

Table A-2 Raw data for compound #4_0

FaDu											
	Compound #4_0 [μ M]	80	40	20	10	5	2,50	1,25	0,625	0,313	0,156
Viability	Average	1,174	1,13	1,329	1,132	1,26	1,086	1,009	1,061	1,051	0,997
	Standard Deviation	0,004	0,111	0,047	0,192	0,056	0,021	0,044	0,001	0,028	0,029
Cytotoxicity	Average	1,017	1,048	1,061	0,915	0,997	0,897	0,929	0,882	0,97	0,941
	Standard Deviation	0,05	0,08	0,187	0,053	0,2	0,115	0,125	0,17	0,111	0,119
Apoptosis	Average	1,756	2,033	1,292	1,286	1,194	1,301	1,131	1,177	1,216	1,218
	Standard Deviation	0,619	0,599	0,447	0,345	0,369	0,438	0,301	0,3	0,453	0,239

HCT-8		Compound #4_0 [μM]	80	40	20	10	5	2,50	1,25	0,625	0,313	0,156
Viability	Average		1,085	1,177	1,276	1,18	1,19	1,084	1,073	1,1	1,007	1,021
	Standard Deviation		0,326	0,326	0,326	0,326	0,326	0,326	0,326	0,326	0,326	0,326
Cytotoxicity	Average		1,084	1,129	1,153	1,063	0,981	0,942	0,931	0,919	0,854	1,089
	Standard Deviation		0,098	0,193	0,032	0,058	0,135	0,005	0,037	0,055	0,015	0,396
Apoptosis	Average		1,874	1,762	1,266	1,224	1,029	1,127	1,127	1,165	1,172	1,034
	Standard Deviation		0,153	0,209	0,057	0,04	0,028	0,025	0,065	0,006	0,088	0,102

HEK293 EpCAM FL		Compound #4_0 [μM]	80	40	20	10	5	2,50	1,25	0,625	0,313	0,156
Viability	Average		0,891	1,039	1,238	1,166	1,255	1,091	1,103	1,168	1,132	1,088
	Standard Deviation		0,096	0,333	0,256	0,205	0,181	0,139	0,131	0,071	0,17	0,175
Cytotoxicity	Average		1,006	1,031	1,589	0,988	1,467	0,975	0,941	1,33	0,988	0,969
	Standard Deviation		0,208	0,005	0,922	0,023	0,723	0,031	0,074	0,658	0,043	0,044
Apoptosis	Average		1,568	1,46	1,345	1,404	1,325	1,359	1,315	1,15	1,305	1,21
	Standard Deviation		0,732	0,49	0,557	0,744	0,694	0,653	0,689	0,49	0,549	0,527

HEK293 wt		Compound #4_0 [μM]	80	40	20	10	5	2,50	1,25	0,625	0,313	0,156
Viability	Average		0,847	0,929	1,223	1,052	1,142	0,966	0,942	1,021	0,984	0,787
	Standard Deviation		0,002	0,039	0,094	0,05	0,116	0,098	0,044	0,069	0,038	0,274
Cytotoxicity	Average		0,985	0,979	0,99	0,912	0,874	0,835	0,807	0,828	0,837	0,684
	Standard Deviation		0,092	0,131	0,057	0,173	0,177	0,166	0,136	0,16	0,124	0,35
Apoptosis	Average		1,409	1,326	1,169	1,146	1,086	1,007	1,002	1,069	0,932	1,105
	Standard Deviation		0,144	0,112	0,358	0,163	0,272	0,024	0,141	0,186	0,051	0,159

Table A-3 Raw data for compound #6_0.

FaDu											
	Compound #6_0 [μM]	80	40	20	10	5	2,50	1,25	0,625	0,313	0,156
Viability	Average	0,532	1,011	0,843	0,814	0,908	0,957	1	1,064	1,066	1,074
	Standard Deviation	0,1	0,105	0,011	0,113	0,21	0,141	0,129	0,082	0,107	0,154
Cytotoxicity	Average	1,668	0,994	1,197	1,037	1,024	1,065	0,92	1,038	1,013	1,053
	Standard Deviation	0,068	0,208	0,19	0,042	0,176	0,126	0,13	0,064	0,255	0,209
Apoptosis	Average	1,986	1,604	3,214	2,228	1,497	1,277	1,027	1,131	1,069	1,038
	Standard Deviation	0,103	0,152	1,126	0,529	0,057	0,182	0,022	0,086	0,059	0,064

HCT-8											
	Compound #6_0 [μM]	80	40	20	10	5	2,50	1,25	0,625	0,313	0,156
Viability	Average	0,456	0,963	0,699	0,809	0,849	0,904	0,891	0,956	0,97	0,976
	Standard Deviation	0,137	0,117	0,13	0,126	0,104	0,098	0,082	0,027	0,046	0,047
Cytotoxicity	Average	1,771	1,135	1,175	1,1	0,967	0,988	0,884	0,909	0,919	0,93
	Standard Deviation	0,345	0,15	0,126	0,072	0,008	0,014	0,044	0,019	0,04	0,095
Apoptosis	Average	2,188	1,637	3,063	2,429	1,487	1,202	0,969	1,045	1,063	1,043
	Standard Deviation	0,108	0,503	1,324	1,273	0,403	0,165	0,066	0,249	0,084	0,188

HEK293 EpCAM FL											
	Compound #6_0 [μM]	80	40	20	10	5	2,50	1,25	0,625	0,313	0,156
Viability	Average	0,475	0,986	0,913	1,019	1,011	1,159	1,13	1,123	1,218	1,316
	Standard Deviation	0,145	0,293	0,272	0,299	0,268	0,352	0,212	0,278	0,336	0,434
Cytotoxicity	Average	1,613	1,478	1,079	1,057	1,057	1,116	1,075	1,045	1,179	1,612
	Standard Deviation	0,305	0,626	0,005	0,068	0,064	0,02	0,038	0,023	0,04	0,481
Apoptosis	Average	0,895	0,819	1,101	1	1,092	1,058	1,169	0,959	1,111	0,931
	Standard Deviation	0,317	0,046	0,104	0,004	0,181	0,327	0,014	0,271	0,019	0,192

HEK293 wt		Compound #6_0 [μ M]	80	40	20	10	5	2,50	1,25	0,625	0,313	0,156
Viability	Average		0,517	1,11	0,901	0,977	0,961	1,056	1,105	1,071	1,134	1,268
	Standard Deviation		0,002	0,235	0,161	0,134	0,107	0,194	0,226	0,141	0,138	0,154
Cytotoxicity	Average		1,909	1,38	1,127	1,147	1,08	1,129	1,149	1,089	1,179	1,258
	Standard Deviation		0,27	0,086	0,093	0,05	0,009	0,12	0,138	0,063	0,2	0,033
Apoptosis	Average		1,257	0,898	0,846	0,987	0,949	0,972	0,882	0,979	0,986	1,042
	Standard Deviation		0,98	0,144	0,121	0,178	0,212	0,03	0,026	0,065	0,144	0,354

Table A-4 Raw data for compound #7_0.

FaDu		Compound #7_0 [μ M]	80	40	20	10	5	2,50	1,25	0,625	0,313	0,156
Viability	Average		0,957	0,945	0,882	1,032	1,046	1,03	0,937	0,972	1,041	1,064
	Standard Deviation		0,049	0,024	0,301	0,084	0,086	0,009	0,155	0,093	0,003	0,07
Cytotoxicity	Average		0,907	0,885	0,857	1,009	1,059	0,957	0,955	0,955	1,007	0,966
	Standard Deviation		0,038	0,005	0,328	0,127	0,176	0,062	0,206	0,134	0,116	0,156
Apoptosis	Average		1,05	1,08	1,042	1,164	1,204	1,179	1,062	1,035	1,086	1,145
	Standard Deviation		0,104	0,239	0,037	0,032	0,246	0,238	0,149	0,23	0,053	0,125

HCT-8		Compound #7_0 [μ M]	80	40	20	10	5	2,50	1,25	0,625	0,313	0,156
Viability	Average		0,9	0,903	1,013	0,983	1,063	1,074	1,037	1,047	1,021	1,007
	Standard Deviation		0,088	0,135	0,044	0,058	0	0,019	0,002	0,003	0,02	0,001
Cytotoxicity	Average		0,925	0,861	0,973	1,011	1,006	1,09	0,975	1,068	0,979	0,983
	Standard Deviation		0,025	0,024	0,027	0,068	0,061	0,075	0,057	0,079	0,003	0,016
Apoptosis	Average		1,083	1,036	0,953	1,064	1,017	1,1	1,092	1,077	0,98	1,063
	Standard Deviation		0,097	0,243	0,05	0,006	0,013	0,05	0,025	0,168	0,004	0,057

HEK293 EpCAM FL		Compound #7_0 [μ M]	80	40	20	10	5	2,50	1,25	0,625	0,313	0,156
Viability	Average		0,834	0,841	0,826	1,083	1,142	1,078	1,075	1,039	1,12	1,15
	Standard Deviation		0,113	0,133	0,096	0,211	0,169	0,163	0,148	0,128	0,178	0,145
Cytotoxicity	Average		1,829	1,019	0,975	1,13	1,413	1,095	1,256	1,034	1,068	2,066
	Standard Deviation		1,245	0,183	0,489	0,116	0,483	0,159	0,395	0,199	0,069	1,476
Apoptosis	Average		1,531	1,305	1,376	1,208	1,352	1,281	1,257	1,246	1,254	1,205
	Standard Deviation		0,191	0,387	0,584	0,182	0,341	0,325	0,274	0,342	0,234	0,258

HEK293 wt		Compound #7_0 [μ M]	80	40	20	10	5	2,50	1,25	0,625	0,313	0,156
Viability	Average		0,837	0,808	0,957	0,979	1,042	0,854	0,978	0,995	1,03	1,067
	Standard Deviation		0,019	0,002	0,005	0,059	0,044	0,287	0,115	0,029	0,047	0,095
Cytotoxicity	Average		1,076	0,989	1,063	0,97	0,98	0,833	0,869	0,917	0,982	0,868
	Standard Deviation		0,152	0,102	0,064	0,15	0,106	0,406	0,148	0,179	0,125	0,165
Apoptosis	Average		0,962	0,995	1,006	0,993	0,988	0,872	0,905	0,922	0,971	0,999
	Standard Deviation		0,249	0,202	0,116	0,035	0,044	0,051	0,128	0,113	0,152	0,215

Table A-5 Raw data for compound #9_0.

FaDu											
	Compound #9_0 [μM]	80	40	20	10	5	2,50	1,25	0,625	0,313	0,156
Viability	Average	0,603	0,719	0,974	0,795	0,916	1,034	1,059	1,043	1,008	1,007
	Standard Deviation	0,05	0,089	0,066	0,041	0,134	0,14	0,095	0,148	0,189	0,158
Cytotoxicity	Average	0,636	0,75	0,938	0,904	1,004	1,029	1,014	1,08	1,013	1,011
	Standard Deviation	0,04	0,141	0,06	0,014	0,17	0,239	0,133	0,217	0,219	0,191
Apoptosis	Average	0,747	0,936	0,902	0,93	0,973	0,979	1,044	0,978	1,006	1,003
	Standard Deviation	0,004	0,023	0,013	0,072	0,138	0,03	0,009	0,083	0,139	0,088

HCT-8											
	Compound #9_0 [μM]	80	40	20	10	5	2,50	1,25	0,625	0,313	0,156
Viability	Average	0,593	0,677	0,872	0,852	0,921	0,992	0,967	0,926	0,999	0,963
	Standard Deviation	0,034	0,032	0,052	0,057	0,098	0,081	0,005	0,003	0,034	0,005
Cytotoxicity	Average	0,819	0,889	1,094	1,089	1,183	1,249	1,213	1,119	1,167	1,15
	Standard Deviation	0,032	0,135	0,15	0,038	0,105	0,222	0,204	0,17	0,189	0,127
Apoptosis	Average	0,846	0,821	0,825	0,881	0,847	0,916	0,83	1,016	1,073	1
	Standard Deviation	0,053	0,001	0,012	0,086	0,061	0,029	0,006	0,129	0,168	0,147

HEK293 EpCAM FL											
	Compound #9_0 [μM]	80	40	20	10	5	2,50	1,25	0,625	0,313	0,156
Viability	Average	0,434	0,538	0,932	0,92	1,036	1,167	1,183	1,122	1,202	1,179
	Standard Deviation	0,19	0,169	0,331	0,288	0,351	0,302	0,422	0,424	0,372	0,33
Cytotoxicity	Average	0,66	0,78	1,554	1,026	1,126	1,777	1,889	1,124	1,693	1,147
	Standard Deviation	0,039	0,019	0,659	0,005	0,017	0,891	1,101	0,042	0,623	0,091
Apoptosis	Average	2,01	1,212	0,823	0,878	1,17	1,066	0,933	1,16	1,002	1,083
	Standard Deviation	0,643	0,49	0,015	0,027	0,033	0,07	0,026	0,188	0,079	0,139

HEK293 wt		Compound #9_0 [μ M]	80	40	20	10	5	2,50	1,25	0,625	0,313	0,156
Viability	Average		0,445	0,569	0,926	0,882	0,775	1,174	1,175	1,109	1,206	1,17
	Standard Deviation		0,113	0,112	0,118	0,031	0,237	0,072	0,14	0,16	0,096	0,223
Cytotoxicity	Average		0,795	0,984	1,069	1,081	0,91	1,183	1,735	1,102	1,251	1,223
	Standard Deviation		0,055	0,177	0,148	0,044	0,203	0,174	0,216	0,095	0,13	0,239
Apoptosis	Average		1,177	0,936	0,884	0,98	1,013	0,945	0,929	0,995	1,063	1,005
	Standard Deviation		0,411	0,099	0,091	0,001	0,052	0,06	0,038	0,055	0,078	0,015

Table A-6 Raw data for compound #10_0.

FaDu		Compound #10_0 [μ M]	80	40	20	10	5	2,50	1,25	0,625	0,313	0,156
Viability	Average		0,717	0,804	0,838	0,861	0,919	0,924	0,929	0,94	0,966	0,917
	Standard Deviation		0,099	0,055	0,051	0,053	0,028	0,018	0,155	0,087	0,058	0,032
Cytotoxicity	Average		0,753	0,868	0,929	1,011	0,998	1,032	0,97	0,959	1,018	0,937
	Standard Deviation		0	0,053	0,206	0,095	0,138	0,173	0,181	0,167	0,11	0,164
Apoptosis	Average		0,893	0,951	0,946	1,17	1,143	1,317	1,131	1,048	1,081	1,105
	Standard Deviation		0,253	0,1	0,02	0,073	0,035	0,026	0,035	0,14	0,077	0,024

HCT-8		Compound #10_0 [μ M]	80	40	20	10	5	2,50	1,25	0,625	0,313	0,156
Viability	Average		0,812	0,923	1,037	1,055	1,065	1,138	1,18	1,133	1,118	1,146
	Standard Deviation		0,187	0,142	0,139	0,221	0,25	0,247	0,199	0,258	0,179	0,316
Cytotoxicity	Average		0,814	0,801	0,953	1,022	0,932	1,079	0,99	1,04	0,951	0,93
	Standard Deviation		0,016	0,038	0,056	0,062	0,045	0,031	0,079	0,098	0,078	0,043
Apoptosis	Average		0,898	0,98	0,948	1,056	1,028	1,066	1,114	1,047	1,106	1,052
	Standard Deviation		0,078	0,039	0,022	0,054	0,013	0,012	0,136	0,1	0,04	0,063

HEK293 EpCAM FL		Compound #10_0	80	40	20	10	5	2,50	1,25	0,625	0,313	0,156
		[μM]										
Viability	Average		0,593	0,79	0,851	0,909	1,034	1,026	1,012	0,984	1,081	1,048
	Standard Deviation		0,023	0,158	0,098	0,097	0,13	0,121	0,123	0,039	0,116	0,061
Cytotoxicity	Average		0,664	0,846	1,17	1,786	1,438	1,118	1,224	1,01	1,079	1,067
	Standard Deviation		0,092	0,028	0,296	1,053	0,544	0,099	0,399	0,157	0,096	0,137
Apoptosis	Average		0,907	0,962	1,085	1,051	1,084	1,064	0,987	1,065	1,153	0,996
	Standard Deviation		0,258	0,181	0,394	0,191	0,242	0,218	0,314	0,158	0,247	0,127

HEK293 wt		Compound #10_0	80	40	20	10	5	2,50	1,25	0,625	0,313	0,156
		[μM]										
Viability	Average		0,666	0,743	0,844	0,86	0,921	0,806	0,932	0,938	0,971	0,955
	Standard Deviation		0,005	0,019	0,024	0,035	0,133	0,324	0,096	0,038	0,029	0,06
Cytotoxicity	Average		0,719	0,851	1,037	1,024	0,969	0,851	0,935	0,921	0,962	0,918
	Standard Deviation		0,122	0,202	0,206	0,202	0,236	0,36	0,175	0,195	0,127	0,231
Apoptosis	Average		0,777	0,858	0,965	0,932	0,973	1,017	0,895	0,94	0,894	0,974
	Standard Deviation		0,019	0,078	0,004	0,128	0,031	0,124	0,068	0,023	0,02	0

Table A-7 Raw data for compound #13_0.

FaDu		Compound #13_0 [μM]	80	40	20	10	5	2,50	1,25	0,625	0,313	0,156
Viability	Average		0,534	0,437	0,723	0,938	1,014	1,048	0,987	0,996	1,043	1,019
	Standard Deviation		0,016	0,136	0,126	0,18	0,22	0,039	0,09	0,207	0,152	0,13
Cytotoxicity	Average		4,068	1,989	1,366	1,233	1,187	1,076	1,027	1,013	0,982	1,048
	Standard Deviation		0,872	0,494	0,033	0,208	0,283	0,115	0,141	0,228	0,206	0,173
Apoptosis	Average		1,572	2,515	1,08	1,031	0,899	0,947	1,074	0,922	0,916	1,049
	Standard Deviation		0,822	0,212	0,075	0,013	0,143	0,054	0,058	0,093	0,074	0,096

HCT-8		Compound #13_0 [μM]	80	40	20	10	5	2,50	1,25	0,625	0,313	0,156
Viability	Average		0,436	0,498	0,748	0,961	1,043	1,092	1,047	0,97	0,995	0,966
	Standard Deviation		0,03	0,001	0,098	0,168	0,189	0,054	0,001	0,059	0,127	0,003
Cytotoxicity	Average		4,961	3,259	1,788	1,408	1,263	1,278	1,175	1,049	1,108	1,097
	Standard Deviation		1,007	0,09	0,121	0,021	0,194	0,187	0,172	0,116	0,058	0,164
Apoptosis	Average		1,623	2,798	1,114	0,973	0,858	0,937	0,952	0,982	0,951	1,087
	Standard Deviation		0,638	0,034	0,029	0,035	0,111	0,038	0,048	0,032	0,157	0,036

HEK293 EpCAM FL											
	Compound #13_0 [μM]	80	40	20	10	5	2,50	1,25	0,625	0,313	0,156
Viability	Average	0,351	0,31	0,66	0,964	1,068	1,032	1,046	1,069	1,213	1,128
	Standard Deviation	0,087	0,093	0,155	0,28	0,288	0,138	0,19	0,239	0,349	0,268
Cytotoxicity	Average	4,982	3,365	1,96	1,332	1,241	1,178	1,095	1,061	1,791	1,091
	Standard Deviation	0,887	1,126	0,462	0,006	0,017	0,108	0,013	0,043	0,793	0,116
Apoptosis	Average	2,344	3,013	1,526	1,217	1,03	1,281	1,016	1,145	0,874	1,112
	Standard Deviation	0,166	0,431	0,205	0,284	0,046	0,066	0,054	0,068	0,038	0,103

HEK293 wt											
	Compound #13_0 [μM]	80	40	20	10	5	2,50	1,25	0,625	0,313	0,156
Viability	Average	0,331	0,369	0,609	0,972	1,069	1,121	1,135	1,126	1,183	1,185
	Standard Deviation	0,128	0,005	0,004	0,115	0,093	0,171	0,152	0,129	0,082	0,188
Cytotoxicity	Average	4,184	4,201	2,486	1,662	1,333	1,282	1,263	1,143	1,27	1,223
	Standard Deviation	0,684	0,661	0,767	0,139	0,014	0,078	0,029	0,006	0,157	0,124
Apoptosis	Average	2,955	2,787	2,169	1,141	1,046	0,972	0,977	1,025	0,903	0,979
	Standard Deviation	2,368	1,805	1,794	0,278	0,102	0,004	0,146	0,079	0,252	0,083

Table A-8 Raw data for compound #51_0.

FaDu		Compound #51_0 [μM]	80	40	20	10	5	2,50	1,25	0,625	0,313	0,156
Viability	Average		1,084	1,093	1,035	0,891	0,851	1,001	0,987	0,994	1,031	1,013
	Standard Deviation		0,152	0,075	0,018	0,128	0,238	0,057	0,015	0,142	0,124	0,098
Cytotoxicity	Average		0,884	1,094	1,051	0,863	0,884	0,982	0,956	0,978	1,006	0,957
	Standard Deviation		0,286	0,041	0,107	0,334	0,445	0,141	0,151	0,109	0,059	0,122
Apoptosis	Average		5,746	1,693	1,301	1,205	1,21	1,227	1,152	1,332	1,272	1,29
	Standard Deviation		0,619	0,599	0,447	0,345	0,369	0,438	0,301	0,3	0,453	0,239

HCT-8		Compound #51_0 [μM]	80	40	20	10	5	2,50	1,25	0,625	0,313	0,156
Viability	Average		1,207	1,184	1,182	1,168	0,947	1,171	1,137	1,146	1,16	1,183
	Standard Deviation		0,542	0,38	0,29	0,313	0,028	0,258	0,255	0,326	0,191	0,228
Cytotoxicity	Average		1,054	1,046	1,159	1,007	0,82	1,007	0,932	0,95	0,901	0,92
	Standard Deviation		0,059	0,023	0,087	0,087	0,155	0,036	0,007	0,086	0,041	0,048
Apoptosis	Average		6,32	1,939	1,478	1,226	1,143	1,24	1,256	1,244	1,341	1,256
	Standard Deviation		0,586	0,169	0,122	0,078	0,007	0,067	0,181	0,03	0,238	0,216

HEK293 EpCAM FL		Compound #51_0 [μ M]	80	40	20	10	5	2,50	1,25	0,625	0,313	0,156
Viability	Average		1,012	1,019	1,045	1,112	0,921	1,106	1,03	0,805	1,079	0,873
	Standard Deviation		0,052	0,139	0,065	0,062	0,21	0,083	0,017	0,276	0,1	0,317
Cytotoxicity	Average		1,311	1,09	1,344	2,021	1,134	1,099	1,223	0,787	1,07	0,834
	Standard Deviation		0,255	0,063	0,535	1,381	0,674	0,111	0,517	0,407	0,119	0,348
Apoptosis	Average		1,924	1,335	1,521	1,293	1,356	1,204	1,161	1,171	1,25	1,254
	Standard Deviation		0,099	0,473	0,598	0,507	0,489	0,433	0,275	0,441	0,375	0,505

HEK293 wt		Compound #51_0 [μ M]	80	40	20	10	5	2,50	1,25	0,625	0,313	0,156
Viability	Average		1,097	0,994	1,015	1,076	1,017	0,969	0,865	1,029	1,064	1,013
	Standard Deviation		0,191	0,113	0,061	0,001	0,034	0,031	0,268	0,065	0,025	0,023
Cytotoxicity	Average		1,135	1,007	1,117	1,115	0,908	0,891	0,809	0,926	0,997	0,916
	Standard Deviation		0,155	0,153	0,192	0,191	0,145	0,218	0,422	0,208	0,114	0,232
Apoptosis	Average		2,369	0,901	1,108	1,067	1,083	0,97	1,037	1,101	1,044	1,036
	Standard Deviation		1,793	0,218	0,003	0,001	0,128	0,123	0,121	0,172	0,221	0,162

Table A-9 Raw data for compound #66_0.

FaDu												
	Compound #66_0 [μM]	80	40	20	10	5	2,50	1,25	0,625	0,313	0,156	
Viability	Average	0,354	0,531	0,742	1,076	1,015	1,02	1,05	1,028	1,1	1,007	
	Standard Deviation	0,017	0,139	0,014	0,09	0,089	0,007	0,038	0,046	0,019	0,109	
Cytotoxicity	Average	1,875	0,975	1,072	0,992	0,916	0,952	0,988	0,998	1,007	0,987	
	Standard Deviation	0,188	0,475	0,086	0,062	0,204	0,151	0,013	0,098	0,145	0,123	
Apoptosis	Average	0,334	0,371	0,256	0,495	0,614	0,845	0,978	1,024	1,077	1,062	
	Standard Deviation	0,14	0,208	0,031	0,115	0,048	0,188	0,204	0,263	0,359	0,307	

HCT-8												
	Compound #66_0 [μM]	80	40	20	10	5	2,50	1,25	0,625	0,313	0,156	
Viability	Average	0,32	0,554	0,751	0,876	0,983	1,073	1,02	0,97	0,979	1,019	
	Standard Deviation	0,012	0,09	0,03	0,33	0,051	0,022	0,033	0,014	0,17	0,025	
Cytotoxicity	Average	2,135	1,458	1,515	0,89	1,051	1,259	1,118	1,089	1,034	1,129	
	Standard Deviation	0,245	0,324	0,03	0,157	0,232	0,259	0,132	0,11	0,091	0,172	
Apoptosis	Average	0,356	0,291	0,32	0,494	0,641	0,86	0,952	1,087	1,104	1,186	
	Standard Deviation	0,054	0,125	0,067	0,071	0,055	0,065	0,191	0,274	0,344	0,278	

HEK293 EpCAM FL											
	Compound #66_0 [μM]	80	40	20	10	5	2,50	1,25	0,625	0,313	0,156
Viability	Average	0,312	0,584	0,874	1,11	1,179	1,125	1,031	1,098	1,055	1,163
	Standard Deviation	0,128	0,216	0,289	0,095	0,23	0,164	0,045	0,259	0,114	0,401
Cytotoxicity	Average	1,274	1,168	1,172	1,021	1,08	1,104	0,967	1,043	1,818	1,049
	Standard Deviation	0,096	0	0,084	0,012	0,067	0,102	0,058	0,034	1,392	0,113
Apoptosis	Average	0,471	0,603	0,574	0,539	0,93	0,968	1,116	1,107	1,063	1,055
	Standard Deviation	0,136	0,122	0,105	0,045	0,181	0,319	0,115	0,198	0,32	0,298

HEK293 wt											
	Compound #66_0 [μM]	80	40	20	10	5	2,50	1,25	0,625	0,313	0,156
Viability	Average	0,365	0,624	0,91	1,223	1,151	0,802	1,195	1,045	1,302	1,211
	Standard Deviation	0,091	0,034	0,086	0,04	0,177	0,501	0,132	0,164	0,228	0,13
Cytotoxicity	Average	2,417	1,714	1,497	1,198	1,09	0,781	1,162	1,002	1,422	1,165
	Standard Deviation	1,091	0,603	0,315	0,006	0,06	0,472	0,069	0,077	0,075	0,125
Apoptosis	Average	0,386	0,664	0,589	0,683	0,874	1,074	1,171	1,661	0,996	1,702
	Standard Deviation	0,049	0,096	0,343	0,378	0,521	0,556	0,525	1,145	0,394	1,245

Table A-10 Raw data for compound #4_7.

FaDu											
	Compound #4_7 [μM]	80	40	20	10	5	2,50	1,25	0,625	0,313	0,156
Viability	Average	0,562	0,806	0,88	0,726	0,91	0,901	0,874	0,933	0,972	0,952
	Standard Deviation	0,055	0,129	0,142	0,14	0,056	0,058	0,053	0,069	0,056	0,154
Cytotoxicity	Average	1,494	1,391	1,14	0,822	0,968	0,938	0,853	0,902	0,92	0,911
	Standard Deviation	0,232	0,235	0,256	0,178	0,081	0,006	0,056	0,018	0,004	0,041
Apoptosis	Average	0,849	1,096	0,971	0,874	0,936	1,009	0,929	1,054	1,02	1,071
	Standard Deviation	0,089	0,06	0,144	0,07	0,095	0,158	0,013	0,025	0,065	0,183

HCT-8											
	Compound #4_7 [μM]	80	40	20	10	5	2,50	1,25	0,625	0,313	0,156
Viability	Average	0,662	0,931	0,989	1,107	1,096	1,045	1,047	1,11	1,078	1,078
	Standard Deviation	0,03	0,233	0,302	0,212	0,309	0,273	0,239	0,23	0,269	0,295
Cytotoxicity	Average	1,342	1,392	1,21	1,301	1,258	1,131	1,166	1,22	1,166	1,195
	Standard Deviation	0,401	0,634	0,572	0,528	0,448	0,312	0,311	0,42	0,317	0,374
Apoptosis	Average	1,03	1,163	1,139	1,205	1,157	1,104	1,096	1,136	1,051	1,072
	Standard Deviation	0,282	0,434	0,269	0,386	0,238	0,326	0,207	0,295	0,2	0,242

HEK293 EpCAM FL											
	Compound #4_7 [μM]	80	40	20	10	5	2,50	1,25	0,625	0,313	0,156
Viability	Average	1,047	1,088	1,001	1,097	1,154	1,117	1,135	1,223	1,18	1,173
	Standard Deviation	0,643	0,348	0,286	0,258	0,222	0,221	0,216	0,168	0,165	0,142
Cytotoxicity	Average	0,999	1,107	0,934	0,891	0,892	0,845	0,891	1,034	1,096	1,091
	Standard Deviation	0,365	0,307	0,358	0,338	0,336	0,251	0,231	0,122	0,008	0,026
Apoptosis	Average	1,581	1,384	1,428	1,366	1,327	1,37	1,197	1,196	1,189	1,159
	Standard Deviation	1,388	0,818	0,743	0,489	0,571	0,422	0,424	0,459	0,384	0,457

HEK293 wt											
	Compound #4_7 [μ M]	80	40	20	10	5	2,50	1,25	0,625	0,313	0,156
Viability	Average	0,532	0,729	0,842	0,785	0,893	0,894	0,946	0,945	0,951	0,939
	Standard Deviation	0,038	0,009	0,031	0,048	0,102	0,127	0,109	0,109	0,093	0,073
Cytotoxicity	Average	1,536	1,383	1,181	1,008	0,991	0,983	1,016	1,023	0,965	0,948
	Standard Deviation	0,267	0,212	0,125	0,016	0,134	0,095	0,085	0,059	0,087	0,055
Apoptosis	Average	0,717	0,97	1,208	1,199	1,088	1,153	0,871	1,112	1,062	0,903
	Standard Deviation	0,009	0,091	0,045	0,066	0,194	0,186	0,116	0,195	0,155	0,189

Table A-11 Raw data for compound #9_0.

FaDu											
	Compound #9_0 [μ M]	80	40	20	10	5	2,50	1,25	0,625	0,313	0,156
Viability	Average	0,708	0,845	0,674	0,735	0,772	0,826	0,827	0,856	0,849	0,844
	Standard Deviation	0,026	0,074	0,036	0,053	0,069	0,035	0,034	0,084	0,064	0,075
Cytotoxicity	Average	0,798	0,869	0,867	0,91	0,969	1,002	1,027	0,955	0,98	0,968
	Standard Deviation	0,109	0,106	0,076	0,035	0,054	0,03	0,092	0,094	0,037	0,058
Apoptosis	Average	0,803	0,793	0,868	0,933	0,931	0,917	1,06	1,01	1,053	1,009
	Standard Deviation	0,01	0,053	0,053	0,047	0,054	0,008	0,045	0,096	0,128	0,022

HCT-8											
	Compound #9_0 [μ M]	80	40	20	10	5	2,50	1,25	0,625	0,313	0,156
Viability	Average	0,839	0,853	0,788	0,78	0,781	0,815	0,837	0,85	0,84	0,826
	Standard Deviation	0,195	0,402	0,186	0,062	0,095	0,08	0,071	0,08	0,108	0,131
Cytotoxicity	Average	0,851	0,988	0,936	1,083	1,072	1,098	1,061	1,059	1,068	1,059
	Standard Deviation	0,087	0,04	0,071	0,07	0,034	0,033	0,044	0,067	0,052	0,009
Apoptosis	Average	0,819	0,97	0,98	1,115	0,993	1,076	1,014	1,022	0,972	1,028
	Standard Deviation	0,255	0,348	0,249	0,157	0,249	0,026	0,127	0,044	0,131	0,096

HEK293 EpcAM FL		Compound #9_0 [μM]	80	40	20	10	5	2,50	1,25	0,625	0,313	0,156
Viability	Average		1,169	0,984	1,078	0,932	0,993	1,015	0,941	0,995	0,992	0,852
	Standard Deviation		0,429	0,527	0,552	0,182	0,197	0,329	0,12	0,012	0,028	0,229
Cytotoxicity	Average		1,583	0,884	1,104	0,794	0,891	0,761	0,809	0,838	0,799	0,719
	Standard Deviation		0,972	0,708	0,905	0,406	0,558	0,446	0,408	0,395	0,385	0,464
Apoptosis	Average		0,716	0,888	0,912	1,07	1,053	0,969	0,918	0,978	0,916	0,909
	Standard Deviation		0,071	0,035	0,127	0,105	0,156	0,08	0,107	0,042	0,129	0,162

HEK293 wt		Compound #9_0 [μM]	80	40	20	10	5	2,50	1,25	0,625	0,313	0,156
Viability	Average		0,862	0,863	0,867	0,833	0,864	0,926	0,895	0,949	0,969	0,95
	Standard Deviation		0,175	0,398	0,265	0,043	0,056	0,028	0,039	0,047	0,08	0,063
Cytotoxicity	Average		1,125	1,073	0,962	0,929	0,991	1,025	1,011	1,005	1,046	1,033
	Standard Deviation		0,144	0,512	0,205	0,044	0,016	0,056	0,088	0,047	0,086	0,006
Apoptosis	Average		0,777	0,798	0,949	0,981	0,968	0,989	1,114	1,018	1,169	1,026
	Standard Deviation		0,002	0,084	0,033	0,033	0,096	0,111	0,288	0,04	0,075	0,016

Table A-12 Raw data for compound #10_4.

FaDu		Compound #10_4 [μM]	80	40	20	10	5	2,50	1,25	0,625	0,313	0,156
Viability	Average		0,499	0,608	0,684	0,74	0,754	0,751	0,815	0,847	0,936	0,863
	Standard Deviation		0,038	0,052	0,005	0,013	0,005	0,045	0,005	0,025	0,064	0,083
Cytotoxicity	Average		0,641	0,793	0,966	0,995	0,976	0,973	0,984	1,001	1,034	0,957
	Standard Deviation		0,099	0,113	0,206	0,123	0,087	0,058	0,051	0,068	0,029	0,043
Apoptosis	Average		0,791	0,924	1,003	0,974	0,976	0,995	1,047	1,011	1,013	0,928
	Standard Deviation		0,156	0,123	0,078	0,149	0,138	0,075	0,067	0,159	0,105	0,003

HCT-8		Compound #10_4 [μM]	80	40	20	10	5	2,50	1,25	0,625	0,313	0,156
Viability	Average		0,672	0,788	0,835	0,963	0,99	1,012	1,039	1,079	1,057	1,073
	Standard Deviation		0,032	0,073	0,175	0,2	0,227	0,146	0,196	0,175	0,158	0,17
Cytotoxicity	Average		0,911	1,06	1,159	1,229	1,296	1,303	1,319	1,324	1,259	1,345
	Standard Deviation		0,271	0,3	0,392	0,407	0,351	0,331	0,358	0,322	0,415	0,369
Apoptosis	Average		1,073	1,164	1,187	1,104	1,197	1,16	1,171	1,156	1,118	1,166
	Standard Deviation		0,274	0,147	0,261	0,294	0,156	0,098	0,145	0,13	0,157	0,257

HEK293 EpCAM FL											
	Compound #10_4 [μM]	80	40	20	10	5	2,50	1,25	0,625	0,313	0,156
Viability	Average	0,799	0,831	0,867	0,954	0,904	0,982	0,95	1,038	1,082	1,001
	Standard Deviation	0,142	0,081	0,111	0,042	0,101	0,041	0,037	0,117	0,03	0,032
Cytotoxicity	Average	0,594	0,712	0,762	0,824	0,841	0,844	0,801	0,823	0,825	0,84
	Standard Deviation	0,302	0,368	0,426	0,398	0,344	0,397	0,334	0,327	0,333	0,349
Apoptosis	Average	0,986	1,074	1,16	1,158	1,044	1,103	1,147	1,083	1,063	1,027
	Standard Deviation	0,429	0,489	0,43	0,499	0,114	0,436	0,216	0,306	0,387	0,408

HEK293 wt											
	Compound #10_4 [μM]	80	40	20	10	5	2,50	1,25	0,625	0,313	0,156
Viability	Average	0,633	0,718	0,8	0,875	0,927	0,937	0,969	0,984	1,009	0,985
	Standard Deviation	0,009	0,044	0,024	0,006	0,032	0,048	0,024	0,055	0,006	0,005
Cytotoxicity	Average	0,649	0,797	0,889	0,942	1,022	1,042	1,024	1,045	1,101	1,009
	Standard Deviation	0,087	0,025	0,031	0,013	0,05	0,046	0,043	0,028	0,027	0,001
Apoptosis	Average	0,767	0,835	0,873	0,908	0,941	0,808	0,89	1,083	1,049	0,925
	Standard Deviation	0,079	0,189	0,076	0,085	0,201	0,027	0,038	0,147	0,187	0,025

Table A-13 Raw data for compound #10_6.

FaDu		Compound #10_6	80	40	20	10	5	2,50	1,25	0,625	0,313	0,156
		[μM]										
Viability	Average		0,558	0,662	0,739	0,79	0,855	0,869	0,904	0,935	0,996	1,039
	Standard Deviation		0,055	0,002	0,004	0,033	0,039	0,067	0,025	0,053	0,028	0
Cytotoxicity	Average		0,655	0,823	0,92	1,022	1,045	1,036	1,041	1,066	1,072	1,112
	Standard Deviation		0,114	0,147	0,129	0,113	0,026	0,034	0,089	0,017	0,051	0,065
Apoptosis	Average		0,709	0,86	0,901	0,951	0,969	0,971	0,954	1,014	0,932	1,086
	Standard Deviation		0,065	0	0,034	0,036	0,134	0,099	0,016	0,164	0,034	0,022

HCT-8		Compound #10_6	80	40	20	10	5	2,50	1,25	0,625	0,313	0,156
		[μM]										
Viability	Average		0,539	0,643	0,71	0,765	0,785	0,867	0,908	0,93	0,903	0,91
	Standard Deviation		0,173	0,15	0,142	0,163	0,139	0,117	0,147	0,18	0,149	0,149
Cytotoxicity	Average		0,763	0,843	1,001	1,002	1,027	1,101	1,161	1,145	1,144	1,162
	Standard Deviation		0,019	0,102	0,062	0,019	0,017	0,129	0,073	0,027	0,047	0,065
Apoptosis	Average		0,992	1,024	1,093	1,091	1,083	1,086	1,073	1,092	1,117	1,098
	Standard Deviation		0,07	0,09	0,043	0,029	0,016	0,084	0,015	0,061	0,027	0,064

HEK293 EpCAM FL		Compound #10_6 [μ M]	80	40	20	10	5	2,50	1,25	0,625	0,313	0,156
Viability	Average	0,721	0,746	0,887	0,873	0,903	0,902	0,989	0,988	1,001	1,033	
	Standard Deviation	0,15	0,302	0,167	0,168	0,111	0,065	0,19	0,083	0,046	0,032	
Cytotoxicity	Average	0,555	0,666	0,763	0,791	0,768	0,757	0,787	0,795	0,821	0,824	
	Standard Deviation	0,241	0,457	0,419	0,399	0,395	0,37	0,412	0,337	0,353	0,345	
Apoptosis	Average	0,872	1,043	1,022	1,204	1,127	1,053	1,027	0,978	0,977	0,967	
	Standard Deviation	0,075	0,042	0,046	0,044	0,17	0,031	0,087	0,009	0,191	0,024	

HEK293 wt		Compound #10_6 [μ M]	80	40	20	10	5	2,50	1,25	0,625	0,313	0,156
Viability	Average	0,538	0,636	0,724	0,809	0,833	0,875	0,955	0,946	0,951	0,949	
	Standard Deviation	0,051	0,115	0,076	0,055	0,046	0,056	0,076	0,096	0,147	0,09	
Cytotoxicity	Average	0,647	0,767	0,885	0,957	1,005	1,017	1,067	1,02	1,04	1,051	
	Standard Deviation	0,012	0,087	0,048	0,075	0,024	0,012	0,047	0,032	0,052	0,081	
Apoptosis	Average	0,75	0,909	0,981	0,991	1,076	0,978	0,946	1,063	0,976	1,037	
	Standard Deviation	0,043	0,001	0,087	0,012	0,087	0,014	0,009	0,113	0,108	0,044	

Table A-14 Raw data for compound #10_9.

FaDu		Compound #10_9	80	40	20	10	5	2,50	1,25	0,625	0,313	0,156
		[μM]										
Viability	Average		0,743	0,92	0,999	1,058	1,038	1,053	1,075	1,163	1,161	1,123
	Standard Deviation		0,154	0,142	0,15	0,117	0,1	0,075	0,094	0,154	0,064	0,049
Cytotoxicity	Average		0,596	0,782	0,887	0,973	0,924	0,971	1,008	1,073	1,062	1,014
	Standard Deviation		0,117	0,133	0,176	0,138	0,055	0,09	0,056	0,081	0,092	0,011
Apoptosis	Average		0,79	0,953	0,911	0,964	0,821	0,94	1,003	1,081	0,958	1,127
	Standard Deviation		0,019	0,123	0,038	0,18	0,022	0,029	0,004	0,133	0,023	0,222

HCT-8		Compound #10_9	80	40	20	10	5	2,50	1,25	0,625	0,313	0,156
		[μM]										
Viability	Average		0,81	0,821	1,042	1,067	1,101	1,179	1,12	1,171	1,142	1,163
	Standard Deviation		0,151	0,079	0,275	0,253	0,254	0,327	0,234	0,213	0,291	0,208
Cytotoxicity	Average		0,882	1,025	1,266	1,274	1,301	1,373	1,356	1,382	1,411	1,373
	Standard Deviation		0,427	0,521	0,635	0,602	0,568	0,619	0,548	0,574	0,663	0,522
Apoptosis	Average		1,206	1,243	1,234	1,267	1,233	1,2	1,215	1,155	1,193	1,279
	Standard Deviation		0,232	0,347	0,315	0,262	0,289	0,279	0,201	0,191	0,139	0,192

HEK293 EpCAM FL											
	Compound #10_9 [μM]	80	40	20	10	5	2,50	1,25	0,625	0,313	0,156
Viability	Average	0,934	1,002	1,08	1,13	1,16	1,097	1,11	1,122	1,194	1,095
	Standard Deviation	0,225	0,309	0,261	0,217	0,116	0,009	0,11	0,068	0,069	0,054
Cytotoxicity	Average	0,631	0,737	0,822	0,816	0,821	0,779	0,836	0,91	1,047	0,944
	Standard Deviation	0,328	0,377	0,453	0,373	0,271	0,212	0,307	0,222	0,057	0,117
Apoptosis	Average	1,005	1,011	1,085	1,121	1,04	0,932	0,902	0,938	0,937	0,844
	Standard Deviation	0,26	0,276	0,171	0,07	0,049	0,122	0,109	0,043	0,017	0,041

HEK293 wt											
	Compound #10_9 [μM]	80	40	20	10	5	2,50	1,25	0,625	0,313	0,156
Viability	Average	0,633	0,808	0,891	0,963	1,022	1,011	0,987	1,01	1,027	1,026
	Standard Deviation	0,046	0	0,032	0,012	0,049	0,023	0,025	0,026	0,048	0,04
Cytotoxicity	Average	0,639	0,824	0,89	0,998	1,055	1,047	1,049	1,027	1,068	1,04
	Standard Deviation	0,122	0,015	0,011	0,012	0,087	0,078	0,114	0,122	0,11	0,047
Apoptosis	Average	1,097	1,205	1,076	1,097	0,931	0,874	0,925	0,891	0,791	0,946
	Standard Deviation	0,055	0,131	0,025	0,04	0,068	0,009	0,018	0,006	0,044	0,027

Table A-15 Raw data for compound #10_10.

FaDu		Compound #10_10 [μM]	80	40	20	10	5	2,50	1,25	0,625	0,313	0,156
Viability	Average		0,635	0,754	0,929	0,918	0,827	1,015	1,027	1,002	1,09	1,122
	Standard Deviation		0,132	0,093	0,16	0,206	0,069	0,19	0,232	0,232	0,107	0,175
Cytotoxicity	Average		0,521	0,62	0,75	0,786	0,75	0,823	0,836	0,82	0,895	0,924
	Standard Deviation		0,064	0,048	0,043	0,057	0,004	0,089	0,16	0,126	0,004	0,023
Apoptosis	Average		0,7	0,78	0,832	0,898	0,824	0,909	0,912	0,849	0,879	0,898
	Standard Deviation		0,013	0,02	0,016	0,207	0,069	0,009	0,013	0,026	0,013	0,072

HCT-8		Compound #10_10 [μM]	80	40	20	10	5	2,50	1,25	0,625	0,313	0,156
Viability	Average		0,508	0,637	0,723	0,721	0,749	0,824	0,811	0,865	0,838	0,849
	Standard Deviation		0,019	0,049	0,041	0,015	0,076	0,004	0,094	0,075	0,016	0,029
Cytotoxicity	Average		0,721	0,835	0,914	0,882	0,893	0,965	0,989	1,006	0,963	1,048
	Standard Deviation		0,265	0,223	0,265	0,182	0,058	0,229	0,376	0,223	0,246	0,214
Apoptosis	Average		0,984	0,976	1,009	0,986	0,977	1	0,945	0,961	0,914	0,997
	Standard Deviation		0,21	0,048	0,151	0,049	0,005	0,031	0,194	0,21	0,144	0,039

HEK293 EpCAM FL											
	Compound #10_10 [μM]	80	40	20	10	5	2,50	1,25	0,625	0,313	0,156
Viability	Average	0,631	0,722	0,882	0,904	0,851	1,053	1,088	1,22	0,996	1,169
	Standard Deviation	0,06	0,22	0,259	0,177	0,048	0,279	0,362	0,361	0,083	0,29
Cytotoxicity	Average	0,46	0,488	0,624	0,642	0,56	0,708	0,677	0,708	0,652	0,745
	Standard Deviation	0,107	0,198	0,248	0,211	0,073	0,32	0,282	0,26	0,212	0,354
Apoptosis	Average	0,873	0,847	0,93	0,951	1,043	0,868	1,014	0,981	0,853	0,907
	Standard Deviation	0,069	0,041	0,018	0,012	0,033	0,031	0,083	0,054	0,032	0,041

HEK293 wt											
	Compound #10_10 [μM]	80	40	20	10	5	2,50	1,25	0,625	0,313	0,156
Viability	Average	0,521	0,578	0,686	0,761	0,793	0,822	0,835	0,908	0,884	0,91
	Standard Deviation	0,011	0,022	0,008	0,04	0,06	0,007	0,036	0,028	0,007	0,021
Cytotoxicity	Average	0,626	0,675	0,779	0,824	0,872	0,893	0,916	0,927	0,893	0,915
	Standard Deviation	0,069	0,06	0,095	0,114	0,146	0,09	0,132	0,122	0,104	0,119
Apoptosis	Average	0,912	0,758	0,952	0,872	0,877	0,909	0,925	0,946	0,891	0,896
	Standard Deviation	0,04	0,058	0,031	0,121	0,166	0,024	0,114	0,009	0,012	0,003

Table A-16 Raw data for compound #10_12.

FaDu		Compound #10_12	80	40	20	10	5	2,50	1,25	0,625	0,313	0,156
		[μM]										
Viability	Average		0,479	0,593	0,663	0,71	0,73	0,819	0,842	0,837	0,886	0,905
	Standard Deviation		0,027	0,024	0,024	0,047	0,033	0,006	0,069	0,034	0,089	0,072
Cytotoxicity	Average		0,555	0,651	0,783	0,843	0,898	0,958	0,962	0,912	1	1,034
	Standard Deviation		0,015	0,011	0,066	0,037	0,042	0,037	0,007	0,038	0,044	0,05
Apoptosis	Average		0,828	0,846	0,922	0,923	0,92	1,065	0,923	0,926	1,01	0,965
	Standard Deviation		0,037	0,009	0,012	0,004	0,057	0,012	0,037	0,027	0,002	0,003

HCT-8		Compound #10_12	80	40	20	10	5	2,50	1,25	0,625	0,313	0,156
		[μM]										
Viability	Average		0,555	0,818	0,92	1,008	1,086	1,104	0,98	1,098	1,241	1,24
	Standard Deviation		0,132	0,312	0,345	0,324	0,35	0,401	0,25	0,326	0,506	0,415
Cytotoxicity	Average		0,757	1,001	1,151	1,296	1,357	1,346	1,138	1,356	1,339	1,386
	Standard Deviation		0,248	0,442	0,505	0,536	0,56	0,569	0,411	0,553	0,645	0,666
Apoptosis	Average		1,014	1,073	1,04	1,1	1,077	1,057	1,082	1,163	1,099	1,162
	Standard Deviation		0,179	0,125	0,204	0,231	0,281	0,209	0,212	0,283	0,199	0,325

HEK293 EpCAM FL											
	Compound #10_12 [μM]	80	40	20	10	5	2,50	1,25	0,625	0,313	0,156
Viability	Average	0,559	0,759	0,773	0,878	0,914	0,975	1,001	0,935	0,967	0,9
	Standard Deviation	0,093	0,162	0,03	0,029	0,011	0,039	0,035	0,131	0,247	0,211
Cytotoxicity	Average	0,4	0,605	0,636	0,702	0,735	0,787	0,746	0,647	0,857	0,657
	Standard Deviation	0,133	0,052	0,229	0,257	0,239	0,313	0,26	0,102	0,055	0,053
Apoptosis	Average	1,009	0,974	1,037	1,102	1,046	1,116	1,053	1,166	1,029	1,069
	Standard Deviation	0,397	0,42	0,444	0,311	0,282	0,295	0,3	0,278	0,389	0,178

HEK293 wt											
	Compound #10_12 [μM]	80	40	20	10	5	2,50	1,25	0,625	0,313	0,156
Viability	Average	0,511	0,732	0,738	0,852	0,885	0,927	0,976	0,952	0,989	0,957
	Standard Deviation	0,045	0,188	0,048	0,116	0,097	0,099	0,147	0,094	0,152	0,052
Cytotoxicity	Average	0,543	0,77	0,803	0,895	0,956	0,993	1,048	0,981	0,985	0,971
	Standard Deviation	0,001	0,116	0,045	0,065	0,096	0,075	0,1	0,079	0,073	0,044
Apoptosis	Average	0,786	0,846	0,888	0,976	0,913	0,895	0,951	0,912	0,891	0,864
	Standard Deviation	0,074	0,032	0,034	0,062	0,033	0,037	0,034	0,125	0,192	0,103

Table A-17 Raw data for compound #13_1.

FaDu		Compound #13_1	80	40	20	10	5	2,50	1,25	0,625	0,313	0,156
		[μM]										
Viability	Average		0,781	0,811	0,828	0,909	0,842	0,909	0,91	0,918	0,891	0,91
	Standard Deviation		0,096	0,054	0,028	0,001	0,067	0,004	0,014	0,025	0,029	0,006
Cytotoxicity	Average		0,98	0,987	1,057	1,039	0,919	1,014	1,017	0,956	0,997	1,009
	Standard Deviation		0,149	0,058	0,013	0,02	0,085	0,017	0,058	0,001	0,029	0,007
Apoptosis	Average		0,883	0,882	1,014	1,04	1,017	0,945	1,016	0,992	1,004	0,975
	Standard Deviation		0,051	0,036	0,125	0,045	0,062	0,024	0,049	0,004	0,011	0,06

HCT-8		Compound #13_1	80	40	20	10	5	2,50	1,25	0,625	0,313	0,156
		[μM]										
Viability	Average		0,802	0,888	0,925	1,022	0,957	0,943	0,934	0,924	0,965	0,926
	Standard Deviation		0,183	0,124	0,046	0,111	0,16	0,051	0,073	0,076	0,011	0,057
Cytotoxicity	Average		0,973	1,028	1,096	1,168	1,088	1,114	1,103	1,099	0,967	1,035
	Standard Deviation		0,017	0,021	0,11	0,144	0,002	0,131	0,063	0,079	0,061	0,175
Apoptosis	Average		1,25	1,294	1,269	1,164	1,054	1,047	1,084	1,104	0,944	0,999
	Standard Deviation		0,265	0,126	0,109	0,144	0,114	0,224	0,019	0,033	0,116	0,137

HEK293 EpCAM FL											
	Compound #13_1 [μM]	80	40	20	10	5	2,50	1,25	0,625	0,313	0,156
Viability	Average	0,863	0,782	0,791	0,955	0,961	0,957	0,937	0,816	0,718	0,683
	Standard Deviation	0,009	0,104	0,081	0,049	0,073	0,047	0,021	0,195	0,371	0,422
Cytotoxicity	Average	0,808	0,779	0,798	0,841	0,796	0,813	0,846	0,768	0,764	0,768
	Standard Deviation	0,348	0,399	0,346	0,362	0,309	0,335	0,269	0,035	0,074	0,244
Apoptosis	Average	1,354	1,314	1,316	1,232	1,144	1,053	1,048	1,065	1,067	0,987
	Standard Deviation	0,432	0,317	0,006	0,158	0,009	0,039	0,057	0,057	0,142	0,155

HEK293 wt											
	Compound #13_1 [μM]	80	40	20	10	5	2,50	1,25	0,625	0,313	0,156
Viability	Average	0,704	0,734	0,775	0,881	0,911	0,916	0,912	0,92	0,93	0,902
	Standard Deviation	0,005	0,027	0,068	0,041	0,064	0,041	0,047	0,006	0,02	0,104
Cytotoxicity	Average	0,916	0,938	0,936	0,957	0,989	1,022	1,013	1,022	0,986	0,998
	Standard Deviation	0,066	0,087	0,022	0,059	0,059	0,034	0,001	0,028	0,032	0,009
Apoptosis	Average	1,066	1,052	1,023	1,121	1,002	0,978	1,039	0,933	1,073	0,899
	Standard Deviation	0,033	0,007	0,033	0,097	0,042	0,014	0,048	0,018	0,158	0,216

Table A-18 Raw data for compound #13-7.

FaDu		Compound #13_7	80	40	20	10	5	2,50	1,25	0,625	0,313	0,156
		[μM]										
Viability	Average		0,881	1,005	0,977	0,986	0,917	0,969	0,969	0,974	0,968	0,986
	Standard Deviation		0,077	0,051	0,073	0,02	0,098	0,067	0,017	0	0,036	0,057
Cytotoxicity	Average		0,987	1,042	1,054	1,031	0,991	1,026	1,042	1,002	1,008	1,015
	Standard Deviation		0,101	0,003	0,013	0,041	0,12	0,04	0,013	0,008	0,045	0,044
Apoptosis	Average		1,045	1,092	1,058	1,101	1,015	1,061	0,981	1,086	1,051	0,989
	Standard Deviation		0,034	0,048	0,258	0,14	0,139	0,069	0,109	0,172	0,02	0,108

HCT-8		Compound #13_7	80	40	20	10	5	2,50	1,25	0,625	0,313	0,156
		[μM]										
Viability	Average		1,055	1,2	0,96	1,197	1,099	1,13	1,072	1,153	1,111	1,121
	Standard Deviation		0,031	0,096	0,096	0,167	0,054	0,165	0,209	0,219	0,209	0,185
Cytotoxicity	Average		1,238	1,407	1,141	1,431	1,291	1,257	1,243	1,172	1,264	1,224
	Standard Deviation		0,342	0,508	0,174	0,485	0,326	0,3	0,392	0,314	0,55	0,438
Apoptosis	Average		1,453	1,288	1,381	1,285	1,161	1,049	1,135	0,985	1,166	1,09
	Standard Deviation		0,282	0,354	0,361	0,237	0,175	0,06	0,207	0,095	0,262	0,119

HEK293 EpCAM FL											
	Compound #13_7 [μM]	80	40	20	10	5	2,50	1,25	0,625	0,313	0,156
Viability	Average	0,866	1,014	0,963	1,033	0,953	0,986	0,955	1,029	0,748	0,809
	Standard Deviation	0,123	0,156	0,115	0,122	0,005	0,041	0,088	0,2	0,367	0,297
Cytotoxicity	Average	0,789	0,792	0,835	0,874	0,839	0,892	0,875	0,981	0,719	0,855
	Standard Deviation	0,137	0,241	0,24	0,239	0,265	0,192	0,105	0,087	0,163	0,093
Apoptosis	Average	1,02	0,997	0,955	0,98	0,922	0,871	0,875	0,828	0,808	0,928
	Standard Deviation	0,064	0,003	0,117	0,044	0,035	0,078	0,07	0,091	0,091	0,022

HEK293 wt											
	Compound #13_7 [μM]	80	40	20	10	5	2,50	1,25	0,625	0,313	0,156
Viability	Average	0,854	0,977	0,992	1,035	1,01	1,011	0,974	1,023	1,003	1,004
	Standard Deviation	0,056	0,057	0,062	0,052	0,06	0,057	0,054	0,149	0,027	0,072
Cytotoxicity	Average	0,977	1,032	1,047	1,056	1,057	1,07	1,088	1,079	1,072	1,012
	Standard Deviation	0,031	0,056	0,066	0,031	0,106	0,096	0,079	0,14	0,081	0,056
Apoptosis	Average	1,088	1,061	1,129	0,99	0,932	1,177	0,892	1,011	0,884	0,915
	Standard Deviation	0,068	0,017	0,128	0,008	0,007	0,346	0,145	0,075	0,149	0,025

B. ApoTox Evaluation

The graphs show the evaluation of ApoTox Assay. Results are depicted for FaDu (black), HCT-8 (dark grey), HEK293 EpCAM-FL (light grey) and HEK293 wild-type cells (white) as fold change from DMSO treated control. The drug staurosporine was used as positive control. The first graph shows the results for viability, the middle one for cytotoxicity and the last for apoptosis. Depicted are mean values and standard deviations from two independent experiments, each consisting of three replicates.

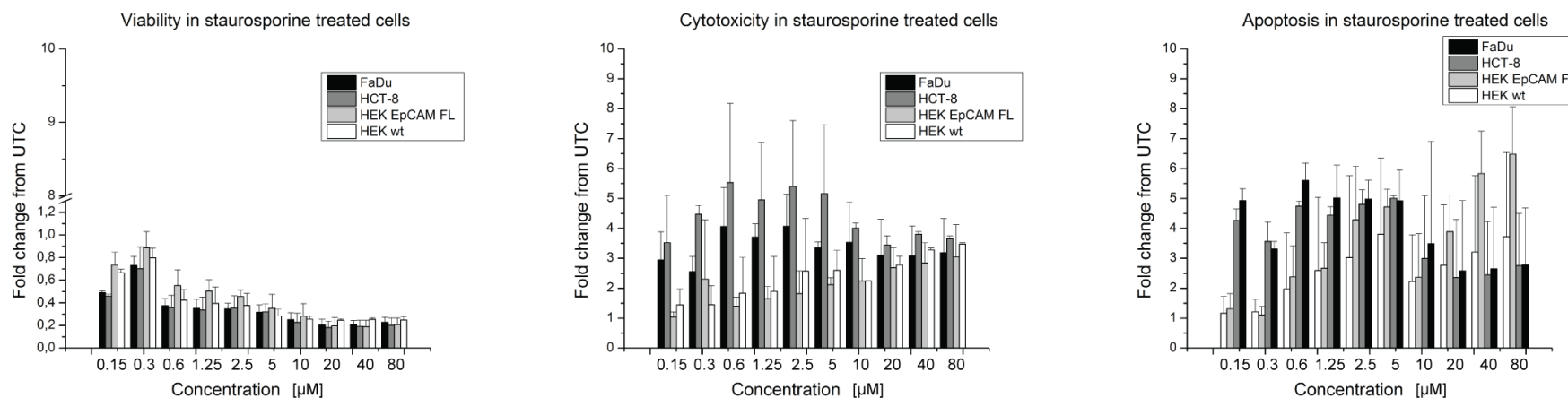


Figure B-1 Results from staurosporine treated cells.

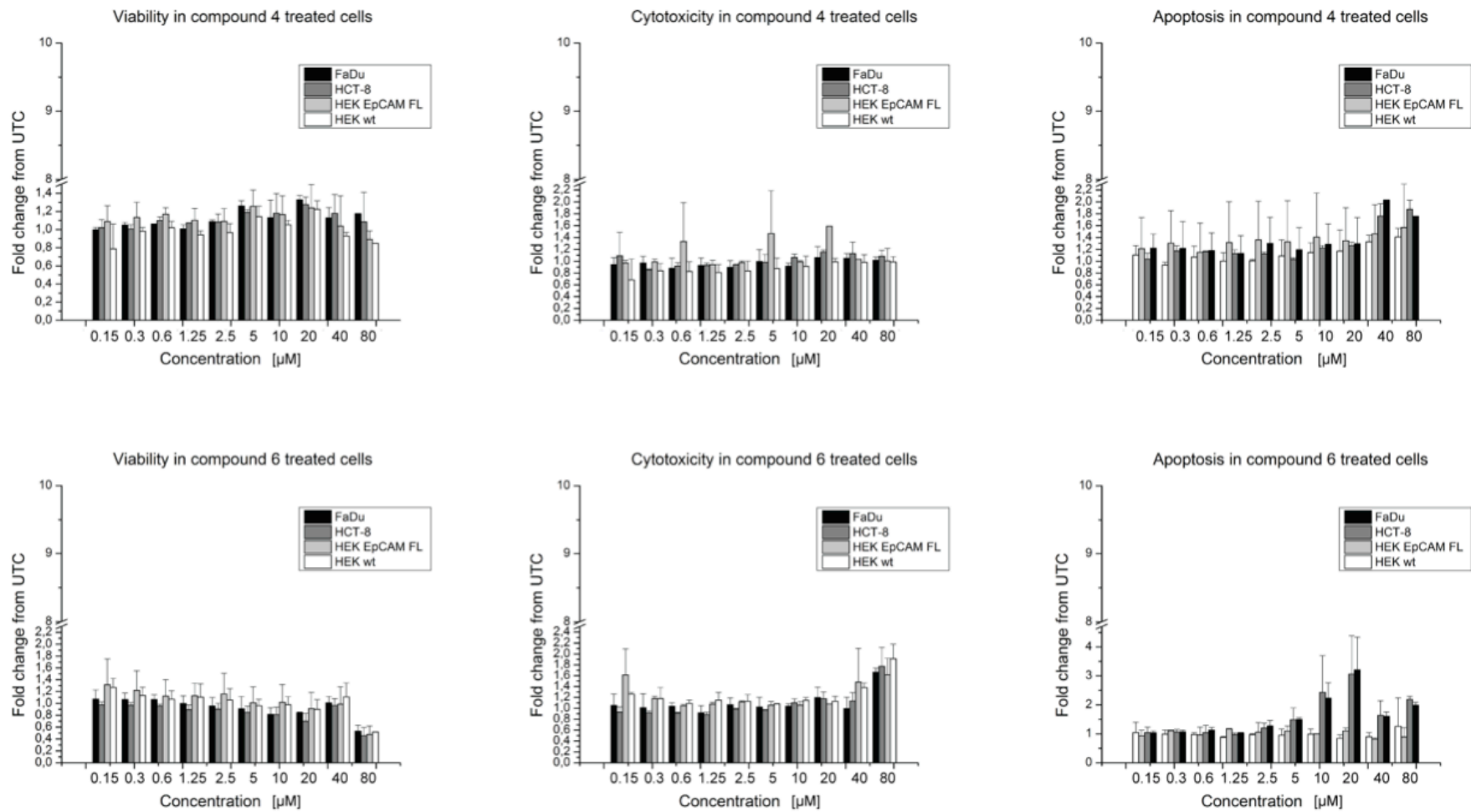


Figure B-2 Results from compound #4_0 (upper panel) and compound #6_0 (lower panel) treated cells.

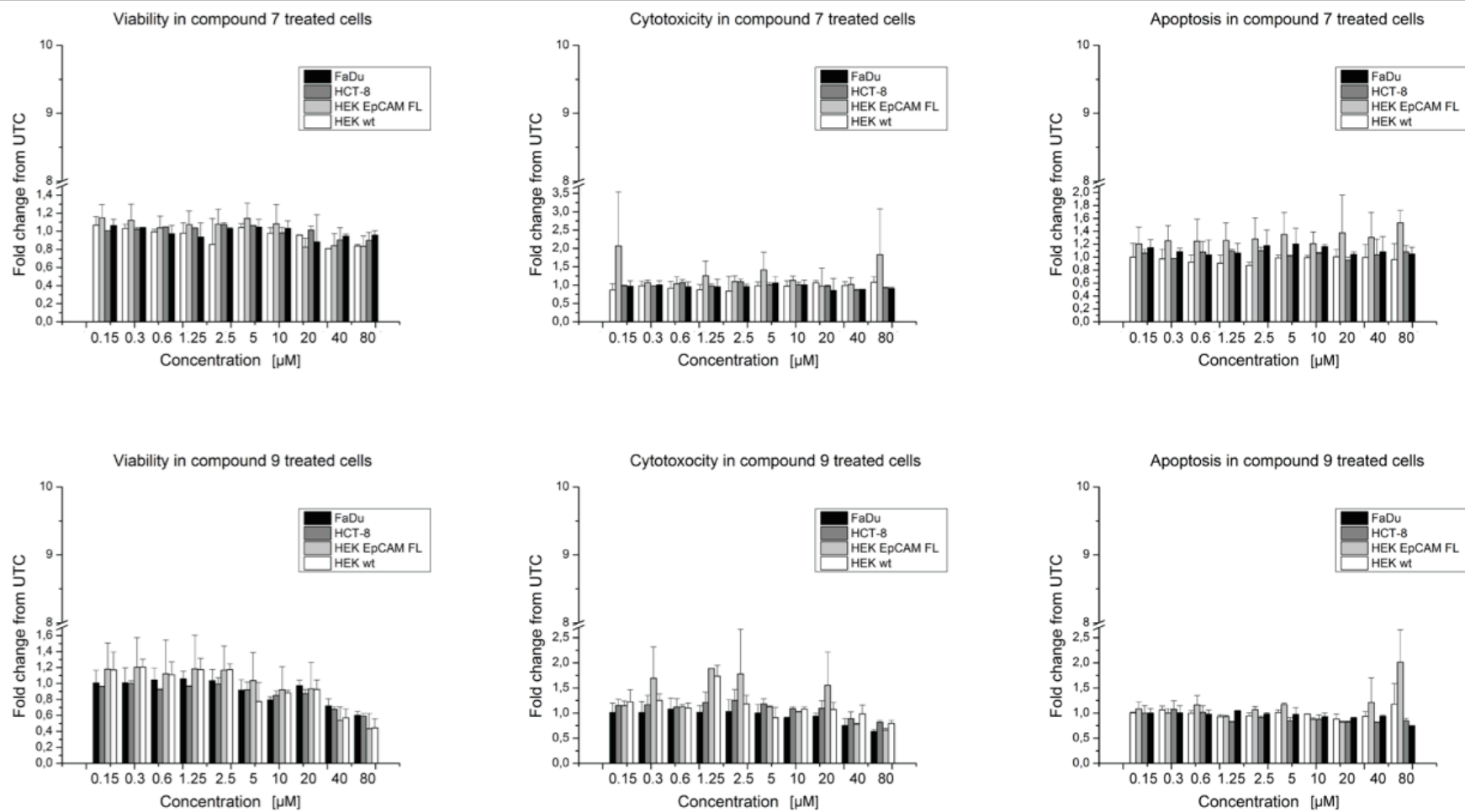


Figure B-3 Results from compound #7_0 (upper panel) and compound #9_0 (lower panel) treated cells.

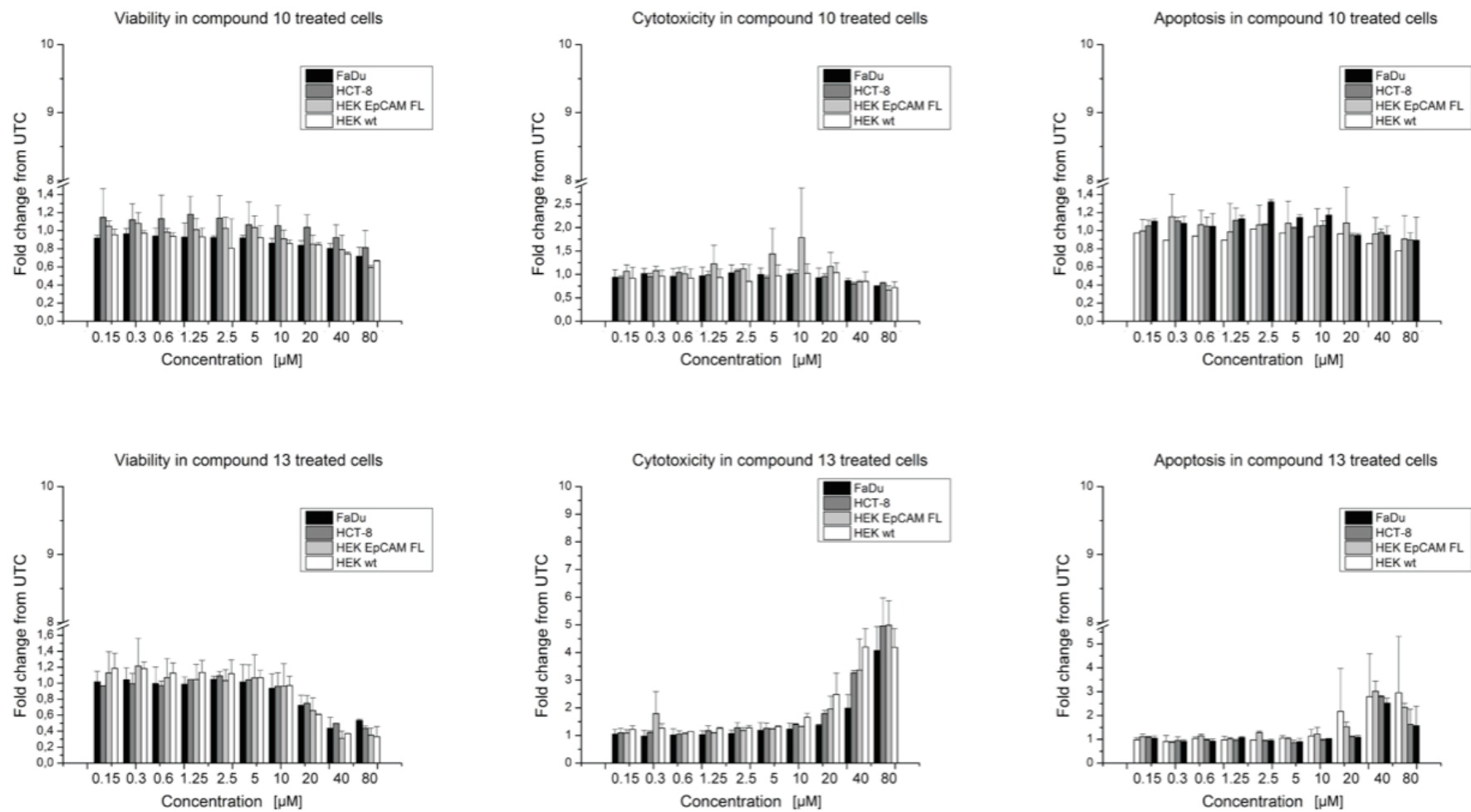


Figure B-4 Results from compound #10_0 (upper panel) and compound #13_0 (lower panel) treated cells.

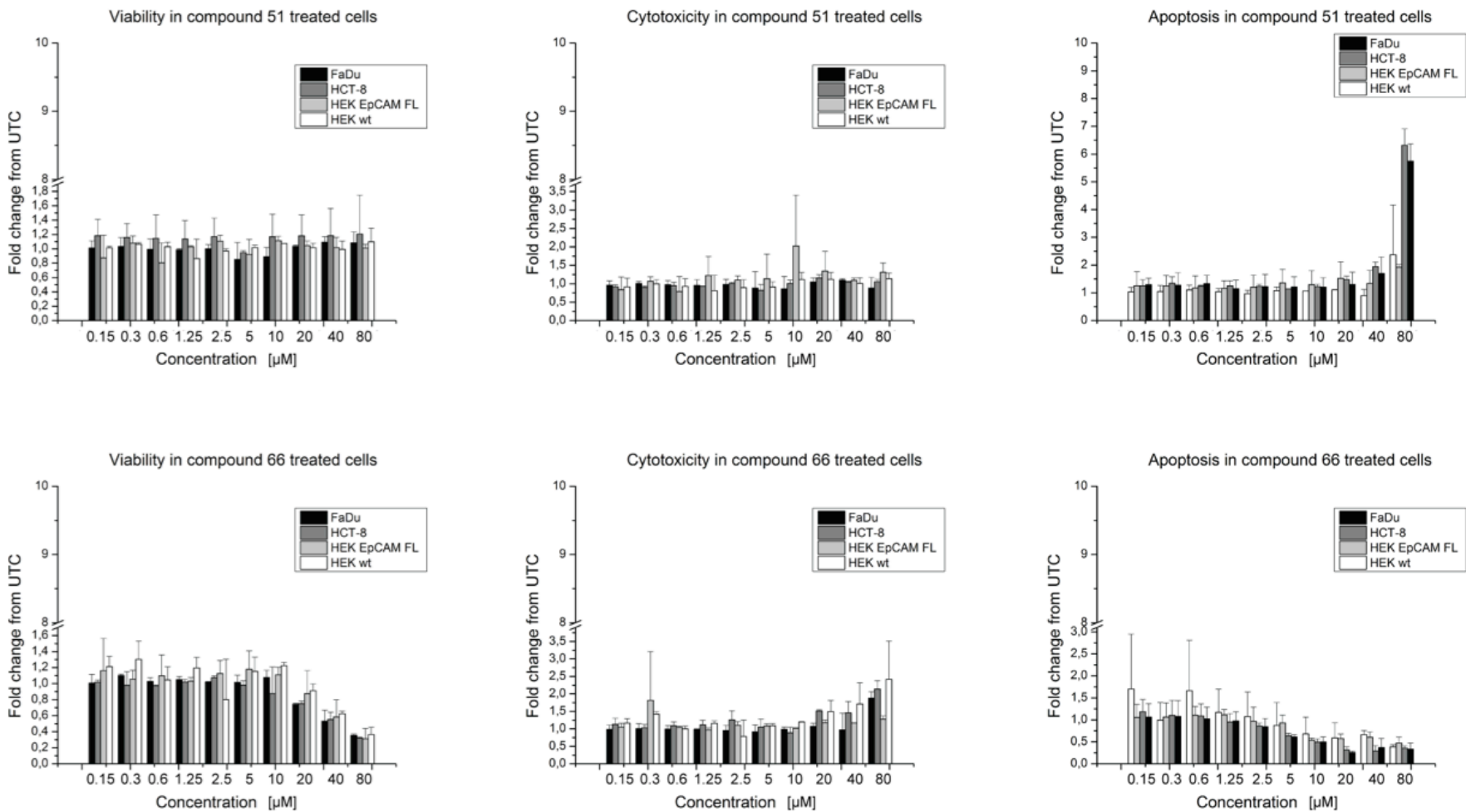


Figure B-5 Results from compound #51_0 (upper panel) and compound #66_0 (lower panel) treated cells.

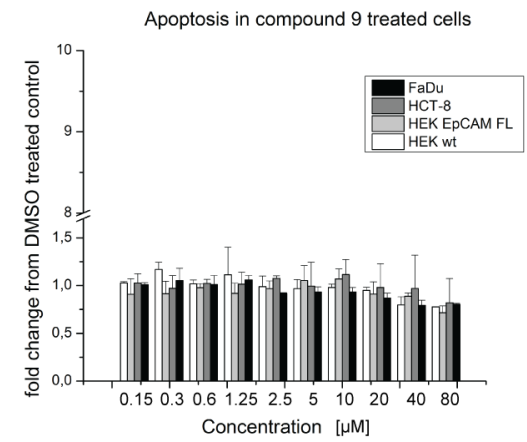
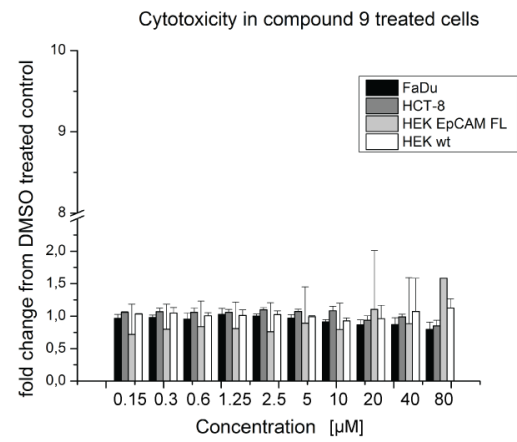
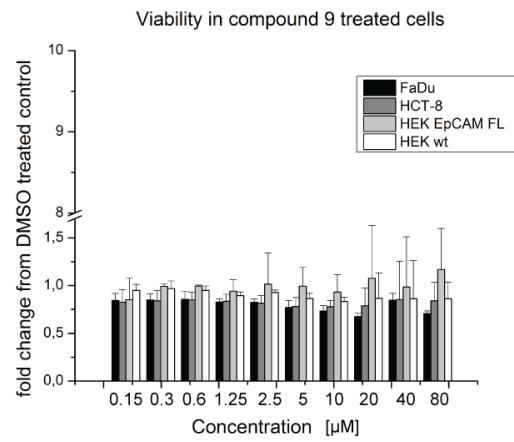
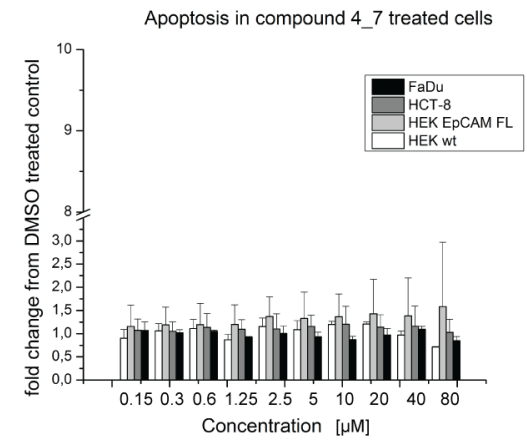
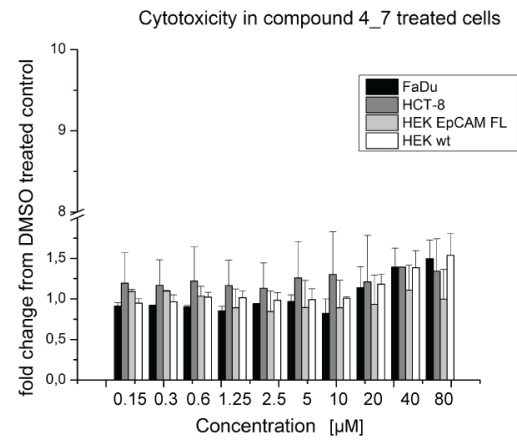
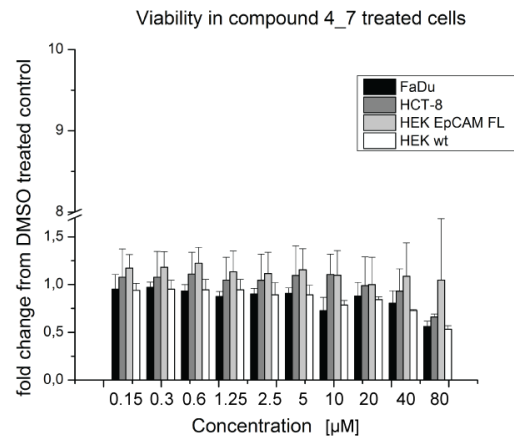


Figure B-6 Results from compound #4_7 (upper panel) and compound #9_0 (lower panel) treated cells.

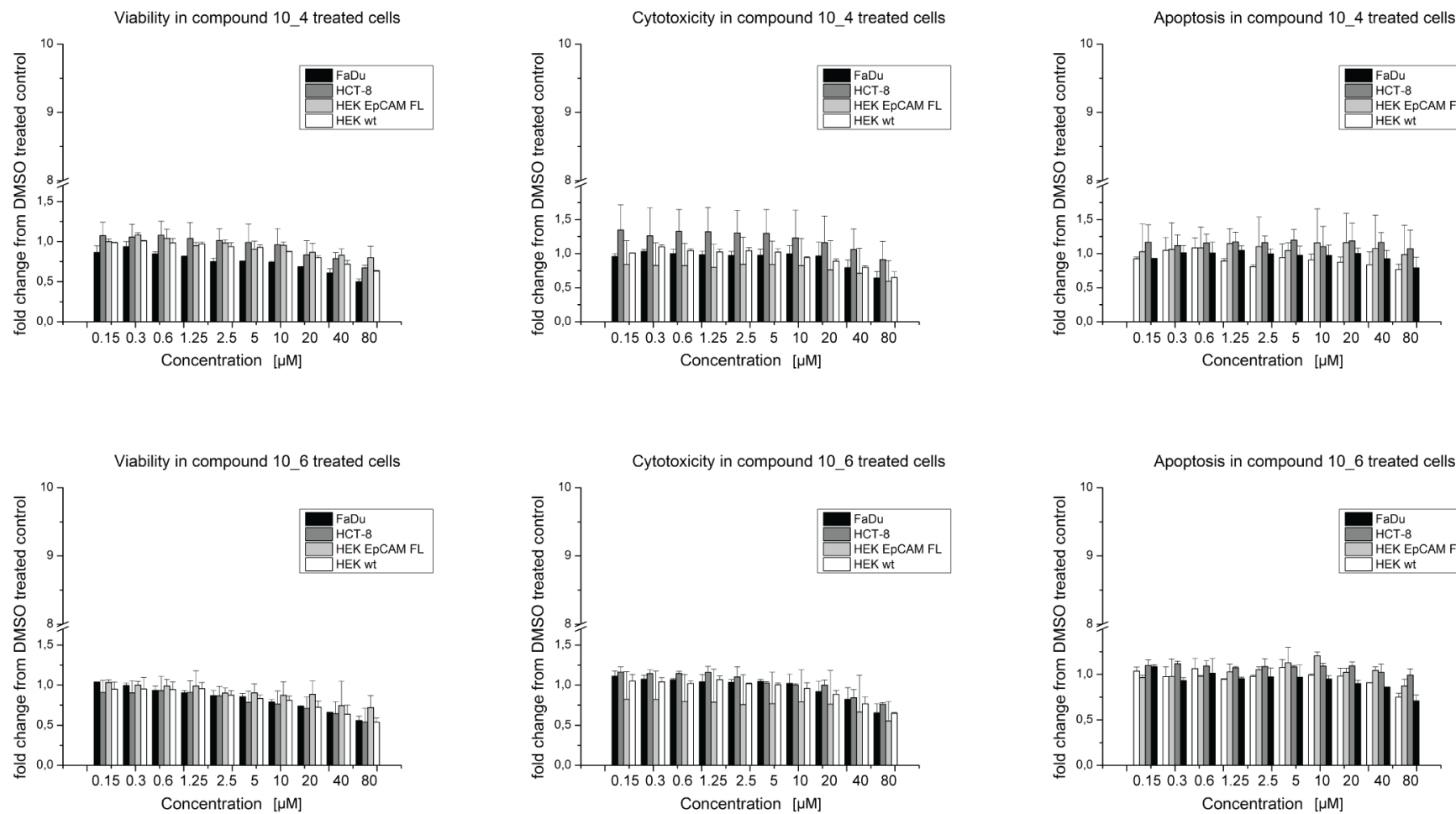


Figure B-7 Results from compound #10_4 (upper panel) and compound #10_6 (lower panel) treated cells.

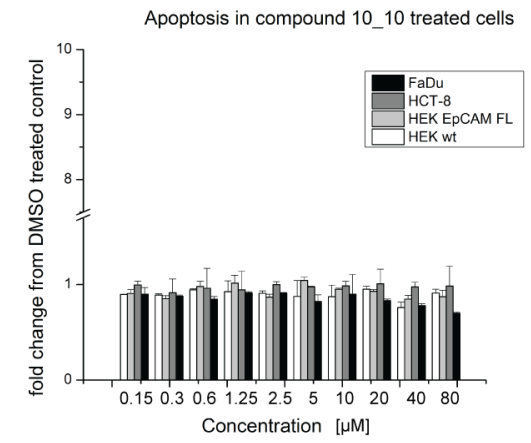
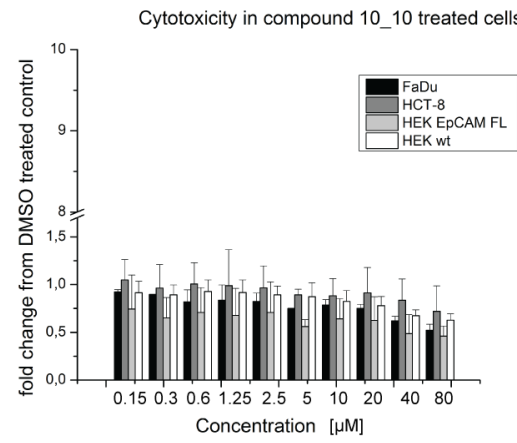
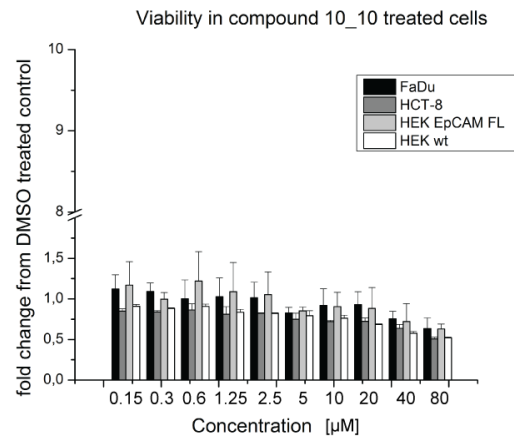
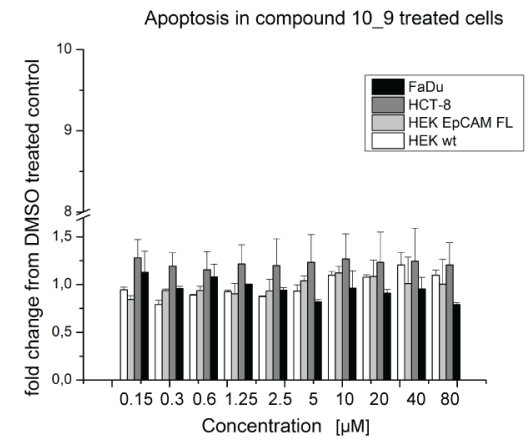
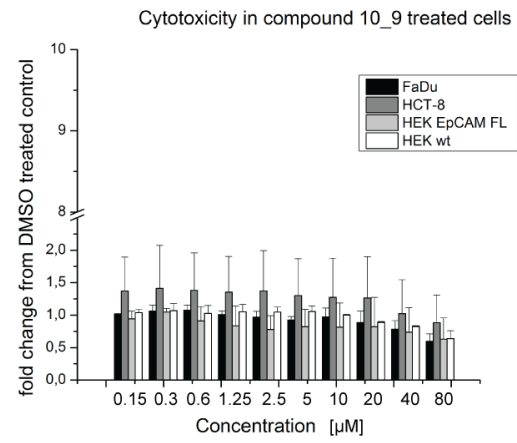
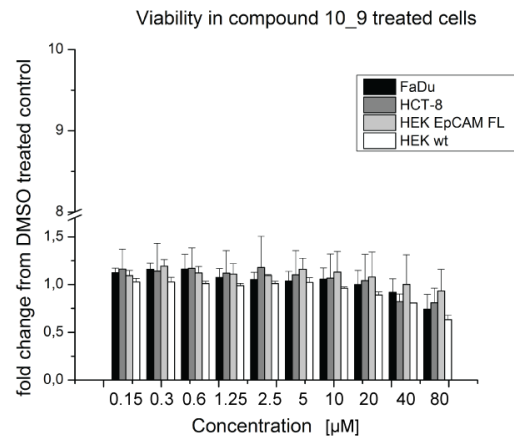


Figure B-8 Results from compound #10_9 (upper panel) and compound #10_10 (lower panel) treated cells.

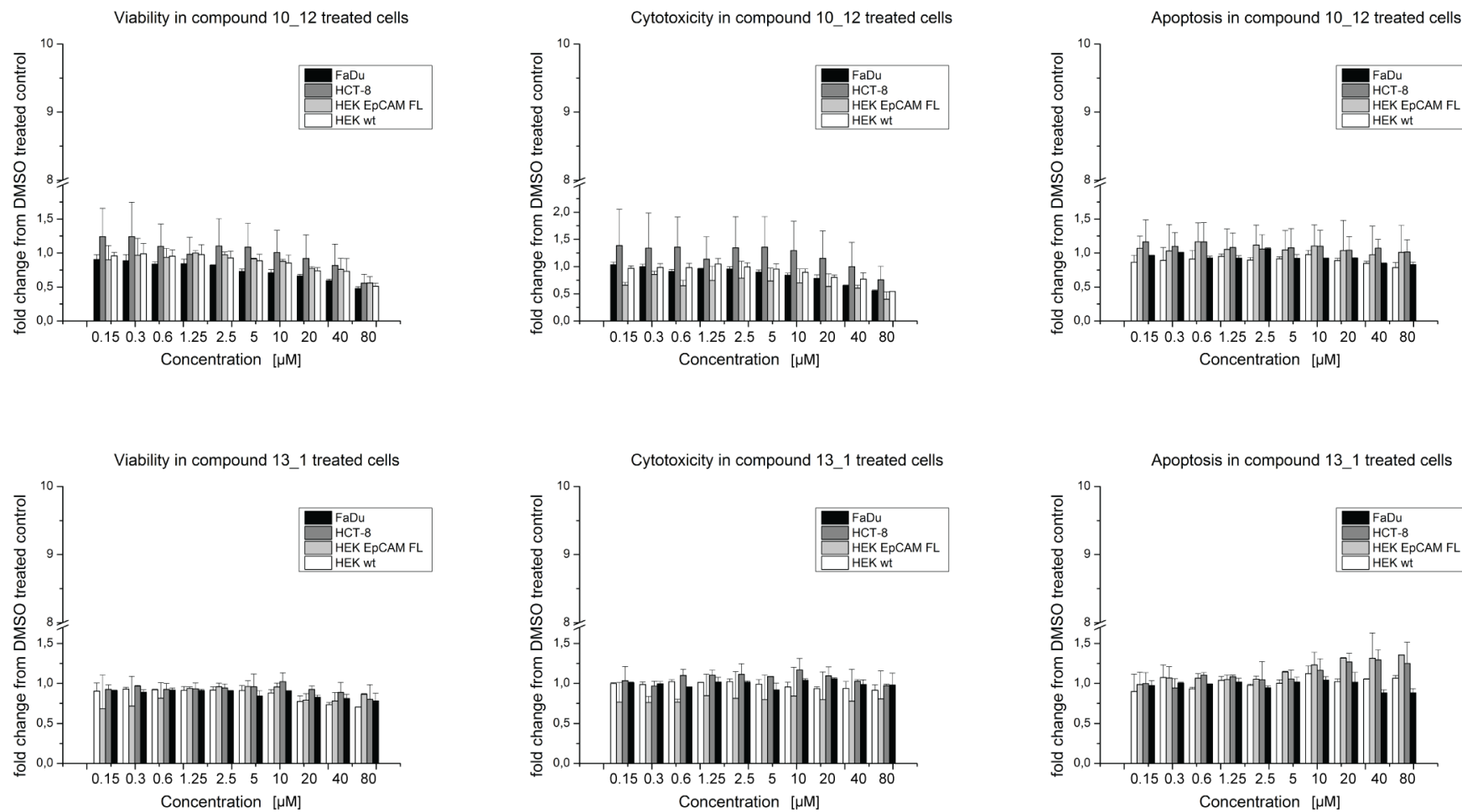


Figure B-9 Results from compound #10_12 (upper panel) and compound #13_1 (lower panel) treated cells.

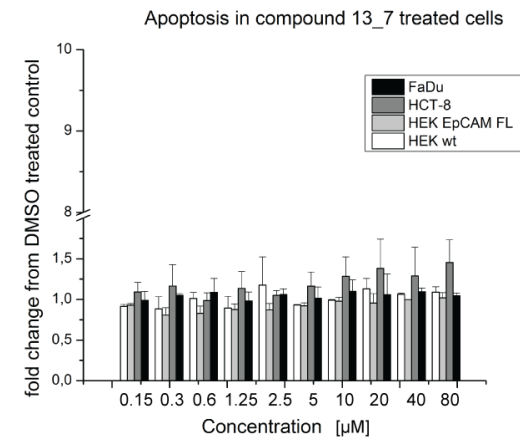
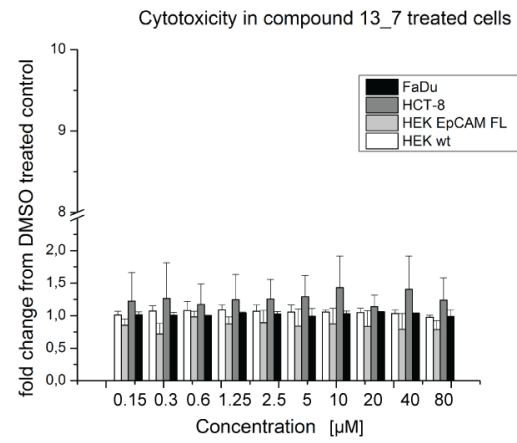
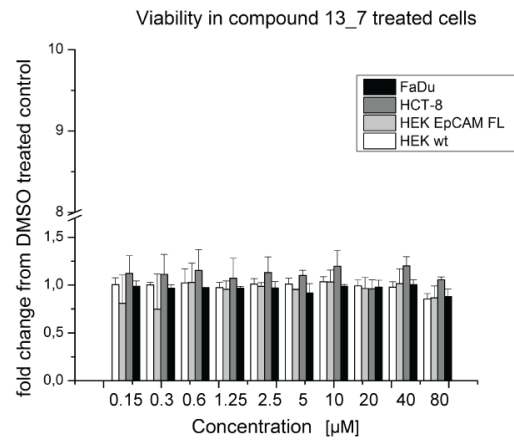
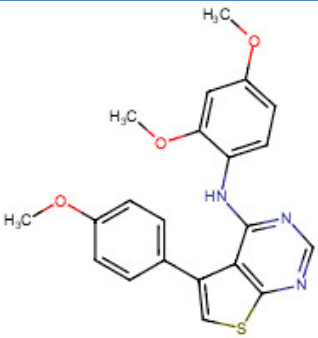
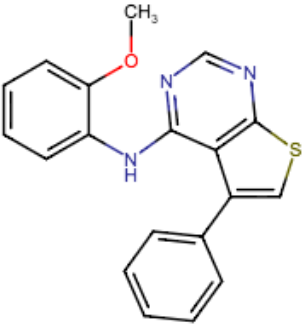
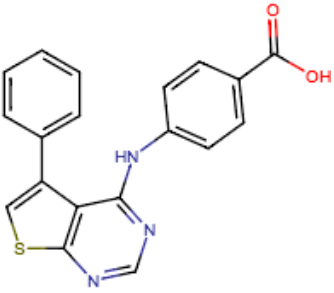
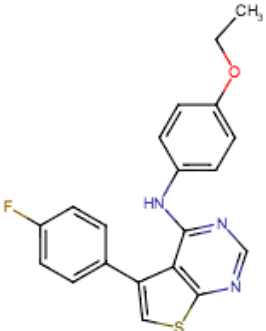


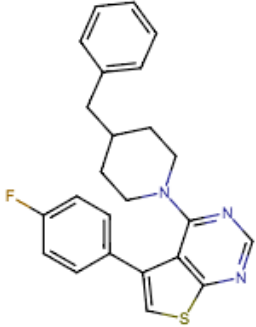
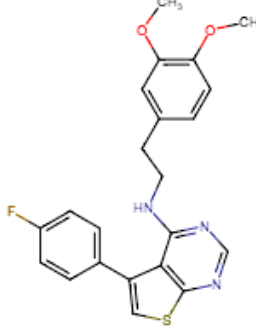
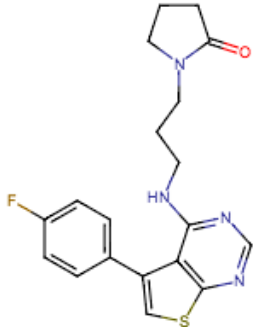
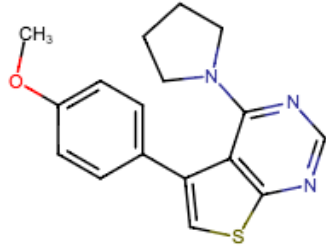
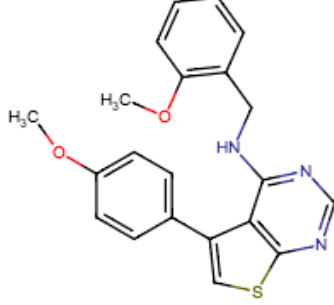
Figure B-10 Results from compound #13_7 treated cells.

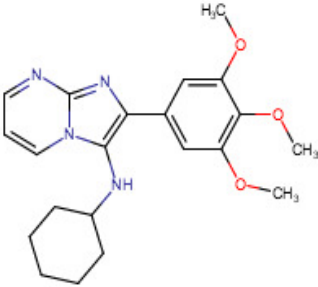
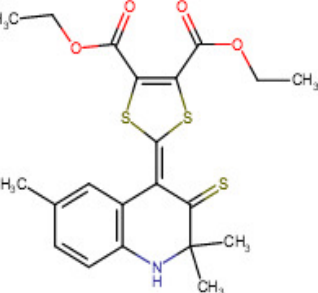
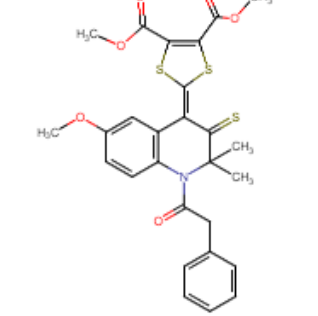
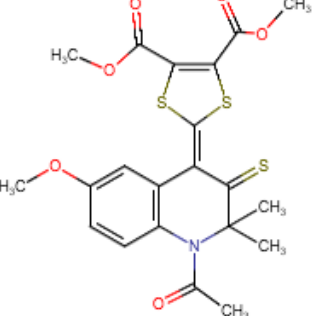
C. Compound structures

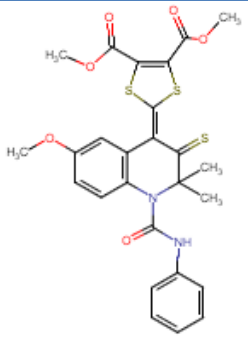
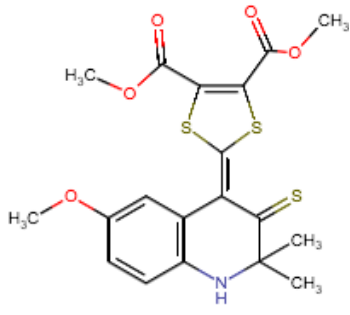
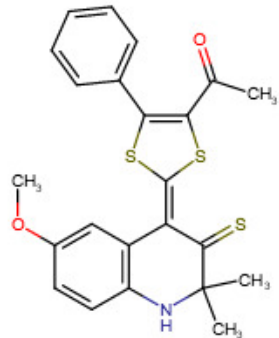
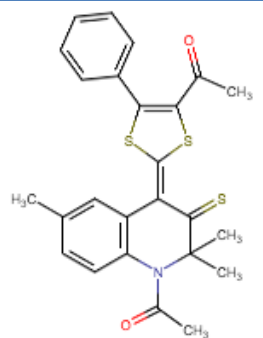
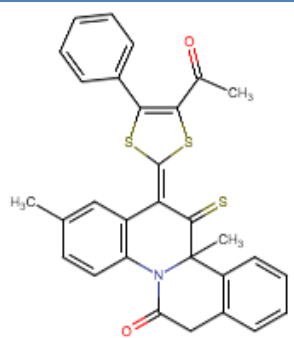
Table C-1 Structures of high-confidence hits and their analogs. Shown are the compound ID, the chemical structure, the molecular formula and the molecular weight

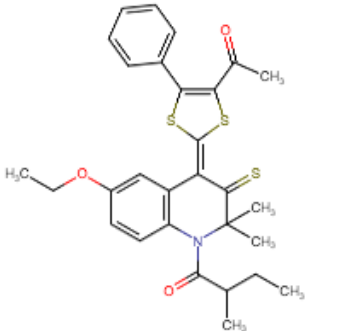
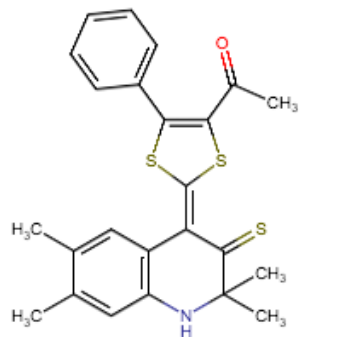
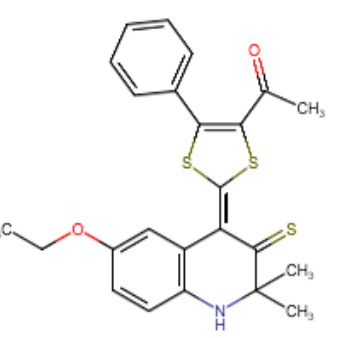
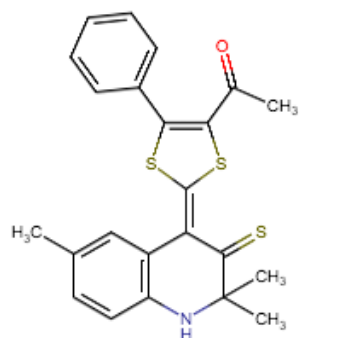
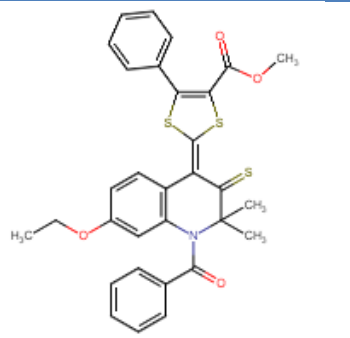
Compound ID	Structure	Formula	Mol Weight [g/mol]
4_0		C ₂₁ H ₁₉ N ₃ O ₃ S	393.46
4_1		C ₁₉ H ₁₅ N ₃ OS	333.41
4_2		C ₁₉ H ₁₃ N ₃ O ₂ S	347.4
4_3		C ₂₀ H ₁₆ FN ₃ OS	365.43

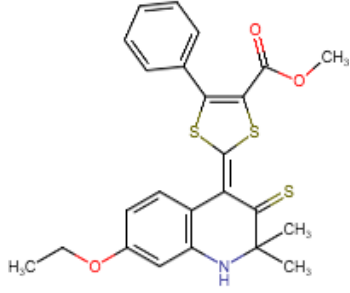
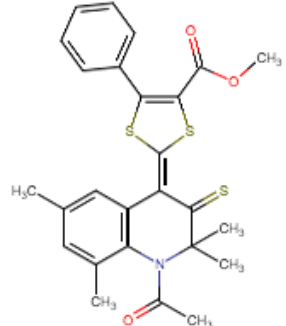
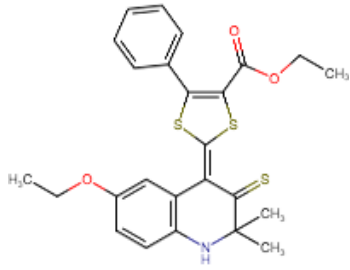
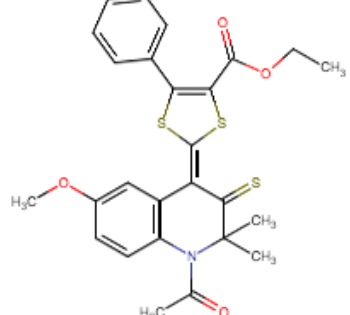
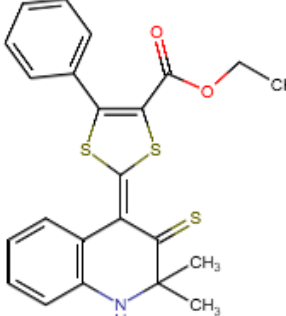
4_4		$C_{19}H_{13}F_2N_3OS$	369.4
4_5		$C_{21}H_{19}N_3O_3S$	393.47
4_6		$C_{18}H_{11}Cl_2N_3S$	372.28
4_7		$C_{24}H_{22}ClFN_4OS$	468.98
4_8		$C_{19}H_{22}N_4OS$	354.48

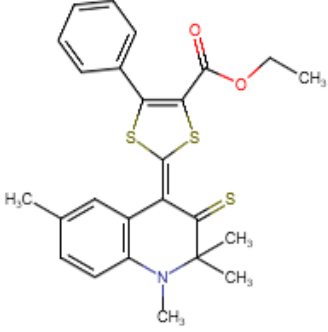
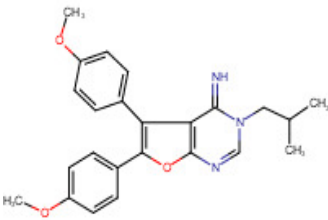
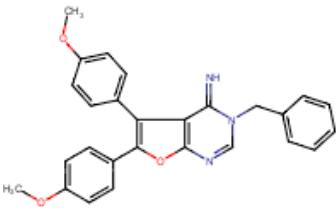
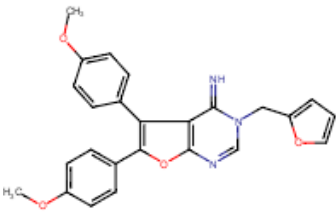
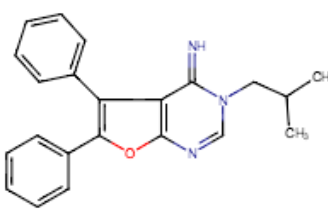
4_9		C ₂₄ H ₂₂ FN ₃ S	403.53
4_10		C ₂₂ H ₂₀ FN ₃ O ₂ S	409.49
4_11		C ₁₉ H ₁₉ FN ₄ OS	370.45
4_12		C ₁₇ H ₁₇ N ₃ OS	311.41
4_13		C ₂₁ H ₁₉ N ₃ O ₂ S	377.47

6_0		C ₂₁ H ₂₆ N ₄ O ₃	382.46
7_0		C ₂₃ H ₂₅ FN ₂ O ₃ S	428.52
9_0		C ₂₁ H ₂₃ NO ₄ S ₃	449.61
9_1		C ₃₀ H ₃₁ NO ₆ S ₃	597.78
9_2		C ₂₁ H ₂₁ NO ₆ S ₃	479.5

9_3		$C_{26}H_{24}N_2O_6S_3$	556.68
9_4		$C_{19}H_{19}NO_5S_3$	437.56
10_0		$C_{23}H_{21}NO_2S_3$	439.61
10_1		$C_{25}H_{23}NO_2S_3$	465.66
10_2		$C_{31}H_{27}NO_2S_3$	541.76

10_3		$C_{29}H_{31}NO_3S_3$	537.77
10_4		$C_{24}H_{23}NOS_3$	437.65
10_5		$C_{24}H_{23}NO_2S_3$	453.65
10_6		$C_{23}H_{21}NOS_3$	423.62
10_7		$C_{31}H_{27}NO_4S_3$	573.76

10_8		$C_{25}H_{25}NO_3S_3$	483.67
10_9		$C_{26}H_{25}NO_3S_3$	495.69
10_10		$C_{25}H_{25}NO_3S_3$	483.67
10_11		$C_{26}H_{25}NO_4S_3$	511.69
10_12		$C_{23}H_{21}NO_2S_3$	439.62

10_13		$C_{25}H_{25}NO_2S_3$	467.68
13_0		$C_{24}H_{25}N_3O_3$	403.47
13_1		$C_{27}H_{23}N_3O_3$	437.5
13_2		$C_{25}H_{21}N_3O_4$	427.46
13_3		$C_{22}H_{21}N_3O$	343.43

13_4		$C_{28}H_{25}N_3O_3$	451.53
13_5		$C_{26}H_{19}N_3O_2$	405.46
13_6		$C_{24}H_{25}N_3O_3$	403.49
13_7		$C_{27}H_{23}N_3O_3$	437.5
13_8		$C_{26}H_{25}N_5O_3$	455.52

13_9		$C_{28}H_{25}N_3O_3$	451.53
51_0		$C_{25}H_{22}N_2O_3$	398.45
66_0		$C_{15}H_{12}N_2O$	236.27